Neuroimaging Changes during Early Recovery from Alcohol Use Disorder

by

Michal Juhas

A thesis submitted in partial fulfillment of the requirements for the degree of

Doctor of Philosophy

Department of Psychiatry
University of Alberta

Abstract

Alcohol use disorder (AUD) is one of the most prevalent, harmful, and costly preventable disorders in the world. AUD is associated with wide-spread structural and functional brain deficits, which are at least partially reversible with sustained abstinence. The most rapid recovery is thought to occur within the initial weeks of sobriety. The mechanism and progression of structural and functional AUD-related brain damage and subsequent recovery during remission remain not fully understood. The objective of this exploratory project was to better characterize the macroscopic and microscopic structural and functional brain changes in recovering AUD patients between approximately two weeks and one month of abstinence, using multi-modal magnetic resonance imaging (MRI) techniques. The data was acquired at two clinical sites in Edmonton, Canada and Mannheim, Germany and together represent one of the largest and most clinically homogeneous, longitudinal, multimodal AUD neuroimaging datasets analyzed to this date. We have conducted six sets of analyses examining: 1) voxel and surface-based morphometry of structural brain changes; 2) region-based morphometry of structural brain changes; 3) white matter microstructure brain changes; 4) regional resting state functional connectivity brain changes; 5) brain changes in large-scale resting state functional network connectivity; and 6) AUD-related brain iron accumulation. The results of these studies have revealed a rich set of complex results across all of the tested modalities. 1) The first analysis revealed a broad high single digit decrease in global gray and white matter densities in AUD at the first time point, which persisted in mid-single digit at the second time point, exhibiting a positive but non-significant structural integrity improvement with sustained abstinence. The AUD group has also exhibited a persistent low single digit decrease in global cortical thickness that persisted through both time points. Clinical severity scales were weakly-to-moderately correlated to the magnitude of the structural atrophy. 2) The second analysis revealed broad high single digit decrease in region-specific cortical, subcortical, and cerebellar regions which showed significant correlation to the clinical severity, especially in the most affected regions. Longitudinal interscan differences associated

with sustained abstinence did not survive multiple comparison correction but indicated a positive recovery trend. 3) The third analysis revealed aberrant diffusion tensor imaging (DTI) scalar pattern consistent with wide-spread neuronal and/or myelin injury in AUD at both time points. Magnitude of the scalar's impairment was in most cases correlated to the clinical severity measures. The longitudinal differences were not significant but alluded to a pattern of microstructural healing during the early AUD recovery. 4) The fourth analysis revealed persistent AUD-related decrease in regional functional connectivity indices in basal ganglia that persisted during both time points, as well as aberrant increase in functional connectivity in the frontal cortex in the AUD patients. Longitudinal differences were mostly not significant. Magnitude of most of the functional deficits was correlated to the AUD clinical severity measures. The longitudinal changes should be considered with caution but might potentially provide evidence of over-compensatory adaptation in the abstinent AUD. 5) The fifth analysis revealed a largely inconsistent complex set of differences in the resting state functional networks derived from an independent component analysis (ICA). Together with hierarchical network analysis, these results suggest a pattern of global hypoconnectivity in the AUD with encouraging functional connectivity convergence across plurality of the networks. Most of the significant changes were correlated with at least one measure of AUD severity. 6) The sixth analysis demonstrated use of a novel quantitative susceptibility technique in a clinical cohort to retrospectively measure brain iron accumulation. This analysis revealed significant high single-digit to low teen percentage increase in iron accumulation in deep brain gray matter in AUD. Altogether, the six sets of analyses completed in this project succeeded in characterizing AUD-related structural and functional deficits in recently detoxified AUD patients but largely failed to detect significant longitudinal differences during the approximately two week to one month interscan remission period. Several of the above analyses were first of their kind and provide unique evidence characterizing early brain recovery dynamics during successful remission from AUD.

Preface

This thesis is original work by Michal Juhas. This research project was approved by the University of Alberta Health Research Ethics Board (study ID: Pro00019424). The project was completed as part of an international TRANSALC research consortium as a part of an international team grant funded by Canadian Institutes of Health Research (NRF 110026) and the European Commission under ERANet Neuron initiative (TRANSALC FKZ 01EW1112).

This project was completed under supervision of Dr. Matthew Brown (Department of Psychiatry, University of Alberta), Dr. Serdar Dursun (Department of Psychiatry, University of Alberta), Dr. Andrew Greenshaw (Department of Psychiatry, University of Alberta), and Dr. Russell Greiner (Department of Computing Science, University of Alberta), together with Edmonton TRANSALC collaborators Dr. Allan Aubry (Alberta Health Services), Dr. James Benoit (Department of Psychiatry, University of Alberta), Dr. Blayne Blackburn (Alberta Health Services), Dr. Ericson Dametto (Department of Psychiatry, University of Alberta), Dr. J. Tim Gillese (Alberta Health Services), Dr. Cindy King (Alberta Health Services), Dr. Mark Loowell (Alberta Health Services), Dr. Marnie Mackay (Department of Psychiatry, University of Alberta), Dr. Manoj Malik (Department of Psychiatry, University of Alberta), Dr. Liana Urichuk (Alberta Health Services), Dr. Glenn Walmsley (Alberta Health Services) and Mannheim TRANSALC team headed by Dr. Wolfgang Sommer (Department of Addictive Behaviour & Addiction Medicine, Central Institute of Mental Health, Medical Faculty Mannheim, University of Heidelberg and Department of Psychopharmacology, Central Institute of Mental Health, University of Heidelberg).

The sixth analysis chapter has been published as Juhás, M., Sun, H., Brown, M., MacKay, M. B., Mann, K. F., Sommer, W. H., Wilman, A. H., Dursun, S. M., & Greenshaw, A. J. (2017). Deep grey matter iron accumulation in alcohol use disorder. *NeuroImage*, 148, 115–122. https://doi.org/10.1016/j.neuroimage. 2017.01.007. The analysis and manuscript preparation was performed in addition to the supervisory and

TRANSALC team described above with Dr. Karl Mann (Department of Addictive Behaviour & Addiction Medicine, Central Institute of Mental Health, Medical Faculty Mannheim, University of Heidelberg), Dr. Hongfu Sun (Department of Biomedical Engineering, University of Alberta), and Dr. Alan Wilman (Department of Biomedical Engineering, University of Alberta). My contribution to this publication included data collection, data analysis, manuscript composition and revisions with collaboration from the other co-authors.

Table of Contents

List of Tables

List of Figures

Chapter 1 - Introduction

This is a paper-based thesis. Each chapter contains its own dedicated introduction, methods, results, and discussion sections. This chapter will, therefore, succinctly provide the main overview and aims of the project as a whole.

Research Problem

Alcohol use disorder (AUD) is one of the most prevalent, harmful and costly preventable disorders in the world, affecting over 283 million people and being responsible for approximately 5.1% of global burden of disease and 5.9% of all deaths globally (Nutt, King, & Phillips, 2010; World Health Organization, 2018). AUD is a chronic relapsing psychiatric disorder characterized by uncontrolled recurrent alcohol abuse, despite its significant interference in the individual's mental wellbeing, physical health, and ability to function in their daily lives (American Psychiatric Association & American Psychiatric Association, 2013). Even though AUD has been systematically studied as a medical disorder of the brain for over 120 years (Marchiafava, 1933; Tabakoff & Hoffman, 2013), AUD patients continue to suffer from only limited treatment options, with plurality of the patients experiencing relapse within the first year (R. H. Moos & Moos, 2006; Walitzer & Dearing, 2006; Witkiewitz, 2011). One of the reasons for the modest knowledge translation and limited therapeutic progress has been the lack of full understanding of the complex mechanism of alcohol on the brain and the progression of structural and functional AUD-related damage and subsequent recovery during prolonged abstinence (Harris, Trudell, & Mihic, 2008; Sutherland, Sheedy, & Kril, 2014b; N. D. Volkow et al., 2017; Zahr & Pfefferbaum, 2017). A growing body of evidence suggests that AUD-related brain deficits are at least partially reversible with sustained abstinence (for reviews, see (Crews & Nixon, 2009; Crowe, Cammisuli, & Stranks, 2019; Fein & Cardenas, 2015; Sullivan & Pfefferbaum, 2005)), and that this process most likely occurs non-linearly with the most rapid recovery in the first few weeks of sobriety (Durazzo, Mon, Gazdzinski, Yeh, &

Meyerhoff, 2015; Gazdzinski, Durazzo, & Meyerhoff, 2005; Pfefferbaum et al., 1995; Y. Zou et al., 2017). There has been a relative scarcity of longitudinal studies that have examined neuroimaging changes during this early period of sustained abstinence, especially in homogeneous clinical cohorts without substantial polysubstance abuse, psychiatric, and somatic comorbidities. The aim of our study was to try to address this gap in the literature and to perform an exploratory analysis to better characterize multimodal neuroimaging changes during the first month of abstinence. I have been involved in all aspects of this project with the exception of design formulation, research consortium building, and grant application, which were completed before my enrollment in the graduate studies.

Goals of the Project

Our study consisted of six different sets of analyses, which have each focused on different neuroimaging modality (structural MRI, DTI, and resting state functional MRI) and/or analysis technique. These are discussed separately in each of the following chapters:

1. Voxel and Surface Based Morphometry of Structural Brain Changes during First Month of Recovery from Alcohol Use Disorder
2. Region-Based Morphometry of Structural Brain Changes during First Month of Recovery from Alcohol Use Disorder
3. White Matter Microstructure Changes during First Month of Recovery from Alcohol Use Disorder
4. Regional Functional Connectivity Changes during First Month of Recovery from Alcohol Use Disorder
5. Independent Component Analysis of Functional Connectivity Changes during First Month of Recovery from Alcohol Use Disorder
6. Deep Grey Matter Iron Accumulation in Alcohol Use Disorder

As an exploratory study, our main goal was to characterize the AUD-related structural and functional differences at both baseline scan at approximately 2 weeks of abstinence and also the interscan differences at the follow-up after 1 month of sustained sobriety in a controlled environment. To this extent, the analyses have generally deployed three sets of contrasts in a general linear model, contrasting the differences between AUD group at the first time point and the reference healthy control group (What brain changes are associated with AUD?), contrasting the differences between AUD group at the second time point and the reference healthy control group (Do the AUD changes persist after the interscan interval?), and the interscan differences within the AUD group between the second time point and the first time point (Is there any significant neuroplasticity observable within the patients during the early remission?). These contrasts provided the main results of our analyses, documenting the neuroimaging differences at baseline and also with the 2-3 week supervised abstinence period.

Additional post-hoc exploratory analyses were conducted on all of the significant results to better contextualize the clinical relevance of the findings (in relation to baseline length of abstinence, average daily alcohol consumption, clinical addiction severity scales, as well as nuisance confounding variables such as age) as well as to other neuroimaging data (to answer follow-up question such as: do regional functional connectivity deficits lead to altered global functional connectivity?) to assist with the interpretation of the significance of our results.

To remain conservative in the discussion of our results, we have generally only considered findings to be relevant if they have survived our *a priori* threshold and indicated at least some significant correlation trend with a clinical severity measure. Especially functional MRI (fMRI) has recently endured extensive criticism for common design, analytical, interpretation, and reproducibility limitations common in the literature, warranting additional caution in our discussion (Button et al., 2013; David et al., 2013; Eklund, Nichols, & Knutsson, 2016; Ioannidis, 2011; Noble, Scheinost, & Constable, 2019; Woo, Krishnan, & Wager, 2014).

The sampling window in our study did not only correspond to what is generally thought to be the period of some of the most dynamic structural brain recovery (Charlet, Rosenthal, Lohoff, Heinz, & Beck, 2018; Gazdzinski et al., 2005), but also to the length of the intensive supervised treatment programs that the patients were enrolled in, effectively providing a multimodal neuroimaging snapshot of recovering AUD patients in early days of enrollment and a snapshot of the recovering AUD patients at or soon after graduation from the established intensive AUD treatment programs provided to the public at both of the clinical nodes. If the residential treatment can meaningfully help patients recover from their alcohol addiction and catalyze the appropriate behavioural and cognitive changes necessary for remission, then there should also be corresponding structural and functional changes in the brain over the same time period. Prior studies have reported detectable evidence of structural recovery using traditional neuroimaging techniques in recently detoxified AUD patients within as little as two weeks (Kühn et al., 2014; van Eijk et al., 2013), thus, supporting the feasibility of being able to measure the anticipated brain changes also in our study.

Based on the available literature, our *a priori* expectations for our analyses included:

1. STRUCTURAL MRI: Wide-spread global structural atrophy in the AUD, with especially noticeable enlargement of ventricles and increased susceptibility of the white matter as well as frontal gray matter regions, which should be at least partially reversible within our interscan interval.
2. DTI: Wide-spread decreased fractional anisotropy due to myelin and glial damage as well as neuronal thinning and deletion, which should be at least partially reversible.
3. RESTING STATE fMRI: Less efficient functional connectivity patterns with possible compensatory aberrant recruitment of additional anatomical regions and either abstinence-related normalization or adaptive excess top-down executive (frontal cortex) and decreased bottom-up reward (basal ganglia) functional connectivity.

4. CLINICAL SEVERITY: More severe magnitude of AUD-related brain deficits are expected to be associated with greater severity of AUD (including increased average daily alcohol consumption).

The literature has, however, provided complex evidence of mixed results for most of the modalities. Studies have reported significant earlier recovery prior to the abstinence window of our study (from detoxification to the first two weeks) as well as persistent structural and functional deficits even in multi-year abstinent AUD participants. Therefore, our expectations are of significant AUD-related deficits at both time points with a positive recovery normalization trend. Some studies have also reported recovery claims despite of unclear abstinence profile (early abstinence could mean a few days to few months in different studies), complex polysubstance abuse history (very common nicotine dependence as well as concurrent stimulant and marihuana abuse), as well cross-sectional design (despite of clear evidence of survival bias of patients with less severe baseline damage exhibiting longer remission probability – for example see (S. F. Sorg et al., 2012)).

Our study should not only help characterize the neuroimaging changes during early remission from AUD using a very homogeneous, carefully controlled clinical cohort with more consistent abstinence profile than other studies, it will be also one of the first few longitudinal studies to examine cortical thickness in recovering AUD patients (third study), subcortical and cerebellar volumes (possibly the second and first, respectively), white matter microstructure, regional functional connectivity differences (possibly the first), independent component whole-brain resting state functional connectivity differences (possibly the first), and brain iron levels in a clinical AUD cohort (the first). The results of our study should, therefore, provide a meaningful addition to the existing literature and our understanding of the underlying structural and functional brain changes during early recovery from AUD.

The chapter-specific introductions provide more in-depth literature overview and hypothesis formulation for each of the six sets of neuroimaging studies.

Chapter 2 - Voxel and Surface Based Morphometry of Structural Brain Changes during First Month of Recovery from Alcohol Use Disorder

Abstract:

Alcohol use disorder (AUD) is associated with widespread structural brain damage, which is partially reversible during prolonged abstinence. To the best of our knowledge, only two prior longitudinal studies have documented cortical changes during AUD recovery. This study performed voxel and surface-based morphometry of longitudinal changes in gray matter density, white matter density, cortical thickness, and associated clinical correlations in 13 male AUD patients undergoing a three week supervised residential treatment, compared to 12 matched healthy controls. The recovering AUD patients have exhibited widespread structural atrophy across all measures at both first and second time points. Although there was a positive trend towards structural recovery between the approximately 9 and 29 days of abstinence, none of the interscan changes survived multiple comparison correction. On average, the AUD patients exhibited 7.11% decrease in overall gray matter density, which improved to 4.68% deficit by the second time point (2.62% interscan increase). White matter density improved from 7.19% deficit to 4.39% deficit (3.01% interscan increase). Whole-brain cortical thickness exhibited only a marginal improvement trend from 2.88% deficit to 2.85% deficit (negligible 0.03% interscan increase), with more pronounced differences in specific regions of interest. Clinical severity scales exhibited weak to moderate negative correlation with most of the atrophy measures (generally with -0.3 to -0.5 Pearson handle). Even though this study was constrained by its modest sample size to draw exhaustive conclusions about the structural patterns of early AUD recovery, it adds valuable insights from a carefully controlled, homogeneous, longitudinal sample in a challenging clinical cohort.

Key terms

alcohol use disorder; abstinence; voxel-based morphometry; cortical thickness; magnetic resonance imaging

1. Introduction

Alcohol use disorder (formerly also classified as alcohol dependence, alcohol addiction, or alcoholism) is a mental disorder characterized by uncontrolled chronic, recurrent alcohol abuse, which significantly interferes with the patients' ability to function in their daily lives (American Psychiatric Association & American Psychiatric Association, 2013). It is one of the most prevalent, harmful, and costly preventable disorders in the world (Nutt et al., 2010; World Health Organization, 2018). Worldwide, WHO estimates that over 283 million people are currently suffering from AUD and that harmful use of alcohol is responsible for approximately 5.9% of all deaths and 5.1% of the global burden of disease (translating to a preventable loss of over 139 million disability-adjusted life years). Even though AUD is a widespread and very costly disorder, which has a long and pervasive history as well as well-characterized clinical symptoms, the exact underlying mechanism of alcohol addiction as well as recovery and sustained maintenance of abstinence remain unclear (Sutherland et al., 2014b; Zahr & Pfefferbaum, 2017). As a result, treatment-seeking AUD patients have only limited therapeutic options, which are associated with poor clinical prognosis for a large portion of the patients, contributing to the chronic, recurrent nature of the disorder (R. H. Moos & Moos, 2006; Walitzer & Dearing, 2006; Witkiewitz, 2011).

Chronic alcohol abuse causes progressive, wide-spread structural damage in the brain. The scientific evidence of these pathological features has been systematically documented for over 120 years (Marchiafava, 1933; Tabakoff & Hoffman, 2013), even as our understanding and clinical definition of AUD has gradually evolved over time. Early post-mortem pathological reports and subsequent animal studies have documented significant brain volume loss, cortical thinning, widespread demyelination and loss of glial cells, as well as thinning of dendritic arbor, shrinking volume of neuronal axons and soma, and region-specific loss of neurons caused by the recurrent toxic alcohol exposure (Harper, Dixon, Sheedy, & Garrick, 2003). Brains of neuro-behaviourally uncomplicated deceased AUD donors have exhibited up to 27% regional loss of neurons (especially in the frontal cortex) and even more pronounced

loss of up to 37% of glial supports cells (in regions such as hippocampus) (Harper et al., 2003; Korbo, 1999; Miguel-Hidalgo et al., 2002). The extent of cellular damage in several regions has been, furthermore, correlated with severity of alcohol abuse, including lifetime amount of alcohol consumption (Harding, Halliday, Ng, Harper, & Kril, 1996).

With technological advances and gradual adoption of non-invasive neuroimaging techniques (such as magnetic resonance imaging (MRI)) since the late 1980s onwards, clinical researchers have been able to corroborate on the histological evidence by documenting structural changes in living patients at different levels of AUD severity, clinical treatment stages, and in progressively finer structural resolution. These studies have replicated global brain atrophy and ventricular enlargement as well as region-specific structural deficits in living AUD patients (Fritz, Klawonn, & Zahr, 2019). Two meta-analyses have summarized the reproducible structural findings across multiple AUD structural studies (Xiao et al., 2015; Yang et al., 2016). The voxel-based morphometry (VBM) meta-analyses reported a consistent decrease in the grey matter density in the prefrontal cortex (especially anterior cingulate cortex), posterior cingulate cortex, and dorsal striatum / insula in AUD patients, compared to matched healthy volunteers. A mega-analysis of pooled AUD datasets has also reported similar wide-spread structural atrophy in AUD patients, affecting most cortical regions, including superior frontal gyrus, orbital frontal gyrus, cingulate cortex, precuneus, superior and inferior temporal gyri, insula, and precentral gyrus (Mackey et al., 2019). One of the most important advantages of the non-invasive neuroimaging techniques is, however, the ability to explore longitudinal changes within the same participants. The advent and wide-spread utilization of the non-invasive neuroimaging systems has thus helped to document not only the extent of the AUD-related brain damage but also the progressive functional and structural changes associated with AUD treatment and successful recovery. Structural MRI remains one of the most effective tools for clinical identification, diagnosis, and monitoring of alcohol-related brain damage (Fritz et al., 2019).

Longitudinal structural neuroimaging studies have documented at least partial recovery of AUD structural brain damage with abstinence, including decreased volume of enlarged ventricles and region-specific volume recovery within as early as the first two weeks of abstinence. (Bartsch et al., 2007; Cardenas, Studholme, Gazdzinski, Durazzo, & Meyerhoff, 2007; Demirakca et al., 2011; Gazdzinski et al., 2005; Kühn et al., 2014; Pfefferbaum et al., 1995; van Eijk et al., 2013). The pattern of structural recovery appears to be non-linear, with most rapid recovery occurring during the early stages (first few weeks) of sustained abstinence, although AUD-related structural deficits might persist even after years of abstinence (Durazzo et al., 2015; Gazdzinski et al., 2005; Pfefferbaum et al., 1995; Y. Zou et al., 2017). Structural brain changes during the early recovery from AUD are of particular interest, because preclinical evidence suggests that underlying tissue repair and regeneration (neuro- and glio-genesis) in the animal models of AUD also occurs primarily within the first month of abstinence (Crews & Nixon, 2009). Clinical magnetic resonance spectroscopy studies have also documented metabolic brain changes consistent with glial and/or neuronal repair and regeneration within the first few weeks of abstinence (Bartsch et al., 2007). These metabolic changes have been directly associated with both macroscopic structural volume recovery as well as functional improvements in the abstinent AUD patients. Synthesis of the preclinical and clinical evidence has been, however, challenging since much of the existing evidence has not been translatable. The existing clinical longitudinal literature only provides sparse and often inconsistent snapshots of the underlying structural changes during recovery from alcohol use disorder, persisting as a bottleneck in our understanding of AUD and its clinical progression.

The aim of this study was to try to address this gap and document both differences in tissue density (voxel-based morphometry) as well as cortical thickness (surface-based morphometry) during the first month of AUD recovery in a clinically homogeneous longitudinal study. Cortical thickness should provide a more sensitive, complementary technique for measuring structural atrophy in addition to the more traditional voxel-based morphometry analysis (Hutton, Draganski, Ashburner, & Weiskopf, 2009).

Our *a priori* hypotheses were that (1) AUD patients will exhibit mid to high single digit average structural atrophy across all of the baseline measures (gray matter density, white matter density, as well cortical thickness) at the first time point, compared to the matched healthy controls; (2) AUD patients will exhibit low to middle single digit average structural atrophy across all of the measures at the second time point; (3) interscan comparison will reveal low to middle single digit longitudinal recovery associated with the sustained abstinence; and (4) AUD-related clinical severity measures will be negatively correlated to the structural parameters (*i.e.* the higher the clinical severity, the greater the structural damage).

To the best of our knowledge, this is only the third longitudinal study to analyse cortical thickness differences during AUD recovery. This study will complement the existing literature by spanning the abstinence range between the two existing studies (P. Bach et al., 2020; G. Y. Wang et al., 2016) and also provide the first evidence from a North American clinical cohort.

2. Materials and Methods

2.1 Subjects

The analysis is based on longitudinal data from 13 recently detoxified adult male alcohol dependent patients (DSM-IV-TR criteria)(American Psychiatric Association, 2000) and matched 12 healthy non-alcohol-abusing men. The demographic and clinical overview of the 25 participants is summarized in Table 2.1.

During the recruitment process, a total of 1,123 AUD patients and 668 healthy controls were screened and interviewed for participating in the study. 29 eligible AUD volunteers and 18 matched healthy control volunteers were enrolled in the study. 24 patients and 17 healthy controls completed the first scanning session. 14 patients and 12 controls completed the second scanning session. One of the 14 patients who

completed both scanning sessions had to be excluded due to severe imaging artifacts. None of the volunteers were provided with any compensation for their participation in the study.

The alcohol-dependent participants were recruited from a pool of patients referred to supervised residential treatment programs in Edmonton, Canada as part of the TRANSALC research project. DSM-IV-TR diagnostic interviews were carried out by a psychiatrist, using the Structured Clinical Interview for the DSM-IV-TR (SCID-I) (First, Spitzer, Gibbon, & Williams, 2002). All of the patients were consistent, steady, heavy drinkers. All of the analyzed patients met the highest Zone IV cut-off score on the Alcohol Use Disorders Identification Test (AUDIT) with an average score of 31 out of 40 (Saunders, Aasland, Babor, de la Fuente, & Grant, 1993). The AUD patients exhibited on average a substantial level of alcohol dependence (third quartile) according to the Alcohol Dependence Scale (ADS) with the average score of 26 out of 47, at the time of the first scanning session (Skinner & Allen, 1982). The patients did not abuse non-beverage ethanol or other substances except nicotine (average Fagerstrom score of 4 out of 10 (Heatherton, Kozlowski, Frecker, & Fagerström, 1991)). The patients were recruited within the first two weeks of abstinence and underwent longitudinal scanning sessions at two time points: first at approximately 9 days of abstinence and second three weeks later at approximately 29 days of abstinence. Abstinence was verified at each scanning session in all participants by an alcohol breathalyser (BACtrack S50 Personal Breathalyzer, Portable Breath Alcohol Tester) and a urine drug screen (nal von minden GmbH Drug-Screen® Diptest, Version 1.0).

Controls were recruited concurrently to match the patients' general demographic profile (including sex, age, handedness, general occupation/education background). The controls had no history of alcohol or drug addiction and consumed alcohol below the Canada's Low-Risk Alcohol Drinking Guidelines (Butt, 2011). Participants in both arms were excluded if they had any history of serious medical (including psychiatric or neurological) complications, brain injury, use of psychotropic medications (other than during the detoxification process), or did not meet magnetic resonance safety criteria for our imaging

facility. The study was approved by the University of Alberta Health Research Ethics Board (study ID: Pro00019424).

Table 2.1 Summary of Key Demographic and Clinical Variables

	AUD Patients (n=13)		Controls (n=12)				
	Mean	**SEM**	**Mean**	**SEM**	**% Δ**	**t-Value**	**corrected p**
Age	41.35	1.85	45.39	1.87	-8.92	-1.52	not sig
TIV	1,704.27	28.09	1715.86	25.90	-0.68	-0.32	not sig
Ethanol (grams/day)	370.15	39.82	3.10	0.87	11,847.59	9.22	***
AUDIT	30.77	0.71	2.50	0.35	1,130.77	35.93	***
ADS	26.15	1.31	0.67	0.20	3,823.08	19.24	***
OCDS	25.23	1.38	1.08	0.23	2,228.99	17.24	***
ODS	10.54	0.81	0.08	0.06	12,546.15	12.88	***
CDS	14.69	0.71	1.00	0.21	1,369.23	18.45	***
Abstinence 1 (days)	8.77	0.35	N/A	N/A			
Abstinence 2	29.00	0.58	N/A	N/A			

*p<0.05, ** p<0.01, *** p<0.001 Bonferroni-corrected; SEM = standard error of mean

2.2 MRI Acquisition

The neuroimaging data was acquired using a 4.7 Tesla Varian Inova whole-body MRI scanner, located at the University of Alberta, Edmonton. The scanning protocol included anatomic imaging using T1-weighted magnetization-prepared rapid acquisition echo (MPRAGE) with acquisition parameters of TR 1,505.9 ms, inversion time 300.0 ms, relaxation delay time (after readout prior to inversion) 300.0 ms, linear phase encoding, TE 3.71 ms, matrix 240×192×128, field of view 240×192×192 mm^3, 1.0×1.0×1.5 mm^3 voxels, whole brain coverage.

The anatomical scans were visually reviewed by two independent neuroimaging experts for gross abnormalities. None of the subjects exhibited any clinically significant structural abnormalities other than what may be expected from normal aging or prolonged alcohol abuse.

The raw data was also anonymized before any pre-processing and the researchers were blinded to the subject or group label key until the final statistical analysis (even though automated morphometry analyses should avoid bias).

2.3 Voxel-Based Morphometry

Voxel-based morphometry (VBM) analysis was performed using Computational Anatomy Toolbox (CAT12; http://www.neuro.uni-jena.de/cat/) (Gaser & Dahnke, 2016) in the Statistical Parametric Mapping software library (SPM 12; http://www.fil.ion.ucl.ac.uk/spm/) (John Ashburner et al., 2014) in MATLAB (version R2018b) (The MathWorks Inc, 2018). Full description of the processing pipeline is included in the above citations. Briefly, the raw reconstructed T1 scans were inspected to exclude any participants without a whole-brain field of view or severe imaging artifacts. A unified segmentation model (J. Ashburner & Friston, 2005) was used to spatially register and segment maps into gray matter (GM), white matter (WM), and cerebrospinal fluid (CSF), bias-correct for intensity non-uniformities, and modulate signal proportionately to the volume changes related to spatial registration, to maintain consistent total amount of segmented tissue to the original scan (using default parameters). The spatial normalization was performed using affine regularization to International Consortium for Brain Mapping (ICBM) European brain tissue probability template and finely warped using non-linear diffeomorphic DARTEL normalization (John Ashburner, 2007) to a tissue template target based on 555 healthy controls from the IXI database (www.brain-development.org) in the Montreal Neurological Institute (MNI) space. The corrected segmented images underwent another quality control step to verify the anatomical tissue classification. Next, the GM and WM segmented images were smoothed using an 8 mm full-width-at-half-maximum (FWHM) Gaussian isotropic kernel and entered into a statistical analysis. Estimates of the total intracranial volume were also computed at this time, so that they could be added as a nuisance variable in the statistical model. Preprocessing steps were performed using the CAT12 default recommended settings (Gaser & Dahnke, 2016).

2.4 Surface-Based Morphometry

Surface-based morphometry (SBM) analysis was performed using the projection-based thickness method (Dahnke, Yotter, & Gaser, 2013). Cortical thickness was calculated based on the segmented data described in the VBM section. The segmented tissue maps were then separated into hemispheres, cerebellum and hindbrain were removed, ventricular and subcortical regions were filled in, and the masked volumes were linearly interpolated to 0.5 mm isotropic resolution. Voxel-based distance from the inner boundary of the gray matter mask was calculated to each gray matter voxel, creating a white matter distance map. Voxel-based distance was also calculated from the outer boundary of the gray matter mask for each gray matter voxel, creating a CSF distance map. The outer boundary local maxima values for the white matter distance were then corrected by the corresponding CSF distance values, representing the cortical thickness values. The corrected thickness values from the outer maxima were then projected back onto all of the other gray matter voxels based on the neighbour relationship described by the white matter distance. To correct for overestimation of the cortical thickness in the sulcal regions due to outer boundary blurring, successor relation projection scheme described in detail in the original publication was used to create a corrected cortical thickness map (Dahnke et al., 2013). In the same step, CAT12 also calculated the central surface at the median distance for both hemispheres. The surface morphometry pipeline also used topology correction, spherical mapping of the surface mesh (resampled to 32k mesh) in a common coordinate space, and estimation of local surface complexity and gyrification (Kurth & Gaser, 2019). The spherical registration was adapted from the volume-based diffeomorphic DARTEL algorithm to the spherical maps (Yotter, Ziegler, Thompson, & Gaser, 2011). Only the cortical thickness estimates were used in our analysis, since we had no *a priori* expectation for altered surface complexity change associated with chronic alcohol abuse in an adult, matured brain (Kühn et al., 2016). The cortical thickness maps were visually inspected for quality. Next, cortical thickness maps were smoothed using a 15 mm full-width-at-half-maximum (FWHM) Gaussian isotropic kernel and entered into a statistical

analysis. Unlike in the VBM analysis, the SBM analysis of the cortical thickness did not include total intracranial volume as a nuisance variable. A post-hoc region-of-interest cortical thickness analysis was also performed, based on Desikan-Killiany Cortical Atlas labels (Desikan et al., 2006), to help refine anatomical localization and quantify the wide-spread cortical thinning observed in the data and its relation to the clinical severity scales.

2.5 Statistical Analysis

After the quality assurance of the VBM and SBM maps was complete, the label key was returned to the blinded researcher to allow for group comparison and statistical analysis. The summary statistics and group comparison was generated using SPSS (version 20) (IBM Corp, 2011) and MATLAB (version R2018b) (The MathWorks Inc, 2018). The summary statistics included group mean and standard error of mean (SEM). After verifying validity of the assumptions (including Levene's test of homogeneity), two sample t-tests were used to compare group differences. The input data for demographic and clinical summary statistics was not corrected for nuisance variables (such as age).

The primary group comparison analysis was done using general linear models. The models included predictors for group status (dummy variables for first and second scans for patients and controls) as well z-normalized nuisance variables (total intracranial volume, age, and length of abstinence at first scan). Cortical thickness SBM analysis did not include the total intracranial volume nuisance variable, as recommended by CAT12 manual (Kurth & Gaser, 2019). The contrasts compared first time point group differences, second time point group differences, as well as interscan longitudinal differences. For completeness and quality assurance purposes, an interscan comparison was also performed on only the healthy control longitudinal data, none of which showed any significant interscan differences during the three weeks and were thus not reported in the figures.

Post-hoc clinical correlation analysis was performed on nuisance-corrected z-normalized data. The significance of the Pearson correlation coefficient was tested using two-tailed t-test.

For all analyses, the null hypothesis was rejected and group differences were considered as significant at a global alpha threshold of 0.05. The p-values were corrected for multiple comparison using Family-Wise Error (FWE) correction. The FWE-corrected statistical map thresholds for the neuroimaging data were estimated using 10,000 permutations with threshold-free cluster enhancement toolbox (Gaser, 2019). Demographic and clinical summary statistics as well as clinical correlations and region-of-interest group comparisons were FWE corrected using the Bonferroni method (Bonferroni, 1936).

3 Results

3.1 Participant profile

The healthy controls were recruited to match the general demographic profile of the AUD patients. As a result, the groups were not significantly different in their general demographic profile. On average, the total intracranial volume was also comparable between the groups. Nonetheless, group comparisons using general linear models as well as post-hoc clinical correlation analyses included age, total intracranial volume, as well as the patients' length of abstinence at first scanning session as nuisance variables since all of these variables are known to impact regional volumes or longitudinal changes in the brain. The clinical measures were in general at least an order of magnitude more severe in the AUD group than in the healthy control, as illustrated in Table 2.1.

3.2 Voxel-Based Morphometry – Gray Matter Changes

AUD patients demonstrated a widespread decrease in gray matter tissue concentration at both time points (9 days and 29 days of abstinence). The interscan differences did not survive multiple comparison correction, but demonstrated a positive trend towards increased gray matter concentration with sustained three week abstinence. Top rows of Figure 2.1, Figure 2.2, and Figure 2.3 illustrate the large widespread decrease in gray matter concentration (dark blue t-maps and bright blue significant clusters) and interscan improvement in the AUD patients (predominantly red t-map but no significant clusters). Table 2.2 and Table 2.3 list the significant clusters and their respective coordinates, corresponding to Figure 2.1 and Figure 2.2. Peak p-values were FWE-corrected and the X, Y, Z coordinates of the peak values (MAX) and centre of gravity (COG) are in the MNI space.

Table 2.2: Significant Clusters of Decreased Gray Matter Concentration at First Scan

Peak Location	Peak corr. p-value	MAX X (mm)	MAX Y (mm)	MAX Z (mm)	# Voxels	COG X (mm)	COG Y (mm)	COG Z (mm)
right cerebellum - right crus II	0.000	47.5	-62.5	-48.5	625547	1.02	-26.4	8.21
right superior frontal gyrus	0.003	20.5	7.5	67.5	6811	22.5	3.27	60.7
right superior frontal gyrus	0.015	16.5	31.5	46.5	359	16	31.4	50.6
left frontal pole	0.017	-3.5	54.5	-25.5	38	-4.05	54.7	-24.9

Table 2.3: Significant Clusters of Decreased Gray Matter Concentration at Second Scan

Peak Location	Peak corr. p-value	MAX X (mm)	MAX Y (mm)	MAX Z (mm)	# Voxels	COG X (mm)	COG Y (mm)	COG Z (mm)
cerebellum - right crus II	0.000	48.5	-55.5	-47.5	463425	1.09	-26.9	11.5
left frontal pole	0.016	-33.5	61.5	-7.5	295	-31	57.8	-9.11
left frontal orbital cortex	0.017	-35.5	21.5	-20.5	54	-34.5	22.9	-18.3
right superior frontal gyrus	0.017	2.5	54.5	29.5	22	2.59	54.8	30.1

The average t-values across the entire gray matter mask were -2.42 (standard deviation 1.82) for group comparison at 9 days of abstinence, -1.80 (σ 1.79) for group comparison at 29 days of abstinence, and +0.54 (σ 0.71) for the interscan improvement in the AUD patients. Examining just the significant cluster, the average t-values were -3.61 (σ 1.28) at first scanning session group comparison and -3.43 (σ 1.12) at second scanning session. The interscan difference comparison did not yield any significant clusters after multiple comparison correction.

The average whole-brain gray matter concentration was 7.1% less at first time point (corrected for nuisance variables) in AUD compared to controls. At the second time point the difference narrowed down to -4.7%, corresponding to a +2.6% interscan increase in the AUD patients. The significant clusters at the first time point demonstrated a difference of -10.4% at first scan, -7.6% at second scan, and AUD interscan change of +3.1%. The significant clusters at the second time point (substantially overlapping with both of the above measurement sets) demonstrated a difference of -10.9% at first time point, -8.74% at second time point, and corresponding +2.5% AUD interscan improvement. Table 2.4 summarizes the raw and nuisance variable corrected gray matter VBM changes for whole-brain (All GM) as well significant clusters which survived multiple comparison correction for group comparison between AUD and healthy controls (CTL) at first time point and at second time point.

Table 2.4: Raw and Nuisance-Corrected Gray Matter Tissue Concentration

	AUD 1		**AUD 2**		**CTL**	
	$\bar{x}$	**σ**	**$\bar{x}$**	**σ**	**$\bar{x}$**	**σ**
All GM	0.45	0.05	0.46	0.05	0.49	0.047
Only significant GM clusters at 1st scan	0.47	0.05	0.48	0.05	0.52	0.054
Only significant GM clusters at 2nd scan	0.47	0.05	0.47	0.05	0.53	0.056
Group Differences						
	AUD 1 vs CTL		**AUD 2 vs CTL**		**AUD2 vs AUD1**	
	Δ Raw	**Δ Corr.**	**Δ Raw**	**Δ Corr.**	**Δ Raw**	**Δ Corr.**
All GM	-7.46%	-7.11%	-6.39%	-4.68%	1.16%	2.62%
Only significant GM clusters at 1st scan	-10.77%	-10.42%	-9.27%	-7.60%	1.68%	3.15%
Only significant GM clusters at 2nd scan	-11.29%	-10.94%	-10.39%	-8.74%	1.01%	2.47%

3.3 Voxel-Based Morphometry – White Matter Changes

AUD patients demonstrated a widespread decrease in white matter tissue concentration at both time points (9 days and 29 days of abstinence). The interscan differences did not survive multiple comparison correction, but demonstrated a positive trend towards increased white matter density with sustained three week abstinence. Bottom rows of Figure 2.1, Figure 2.2, and Figure 2.3 illustrate the large widespread decrease in white matter concentration (dark blue t-maps and bright blue significant clusters) and interscan improvement in the AUD patients (predominantly red t-map but no significant clusters). Table 2.5 and Table 2.6 list the significant clusters and their respective coordinates, corresponding to Figure 2.1 and Figure 2.2. Peak p-values were FWE-corrected and the X, Y, Z coordinates of the peak values (MAX) and centre of gravity (COG) are in the MNI space.

Table 2.5: Significant Clusters of Decreased White Matter Concentration at First Scan

Peak Location	Peak corr. p-value	MAX X (mm)	MAX Y (mm)	MAX Z (mm)	# Voxels	COG X (mm)	COG Y (mm)	COG Z (mm)
right inferior temporal gyrus WM	0.000	54.5	-21.5	-25.5	356505	0.797	-15.7	16.4
right superior cerebellar peduncle	0.006	9.5	-50.5	-31.5	3366	15.5	-47.2	-33.9
left precentral gyrus WM	0.015	-37.5	-13.5	44.5	528	-38.8	-10.5	45.7

Table 2.6: Significant Clusters of Decreased White Matter Concentration at Second Scan

Peak Location	Peak corr p-value	MAX X (mm)	MAX Y (mm)	MAX Z (mm)	# Voxels	COG X (mm)	COG Y (mm)	COG Z (mm)
left V3/V4 visual cortex occipital WM	0.000	-21.5	-83.5	-3.5	271315	0.569	-15.1	16.2
right middle cerebellar peduncle	0.009	22.5	-41.5	-28.5	312	20.4	-42.7	-28.5
right precentral gyrus WM	0.015	38.5	0.5	41.5	251	37.1	0.966	43.6

The average t-values across the entire white matter mask were -1.92 (standard deviation 1.76) for group comparison at 9 days of abstinence, -1.31 (σ 1.91) for group comparison at 29 days of abstinence, and

+0.66 (σ 0.64) for the interscan improvement in the AUD patients. Examining just the significant cluster, the average t-values were -3.41 (σ 0.90) at first scanning session group comparison and -3.31 (σ 0.84) at second scanning session. The interscan difference comparison did not yield any significant clusters after multiple comparison correction.

The average whole-brain white matter concentration was 7.2% less at first time point (corrected for nuisance variables) in AUD compared to controls. At the second time point the difference narrowed down to -4.4%, corresponding to a +3.0% interscan increase in the AUD patients. The significant clusters at the first time point demonstrated a difference of -10.6% at first scan, -8.2% at second scan, and AUD interscan change of +2.7%. The significant clusters at the second time point (substantially overlapping with both of the above measurement sets) demonstrated a difference of -10.9% at first time point, -8.88% at second time point, and corresponding +2.3% AUD interscan improvement. Table 2.7 summarizes the raw and nuisance variable corrected white matter VBM changes for whole-brain (All WM) as well significant clusters which survived multiple comparison correction for group comparison between AUD and healthy controls (CTL) at first time point and at second time point.

Table 2.7: Raw and Nuisance-Corrected White Matter Tissue Concentration

	AUD 1		**AUD 2**		**CTL**	
	$\bar{x}$	**σ**	**$\bar{x}$**	**σ**	**$\bar{x}$**	**σ**
All WM	0.522	0.059	0.53	0.057	0.564	0.053
Only significant WM clusters at 1st scan	0.592	0.071	0.599	0.069	0.664	0.071
Only significant WM clusters at 2nd scan	0.613	0.074	0.618	0.072	0.69	0.077
Group Differences						
	AUD 1 vs CTL		**AUD 2 vs CTL**		**AUD2 vs AUD1**	
	Δ Raw	**Δ Corr.**	**Δ Raw**	**Δ Corr.**	**Δ Raw**	**Δ Corr.**
All WM	-7.48%	-7.19%	-6.06%	-4.39%	1.54%	3.01%
Only significant WM clusters at 1st scan	-10.86%	-10.60%	-9.80%	-8.22%	1.20%	2.67%
Only significant WM clusters at 2nd scan	-11.18%	-10.93%	-10.44%	-8.88%	0.84%	2.30%

3.4 Voxel-Based Morphometry – Clinical Correlates

Post-hoc exploratory analysis of the correlations between the VBM values and clinical parameters in AUD patients did not reveal significant results with the exception of age, in data which was not corrected for nuisance variables. Data corrected only for total intracranial volume have shown a strong negative correlation between gray matter density (total as well as significant clusters) and age (at Pearson's correlation of -0.86 to -0.87). There was no significant correlation between AUD patients' white matter density and age. The only clinical measure which approached significance but did not survive Bonferroni correction for multiple comparisons was the total length of abstinence at the first time point. It was correlated with gray matter density (total as well as significant cluster at Pearson's correlation of 0.39 to 0.45). White matter density was positively correlated with length of abstinence as well (0.26 to 0.29), but was not significant, even before Bonferroni correction. Note that both age and length of abstinence at first time point were included as nuisance variables in the main analysis to help explore longitudinal structural differences in the recovering AUD brain during the interscan interval.

If we include also the data for healthy controls, all of the clinical severity measures demonstrate significant negative correlation with tissue density. The Pearson's correlations for gray matter and white matted for total whole-brain tissue mask, significant cluster at first time point, and significant cluster at second time point are respectively: ADS -0.41, -0.51, -0.54 and -0.36, -0.51, -0.53; AUDIT -0.40, -0.52, -0.56 and -0.39, -0.55, -0.57; OCDS -0.42, -0.53, -0.56 and -0.34, -0.49, -0.50; ODS -0.43, -0.52, -0.55 and -0.26, -0.40, -0.41; CDS -0.40, -0.52, -0.55 and -0.40, -0.54, -0.56; and average daily ethanol consumption (prior to treatment) -0.30, -0.39, -0.42 and -0.35, -0.46, -0.46. The age was also significantly correlated in the data which was only corrected for the total intracranial volume (-0.50 to -0.60 for gray matter and -0.12 to -0.16 for white matter regions). All of these correlations had Bonferroni corrected p-values of less than 0.01, meeting the *a priori* α threshold of 0.05 for rejection of the null hypothesis.

3.5 Surface-Based Morphometry – Cortical Thickness

AUD patients demonstrated a widespread decrease in cortical thickness at both time points (9 days and 29 days of abstinence). The interscan differences did not survive multiple comparison correction, but demonstrated a positive trend towards increasing global cortical thickness with sustained three week abstinence. Figure 2.4, Figure 2.5, and Figure 2.6 illustrate these differences by depicting t-maps of the comparisons as well as outlines of the significant clusters (saturated clusters with pink outline over unsaturated t-maps on the right side of the figures), which have survived FWE multiple comparison correction. The figures depict large, widespread negative trend at the first time point (almost exclusive negative blue and blue-green t values), somewhat less large and less widespread negative trend at the second time point (almost exclusive negative blue and blue-green t values but more green, closer to neutral), and primarily yellow-green interscan positive difference in the AUD patients. The greatest interscan increase was in the precentral and postcentral sulci of the primary motor cortex and visual cortex of the occipital lobe.

To quantify the cortical thickness changes and provide greater granularity of the findings, beyond large, wide-spread patterns, we have also conducted a post-hoc region-of-interest analysis based on Desikan-Killiany Cortical Atlas labels (Desikan et al., 2006). The whole-brain average shows a -2.88% cortical thickness difference at first time point, -2.85% difference at second time point, corresponding to a 0.03% interscan whole-brain increase in the cortical thickness in the recovering AUD patients during the last three weeks of the first month of sustained abstinence. Table 2.8 and Table 2.9 provide a summary of the significant differences after the FWE correction. The significant changes occurred 79% across bilateral anatomical regions, with only 5 out of the 24 significantly different regions being limited to a single hemisphere (banks of superior temporal sulcus only significantly different in left hemisphere while parahippocampal, cuneus, pars triangularis, frontal pole, and pars orbitalis only significantly different in the right hemisphere).

3.6 Surface-Based Morphometry – Clinical Correlates

Essentially all of the Desikan-Killiany atlas regions of interest demonstrated a negative correlation with age (average of -0.34) in the cortical thickness data not corrected for the nuisance variables, with approximately 43% of the anatomical regions exhibiting statistically significant Pearson correlation after Bonferroni correction (average of significant regions -0.45). The nuisance-corrected cortical thickness data has demonstrated a broadly negative correlation with most of the clinical measures: daily alcohol consumption -0.18 (significant only -0.37), ADS -0.16 (significant only -0.27), AUDIT -0.22 (-0.39), OCDS -0.17 (-0.39), ODS -0.15 (-0.18), and CDS -0.17 (significant only -0.39). Although the majority of the Desikan-Killiany regions of interest demonstrated a significant negative correlation with the clinical severity measures, only a minority survived FWE multiple comparison correction. Daily alcohol consumption was significantly correlated with cortical thinning in the following regions: right caudal middle frontal gyrus (-0.39), left inferior parietal lobule (-0.35), right postcentral gyrus (-0.36), left rostral middle frontal gyrus (-0.33), left superior frontal gyrus (-0.34), right superior frontal gyrus (-0.36), left superior parietal lobule (-0.44), right superior parietal lobule (-0.37), left supramarginal gyrus (-0.33), right supramarginal gyrus (-0.42). ADS score was significantly correlated with cortical thinning in the following regions: right postcentral gyrus (-0.35), left superior parietal lobule (-0.36), and right supramarginal gyrus (-0.37). AUDIT score was significantly correlated with cortical thinning in the following regions: left inferior parietal lobule (-0.37), left paracentral lobule (-0.34), left pars opercularis (-0.36), left postcentral gyrus (-0.36), right postcentral gyrus (-0.50), left rostral middle frontal gyrus (-0.37), left superior frontal gyrus (-0.36), right superior frontal gyrus(-0.34), left superior parietal lobule (-0.47), right superior parietal lobule (-0.45), left superior temporal gyrus (-0.37), left supramarginal gyrus (-0.35), and right supramarginal gyrus (-0.42). OCDS, ODS subscale, and CDS subscale scores were significantly correlated with cortical thinning in the following regions (respectively): right postcentral gyrus (-0.42, -0.37, -0.43), left superior parietal lobule (-0.39, -0.36, -0.38), right superior parietal lobule

(-0.38, -0.35, -0.38), and right supramarginal gyrus (-0.37, -0.35, -0.37). Pearson correlation coefficients for each of the clinical severity scales and respective anatomical regions are listed in the parentheses.

4 Discussion

The aim of this study was to analyze changes in gray matter density, white matter density, and cortical thickness in detoxified recovering AUD patients during the first month of abstinence. This study also explored the respective clinical context of these findings using post-hoc correlation analyses between the structural results and several clinical and demographic variables. Our results generally supported our *a priori* hypotheses, with the exception of the lack of significance of the generally positive trend in longitudinal structural recovery in the AUD patients across most measures. The relevance of this study stems primarily from its longitudinal design with paired follow-up scans and homogeneous, strictly controlled clinical cohort. Findings of our study should be interpreted with caution due to its modest sample size and spatial resolution.

Our voxel-based morphometry (VBM) analysis has revealed wide-spread significant atrophy across both grey and white matter at both 9 and 29 days of abstinence, compared to the healthy controls. On average, the AUD patients exhibited 7.11% decrease in overall gray matter density, which improved to 4.68% deficit by the second time point (2.62% interscan increase). As summarized in Table 2.4, both the raw as well as nuisance-corrected differences yielded comparable results. The differences in the significant clusters have on average exhibited more pronounced structural deficits, with an average of over 10% at both time points. None of the four significant clusters at both first and second time-point comparison demonstrated distinct anatomical compartmentalisation and spanned multiple diverse brain regions. As a result, comparison of the peak or centre-of-gravity coordinates to other VBM studies would not be very meaningful. Nonetheless, the significant clusters (light blue) depicted on both Figure 2.1 and Figure 2.2 overlap with the results of Yang *et al*. meta-analysis (green colour in the figures). Our gray matter density results are, therefore, largely anatomically consistent with the published literature.

Similarly to the gray matter VBM analysis, the white matter analysis has also revealed significant wide-spread structural deficits which have improved from 7.19% at 9 days of abstinence to 4.39% deficit (3.01% interscan increase) overall. The raw and nuisance-corrected values were also comparable for the white matter analysis, as summarized in Table 2.7. Deficits in white matter density in significant only clusters also exceed 10% at both time points. Similarly to the gray matter results, the significant clusters of white matter VBM analysis were also anatomically diffuse and did not compartmentalize to any distinct anatomical region, limiting the insights which could be inferred by comparing the centre-of-gravity or peak coordinates to those in the published literature. The results of VBM analysis suggest that both gray and white matter were affected comparably in our study and overall structural atrophy at both time points was not dominated by white matter changes.

Contrary to our expectations, we have failed to observe a significant improvement in the AUD VBM following the three-week interscan period of supervised abstinence. The overwhelmingly red t-maps (i.e. positive trend) depicted in Figure 2.3, nonetheless suggest an underlying wide-spread structural improvement across both gray as well as white matter. Contrasting Figure 2.2 (second time point) to Figure 2.1 (first time point) also alludes to this underlying trend. The anatomical extent of the significant clusters at the second time point has become noticeably smaller (the retreating trend is apparent especially in the frontal lobes). The positive trend associated with longer abstinence was also observed in the weakly positive correlation between structural density of both gray and white matter and the length of abstinence at the first time point (baseline range of 6 to 12 days). This post-hoc correlation has, however, also failed to reach statistical significance after multiple-comparison correction.

Although AUD-related structural brain atrophy has been documented quite widely in the literature, with voxel-based morphometry being one of the most common analysis techniques, there is still a scarcity of multiple time point studies characterizing the structural trends during both short-term and long-term AUD

recovery. To the best of our knowledge, there are less than 40 anatomical AUD studies (including both CT and MRI/DTI) examining data from multiple time points, including cross-sectional, mixed, and longitudinal designs which have been published in English scientific journals from 1978 to 2020 (with notable full or partial neuroimaging dataset overlap in multiple studies). Out of these, only a small minority (less than a fifth) have reported quantitative results which could be directly compared to our study (ROI volume or VBM density for overall gray or white matter) and only two studies focused on VBM (Demirakca *et al.* and Bach *et al.*). The clinical profile of the participants in these studies was also quite heterogeneous, with an average abstinence range of 0 to 29 days at first time point (which spans the entire duration of our longitudinal study) and 14 to 1,921 days at second time point (and 91 to 226 days at third time point) and inconsistent exclusion criteria for confounding comorbidities such as history of polysubstance use or other concurrent psychiatric conditions (Agartz et al., 2003; P. Bach et al., 2020; Durazzo et al., 2015; Durazzo et al., 2011; Mon et al., 2013; Pfefferbaum et al., 1995; Shear, Jernigan, & Butters, 1994; van Eijk et al., 2013).

Although some studies have reported structural improvement within as little as two weeks of abstinence (day zero to two of abstinence and two weeks later for example (Agartz et al., 2003; van Eijk et al., 2013)), other studies with much long longer comparison ranges (months to even years) have failed to report substantially greater magnitude of structural recovery. The average differences in AUD cohorts from the second to first time point for all of gray matter ranged from +0.47% to +0.97% and for all white matter from -0.27% to +11.26% (but most falling to similar low range as the gray matter, except for two outlying studies). These differences should be considered in the context of baseline whole-brain gray matter contrast of -6.99% to -1.38% between AUD and healthy control groups at first time point and -6.21% to -3.29% at second time point and -2.95% to -0.94% and -0.79% to -0.53% for first and second time point white matter contrasts. Note that some of these values were not tested for significance in the original publications and sometimes had to be extrapolated from figures, since the publications usually quantify only the changes in the significant clusters or specific regions of interest, which by definition

exhibited more pronounced differences but might not be readily compared between studies due to their anatomical heterogeneity. The inconsistency and relatively small overall differences in the literature suggest that even though there is an underlying trend of widespread structural recovery with sustained abstinence, the effect size is likely quite weak and might be difficult to consistently characterize across different samples, especially in smaller or more heterogeneous studies. The strict clinical homogeneity and consistent longitudinal design of our study are, therefore, very relevant in the broader context of the existing literature.

Adoption of higher field strength MRI scanners, such as the 4.7 Tesla scanner used in this study, has enabled increased resolution as well as tissue contrast without excessively prolonging the total scanning time. This has in turn enabled use of surface-based morphometry (SBM) techniques such as cortical thickness analysis to complement the more commonly used VBM. Cortical thickness might offer greater sensitivity to characterize neurodegenerative processes of various pathologies as well as normal aging (Hutton et al., 2009). Although cortical thickness is closely related to both volume and tissue density measures, it may serve as a better proxy for cortical cytoarchitectural integrity (Durazzo, Nguyen, & Meyerhoff, 2020). Cortical thickness might be the most relevant of the commonly used SBM measures, since other measures such as gyrification indices or total surface area might be determined predominantly by genetics or early childhood development (Kühn et al., 2016), and thus should not be substantially impacted by chronic alcohol abuse in adulthood (Im et al., 2016).

Our SBM analysis has revealed wide-spread cortical thinning in the AUD patients at both 9 and 29 days of abstinence. The longitudinal interscan improvement has been, however, only marginal and failed to reach significance. The average whole-brain cortical thickness exhibited only negligible interscan increase of 0.03% from a baseline deficit of 2.88% to a 2.85% deficit at the second time point. The cortical thinning in the AUD cohort was significant across almost all of the Desikan-Killiany atlas regions for both time points, ranging from -6.65% to -2.47% at baseline and -5.69% to -2.16% at the second time

point (Table 2.8 and Table 2.9). The longitudinal interscan changes were not significant across any of the Desikan-Killiany atlas regions and ranged from -0.68% to +1.04% in the atlas regions (with about a third of the regions exhibiting negligibly negative change).

As illustrated by Figure 2.4 and Figure 2.5, anatomical regions associated with the most significant AUD-related cortical thinning included postcentral gyrus, superior parietal lobule, superior frontal gyrus, multiple regions in the temporal lobe, and other smaller areas throughout parietal, occipital and frontal lobes. Although some studies, such as Fortier *et al.* (2011) have interpreted similar results by claiming that AUD might be associated with anatomically selective structural atrophy (affecting primarily the frontal cortex), our results, especially in the context of the broader t-maps, suggest a more diffuse pattern of wide-spread structural damage, which has been also replicated in recent pooled multi-database analysis such as Mackey *et al* (2019). Comparing Figure 2.5 to Figure 2.4 further outlines the positive trend between cortical thickness and sustained abstinence as documented by the reduced anatomical extent of the significant clusters after the three weeks of sustained abstinence. Figure 2.6 also depicts an overall weakly positive trend by widespread warm colour shades on the interscan t-map. The most positive trend in the longitudinal cortical thickness recovery (orange in Figure 2.6) was observed in the medial paracentral lobule, cuneus and lingual gyri, medial orbito-frontal gyrus, parts of the middle and inferior frontal gyri, and some other more diffuse regions. Post-hoc exploratory analysis has also revealed a weak negative trend between cortical thickness and clinical severity scores, although these were in general weaker and fewer survived statistical correction compared to the VBM results.

To the best of our knowledge, the scientific literature discussing cortical thickness changes in AUD remains quite sparse. There have been only six single time point AUD cortical thickness studies (including one multi database mega-analysis) (S. Bae et al., 2016; Durazzo et al., 2011; Im et al., 2016; Mackey et al., 2019; Momenan et al., 2012; Tomasi et al., 2019), one cross sectional study (Fortier et al., 2011), and two longitudinal studies (P. Bach et al., 2020; G. Y. Wang et al., 2016) published to this date.

The length of abstinence reported in these studies ranged from the first day of detoxification to 26 years and included 19 to 885 AUD patients per cohort. Overall, the literature supports wide-spread and persistent cortical thinning in the AUD groups compared to the healthy controls. At baseline, the magnitude of cortical thinning ranged from 3.23% to 8.18% for the overall brain, while longitudinal interscan recovery was less than 2%. Compared to the results of our study, magnitudes of both baseline deficits as well as subsequent recovery were greater, even though our study has shared a similar abstinence period spanning the clinical window between both of the longitudinal studies.

For the single time point studies, Tomasi *et al.* reported 4.4% cortical thinning at 3.8 days of abstinence in the AUD group compared to the healthy controls. Durazzo *et al.* reported 4.21% decrease in overall cortical thickness (region-specific changes from -5.88% to increase of 0.80%, also reporting association between more severe structural atrophy and worse clinical outcomes) at 7 days of abstinence. Bae *et al.* described 8.18% decrease after 2 weeks of detoxification. Momenan *et al.* reported a 14.09% decrease in specific significant clusters in AUD patients with complex comorbidities who were abstinent at least 23 days. Im *et al* revealed a 3.23% deficit at 13.2 months of abstinence. Mackey *et al.* multi-dataset mega-analysis reported wide-spread structural atrophy in both cortical thickness as well as region-specific volumes spanning most brain regions but only with small magnitude. The magnitude of the overall cortical thinning in the published AUD cohorts does not seem to show a strong positive or negative trend when considered in the context of the average length of abstinence of the cohorts (4.4%, 4.21%, 8.18%, 3.23% at 3.8 days, 7 days, 14+days, 13.2 months, respectively).

Cross-sectional study by Fortier *et al*. has reported average cortical thinning of 4% across the entire cortex (region-specific differences of 4-11%) for a range of abstinence from one month to 26 years (average abstinence of 5.6 years). The limited sample size (31 patients) over such a broad range of abstinence, inherent survivor bias in the design, and lack of data for the early recovery period (within the first month) constrain our ability to relate these findings to our study. Nonetheless, Fortier *et al.* reported

an important observation, suggesting that the relationship between length of abstinence and cortical thickness might be second-order quadratic rather than linear (peaking at about 2 years and declining after 8 years of abstinence). Other studies have also reported non-linear pattern of structural recovery, but observed the most rapid recovery at earlier stages of sustained abstinence with taper in long-term abstinence (Durazzo et al., 2015; Gazdzinski et al., 2005; Pfefferbaum et al., 1995; Y. Zou et al., 2017). It was even suggested that structural recovery might occur up to six times faster (and up to 50% of the total recovery) during the first 3 weeks than during the subsequent year (Charlet et al., 2018; Gazdzinski et al., 2005). Because our study examined a relatively narrow abstinence range during the early recovery period and we did not observe unusual residual distribution, using a general linear model in our analysis should still be acceptable but future studies examining structural recovery over extended abstinence ranges should be cautious.

Longitudinal study by Wang *et al*. compared cortical thickness at the first day of abstinence to 14 days of abstinence with an average baseline deficit in cortical thickness of 6.7% (12.45% in significant only cluster) and reported only a marginal interscan improvement of 0.028% to 1.97% compared to the baseline levels, similar to our negligible three-week interscan improvement. Wang *et al* also reported substantial decline in the anatomical extent of the clusters of significantly lower cortical thickness when contrasting baseline and follow-up contrasts between AUD and healthy controls, noting a similar underlying positive trend as observed in our study. The second longitudinal study of Bach *et al* compared cortical thickness differences at 12 days and 27 days of abstinence. The comparison revealed persistent deficits in both tissue density as well as cortical thickness at both baseline and follow-up scans (similar to our study). The AUD cohort has exhibited a 1.00% (-1.85% to 7.69%) increase in VBM grey matter density and similar small increase in cortical thickness (overall increase was not reported, but greatest increase was observed in right insula and superior frontal gyrus cluster of 1.1% and left insula cluster of 0.8%). Our study had 3.8 to 4.8 times fewer AUD patients and 1.7 to 6.2 times fewer controls than the two longitudinal studies. It is, therefore, possible that any unrepresentative individual data could result in

skewing our results, thus further constraining our ability to detect weak group effects, such as the interscan changes in cortical thickness, which even the larger studies had difficulty characterizing.

It is not clear why our study failed to observe higher baseline atrophy, which would be more comparable to the published literature on our *a priori* hypotheses. Compared to the literature in general, our study has implemented a more consistent longitudinal design with stricter recruitment criteria and thus a more homogeneous sample. Moreover, compared to the two other longitudinal cortical thickness studies, our study included clinical cohort with greater AUD severity who self-reported on average 75% and 88% more daily alcohol consumption prior to detoxification (as steady chronic drinkers) while our controls self-reported consuming on average 61% and 86% less alcohol than the controls in the other studies. This should have translated to an enhanced rather than reduced alcohol-related baseline contrast between the groups. On average, our AUD group was also 12% and 13% younger than the other AUD cohorts, which should have translated to an increased recovery potential and thus potentially larger interscan differences. Other factors such as underlying genetic, cultural, or treatment differences (our study collected data from north-western Canada while the other two studies collected data from south-western Germany) or potentially publication bias against non-significant findings could also help explain the disparity between our results and the existing literature.

When interpreting our findings, it is also important to remember the sensitivity limitations of the underlying analysis. Whole-brain high resolution structural scans have most commonly $1.0\times1.0\times1.0$ mm^3 or $1.0\times1.0\times1.5$ mm^3 resolution. Even though the resolution is artificially upsampled by linear interpolation to 0.5 mm isotropic voxels during the SBM analysis, this does not eliminate the original resolution limitations. Most anatomical regions will have cortical thickness spanning only 2-4 voxels (about 2.5 mm). Detecting a change in a single voxel would thus require 25-50% difference in the thickness. In other words, a 5% change in cortical thickness (which is within the published results range) would represent a difference of only about $1/10^{th}$ of the voxel in the source data. This might not be a very

large effect in comparison to imaging artifacts or normal interscan variability at such resolution (due to different head orientation or differently sampled field of view and thus different partial volume distribution). Smoothing, group averaging across many participants, and stringent multiple-comparison correction of the results should largely neutralize such errors. Nonetheless, extrapolating biological meaning to very small changes in cortical thickness (especially in very specific anatomical sub-regions spanning only a few mm^3) should be done with more caution than frequently practiced in the literature.

To more conclusively characterize patterns of early structural changes during recovery from AUD, future studies should consider increasing the resolution of their structural scans, increasing their sample size, and potentially lengthening their interscan interval in order to better capture the underlying wide-spread but small effect. Increasing tissue contrast and precision of tissue segmentation during pre-processing through scanning sequence optimisation or multimodal data acquisition could also help minimize interscan variability. Minimizing natural variability within the study cohorts by implementing a longitudinal instead of cross-sectional design and restricting recruitment parameters such as age, handedness, or clinical comorbidities such as smoking or polysubstance abuse could also help decrease intra-group variability. Future studies including these design parameter suggestions should help improve our understanding of underlying processes occurring during AUD recovery. However, they will also further exacerbate limitations of our study, such as poor translatability of our findings to the broader clinical population. Treatment-seeking individuals include both sexes, often engage in poly-substance abuse, have other concurrent psychiatric and somatic comorbidities, and might exhibit a more diverse AUD clinical profile. We had to exclude over 85 treatment-seeking AUD patients for every 1 patient included in the final analysis. All future studies should, nonetheless, strive for greater transparency and intercomparability. Publishing more thorough characterisation of the clinical participants (disclosing the baseline length of abstinence, clinical pattern and severity of AUD, etc.) as well as quantifying their findings (disclosing raw and nuisance-corrected structural measures in addition to figures or summary of cluster statistical parameters) would help readers better contextualize future findings compared to the existing literature.

5 Conclusion

In conclusion, our voxel and surface-based morphometry analyses have successfully documented wide-spread structural atrophy in recovering AUD patients during the first month of sustained abstinence. The AUD patients exhibited high single digit and mid single digit whole-brain grey matter and white matter density reduction at first and second time point (9 and 29 days of abstinence), respectively. Longitudinal changes during the interscan period of supervised abstinence were associated with an underlying positive trend but did not reach statistical significance. Concurrently, the AUD patients exhibited low single digit cortical thinning, which changed only marginally during the three week interscan period. Although our study did not have sufficient sample size and resolution to conclusive characterize the early longitudinal structural recovery and did not observe as large differences as reported in the literature, it has made a relevant contribution to a sparsely documented field as only the third longitudinal AUD surface-based morphometry study and the first based on a North American clinical cohort. Our study also remains one of only very few multiple time point AUD neuroimaging studies which have analyzed structural recovery during the early AUD recovery based on a homogeneous clinical sample without polysubstance abuse or other clinical comorbidities with a consistent AUD clinical profile and supervised interscan abstinence period.

Figure 2.1: AUD-associated decreased tissue density at first time point (9 days)

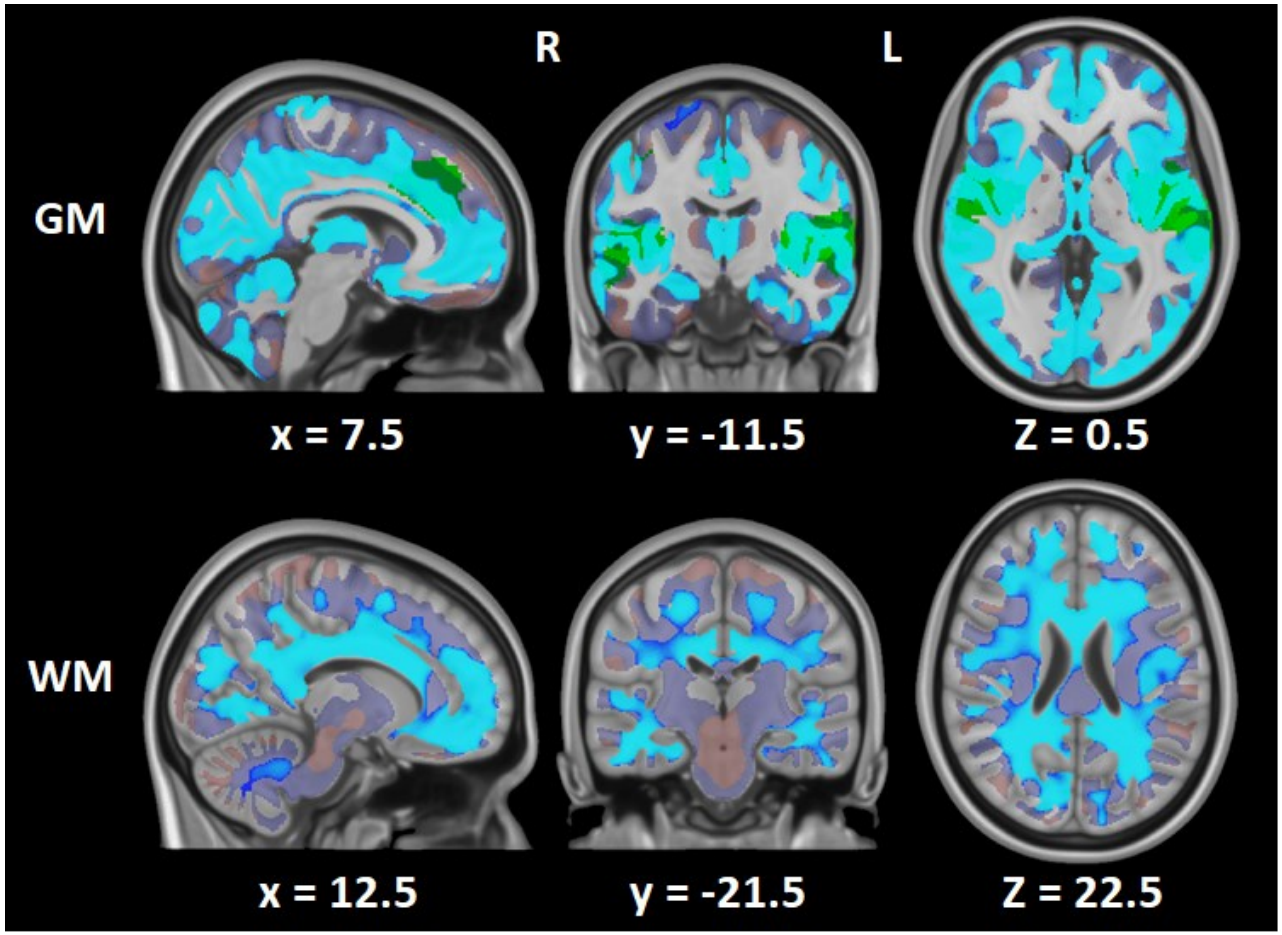

Top row indicates gray matter (GM) differences. Bottom row indicates white matter (WM) differences. Dark blue and dark red depict t-maps (positive = red, negative = blue). Bright azure clusters depict significantly decreased tissue density (FWE corrected). Green clusters indicate anticipated gray matter deficits (Yang *et al*. 2016). Coordinates are in MNI space. There is a wide-spread significant AUD-related decrease in GM and WM density at first time point.

Figure 2.2: AUD-associated decreased tissue density at second time point (29 days)

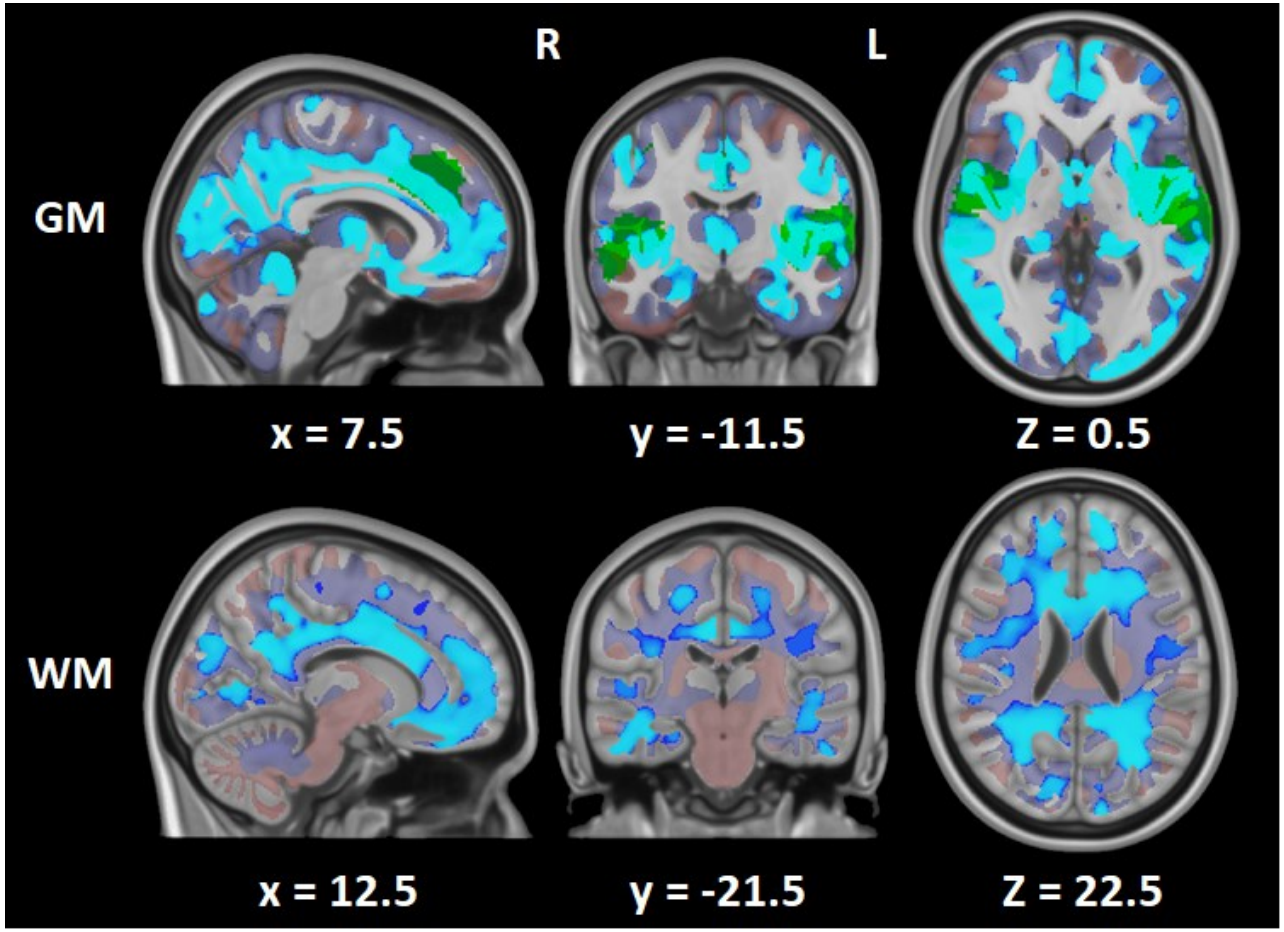

Top row indicates gray matter (GM) differences. Bottom row indicates white matter (WM) differences. Dark blue and dark red depict t-maps (positive = red, negative = blue). Bright azure clusters depict significantly decreased tissue density (FWE corrected). Green clusters indicate anticipated gray matter deficits (Yang *et al*. 2016). Coordinates are in MNI space. There is a wide-spread significant AUD-related decrease in GM and WM density at second time point, although at a lesser extent compared to the first time point.

Figure 2.3: Inter-scan differences in the AUD patients (9 to 29 days of abstinence)

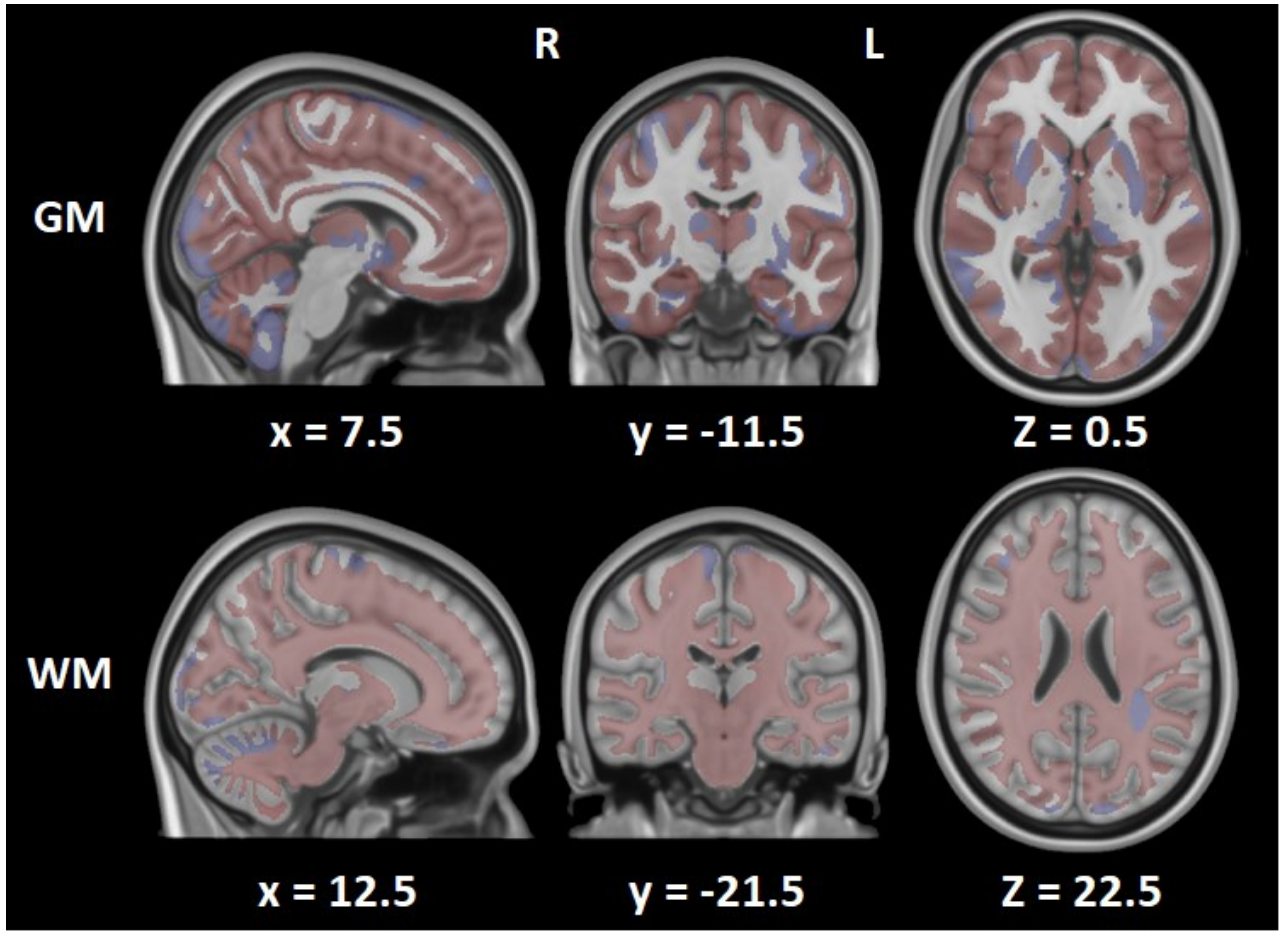

Top row indicates gray matter (GM) differences. Bottom row indicates white matter (WM) differences. Dark blue and dark red depict t-maps (positive = red, negative = blue). Coordinates are in MNI space. There was an overall positive longitudinal trend in increased GM and WM density in AUD patients with increased abstinence, but none of the changes survived FWE multiple comparison correction.

Figure 2.4: AUD-associated cortical thinning at first time point (9 days)

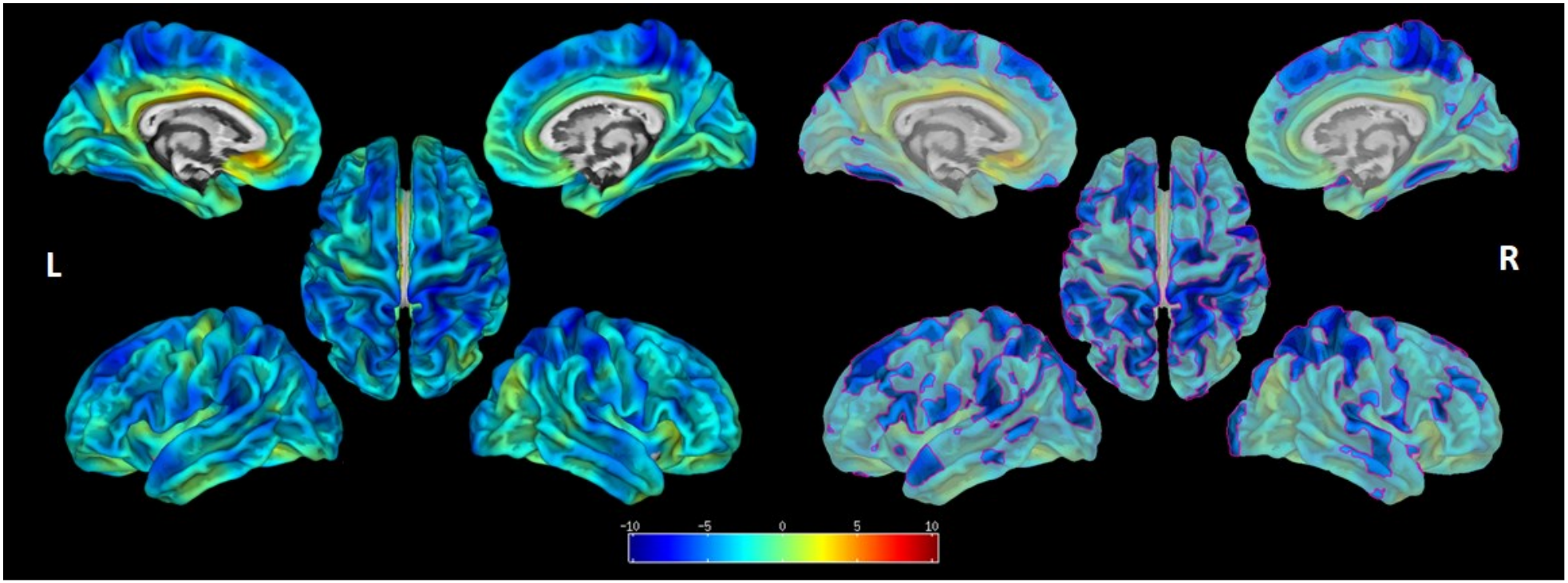

The five maps on the left depict t-map of cortical thickness difference between AUD patients and healthy controls at 9 days of abstinence. The five maps on the right outline in pink and saturated colour significant clusters at 0.05 α (FWE corrected).

Figure 2.5: AUD-associated cortical thinning at second time point (29 days)

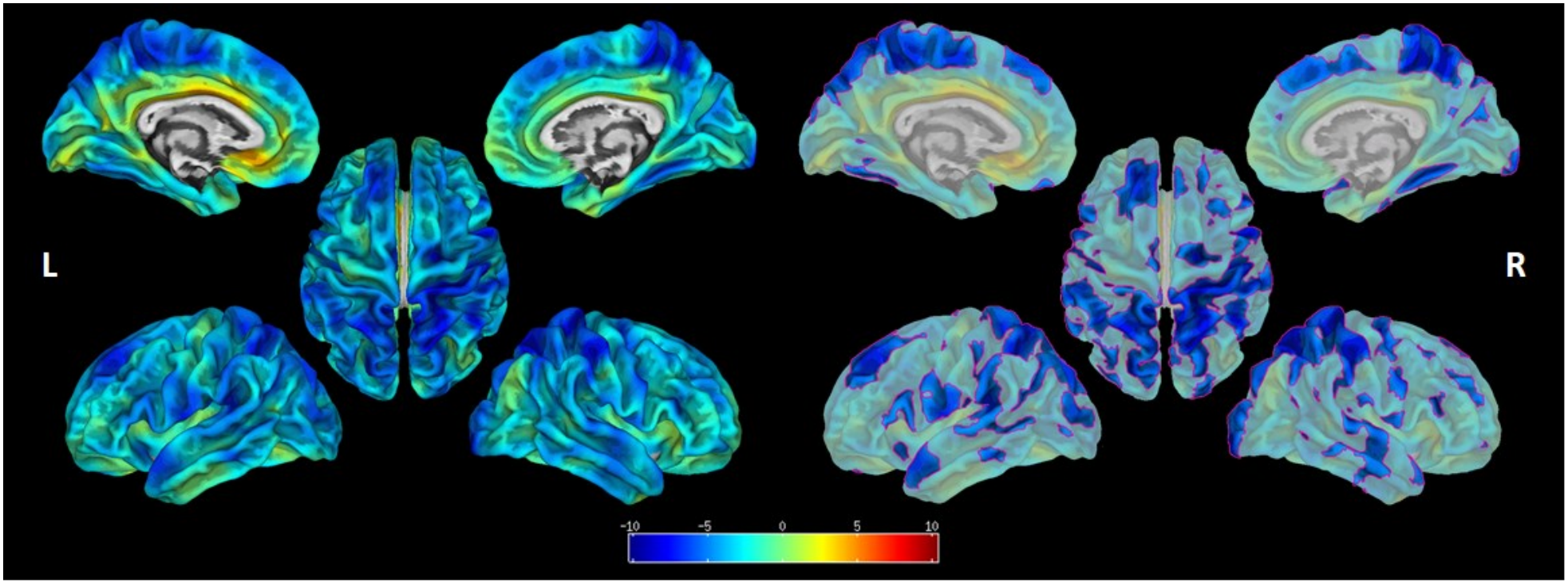

The five maps on the left depict t-map of cortical thickness difference between AUD patients and healthy controls at 29 days of abstinence. The five maps on the right outline in pink and saturated colour significant clusters at 0.05 α (FWE corrected).

Figure 2.6: Inter-scan differences in the AUD patients (9 to 29 days of abstinence)

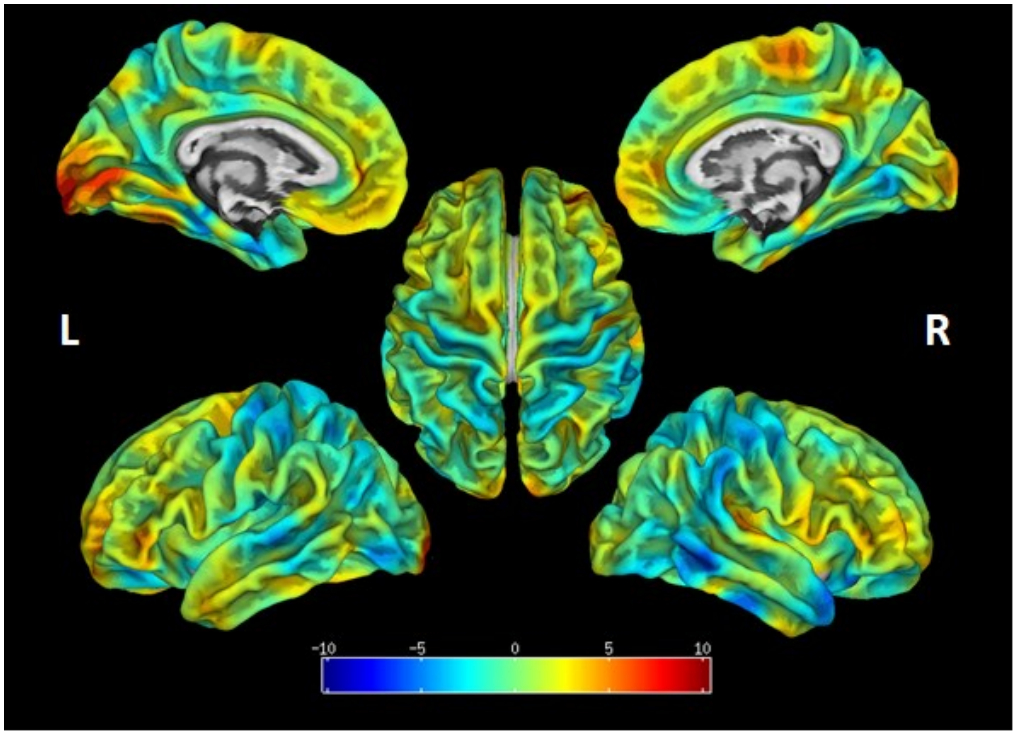

The five maps on the left depict t-map of cortical thickness difference between AUD patients at 9 days and 29 days of abstinence. Despite of the positive trend, none of the differences reached significance after multiple comparison correction.

Table 2.8: Cortical Thickness Differences in the Left Hemisphere during the First Month of AUD Recovery

		AUD 1		AUD 2		CTL		AUD 1 vs CTL		AUD 2 vs CTL		AUD 2 vs AUD1	
Left Hemisphere	**Lobe**	**$\bar{x}$**	**σ**	**$\bar{x}$**	**σ**	**$\bar{x}$**	**σ**	**% Δ**	**p-value**	**% Δ**	**p-value**	**% Δ**	**p-value**
Superior Parietal	parietal	2.29	0.10	2.29	0.10	2.40	0.12	-4.57	0.0000	-4.50	0.0000	0.07	not sig
Superior Temporal	temporal	2.89	0.11	2.89	0.13	3.02	0.17	-4.46	0.0000	-4.45	0.0000	0.00	not sig
Supramarginal	parietal	2.65	0.12	2.66	0.10	2.76	0.14	-4.05	0.0000	-3.91	0.0000	0.15	not sig
Paracentral	frontal	2.32	0.18	2.34	0.15	2.47	0.16	-5.91	0.0000	-5.38	0.0000	0.57	not sig
Pars Opercularis	frontal	2.82	0.11	2.83	0.11	2.94	0.13	-3.83	0.0000	-3.56	0.0000	0.28	not sig
Postcentral	parietal	2.18	0.12	2.19	0.11	2.28	0.13	-4.60	0.0000	-4.18	0.0000	0.44	not sig
Superior Frontal	frontal	2.86	0.13	2.87	0.13	2.98	0.13	-3.93	0.0000	-3.71	0.0000	0.23	not sig
Inferior Parietal	parietal	2.59	0.12	2.59	0.10	2.68	0.12	-3.38	0.0000	-3.54	0.0000	-0.16	not sig
Rostral Middle Frontal	frontal	2.61	0.10	2.62	0.09	2.70	0.10	-3.13	0.0000	-2.70	0.0001	0.45	not sig
Transverse Temporal	temporal	2.43	0.21	2.43	0.24	2.57	0.22	-5.52	0.0002	-5.33	0.0004	0.20	not sig
Middle Temporal	temporal	3.01	0.17	3.01	0.16	3.12	0.19	-3.49	0.0006	-3.39	0.0010	0.10	not sig
Precentral	frontal	2.51	0.15	2.52	0.14	2.61	0.19	-3.80	0.0004	-3.59	0.0013	0.22	not sig
Precuneus	parietal	2.49	0.13	2.48	0.11	2.56	0.13	-2.95	0.0012	-3.12	0.0005	-0.17	not sig
Lingual	occipital	2.11	0.11	2.12	0.11	2.18	0.11	-2.98	0.0002	-2.65	0.0019	0.35	not sig
Pars Triangularis	frontal	2.69	0.15	2.70	0.14	2.78	0.13	-3.29	0.0002	-2.86	0.0030	0.45	not sig
Lateral Occipital	occipital	2.21	0.12	2.22	0.11	2.28	0.11	-3.12	0.0006	-2.83	0.0029	0.29	not sig
Fusiform	temporal	2.71	0.15	2.70	0.12	2.79	0.15	-2.92	0.0032	-3.18	0.0008	-0.26	not sig
Banks of Superior Temporal Sulcus	temporal	2.56	0.16	2.54	0.12	2.64	0.16	-3.00	0.0056	-3.67	0.0002	-0.69	not sig
Inferior Temporal	temporal	2.78	0.13	2.78	0.12	2.85	0.16	-2.53	0.0126	-2.55	0.0113	-0.03	not sig
Caudal Middle Frontal	frontal	2.72	0.13	2.73	0.12	2.79	0.15	-2.47	0.0228	-2.16	not sig	0.32	not sig

Table 2.9: Cortical Thickness Differences in the Right Hemisphere during the First Month of AUD Recovery

		AUD 1		AUD 2		CTL		AUD 1 vs CTL		AUD 2 vs CTL		AUD 2 vs AUD1	
Right Hemisphere	**Lobe**	**$\bar{x}$**	**σ**	**$\bar{x}$**	**σ**	**$\bar{x}$**	**σ**	**% Δ**	**p-value**	**% Δ**	**p-value**	**% Δ**	**p-value**
Postcentral	parietal	2.12	0.11	2.14	0.12	2.27	0.14	-6.59	-	-5.69	0.0000	0.96	not sig
Superior Parietal	parietal	2.27	0.10	2.27	0.10	2.38	0.11	-4.69	0.0000	-4.76	0.0000	-0.08	not sig
Supramarginal	parietal	2.61	0.09	2.62	0.10	2.73	0.12	-4.14	0.0000	-3.99	0.0000	0.16	not sig
Superior Temporal	temporal	2.93	0.14	2.92	0.15	3.05	0.18	-4.18	0.0000	-4.30	0.0000	-0.12	not sig
Middle Temporal	temporal	2.96	0.14	2.95	0.14	3.08	0.17	-3.84	0.0000	-4.20	0.0000	-0.37	not sig
Superior Frontal	frontal	2.90	0.15	2.91	0.14	3.01	0.13	-3.67	0.0000	-3.55	0.0000	0.13	not sig
Precentral	frontal	2.40	0.16	2.42	0.16	2.54	0.19	-5.34	0.0000	-4.76	0.0000	0.61	not sig
Caudal Middle Frontal	frontal	2.72	0.13	2.73	0.13	2.83	0.14	-3.72	0.0000	-3.56	0.0000	0.16	not sig
Paracentral	frontal	2.35	0.15	2.37	0.14	2.48	0.17	-5.31	0.0000	-4.50	0.0000	0.86	not sig
Precuneus	parietal	2.55	0.12	2.54	0.11	2.64	0.14	-3.41	0.0000	-3.51	0.0000	-0.10	not sig
Inferior Parietal	parietal	2.58	0.11	2.57	0.09	2.66	0.12	-3.08	0.0000	-3.18	0.0000	-0.10	not sig
Inferior Temporal	temporal	2.69	0.13	2.67	0.14	2.79	0.16	-3.59	0.0001	-4.21	0.0000	-0.64	not sig
Fusiform	temporal	2.69	0.16	2.67	0.15	2.79	0.17	-3.67	0.0004	-4.33	0.0000	-0.68	not sig
Transverse Temporal	temporal	2.40	0.24	2.42	0.25	2.57	0.22	-6.65	0.0000	-5.68	0.0005	1.04	not sig
Lateral Occipital	occipital	2.20	0.11	2.20	0.11	2.28	0.15	-3.71	0.0001	-3.50	0.0004	0.22	not sig
Rostral Middle Frontal	frontal	2.60	0.14	2.61	0.13	2.69	0.12	-3.41	0.0001	-2.90	0.0021	0.53	not sig
Lingual	occipital	2.13	0.13	2.14	0.13	2.21	0.14	-3.42	0.0007	-3.30	0.0016	0.13	not sig
Pars Opercularis	frontal	2.81	0.14	2.83	0.15	2.89	0.15	-3.03	0.0013	-2.28	not sig	0.78	not sig
Parahippocampal	temporal	2.58	0.20	2.58	0.19	2.70	0.24	-4.14	0.0061	-4.31	0.0036	-0.18	not sig
Cuneus	occipital	2.04	0.14	2.03	0.13	2.10	0.13	-2.98	0.0306	-3.29	0.0079	-0.33	not sig
Pars Triangularis	frontal	2.73	0.14	2.75	0.13	2.81	0.15	-2.87	0.0029	-2.29	0.0495	0.60	not sig
Frontal Pole	frontal	2.76	0.21	2.81	0.21	2.86	0.23	-3.55	0.0354	-2.00	not sig	1.60	not sig
Pars Orbitalis	frontal	2.89	0.16	2.89	0.19	2.98	0.21	-2.93	0.0499	-3.14	0.0257	-0.22	not sig

Chapter 3 - Region-Based Morphometry of Structural Brain Changes during First Month of Recovery from Alcohol Use Disorder

Abstract

Alcohol use disorder (AUD) is associated with widespread structural brain damage. A growing body of evidence suggests that structural atrophy as well as associated functional deficits are at least partially reversible during AUD recovery and sustained abstinence. Only a few structural studies have documented longitudinal changes in non-cortical brain regions with sustained abstinence to this date. This study performed region-based morphometry analysis of longitudinal changes in 57 male AUD patients undergoing supervised treatment at 16 and 34 days of abstinence compared to 52 matched healthy controls, measuring changes in volume of basal ganglia, hippocampal subfields, and cerebellar lobules. Our results indicate a broad single digit percentage volume decrease across most of the examined structures/compartments (except cerebrospinal fluid and ventricles which exhibited double digit increases) in AUD patients compared to the healthy controls. The most significant differences were observed in the hippocampal subfields while no significant changes were observed in the cerebellar lobules. The magnitude of structural deficits was positively correlated with AUD clinical severity scales, especially AUDIT score. The highest correlations were observed in the regions which demonstrated the most substantial deficits compared to the healthy controls. Even though there was an overall positive recovery trend with the sustained abstinence, none of the differences were significant after correction for multiple comparisons. Because of mixed evidence of structural recovery during early abstinence in AUD in our study, which is echoed by the few prior studies indicates the need for further detailed studies of these relatively short-term abstinence effects.

Key terms

alcohol use disorder; abstinence; hippocampus; cerebellum; basal ganglia

1. Introduction

Harmful use of alcohol is a leading preventable cause of death (5.9% of all deaths), disease (causal link to over 200 diseases and injuries), and disability (5.1% of global burden of disease, responsible for loss of 139 million disability-adjusted life years) worldwide (World Health Organization, 2018). Alcohol use disorder (formerly also classified as alcohol dependence, alcohol addiction, or alcoholism) is a mental disorder characterized by chronic, recurrent alcohol abuse (American Psychiatric Association & American Psychiatric Association, 2013). The prevalence of alcohol use disorder (AUD) is estimated at 5.1% (2.6% dependence) worldwide and 8.0% (4.1% dependence) in Canada in the general population over the age of fifteen (World Health Organization, 2018). Globally, approximately 237 million men and 46 million women currently suffer from AUD. According to some estimates, alcohol might be the most harmful drug in our society, especially when considering all of its indirect harm (Nutt et al., 2010). The total financial cost of AUD is difficult to estimate. In Canada alone, the most recent comprehensive study estimated the total cost of alcohol harm at $14.6 billion per year or 38.1% of all substance abuse costs (Canadian Substance Use Costs and Harms Scientific Working Group, 2018). In addition to the substantial economic burden, alcohol use disorder leads to immeasurable human suffering. AUD is a chronic, recurrent condition. AUD patients have only limited treatment options with many patients experiencing relapse within the first year (R. H. Moos & Moos, 2006; Walitzer & Dearing, 2006; Witkiewitz, 2011). Individual suffering is usually compounded in communities by the multi-generational nature of AUD, which is estimated to have 40% to 60% heritability (Agrawal et al. 2008). Even though AUD is a significant, widespread, and costly health problem with a long pervasive history and well-recognized clinical symptoms, both the exact mechanism of action of alcohol on the brain as well as the mechanism of recovery during prolonged abstinence remain unclear (Sutherland et al., 2014b; Zahr & Pfefferbaum, 2017).

Since 1897 (Marchiafava, 1933), an association of chronic alcohol abuse with progressive, widespread brain atrophy and enlargement of the pericerebral space has been systematically documented. Earliest pathological case reports and post-mortem histological observations were gradually complemented with clinical studies in living patients using pneumoencephalography since the 1950s, computed tomography (CT) in the 1970s, and magnetic resonance imaging (MRI) since the late 1980s, with progressively greater resolution. The literature has also refined its focus from complex neurological patients with a history of chronic alcohol abuse (which might today be associated with hepatic encephalopathy or nutritional deficiencies such as that leading to the Wernicke-Korsakoff Syndrome) to include "uncomplicated" contemporary AUD diagnosis patients and recovering AUD patients at various times of abstinence.

Human neuropathological studies have revealed significant brain tissue loss with widespread demyelination, loss of glial cells, dendritic thinning, and region-specific loss and shrinkage of neurons (Harper et al., 2003). Post-mortem regional neuronal loss even in an "uncomplicated" AUD brain can reach up to 27% on average, especially in the frontal cortex. Glial cells may respond to toxic effects of alcohol even more than neurons and exhibit up to 37% loss in regions such as the hippocampus (Korbo, 1999; Miguel-Hidalgo et al., 2002). The extent of cellular damage in several regions is correlated with severity of alcohol abuse, including lifetime amount of alcohol consumption (Harding et al., 1996).

Clinical neuroimaging studies have corroborated histological evidence by documenting global brain atrophy and ventricular enlargement as well as region-specific structural deficits in the frontal lobes, thalamus, mammillary bodies, basal ganglia (caudate nucleus, putamen, amygdala, nucleus accumbens), insula, temporal lobes (including hippocampus), brainstem and the cerebellum in living AUD patients (Fritz et al., 2019). Structural damage and subsequent recovery may also correlate with clinical severity, risk of relapse, and cognitive function (M. J. Rosenbloom et al., 2007; Sullivan, Rosenbloom, Lim, & Pfefferbaum, 2000). Two voxel-based morphometry meta-analyses on structural changes in AUD have

been published to this date (Xiao et al., 2015; Yang et al., 2016), summarizing findings of 9 and 12 different studies, respectively, with 5 overlapping studies (and less homogeneous inclusion criteria used by Yang *et al.*). The meta-analyses reported a consistent decrease in the grey matter density in the prefrontal cortex (especially anterior cingulate cortex), posterior cingulate cortex, and dorsal striatum / insula in AUD patients, compared to matched healthy volunteers.

Longitudinal neuroimaging studies have demonstrated potential for at least partial recovery of AUD structural damage with abstinence, including decreased volumes of enlarged ventricles and increased volumes in anterior cingulate cortex, temporal lobe (including hippocampus), insula, amygdala, brainstem, and cerebellar cortex (Bartsch et al., 2007; Cardenas et al., 2007; Demirakca et al., 2011; Gazdzinski et al., 2005; Kühn et al., 2014; Pfefferbaum et al., 1995; van Eijk et al., 2013). From 1978 until 2019, approximately 35 cross-sectional and longitudinal structural neuroimaging studies have been published in English peer-reviewed academic publications. Some evidence of recovery was observed as early as within the first two weeks of abstinence with a more rapid recovery in the early weeks of sustained abstinence. Nonetheless, global structural damage persisted even in the long-term abstinent AUD subjects who have remained abstinent for years and might not be reversible (Harper, 2007; Zahr & Pfefferbaum, 2017).

Results of preclinical AUD models indicate that structural brain damage may follow repeated acute intoxication (increased oxidative stress, toxic acetaldehyde and aldehydic metabolites, inflammation, chronic glutamate / calcium excitotoxicity, decreased pro-survival factors such as BDNF, decreased neurogenesis) and that subsequent structural regeneration may be associated with rapid repair and neuro- and glio-genesis, occurring primarily within the first month of abstinence (Crews & Nixon, 2009). Mechanisms of structural brain damage and subsequent recovery in humans, however, are not fully understood (Zahr & Pfefferbaum, 2017). Preclinical findings are difficult to translate well into this

clinical domain, partly because the synthesis of existing clinical neuroimaging evidence on structural damage and longitudinal AUD recovery during sustained abstinence remains quite challenging.

Clinical studies reported to date have numerous challenges. These include: inconsistent results; numerous methodological differences (e.g. different severity of AUD, different length /range of abstinence, inclusion of patients with concurrent substance abuse and/or other psychiatric and somatic comorbidities), and recurrent limitations (small sample size, inconsistent multiple comparison correction, high dropout rate without follow-up, group mismatch on non-AUD clinical severity status etc.). Moreover, many contemporary structural AUD studies used automated whole-brain voxel-based morphometry analyses, which rely on inherently limited anatomical resolution due to extensive smoothing and complex tissue segmentation boundaries in deep brain structures. This has created a gap in the literature between early low-resolution region-of-interest gross anatomical studies and modern high-resolution voxel-based morphometry neuroimaging studies. Our study aimed to address this gap and examine longitudinal structural changes in a very homogeneous clinical AUD sample within the first month of abstinence using a best-in-class region-based morphometry analysis pipeline on high resolution structural MRI scans. Our aim was to replicate gross anatomical brain atrophy and subsequent recovery as well as test our *a priori* hypotheses of region-specific partial structural recovery in subcortical, hippocampal, and cerebellar volumes during early stages of sustained abstinence in recovering AUD patients, compared to matched healthy volunteers. Based on existing evidence from neuropathological and multimodal neuroimaging studies, we also hypothesized a positive correlation between structural atrophy and clinical severity scores of AUD.

2. Materials and Methods

2.1 Subjects

Sixty recently detoxified adult male alcohol dependent patients (DSM-IV-TR criteria)(American Psychiatric Association, 2000) and matched fifty-five healthy non-alcohol abusing men were recruited to the AUD and control groups, respectively. Three patients and controls were excluded from the analysis because they dropped out before completing their first neuroimaging session or because of severe neuroimaging artifacts. The demographic and clinical overview of the remaining 109 participants is summarized in Table 3.1.

The alcohol dependent participants were recruited from a pool of patients referred to supervised residential treatment programs in Edmonton, Canada and Mannheim, Germany as part of the TRANSALC research project. DSM-IV-TR diagnostic interviews were carried out by a psychiatrist, using the Structured Clinical Interview for the DSM-IV-TR (SCID-I) (First et al., 2002). All of the patients were consistent, steady, heavy drinkers. All of the analyzed patients met the highest Zone IV cut-off score on the Alcohol Use Disorders Identification Test (AUDIT) with an average score of 28 out of 40 (Saunders et al., 1993). The AUD patients exhibited on average an intermediate level of alcohol dependence (second quartile) according to the Alcohol Dependence Scale (ADS) with the average score of 19 out of 47 (Skinner & Allen, 1982). The patients did not abuse non-beverage ethanol or other substances except nicotine. The patients were recruited within the first two weeks of abstinence and underwent longitudinal scanning sessions at two time points: first at approximately two weeks of abstinence and second at approximately one month of abstinence. Abstinence was verified at each scanning session in all participants by an alcohol breathalyser (BACtrack S50 Personal Breathalyzer, Portable Breath Alcohol Tester) and a urine drug screen (nal von minden GmbH Drug-Screen® Diptest, Version 1.0).

Controls were recruited concurrently to match the patients' general demographic profile (including sex, age, handedness, general occupation/education background). The controls had no history of alcohol or drug addiction and consumed alcohol below the Canada's Low-Risk Alcohol Drinking Guidelines (Butt, 2011). Participants in both arms were excluded if they had any history of serious medical (including psychiatric or neurological) complications, brain injury, use of psychotropic medications (other than during the detoxification process), or did not meet magnetic resonance safety criteria for our imaging facilities. The study was approved by the University of Alberta Health Research Ethics Board (study ID: Pro00019424)

Table 3.1: Summary of Key Demographic and Clinical Variables

	AUD Patients (n=57)		Controls (n=52)				
	Mean	**SEM**	**Mean**	**SEM**	**% Δ**	**t-Value**	**corrected p**
Age	44.11	1.33	42.08	1.36	4.82	1.07	not sig
TIV	1,513.89	18.12	1,563.10	16.61	-3.15	-1.99	not sig
Ethanol (grams/day)	285.82	25.75	5.24	0.74	5,359.57	10.89	***
AUDIT	28.38	0.79	2.65	0.29	971.94	30.56	***
ADS	18.93	1.24	1.69	0.30	1,022.51	13.50	***
OCDS	20.00	1.14	1.33	0.18	1,400.00	16.17	***
ODS	7.39	0.63	0.19	0.10	3,839.18	11.22	***
CDS	12.61	0.60	1.15	0.15	1,000.86	18.57	***
Abstinence 1 (days)	16.44	1.02	N/A				
Abstinence 2	34.23	1.3	N/A				

*p<0.05, ** p<0.01, *** p<0.001 Bonferroni-corrected; SEM = standard error of mean

2.2 MRI Acquisition

Neuroimaging data were acquired at two clinical sites. Canadian data were acquired using a 4.7 Tesla Varian Inova whole-body MRI scanner, located at the University of Alberta, Edmonton. German data were acquired using a 3 Tesla Siemens MAGNETOM TRIO whole-body MRI scanner, located at the Central Institute of Mental Health, Mannheim. The scanning protocol included anatomic imaging using T1-weighted magnetization-prepared rapid acquisition echo (MPRAGE) with acquisition parameters of TR 1505.9 ms, inversion time 300.0 ms, relaxation delay time (after readout prior to inversion) 300.0 ms,

linear phase encoding, TE 3.71 ms, matrix 240×192×128, field of view 240×192×192 mm^3, 1.0×1.0×1.5 mm^3 voxels, whole brain coverage.

The anatomical scans were visually reviewed by two independent neuroimaging experts for gross abnormalities. None of the subjects exhibited any clinically significant structural abnormalities other than what may be expected from normal aging or prolonged alcohol abuse.

2.3 Region-Based Morphometry

The region-based morphometry was performed using volBrain automated preprocessing library (https://volbrain.upv.es). The analysis was split into three streams – gross anatomical analysis using volBrain pipeline (Coupé et al., 2011; Manjón & Coupé, 2016); hippocampal subfield analysis using HIPS pipeline (Romero, Coupé, & Manjón, 2017); and cerebellar analysis using CERES pipeline (Romero, Coupé, Giraud, et al., 2017). The full description of each pipeline is included in the cited papers. Briefly, the analysis consisted of blinded data anonymization, quality assurance of all structural scans and exclusion of any scans with severe imaging artifacts or scans without full brain coverage, preprocessing using the automated pipelines, quality assurance of the segmented maps on both native anatomical scans and the appropriate template, and another quality assurance of the quantitative output to check for outliers or inconsistencies (left/right) in the individual as well as the overall dataset and group. All of the pipelines consisted of: denoising, coarse inhomogeneity correction, MNI space registration, fine inhomogeneity correction, intensity normalization, cropping, and tissue classification and/or non-local segmentation based on manually segmented libraries. VolBrain included non-local intracranial cavity extraction, tissue classification, non-local hemisphere segmentation, and non-local subcortical structure segmentation. HIPS included non-local patch based segmentation (based on 3 label Kulaga-Yoskovitz dataset and 5-label Winterburn dataset) (Kulaga-Yoskovitz et al., 2015; Winterburn et al., 2013). CERES included tissue classification as well as non-local patch based lobule segmentation.

2.4 Statistical Analysis

After the quality assurance of the segmented maps and quantitative measures was complete, the label key was returned to the blinded researcher to allow for group comparison and statistical analysis. The summary statistics and group comparison was generated using SPSS (version 20)(IBM Corp, 2011) and MATLAB (version R2018b) (The MathWorks Inc, 2018).

The summary statistics included group mean and standard error of mean (SEM). After verifying validity of the statistical assumptions (including Levene's test of homogeneity), two sample t-tests were used to compare group differences. The input data for summary statistics were not corrected for nuisance variables (such as site/scanner or age).

The primary group comparison analysis was completed using general linear models on z-normalized data. The models included predictors for group status (dummy variables for patient scan one, patient scan two, and control) as well nuisance variables (scanner site dummy variable, total intracranial volume, age, and length of abstinence at first scan). The contrasts compared group differences at first time point (patient scan one *versus* control), at second time point (patient scan two *versus* control), as well as interscan difference (patient scan two *versus* patient scan one).

Post-hoc clinical correlation analysis was performed on nuisance-corrected z-normalized data. The significance of the Pearson correlation coefficient was tested using two-tailed t-test.

For all analyses, the null hypothesis was rejected and group differences were considered as significant at a global alpha threshold of 0.05. The p-values were corrected for multiple comparison for each of the analyses using Bonferroni method (Bonferroni, 1936).

3 Results

3.1 Participant profile

Healthy controls were recruited to match the general demographic profile of the AUD patients. As a result, the groups were not significantly different in their general demographic profile or scanning site location. On average, the total intracranial volume was also comparable between the groups. Nonetheless, group comparisons using general linear models as well as post-hoc clinical correlation analyses included age, scanning site, total intracranial volume, as well as the patients' length of abstinence at first scanning session as nuisance variables since all of these variables are known to impact regional volumes or longitudinal changes in the brain. The clinical measures were in general an order of magnitude more severe in the AUD group than in the healthy controls, as illustrated in Table 3.1.

3.2 Gross Anatomical Differences (VolBrain)

The gross anatomical differences from the VolBrain pipeline are summarized in Table 3.2. In general, the AUD group exhibited gross decreases in both grey matter and white matter volumes and a corresponding increase in cerebrospinal fluid volume at both first (two weeks of abstinence) and second time point (one month of abstinence). This trend persisted in cerebrum, cerebellum, as well as brainstem, but was only statistically significant in the whole brain and cerebrum measures. Only the following differences survived Bonferroni correction for multiple comparison: 4% decrease in global gray matter at first time point, 32% increase in global cerebrospinal fluid at first time point, 8% decrease in global white matter at second time point, 30% increase in global cerebrospinal fluid at second time point, as well as 6% decrease in cerebrum volume at first time point, 5% decrease in cerebrum grey matter volume at first time point, 6% decrease in cerebrum volume at second time point, and 8% increase in cerebrospinal fluid volume at

second time point. Even though not significant, longitudinal changes within the patient group were associated with a nonsignificant trend towards increased grey matter volume, only marginally decreased cerebrospinal fluid volume, and an unexpected continued decrease in the white matter volume. The normal data variability associated with natural aging as well interpersonal brain variability (as illustrated in **Error! Reference source not found.**) was quite large and comparable to the effect of alcohol-related structural deficits. Moreover, the interscan interval of supervised abstinence was only approximately 18 days. Together, these factors might explain why we failed to observe significant longitudinal changes in the AUD group.

Figure 3.1: Gross Anatomical Differences Associated with Alcohol Use Disorder and Aging

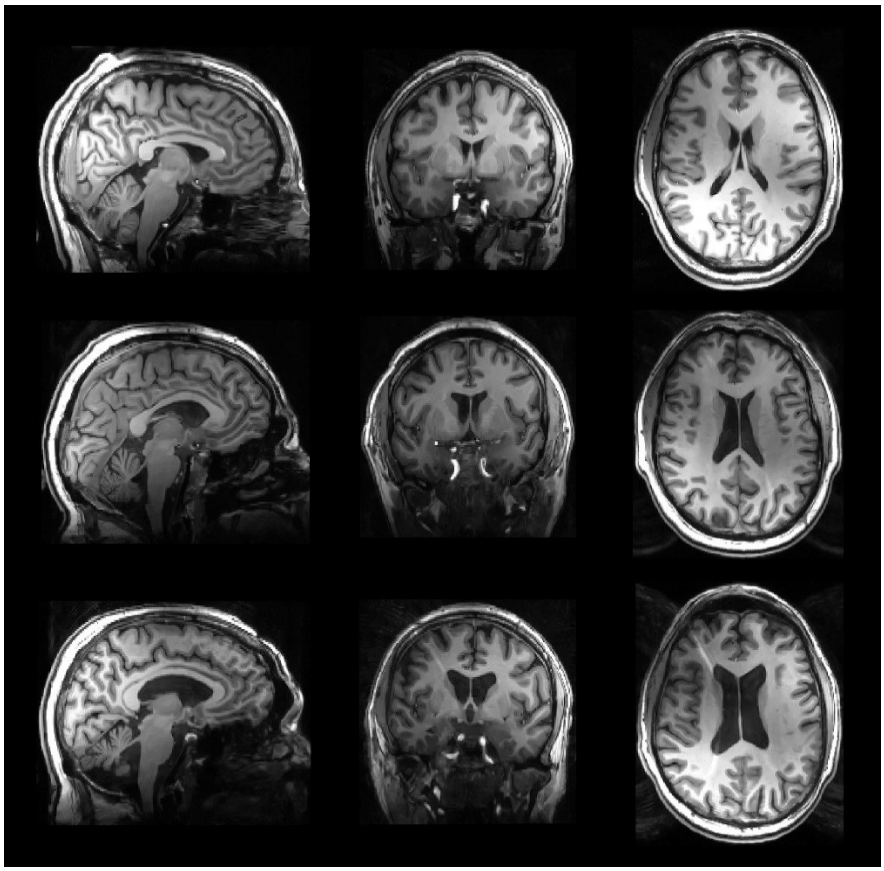

All of the scans are in native space. **Top row** illustrates a structural scan of a **healthy volunteer** who was **45 years old** and an infrequent social drinker (who drank on average 0.01 units of alcohol per day and has been abstinent for 20 days at the time of scanning). **Middle row** illustrates a structural scan of an **AUD patient** who was the same age as the top row control (**45 years old**) but was a chronic heavy drinker (drinking on average 25.32 units of alcohol per day and has been abstinent for 8 days). Note the enlarged ventricles and atrophied cerebellum compared to the matched control above. **Bottom row** illustrates a structural scan of a **healthy volunteer** who was **59 years old** and an infrequent social drinker (who drank on average 0.25 units of alcohol per day and has been abstinent for 16 days). Note that an older healthy control (bottom row) exhibited greater structural atrophy than even an AUD patient (middle row) who was the same age as the top row healthy volunteer. Alcohol use disorder is associated with brain atrophy which in some cases can be noticeable even without quantitative analysis. Nonetheless, normal data variability and confounding variables such as age can have greater impact than AUD history. Age must, therefore, be accounted for as a nuisance variable for the group analysis. Canadian standard unit of alcohol is 17.05 mL or 13.45g of pure ethanol (Butt, 2011).

3.3 Deep Brain Anatomical Differences (VolBrain)

The deep brain anatomical differences from the VolBrain pipeline are summarized in Table 3.3. Deep brain regions exhibited generally the same trend as the whole-brain changes. Most of the regions (except for negligible difference in amygdala and caudate nucleus) exhibited a decreased volume with an increasing longitudinal trend in the recovering alcohol dependent patients compared to healthy controls. The inverse trend occurred in the ventricles. After multiple comparison correction, only the 7% decrease in thalamus at first time point, 3% decrease in hippocampus at first time point, and 5% decrease in the thalamus volume at the second time point were significant. None of the interscan differences within the alcohol dependent group were significant.

3.4 Hippocampal Differences (HIPS)

The anatomical differences in the hippocampal subfields from the HIPS pipeline are summarized in Table 3.4. Hippocampal volume as a whole as well as its subfields exhibited decreased volume in the patient group at both scan intervals in both three (Kulaga-Yoskovitz) and five subfield (Winterburn) segmentation protocols. The interscan longitudinal changes in the patient group did not yield significant changes and showed mixed trends with a positive trend in the three subfield segmentation and unclear trend in the five subfield segmentation. The Winterburn segmentation resulted in the following significant differences: 7% overall hippocampus decrease at first time point; 6% CA1 decrease at first time point, 9% CA4-DG decrease at first time point, 7% decrease in SR-SL-SM at first time point, as well as 6% decrease in hippocampus as a whole at second time point, 6% decrease in CA1 at second time point, 7% decrease in CA4-DG at second time point, and 7% decrease in SR-SL-SM at second time point. The Kulaga-Yoskovitz segmentation resulted in the following significant differences: 5% decrease in overall hippocampus volume at first time point, 5% decrease in CA4-DG at first time point, and 4% decrease in Subiculum at first time point, as well as 3% decrease in overall hippocampus at second time point.

3.5 Cerebellar Differences (CERES)

The anatomical differences in the cerebellar lobules from the CERES pipeline are summarized in Table 3.5. None of the differences were statistically significant. The inter-subject variability was likely greater than the changes which could be associated with alcohol use disorder. The longitudinal differences were also negligible and in some lobules even suggest an unexpected negative trend within the first month of abstinence. Greater scan inhomogeneities in the cerebellar regions close to the edge of the field of view and smaller region of interest size might have also contributed to tissue classification variability and unclear results.

3.6 Clinical Correlations

The clinical correlations between nuisance-corrected volumetric data and clinical scale scores in the patients are summarized in Table 3.6 to 76Table 3.9. The higher severity of alcohol use disorder measure by the AUDIT scale was associated with a significant increase in cerebrospinal fluid volume (Pearson correlation coefficient of 0.40) and unexpected increase in cerebellar white matter (0.37) as well as decrease in whole brain grey matter (-0.45), total cerebrum volume (-0.43), cerebral grey matter (-0.45), thalamus (-0.50), hippocampus (-0.46 in Winterburn HIPS, -0.41 in Kulaga-Yoskovitz HIPS and -0.37 in VolBrain), nucleus accumbens (-0.36), all of the Winterburn hippocampal subfields (-0.34 CA1, -0.30 CA2-CA3, -0.42 CA4-DG, -0.40 SR-SL-SM, -0.41 Subiculum), and CA1-3 Kulaga-Yoskovitz hippocampal subfield. The dependence severity of the ADS scale was positively correlated with cerebrospinal fluid volume (0.40), lateral ventricles (0.61) and unexpectedly with cerebellar white matter (0.27) and subiculum (0.34) as well as decrease in total grey matter (-0.49), total cerebrum (-0.41), cerebral grey matter (-0.52), nucleus accumbens (-0.41), lobule V of cerebellum (-0.47), and Winterburn hippocampal subfields of CA1 (-0.42) and CA2-CA3 (-0.34). The severity of daily alcohol consumption was unexpectedly positively correlated with cerebellar total volume (0.40), cerebellar white matter (0.49), brainstem (0.44), cerebellar Crus I (0.48). The severity of the OCDS was positively correlated with

cerebrospinal fluid volume (0.26), lateral ventricles (0.41), and unexpectedly with Kulaga-Yoskovitz subiculum (0.31) and negatively correlated with caudate (-0.40), thalamus (-0.31), globus pallidus (-0.36), and Winterburn CA2-CA3 hippocampal subfield (-0.30). The compulsive drinking subscale (CDS) of the OCDS scale was significantly correlated with increased volume of cerebrospinal fluid (0.29), lateral ventricles (0.41), as well as unexpectedly with subiculum from both Winterburn (0.33) and Kulaga-Yoskovitz (0.39) segmentations and also decreased volumes in caudate nucleus (-0.33), Winterburn hippocampal subfields CA2-CA3 (-0.43) and CA4-DG (-0.47) and Kulaga-Yoskovitz hippocampal subfields CA1-3 (-0.36). Increased severity on the obsessive drinking subscale (ODS) from the OCDS correlated with increased volume of lateral ventricles (0.36) and decreased volumes of caudate nucleus (-0.39) and globus pallidus (-0.40). In summary, clinical severity scales were generally positively correlated with increased cerebrospinal fluid and lateral ventricle volumes and negatively correlated with most other grey matter regions. AUDIT severity was significantly correlated with 52% of analyzed brain regions, ADS with 27%, daily ethanol consumption with 10%, OCDS with 17%, CDS with 22%, and ODS only with 7%. The strongest and most commonly significant correlation was observed between increased clinical severity and increased ventricular volume. Of note is the regionally specific correlation of striatal subfields with different addiction scales. Decreased volumes of potentially reward-dominated ventral striatum regions such as nucleus accumbens were correlated with increased dependency scores on scales like ADS and AUDIT while decreased volume of dorsal striatum regions such as caudate nucleus which are potentially dominant in executive function (impulsivity / response inhibition) were associated with increased severity on the OCDS and its obsessive and compulsive subscales.

4 Discussion

The aim of this study was to analyze longitudinal volumetric changes in deep brain structures, hippocampal subfields, and cerebellar lobules in recovering AUD patients during their first month of abstinence in comparison to matched healthy volunteers. Our results indicate a broad single digit

percentage volume decrease across most of the examined structures (except cerebrospinal fluid and ventricles which exhibited double digit increases) in AUD patients compared to the healthy controls (in accord with our *a priori* hypothesis). The most significant differences were observed in the hippocampal subfields while no significant changes were observed in the cerebellar lobules. These structural deficits persisted in the approximately two and a half weeks between the first (approximately 16 days of abstinence) and second (approximately 34 days of abstinence) scanning session, with only small, non-significant interscan differences (contrary to our *a priori* hypothesis). The magnitude of structural deficits was positively correlated with AUD clinical severity scales, especially AUDIT score. The highest correlations were observed in the regions which demonstrated the most substantial deficits compared to the healthy controls. Even though this study included a larger sample size (which was approximately one and a half times larger than average of previously published AUD cross-sectional and longitudinal neuroimaging studies) and included more clinically homogeneous sample with above average clinical severity, the results did not replicate several previously published findings or observe anticipated significant structural recovery during the approximately two and a half week interscan interval. These differences may be due to large natural variability in the data (associated for example with age range of 23 to 64) as well as a relatively short interscan interval in our study.

There is a scarcity of longitudinal AUD neuroimaging studies compared to other common neurodegenerative disorders. The first longitudinal structural neuroimaging study in AUD was published in 1978 and since then at least 35 cross-sectional and longitudinal (CT, MRI, and DTI) studies (including multiple publications based on the same or partially same neuroimaging datasets) have been published in English language peer-reviewed journals (Agartz et al., 2003; Artmann, Gall, Hacker, & Herrlich, 1981; Bartsch et al., 2007; Cardenas et al., 2007; Carlen & Wilkinson, 1980; Carlen, Wilkinson, Wortzman, & Holgate, 1984; Carlen, Wortzman, Holgate, Wilkinson, & Rankin, 1978; Demirakca et al., 2011; Deshmukh, Rosenbloom, De Rosa, Sullivan, & Pfefferbaum, 2005; Durazzo & Meyerhoff, 2019; Durazzo, Mon, Gazdzinski, & Meyerhoff, 2017; Durazzo et al., 2015; Fein & Fein, 2013; Gazdzinski et

al., 2005; Hoefer et al., 2014; Kühn et al., 2014; R. S. Liu, Lemieux, Shorvon, Sisodiya, & Duncan, 2000; Mann et al., 2005; Mon, Delucchi, Durazzo, Gazdzinski, & Meyerhoff, 2011; Muuronen, Bergman, Hindmarsh, & Telakivi, 1989; Pfefferbaum et al., 2014; Pfefferbaum et al., 1995; Ron, Acker, Shaw, & Lishman, 1982; Schroth, Naegele, Klose, Mann, & Petersen, 1988; Segobin et al., 2014; Shear et al., 1994; van Eijk et al., 2013; G. Y. Wang et al., 2016; Wobrock et al., 2009; Yeh, Gazdzinski, Durazzo, Sjöstrand, & Meyerhoff, 2007; Zipursky, Lim, & Pfefferbaum, 1989; X. Zou, Durazzo, & Meyerhoff, 2018; Y. Zou et al., 2017). Published evidence ranges from longitudinal case reports (single individual) to large cross-sectional studies (100 participants); including on average about 39 AUD participants. The literature is inconsistent in the terminology and clinical profile of the participants. The range of average abstinence at first scanning time point extends from 0 to 503 days (overall average of 46 days across 33 studies) to a second time point from 14 to 2,722 days (overall average of 290 days across 29 studies) and a third time point from 91 to 226 days (overall averages of 226 days across 8 studies). This is particularly relevant, since structural brain recovery occurs non-linearly, with most rapid recovery over the first few weeks of sustained abstinence (Durazzo et al., 2015; Gazdzinski et al., 2005; Pfefferbaum et al., 1995; Y. Zou et al., 2017). In fact, structural recovery might occur up to six times faster (and up to 50% of the total recovery) during the first 3 weeks than during the subsequent year (Charlet et al., 2018; Gazdzinski et al., 2005). Hence, the results from longitudinal studies with such disparate lengths of abstinence might yield inconsistent results and may fail to detect significant recovery due to underestimation of the extent of the initial AUD-related brain damage. A small number of studies did not disclose the duration of abstinence in their clinical cohort, including recent single time point studies such as (Shim, Kim, Kim, & Baek, 2019). Many studies also did not disclose other variables such as presence or absence of clinical comorbidities. Studies reporting comorbidities have disclosed up to 91% comorbid nicotine dependence (and significantly higher percentage of smokers in AUD than controls in almost all studies), up to 29% comorbid substance use disorder (including stimulants, marihuana, and benzodiazepines), up to 63% comorbid psychiatric disorders (most commonly unipolar mood disorders), and up to 51% other somatic disorders (Hepatitis C etc.). Despite such liberal inclusion criteria, many studies still reported issues with

recruitment, retention, and relapse in the longitudinal AUD samples. Most AUD studies focused primarily on male working age adults (average of average ages of 47 years, which is slightly older but comparable to our study). The average amount of alcohol abused prior to treatment ranged from 115 grams to 264 grams of ethanol per day, with an overall average of 178 grams, which is substantially less than our cohort's 286 grams per day.

Most published longitudinal and cross-sectional studies did not quantify the volume or percentage changes in deep brain regions, hippocampal subfields, or cerebellar lobules. Some earlier studies only reported case observations or provided qualitative rankings of perceived severity of brain atrophy. More recent voxel-based morphometry studies typically did not quantify regional changes and usually reported only significant cluster location, size, and level of significance. Most commonly quantified longitudinal changes included sizes of ventricles and cerebrospinal fluid volume. The summary below lists the publicly available volumetric changes. It is important to note that the discussed values were not always explicitly listed or tested for significance in the original publications. Moreover, most of the values obtained from the literature were not corrected for natural variability in total intracranial volume, age, sex, and other variables, although we tried to normalize the values at least for total intracranial volume, when the data was disclosed in the publication.

In terms of gross anatomical changes, there are structural data available on total cerebral volume, grey matter volume, white matter volume, and cerebrospinal fluid volume. Our study reported a non-significant increase of 0.18% (although a negative t-value when correcting for nuisance variables) from 5.70% to 5.53% atrophy at 16.44 and 34.23 days of abstinence. A case report by Liu *et al.* (2000) reported an 11% increase from 0 to 1,278 days of abstinence. Bartsch *et al*. (2007) reported 1.85% increase from 4.23% to 3.14% atrophy from 3 to 38 days of abstinence (24 and 15 subjects). Gazdzinski *et al.* (2005) reported a 0.96% and subsequent 1.00% increase in a mixed study from 6 to 33 to 212 days of abstinence (23, 18, and 7 subjects). Yeh *et al*. (2007) reported a 1.36% increase and subsequent 3.18% increase from

3.97% to 2.66% to 0.89% atrophy from 5.76 to 31.98 to 209.90 days of abstinence (44, 46, and 17 subjects). Finally, Mann *et al.* (2005) reported 1.15% increase from 4.23% to 3.14% atrophy in a longitudinal study of 76 AUD patients from 20.26 to 55.26 days of abstinence.

Our study indicates a non-significant increase of 1.30% in total grey matter from atrophy of 4.30% to 3.06% over 16.44 to 34.23 days of abstinence. Agartz *et al.* (2003) reported 0.60% and 0.41% recovery respectively, from 0 to 28 to 91 days of abstinence (7 and 6 subjects). Van Eijk (2013) reported a 0.95% increase from atrophy of 6.99% to 6.21% over 1 to 14 days of abstinence (49 subjects). Cardenas *et al*. (2007) reported 7-12% faster volumetric recovery from 5.8 to 243.5 days of sustained abstinence in parietal and frontal lobes in AUD patients compared to light drinkers in 47 versus 25 subjects. Mon *et al*. (2013) reported a 0.72% increase from 6 to 34 days of abstinence (62 and 41 subjects). Durazzo *et al.* (2015) reported 0.97% and subsequent 0.78% recovery from atrophy of 4.23% to 3.29% to 2.54% from 7 to 32.88 to 226.12 days of abstinence respectively (in 82 subjects). Pfefferbaum *et al.* (1995) reported a 3% anterior grey matter increase in 12 to 23.4 days of abstinence (58 subjects). Demirakca *et al.* (2011) reported 0.47% increase from 1.38% atrophy from 21 to 1,921.5 days of abstinence (50 and 14 subjects). Shear *et al* (1994) reported a 0.68% increase from 28.7 to 107 days of abstinence (24 and 15 subjects).

Our study reported a non-significant decrease of 1.35% in total white matter from atrophy of 6.58% to 7.84% from 16.44 to 34.23 days of abstinence. This was contrary to our expectations and most published evidence. Agartz *et al.* (2003) reported a respective 11.26% and 3.21% recovery over 0 to 28 to 91 days of abstinence (7 and 6 subjects). Van Eijk *et al.* (2013) reported a 0.27% decrease from atrophy of 0.66% to 0.79% over 1to 14 days of abstinence in 49 subjects. Cardenas *et al*. (2007) reported a faster recovery from 5.8 to 243.5 days of abstinence respectively in parietal and frontal lobes compared to light drinkers in 47 versus 25 AUD subjects. Mon *et al.* (2013) reported 0.41% increase from 6 to 34 days of abstinence (62 and 41 subjects). Durazzo *et al.* (2015) reported 0.42% and subsequent 1.82% from atrophy of 0.94 to atrophy of 0.53% to hypertrophy of 1.28% in 7 to 32.88 to 226.12 days of abstinence in 82 subjects.

Demirakca *et al.* (2011) reported 1.54% increase from atrophy of 2.95% between 21 and 1,921.5 days of abstinence (50 and 14 subjects). Shear *et al.* (1994) reported 3.99% increase from 28.7 to 107 days of abstinence (24 and 15 subjects).

Our study indicates a non-significant decrease of 1.27% in cerebrospinal fluid (CSF) from enlargement of 31.53% to 29.86% from 16.44 to 34.23 days of abstinence. Agartz *et al.* (2003) reported 11.51% and 4.53% decrease in CSF volume from 0 to 28 to 91 days of abstinence (7 and 6 subjects). Van Eijk *et al.* (2013) reported 0.99% decrease from 19.41% to 18.24% enlargement from 1 to 14 days of abstinence in 49 subjects. Schroth *et al.* (1988) reported a 30.50% decrease from 5.2 to 40.2 days of abstinence in 9 subjects. Gazdzinski *et al.* (2005) reported 0.48% and 0.50% decrease from 6 to 33 to 212 days of abstinence in a mixed design study (23, 18, and 7 subjects). Mann *et al.* (2005) reported 8.17% decrease from 46.15% to 34.22% enlargement from 20.26 to 55.26 days of abstinence in 76 subjects. Demirakca *et al.* (2011) reported 3.27% decrease from a 7.49% enlargement from 21 to 1,921.5 days of abstinence (50 and 14 subjects). Shear *et al.* (1994) reported 12.42 decrease from 28.7 to 107 days of abstinence (24 and 15 subjects).

In terms of deep brain structures, existing literature has documented recovery in the ventricular enlargement and generally non-significant or mixed evidence on deep grey matter brain structures. Our study indicates a non-significant 6.77% decrease in the lateral ventricle volume from 18.68% to 10.64% enlargement from 16.44 to 34.23 days of abstinence. Schroth *et al.* (1988) reported a 14.70% decrease from 5.2 to 40.2 days of abstinence in 9 subjects. Yeh *et al.* (2007) reported 8.18% decrease and a 4.60% enlargement from 21.94% to 33.39% to 53.64% compared to healthy controls from 5.76 to 31.98 to 209.90 days of abstinence (44, 46, 17 subjects). Gazdzinski *et al.* (2005) reported a 0.18% and 0.12% decrease from 6 to 33 to 212 days of abstinence in a mixed design study with 23, 18, and 7 subjects. Durazzo *et al.* (2015) reported 2.96% and 2.79% decrease from 10.92% to 7.64% to 4.63% from 7 to 32.88 to 226.12 days of abstinence in 82 subjects. Zipursky *et al.* (1989) reported a decrease of 15.22%

from 37.31% to 16.42% in 10 patients from 7.4 to 22.6 days of abstinence. Wobrock *et al.* (2009) reported a 5.50% decrease from 37% enlargement from 11 to 228.28 days of abstinence in 56 subjects with substantial mental health comorbidities. Pfefferbaum *et al.* (1995) reported an 8% and 16% decrease in third ventricle volume from 12 to 23.4 to 121.6 days of abstinence (58, 58, 19 subjects). Mann *et al.* (2005) reported 7.04% decrease from 21.94% to 13.35% enlargement from 20.26 to 55.26 days of abstinence in 76 subjects.

A number of studies such as Pfefferbaum (1995) reported no significant changes in basal ganglia. For caudate nucleus, our study reported a non-significant increase of 1.67% from 0.10% to 1.78% enlargement during the interscan interval. Mon *et al.* (2013) reported a 2.11% decrease in caudate volume from 6 to 34 days of abstinence (62 versus 41 subjects). Fein *et al.* (2013) reported a 5.23% increase from 4.19% atrophy to 0.82% hypertrophy from 69 to 2,722.49 days abstinence (36 and 47 subjects).

For nucleus accumbens, our study reported a non-significant increase of 0.19% from atrophy of 5.90% to 5.73% from 16.44 to 34.23 days of abstinence. Fein *et al.* (2013) reported 4.22% increase from atrophy of 8.90% to 5.05% from abstinence of 69 to 2,722.49 days.

Our study has measured a non-significant 0.06% increase in putamen atrophy from 2.19% to 2.24% during the interscan interval. Even though we did not expect an increase in the putamen atrophy, the same trend has been reported in the literature. Durazzo *et al.* (2015) reported a 1.46% and 0.93% increase in lenticular nucleus (putamen and globus pallidus) atrophy from 6.34% to 7.71% to 8.57% atrophy from 7 to 32.88 to 226.12 days of abstinence in 82 subjects. Fein *et al.* (2013) reported a 1.49% increase in atrophy from 1.35% to 2.82% from 69 to 2,722.49 days of abstinence (36 and 47 subjects).

For globus pallidus, our study has measured a 2.55% recovery from atrophy of 3.44% to 0.98% during the interscan interval. Durazzo *et al.* (2015) reported the lenticular nucleus change described above. Fein *et*

al. (2013) reported 1.76% increase from atrophy of 5.28% to 3.60% from 69 to 2,722.49 days of abstinence.

For thalamus, our study has measured a non-significant increase of 1.70% from atrophy of 6.82% to 5.24% during the interscan interval. Mon *et al.* (2013) reported a 2.70% improvement from 6 to 34 days of abstinence (62 and 41 subjects). Durazzo *et al.* (2015) reported a decrease of 0.29% and an increase of 5.41% from atrophy of 14.09% to 14.33% to 9.70% from 7 to 32.88 to 226.12 days of abstinence in 82 subjects. Pfefferbaum *et al.* (1995) reported no significant change and did not quantify the volumetric change in thalamus from 12 to 23.4 to 121.6 days of abstinence. Demirakca *et al.* (2011) reported 4.35% improvement from 0.54% atrophy between 21 and 1,921.5 days of abstinence (50 and 14 subjects). Fein *et al.* (2013) reported 1.48% decrease from 0.71% hypertrophy to 0.78% atrophy from 69 to 2,722.49 days of abstinence (36 and 47 subjects).

For amygdala, our study has measured a non-significant decrease of 0.34% from 0.52% hypertrophy to 0.17% hypertrophy. Zou *et al.* (2018) reported mixed changes in the amygdala atrophy from 3.25% to 2.49% to 4.18% from comparison of 6.5, 33.5, and 218.3 days of abstinence (mixed study with 65, 82, and 36 subjects). Demirakca *et al.* (2011) reported 2.04% improvement from 5.92% atrophy between 21 and 1,921.5 days of abstinence (50 and 14 subjects). Fein *et al.* (2013) reported 1.26% increase in atrophy from 1.03% to 2.27% in 69 to 2,722.49 days of abstinence (36 and 47 subjects)

For hippocampus, our study has revealed a range of results, depending on the segmentation protocol used: non-significant longitudinal improvements of 1.07%, 1.49%, and 1.80% from an atrophy of 7.12% to 6.12%, 4.68% to 3.27%, and 2.63% to 0.88%, respectively. Liu *et al.* (2000) reported a 7.70% increase from 0 to 1,278 days of abstinence in a single case report. Van Eijk *et al.* (2013) reported no improvement from an initial 3.45% atrophy from 1 to 14 days of abstinence in 49 subjects. Zou *et al.* (2018) reported 1.47% and no subsequent improvement from estimated 9.53% to 8.20% to 8.20% atrophy from 6.5 to

33.5 to 218.3 days of abstinence in a mixed study of 65, 82, and 36 subjects. Hoefer *et al.* (2014) reported mixed results of 6% to 8% to 6% atrophy from 7 to 33 to 213 days of abstinence in a mixed study of 84, 121, and 37 subjects. Kühn *et al.* (2014) reported 4.56% increase from atrophy of 5.83% to 1.54% from 9.4 to 23.2 days of abstinence specifically in the cornu ammonis (CA) 2 and 3. Demirakca *et al.* (2011) reported 2.04% increase from atrophy of 5.92% in amygdala and hippocampus region from 21 to 1,921.5 days of abstinence (50 and 14 subjects). Fein *et al.* (2013) reported 1.14% increase from atrophy of 5.88% to 4.81% from 69 to 2,722.49 days of abstinence (36 and 47 subjects). A recent meta-analysis has revealed a moderate effect size (d=-0.53) for AUD-related hippocampal atrophy from 23 AUD versus control group single time point analyses (but it did not fully explore the effect of abstinence other than excluding studies with more than a year of abstinence) (Wilson, Bair, Thomas, & Iacono, 2017). The meta-analysis has also revealed a publication bias with small sample studies reporting larger effects. Post-hoc power analysis suggested future studies should enroll at least 60 subjects per group when studying hippocampal atrophy in AUD compared to healthy controls (with 83% of published papers relying on smaller datasets). Wilson also commented on similar issues which we noted in the longitudinal AUD literature, such as substantial clinical heterogeneity, modest sample sizes, and lack of correction for nuisance variables such as total intracranial volume in the reported results.

Other than Kühn *et al.* (2014), only single time point studies, such as Zahr *et al.* (2019), Lee *et al.* (2016), and Shim *et al.* (2019) reported measurements of comparable hippocampal subfields in AUD in comparison to controls (at average abstinence lengths of 105.7, 402.6, and unknown days). Zahr reported a significantly lower CA2+3 volumes in the AUD group at over three months of abstinence and a significant AUD-age interaction associated with the hippocampal atrophy (Zahr, Pohl, Saranathan, Sullivan, & Pfefferbaum, 2019). Lee reported significant hippocampal atrophy in presubiculum, subiculum, and fimbria and a non-significant trend in all other measured regions, even at more than a year of abstinence (Lee et al., 2016). Shim did not disclose the length of abstinence in their clinical cohort and did not quantify hippocampal subfield changes other than reporting surface reduction in the presubiculum,

hippocampal tail, hippocampal molecular layer, hippocampal fissure, fimbria, and CA3 in their vertex analysis (Shim et al., 2019). These studies suggest that despite the potential for adult neurogenesis and some encouraging clinical and preclinical results, AUD-related structural damage in the hippocampus and its subfields can persist for many months and years. Histological cadaver studies, moreover, suggest structural recovery of the hippocampus would most likely be due to white matter repair rather than neuronal proliferation (Sutherland et al., 2014b).

For cerebellum and its lobules, our study has revealed mixed non-significant results without a clear improvement trend, potentially driven by an underlying structural improvement in grey matter volume while continued white matter volume deterioration during the early recovery phase. Liu *et al.* (2000) reported a 20% improvement from 0 to 1,278 days of abstinence in a single patient. Van Eijk *et al.* (2013) reported 1.95% improvement from an 8.89% to 7.39% atrophy from 1 to 14 days of abstinence in 49 subjects. Mon *et al.* (2013) reported 0.51% improvement from 6 to 34 days (62 and 41 subjects). Durazzo *et al.* (2015) reported 1.42% and subsequent 1.44% improvement from atrophy of 3.32% to 1.95% to 0.54% from 7 to 32.88 to 226.12 days of abstinence in 82 subjects.

The published data on structural changes in cerebellar lobules in uncomplicated AUD (not Wernicke-Korsakoff syndrome) is sparse and available only from single time point AUD versus control group comparisons. Sullivan *et al.* (2019) studied an AUD cohort with the shortest abstinence (105.7 days) and used the closest segmentation technique to our analysis (CERES pipeline), reporting significant atrophy in lobules I-V, Crus I, VIIIB, and IX in 24 AUD subjects compared to 20 matched controls (Sullivan, Zahr, Saranathan, Pohl, & Pfefferbaum, 2019). Zhao *et al.* (2019) reported significant atrophy in total corpus medullare and surface shrinkage in lobules I-V, IX, and vermian X at 248 days of abstinence in 135 AUD patients compared to 128 controls (Zhao, Pfefferbaum, Podhajsky, Pohl, & Sullivan, 2019). Sawyer *et al.* (2016) reported persistent cerebellar atrophy even at 8 years of abstinence in 44 AUD subjects (Sawyer et al., 2016). The overall results were mixed: -1.89% total cerebellum, -5.50% cerebellar

white matter, -0.31% cerebellar gray matter, 6.36% anterior lobe, -1.93% posterior lobe, 0% vestibulocerebellum, -1.34% cerebrocerebellum, 1.41% spinocerebellum. Length of abstinence was positively associated with smaller atrophy in vestibulocerebellum and vermal portions of lobule I-II. The vestibulocerebellum in AUD was 0.6% larger with each year of abstinence. Sullivan *et al.* (2000) reported grey but not white matter cerebellar hemisphere volume deficits as well as grey and white matter deficits in the anterior superior (lobules I-VII) but not posterior inferior vermis (lobules VIII-X) in 25 AUD men of unknown duration of abstinence (Sullivan, Deshmukh, Desmond, Lim, & Pfefferbaum, 2000). Therefore, cerebellar lobules in the anterior superior vermis (I-V) seem to be most commonly affected by AUD-related atrophy. The anterior superior vermis atrophy has been well documented in Wernicke-Korsakoff syndrome, where it is associated especially with a significant loss of Purkinje cells and associated neurocognitive deficits (Sullivan, Deshmukh, et al., 2000). Even though there is some evidence of rapid cerebellar recovery in AUD with sustained abstinence in as little as two weeks (van Eijk et al., 2013), structural damage appears to persist even after multi-year abstinence. Because cerebellum is susceptible to poor imaging quality (partial field of view, movement artifacts, inhomogeneity due to poor shimming etc) as well as because of its tightly folded anatomy with many tissue boundaries, segmentation of traditional non-specific $1mm^3$ whole-brain structural scans might not have sufficient resolution (mixed tissue partial volumes across multiple voxels) and quality (artifacts and poor tissue contrast) to reliably measure cerebellar lobules or detect changes in such a small and structurally complex anatomical region.

Our study aimed to document longitudinal changes in less commonly examined brain regions, including basal ganglia, hippocampus, and cerebellum during the first month of recovery from AUD. Even though, all of these regions are important components of addiction-related reward, executive control, and stress pathways as well as important functional hubs implicated in a range of cognitive, neurological, and behaviour deficits observed in AUD and other alcohol-related neurological conditions (for reviews and meta-analyses see: (Crews & Nixon, 2009; Crowe et al., 2019; Fein & Cardenas, 2015; Koob & Volkow, 2010; Moulton, Elman, Becerra, Goldstein, & Borsook, 2014; Stavro, Pelletier, & Potvin, 2013; Wilcox,

Dekonenko, Mayer, Bogenschutz, & Turner, 2014; Zahr & Sullivan, 2008)), they remain sparsely studied and are often ignored or misrepresented by more traditional modern structural analytical techniques, such as voxel-based morphometry (Bergouignan et al., 2009; G. Y. Wang et al., 2016). Although we have failed to observe a significant volumetric recovery over the approximately two and a half weeks interscan interval, our study has still documented a broadly positive trend from single digit percentage atrophy, which is generally comparable to the sparsely documented longitudinal changes during sustained abstinence and AUD recovery, which we summarized above. The lack of significant improvement or clear and consistent results in the literature suggest that the structural recovery of the basal ganglia, hippocampus, and cerebellum during early abstinence is not very robust and should be interpreted with caution.

Moreover, the timeline of longitudinal structural changes as well as functional improvement in neurocognitive and behavioural measures from acute withdrawal and detoxification (first few days), early recovery (first few weeks), to prolonged sustained abstinence (months or years) is even less consistently documented in the literature and remains poorly understood. Our study aimed to compare detoxified patients after their withdrawal symptoms have subsided (verified by CIWA scale during structured clinical interview) – unlike several other studies which have relied on sometimes still intoxicated or acutely withdrawing patients (usually with appropriate pharmacological treatment) (for example (Agartz et al., 2003; Bartsch et al., 2007; R. S. Liu et al., 2000; van Eijk et al., 2013; G. Y. Wang et al., 2016)). Although some of these studies have demonstrated significant structural recovery within the acute withdrawal phase and there is even some evidence of limited neurocognitive functional improvement (Petit et al., 2017), the early detoxification phase is still marked by a number of potentially confounding underlying processes undergoing biochemical allostatis for example from abnormally elevated levels of glutamate (Hermann et al., 2012), cortisol (Stephens & Wand, 2012), and systemic inflammation (Leclercq, De Saeger, Delzenne, de Timary, & Stärkel, 2014). These confounding biochemical imbalances should be mostly normalized by the time of our first scanning time point. Studies with

prolonged abstinence at first time point (such as (Carlen et al., 1978; Fein & Fein, 2013; Pfefferbaum et al., 2014)) also might have understimated level of initial AUD damage since other studies have revealed more rapid rate of structural recovery in the first few weeks of sustained abstinence (i.e. before their baseline scan) rather than subsequent months (Charlet et al., 2018; Durazzo et al., 2015; Gazdzinski et al., 2005; Pfefferbaum et al., 1995; Y. Zou et al., 2017).

It is also important to consider potential limitations when comparing our results to second-time point findings of cross-sectional studies. Due to high AUD relapse and dropout rates (R. H. Moos & Moos, 2006; Walitzer & Dearing, 2006; Witkiewitz, 2011), cross-sectional studies might be exaggerating the magnitude of structural recovery by underestimating baseline structural damage. Several studies reported an underlying survival bias, with patients who exhibit less structural atrophy and better initial neurocognitive performance having higher prospective likelihood of sustaining their abstinence (for example (Beck et al., 2012; J. Camchong, A. Stenger, & G. Fein, 2013a; Durazzo et al., 2017; Rando et al., 2011; S. F. Sorg et al., 2012; Zois et al., 2017; Y. Zou et al., 2018)). This is especially relevant when interpreting very long term cross-sectional analyses (for example (Fein & Fein, 2013)) since most likely only the least affected and highest functioning minority of AUD patients would likely successfully sustained their abstinence for multiple years after their initial treatment.

Even though the effect of sustained abstinence on structural changes might not be very robust, there is encouraging evidence suggesting active brain plasticity during AUD recovery. For a successful recovery and sustained long-term abstinence, all of the regions examined in this study need to undergo extensive plasticity, due to their involvement in the addiction related circuitry (Fein & Cardenas, 2015; Koob & Volkow, 2010; Moulton et al., 2014; Zahr & Sullivan, 2008). The recovering brain needs to repair damage associated with chronic ethanol abuse as well as remodel and optimize its physical connections to help over-compensate for maladaptively reinforced addiction pathways and less efficient compensatory recruitment of parallel pathways. Although the mechanism of AUD damage and recovery has been

extensively documented in preclinical models (for review of model timeline of neuronal and glial changes as well as degeneration stimulated regeneration hypothesis and global abstinence-stimulated trophic NMDA receptor hyperactivity hypothesis see (Crews & Nixon, 2009)), the precise mechanism in human brain is still not fully understood and often confronted by contradictory evidence (N. D. Volkow et al., 2017; Zahr & Pfefferbaum, 2017). Nonetheless, the functional and behavioural improvements observed in patients during their detoxification (our baseline scan) and subsequent residential treatment (our follow-up scan) support underlying brain plasticity. Some studies report significant recovery of most neurocognitive domains within the first month to a year of abstinence (Munro, Saxton, & Butters, 2000; Sullivan, Rosenbloom, Lim, et al., 2000; Sullivan, Rosenbloom, & Pfefferbaum, 2000) and largely normalized cognitive performance (except for spatial processing) in very long-term abstinent AUD patients (Fein, Torres, Price, & Di Sclafani, 2006; Stavro et al., 2013). A recent comprehensive cross-sectional meta-analysis (Crowe et al., 2019) has contradicted these findings, suggesting significant cognitive impairment in AUD might persist not only beyond the first few weeks but also beyond one year. The results of this meta-analysis should, however, be considered with caution since it did not examine longitudinal changes in AUD during these intervals, unlike Sullivan *et al*., but only compared significance of differences between controls and recovering AUD patients, which persisted across most domains at all stages.

Structural human neuroimaging studies have validated an association between functional neurocognitive improvements (memory/learning, processing speed, visuo-spatial function, attention, ataxia, static balance) and longitudinal volumetric brain recovery with both short- and long-term abstinence (Mon et al., 2013; Muuronen et al., 1989; M. J. Rosenbloom et al., 2007; Sullivan, Rosenbloom, Lim, et al., 2000; Yeh et al., 2007). These macroscopic findings have been corroborated by magnetic resonance spectroscopy (MRS) studies, which have revealed that metabolite changes (lower ratios of N-acetylaspartate (NAA) and choline-containing compounds (Cho) as well as elevated myo-inositol (mI) to total creatine and phosphocreatine (tCr)) appear to largely normalize with sustained abstinence (1-3 days

up to 1.7 years) (Bendszus et al., 2001; Durazzo, Gazdzinski, Rothlind, Banys, & Meyerhoff, 2006; Parks et al., 2002; B. C. Schweinsburg et al., 2000). These metabolite changes suggest increased neuronal integrity (NAA), increased cell-membrane synthesis and turnover as well as cellular density (Cho), and greater osmolar stability or reduced glial cell activation (mI) with sustained abstinence. These changes could represent neuronal healing as well remyelination and white matter recovery during sustained abstinence. The molecular MRS findings have been further supported by diffusion tensor imaging (DTI) which has revealed significant white matter microstructure recovery from a week to first month of abstinence (Gazdzinski, Durazzo, Mon, Yeh, & Meyerhoff, 2010; Y. Zou et al., 2017) as well as from weeks to years of sustained abstinence (Alhassoon et al., 2012; Pfefferbaum et al., 2014). These molecular and microstructural markers have been also correlated to functional improvements in the recovering AUD patients (Alhassoon et al., 2012; Bendszus et al., 2001; Durazzo et al., 2006). Underlying processes responsible for functional recovery during sustained AUD abstinence occur at the cellular level and might not occur at sufficiently pronounced scale or sufficiently rapid timeline (progenitor cell generation, migration, maturation etc. takes multiple weeks in preclinical models) to manifest themselves as a significant change at the macroscopic resolution of structural MRI, especially only after a relatively brief interscan interval of this study and in the context of large natural anatomical variability (due to aging, interscan variability, etc.).

Future studies should rely on larger sample sizes (exceeding 60 participants per group: (Wilson et al., 2017), higher resolution and more sensitive scanning parameters (multimodal T1 and T2 scans to assist with segmentation), longer interscan intervals, and more homogeneous longitudinal samples (narrower age range) in order to measure the relatively small volumetric changes during the early recovery of AUD patients with greater accuracy and certainty. Due to inherent issues with recruitment and subject retention, future longitudinal studies should strive for collaboration and concurrent recruitment from multiple clinical sites. Future studies should also specify and declare whether their aim is to obtain a representative clinical sample or a homogeneous AUD-specific sample to test their hypotheses. Our study, for example,

has helped to document longitudinal changes in AUD during early abstinence but it is not broadly representative of the typical clinical population. We had to screen out approximately 19 patients for every participant and only included otherwise healthy working age adult men who were steady, chronic AUD patients right after acute detoxification phase (excluding most of the clinical volunteers due to comorbid substance abuse, concurrent psychiatric complications, and magnetic resonance safety criteria). Other studies have chosen much more liberal recruitment criteria and included convenience samples with some less severe secondary comorbidities and also participants who engaged primarily in binge drinking rather than steady chronic alcohol abuse as well as participants with broad ranges of baseline abstinence. Liver health and its potential impact on brain atrophy as well as other characteristics, such as iron deposition in the basal ganglia (Juhás et al., 2017), should be also documented in future studies and considered when interpreting results of studies which included AUD patients with concurrent Hepatitis C. Correction for smoking, aging, and natural brain volume variability should be also included in future statistical designs and reported results should be corrected for multiple comparison correction.

5 Conclusion

In conclusion, our region-based morphometry study has successfully documented single digit atrophy across most measured regions in basal ganglia and hippocampal subfields, with unclear results in the cerebellar lobules of recovering AUD patients. The atrophy persisted from 16 to 34 days of abstinence, although a broadly positive nonsignificant trend towards recovery was noted across multiple regions. The magnitude of structural atrophy was correlated with several AUD clinical severity scores. These findings broadly agree with the published literature, despite of the inconsistent and poorly documented published evidence on longitudinal structural recovery with sustained abstinence. Our study used larger and more homogeneous clinical sample compared to existing literature. It is also one of only a few longitudinal studies reporting on structural changes in non-cortical regions during AUD recovery. To our knowledge this is the second longitudinal study which has documented changes in hippocampal subfields as well as

the first to measure cerebellar lobules during AUD recovery. The mixed results of our study as well as the published literature suggest that the structural recovery during sustained abstinence is not a very robust finding and should be considered with caution, until larger studies with higher neuroimaging resolution and more as well as longer interscan intervals can replicate these findings with higher accuracy and confidence. Future structural studies should strive for more robust design, greater transparency about the clinical profile of their participants (such as the length of abstinence at baseline), as well as the evaluation of under-studied non-cortical regions, such as those included in this study.

Table 3.2: Large Brain Structural Differences

	AUD 1		AUD 2		CTL		AUD 1 vs CTL		AUD 2 vs CTL		AUD 2 vs AUD 1	
	x̄ %	SEM	x̄ %	SEM	x̄ %	SEM	% Δ	t-Value	% Δ	t-Value	% Δ	t-Value
Grey Matter (GM)	47.369	0.358	47.983	0.522	49.497	0.395	-4.30	**-4.94*** **	-3.06	-2.64	1.30	0.90
White Matter (WM)	34.070	0.505	33.611	0.492	36.469	0.522	-6.58	-2.16	-7.84	**-3.18***	-1.35	-1.01
Cerebrospinal Fluid	18.630	0.656	18.393	0.699	14.164	0.489	31.53	**5.26*** **	29.86	**4.99*** **	-1.27	0.21
Cerebrum Total	70.309	0.639	70.432	0.639	74.558	0.456	-5.70	**-5.06*** **	-5.53	**-5.05*** **	0.18	-0.31
Cerebrum GM	39.769	0.322	40.315	0.466	41.869	0.344	-5.02	**-5.19*** **	-3.71	-2.81	1.37	0.91
Cerebrum WM	30.540	0.471	30.117	0.431	32.689	0.461	-6.58	-2.13	-7.87	**-3.17***	-1.38	-1.00
Cerebellum Total	9.497	0.122	9.532	0.137	9.718	0.108	-2.28	-1.70	-1.92	-1.50	0.36	-0.16
Cerebellum GM	7.307	0.096	7.356	0.105	7.347	0.103	-0.55	-0.99	0.12	-0.57	0.67	0.20
Cerebellum WM	2.190	0.055	2.176	0.073	2.371	0.076	-7.63	-1.33	-8.24	-1.66	-0.66	-0.53
Brainstem	1.643	0.020	1.688	0.022	1.718	0.019	-4.41	-2.56	-1.74	-0.86	2.79	0.77

Table 3.3: Deep Brain Structural Difference

	AUD 1		AUD 2		CTL		AUD 1 vs CTL		AUD 2 vs CTL		AUD 2 vs AUD 1	
	x̄ %	SEM	x̄ %	SEM	x̄ %	SEM	% Δ	t-Value	% Δ	t-Value	% Δ	t-Value
Lateral Ventricles	1.336	0.092	1.246	0.093	1.126	0.081	18.68	1.76	10.64	1.47	-6.77	-0.23
Caudate	0.488	0.007	0.496	0.008	0.487	0.007	0.10	0.12	1.78	0.71	1.67	0.29
Putamen	0.573	0.009	0.572	0.011	0.585	0.009	-2.19	-1.65	-2.24	-1.98	-0.06	-0.54
Thalamus	0.756	0.008	0.769	0.010	0.811	0.010	-6.82	**-5.21*** **	-5.24	**-3.79** **	1.70	0.29
Globus Pallidus	0.157	0.003	0.161	0.003	0.162	0.003	-3.44	-1.25	-0.98	-0.93	2.55	-0.18
Hippocampus	0.537	0.007	0.546	0.008	0.551	0.006	-2.63	**-2.84***	-0.88	-1.83	1.80	0.38
Amygdala	0.120	0.001	0.120	0.002	0.119	0.002	0.52	-0.22	0.17	0.07	-0.34	-0.57
Accumbens	0.042	0.001	0.042	0.001	0.044	0.001	-5.90	-1.90	-5.73	-1.87	0.19	-0.37

Table 3.4: Hippocampal Structural Differences

	AUD 1		AUD 2		CTL		AUD 1 vs CTL		AUD 2 vs CTL		AUD 2 vs AUD 1	
	x̄ %	**SEM**	**x̄ %**	**SEM**	**x̄ %**	**SEM**	**% Δ**	**t-Value**	**% Δ**	**t-Value**	**% Δ**	**t-Value**
Winterburn segmentation												
Hippocampus	0.321	0.005	0.324	0.006	0.345	0.004	-7.12	**-4.44*** **	-6.12	**-3.59** **	1.07	-0.04
CA1	0.118	0.002	0.118	0.002	0.126	0.002	-6.45	**-3.46** **	-5.85	**-2.98** *	0.64	-0.07
CA2-CA3	0.024	0.001	0.024	0.001	0.025	0.001	-3.62	-1.36	-2.87	-1.28	0.77	-0.01
CA4-DG	0.087	0.002	0.089	0.002	0.095	0.002	-8.73	**-3.71*** **	-6.78	**-2.49** *	2.14	0.20
SR-SL-SM	0.059	0.001	0.059	0.002	0.064	0.001	-7.25	**-3.36** **	-7.47	**-3.21** **	-0.23	-0.16
Subiculum	0.033	0.001	0.034	0.001	0.036	0.001	-7.33	-1.84	-5.17	-1.59	2.33	-0.33
Kulaga-Yoskovitz segmentation												
Hippocampus	0.482	0.006	0.489	0.007	0.505	0.005	-4.68	**-4.19*** **	-3.27	**-2.58** *	1.49	0.46
CA1-3	0.310	0.005	0.315	0.006	0.327	0.005	-5.23	**-3.90*** **	-3.87	-2.26	1.43	0.53
CA4-DG	0.049	0.001	0.049	0.001	0.050	0.001	-2.08	-0.90	-1.81	-0.96	0.27	-0.31
Subiculum	0.123	0.002	0.125	0.002	0.128	0.002	-4.30	**-2.71** **	-2.28	-1.89	2.12	0.28

Table 3.5: CERES Cerebellar Lobule Structural Differences

	AUD 1		AUD 2		CTL		AUD 1 vs CTL		AUD 2 vs CTL		AUD 2 vs AUD 1	
	x̄ %	**SEM**	**x̄ %**	**SEM**	**x̄ %**	**SEM**	**% Δ**	**t-Value**	**% Δ**	**t-Value**	**% Δ**	**t-Value**
Cerebellum	9.119	0.119	9.099	0.123	9.159	0.101	-0.44	-0.85	-0.65	-1.15	-0.21	-0.37
Lobule I-II	0.008	0.000	0.008	0.000	0.008	0.000	-0.81	-0.11	-5.06	-0.66	-4.29	-0.90
Lobule III	0.092	0.003	0.093	0.003	0.093	0.003	-0.72	-0.39	-0.47	-0.58	0.25	-0.22
Lobule IV	0.304	0.009	0.312	0.010	0.313	0.008	-2.73	-1.14	-0.42	-0.59	2.37	0.16
Lobule V	0.578	0.012	0.581	0.011	0.547	0.010	5.68	1.95	6.20	1.83	0.50	-0.24
Lobule VI	1.269	0.020	1.283	0.024	1.244	0.024	1.98	0.95	3.11	1.33	1.11	0.17
Lobule Crus I	1.884	0.046	1.877	0.049	1.901	0.044	-0.89	-0.58	-1.24	-0.87	-0.36	-0.50
Lobule Crus II	1.223	0.031	1.201	0.030	1.195	0.029	2.40	-0.19	0.51	-0.76	-1.85	-0.50
Lobule VIIB	0.696	0.015	0.690	0.017	0.681	0.011	2.32	-0.53	1.44	-1.21	-0.86	-0.31
Lobule VIIIA	0.851	0.018	0.837	0.019	0.863	0.016	-1.39	0.70	-2.92	-1.41	-1.55	-0.20
Lobule VIIIB	0.573	0.009	0.581	0.011	0.592	0.011	-3.11	1.03	-1.76	-0.40	1.40	0.50
Lobule IX	0.498	0.016	0.505	0.015	0.515	0.014	-3.38	-1.08	-2.02	-0.70	1.41	0.29
Lobule X	0.093	0.002	0.094	0.002	0.094	0.002	-1.60	-0.88	-0.65	-0.56	0.97	0.29

Table 3.6: Correlations of Large Brain Structural Changes

	AUDIT	ADS	Ethanol g/day	OCDS	CDS	ODS
Grey Matter	**-0.45*** **	**-0.49*** **	-0.17	-0.22	-0.26	-0.15
White Matter	-0.18	-0.04	-0.21	-0.21	-0.22	-0.17
Cerebrospinal Fluid	**0.40***	**0.40***	0.29	**0.26***	**0.29***	0.19
Cerebrum Total	**-0.43****	**-0.41****	-0.30	-0.21	-0.24	-0.13
Cerebrum GM	**-0.45*** **	**-0.52*** **	-0.21	-0.18	-0.21	-0.11
Cerebrum WM	-0.21	-0.04	-0.24	-0.21	-0.22	-0.16
Cerebellum Total	0.29	0.30	**0.40***	-0.23	-0.22	-0.20
Cerebellum GM	-0.18	-0.10	-0.01	-0.31	-0.30	-0.25
Cerebellum WM	**0.37***	**0.27***	**0.49***	-0.15	-0.14	-0.14
Brainstem	-0.09	0.03	**0.44****	-0.25	**-0.27***	-0.18

Table 3.7: Correlations of Deep Gray Matter Structural Changes

	AUDIT	ADS	Ethanol g/day	OCDS	CDS	ODS
Lateral Ventricles	0.29	**0.61*** **	0.04	**0.41*** **	**0.43*** **	**0.35****
Caudate	-0.41	-0.38	0.23	**-0.40****	**-0.33****	**-0.39****
Putamen	-0.31	-0.23	-0.13	-0.18	-0.05	-0.28
Thalamus	**-0.50***	-0.19	-0.12	**-0.31***	-0.27	-0.30
Globus Pallidus	-0.18	-0.24	-0.06	**-0.36***	-0.24	**-0.40****
Hippocampus	**-0.37****	-0.26	-0.27	-0.10	-0.20	-0.05
Amygdala	-0.22	-0.07	-0.24	-0.27	-0.25	-0.25
Accumbens	**-0.36***	**-0.41***	-0.23	-0.30	-0.24	-0.30

Table 3.8: Correlations of Hippocampus Structural Changes

	AUDIT	ADS	Ethanol g/day	OCDS	CDS	ODS
Winterburn segmentation						
Hippocampus	**-0.46*** **	-0.27	-0.31	-0.18	-0.27	-0.10
CA1	**-0.34***	**-0.42****	-0.31	-0.20	-0.23	-0.13
CA2-CA3	**-0.30****	**-0.34***	-0.23	**-0.30****	**-0.43*** **	-0.21
CA4-DG	**-0.42*** **	-0.05	-0.20	-0.24	**-0.47*** **	-0.08
SR-SL-SM	**-0.40****	-0.30	-0.29	-0.04	0.14	-0.09
Subiculum	**-0.41***	**0.34****	-0.11	0.24	**0.33****	0.14
Kulaga-Yoskovitz segmentation						
Hippocampus	**-0.41*** **	-0.14	-0.29	-0.11	-0.19	-0.03
CA1-3	**-0.39*** **	-0.19	-0.29	-0.27	**-0.36****	-0.15
CA4-DG	-0.20	-0.03	-0.09	-0.08	-0.14	-0.03
Subiculum	-0.25	-0.01	-0.19	**0.31****	**0.39****	0.21

Table 3.9: Correlations of CERES Cerebellar Lobule Structural Changes

	AUDIT	ADS	Ethanol g/day	OCDS	CDS	ODS
Cerebellum	0.33	0.24	0.36	-0.17	-0.14	-0.17
Lobule I-II	-0.08	-0.09	-0.22	0.23	-0.09	0.36
Lobule III	0.16	-0.20	0.18	-0.19	-0.34	-0.06
Lobule IV	-0.07	-0.30	0.23	-0.27	-0.26	-0.24
Lobule V	0.09	**-0.47***	0.10	-0.09	-0.07	-0.10
Lobule VI	-0.05	-0.31	0.05	-0.24	-0.31	-0.16
Lobule Crus I	0.30	0.25	**0.48*****	-0.19	-0.19	-0.16
Lobule Crus II	0.36	0.27	0.09	-0.09	0.10	-0.17
Lobule VIIB	0.27	0.27	0.13	0.06	0.10	0.01
Lobule VIIIA	0.18	0.25	0.07	0.03	0.01	0.04
Lobule VIIIB	0.22	0.35	0.06	0.05	0.09	-0.07
Lobule IX	0.16	0.43	0.15	-0.05	0.04	-0.08
Lobule X	0.21	0.01	0.18	-0.06	-0.16	0.08

Chapter 4 - White Matter Microstructure Changes during First Month of Recovery from Alcohol Use Disorder

Abstract

Alcohol use disorder (AUD) is associated with widespread structural brain damage, which is thought to disproportionately affect white matter microstructure. This damage might be at least partially reversible with sustained abstinence during recovery from AUD. Mechanism and timeline of the white matter recovery remain poorly understood. This study measured longitudinal differences in commonly used diffusion tensor imaging (DTI) scalars in 40 recently detoxified AUD men compared to 51 matched healthy volunteers at two time points – a baseline at 18 days of abstinence and follow-up at 35 days. AUD patients exhibited significantly lower axial diffusivity (AD) and fractional anisotropy (FA) while significantly higher radial diffusivity (RD) and mean diffusivity (MD) at both time points (AD -4.81%, -3.75%; FA -6.20%, -5.71%; MD +5.60%, +4.41%; RD +7.37%, +6.09%, respectively). Longitudinal changes in the patients were not significant but described a normalizing trend across all scalars (AD +1.12%; FA +0.52%; MD -1.13%; RD -1.20%). These changes suggest that AUD is associated with diffuse microstructural white matter damage which appears consistent with an axonal and/or myelin injury pattern, which experiences a small but positive recovery trend during the first month of sustained abstinence. Anatomical distribution of the affected white matter tracts spanned most of the brain, especially for FA. AD was not significantly decreased in the frontal and superior regions while MD and RD were not significantly increased in right posterior regions and cerebellum. Clinical severity scales were correlated with the magnitude of most of the DTI scalars' impairment. This study alludes to an encouraging trend of a microstructural brain healing process corresponding to the early stages of clinical AUD recovery.

Key terms

alcohol use disorder; abstinence; diffusion tensor imaging; fractional anisotropy; magnetic resonance imaging

1. Introduction

Alcohol use disorder (AUD) is one of the most prevalent, harmful and costly preventable disorders in the world, affecting over 283 million people and being responsible for approximately 5.1% of global burden of disease and 5.9% of all deaths globally (Nutt et al., 2010; World Health Organization, 2018). AUD (formerly also classified as alcohol dependence, alcohol addiction, harmful use of alcohol, or alcoholism) is a mental disorder characterized by uncontrolled recurrent excessive consumption of alcohol despite its significant interference in the individual's mental wellbeing, physical health, and ability to function in their daily lives (American Psychiatric Association & American Psychiatric Association, 2013). Cognitive and behavioural deficits underlying AUD's clinical progression and potential recovery are modulated through functional and structural changes in the alcohol dependent brain.

There is extensive evidence documenting structural brain damage associated with AUD (for reviews see (Bühler & Mann, 2011; Fritz et al., 2019; Harper et al., 2003)). Recurrent toxic exposure to alcohol, leads to wide-spread brain atrophy, enlargement of pericerebral spaces, as well as region-specific microstructural damage (including demyelination and glial cell loss; dendritic thinning, shrinking of cell bodies, and region-specific neuronal loss; inflammation, cell membrane damage, blood-brain barrier injury; *et cetera*) (Harper et al., 2003; Sutherland, Sheedy, & Kril, 2014a). The extent of cellular damage can be quite substantial, even in functionally neurocognitively uncomplicated AUD brains, with up to 27% regional neuronal loss (especially in the frontal cortex) and even more severe loss in the glial cells, with up to 37% regional loss in hippocampus (Korbo, 1999; Miguel-Hidalgo et al., 2002). Severity of alcohol abuse, including cumulative lifetime amount of alcohol consumption, has been correlated to the extent of cellular brain damage (Harding et al., 1996). White matter is often considered as especially vulnerable to alcohol-related damage and was historically thought to account for most of the overall AUD-related brain atrophy (Agartz et al., 2003; Fortier et al., 2014; Kril, Halliday, Svoboda, & Cartwright, 1997).

Neuroimaging studies have demonstrated wide-spread as well as region-specific structural white matter damage in AUD (for an overview see (M. Rosenbloom, Sullivan, & Pfefferbaum, 2003)). AUD has been associated with a complex pattern of structural deficits affecting disproportionately frontal and superior brain regions, including tracts linking prefrontal and limbic regions (Sullivan, Harris, & Pfefferbaum, 2010). Region-specific changes include thinning and microstructural deficits in corpus callosum (primarily in genu / anterior regions), pons / brain stem, cerebellar white matter, cingulum bundles, centrum semiovale, internal and external capsules, fornix, superior and inferior longitudinal fasciculi, fronto-occipital fasciculus, uncinate fasciculus, arcuate fasciculus, corona radiata, orbitofrontal white matter, frontolimbic fibres, hippocampus, corticopontine bundles, as well as more diffuse deficits in wider regions occupied by regional association fibres (Alhassoon et al., 2012; Monnig et al., 2014; Sullivan et al., 2010; Sullivan & Pfefferbaum, 2005; Yeh, Simpson, Durazzo, Gazdzinski, & Meyerhoff, 2009; Zahr, 2014). The complexity of the reported structural changes has made a synthesis of a unified narrative on AUD-related structural damage quite challenging. Monnig *et al.* has, therefore, performed a meta-analysis and reliably confirmed the robustness of the negative association between AUD and white matter structural integrity. This meta-analysis has also revealed a significant inverse association between the length of abstinence and magnitude of the AUD-related white matter structural damage (Monnig, Tonigan, Yeo, Thoma, & McCrady, 2013).

Several longitudinal and cross-sectional studies have confirmed this trend by demonstrating that alcohol-related structural damage is at least partially reversible with sustained abstinence (Sullivan & Pfefferbaum, 2005). Longer abstinence has been associated with white matter volume recovery (Agartz et al., 2003; Demirakca et al., 2011; Durazzo et al., 2015; Gazdzinski et al., 2010; O'Neill, Cardenas, & Meyerhoff, 2001; Shear et al., 1994), white matter microstructural recovery (Alhassoon et al., 2012; Gazdzinski et al., 2010; Pfefferbaum et al., 2014; Y. Zou et al., 2017), as well as normalization of underlying molecular neurochemical markers (Bendszus et al., 2001; Durazzo et al., 2006; Parks et al.,

2002; B. C. Schweinsburg et al., 2000) which are thought to describe underlying patterns of physiological stabilisation, increased neuronal integrity, as well as re-myelination and white matter recovery. Changes in these volumetric, microstructural, and molecular marker measurements have been also correlated to functional improvements in the recovering AUD patients (Alhassoon et al., 2012; Bendszus et al., 2001; Durazzo et al., 2006). Several studies have attempted to better characterize the trajectory of structural white matter recovery with sustained abstinence by deriving mathematical models describing the non-linear positive relationship between the variables (Mon et al., 2011). However, the clinical evidence documenting trajectory of white matter structural changes during sustained abstinence and recovery from AUD remain conflicting and incomplete (De Santis et al., 2019; Monnig, Tonigan, et al., 2013). Several studies have reported opposite findings, non-significant results, or failed to replicate published findings from independent modalities in comprehensive, unified, multimodal analyses.

Preclinical models of AUD have extensively documented possible mechanisms of AUD-related structural brain damage and subsequent recovery. The neurotoxic effect of AUD may follow repeated sequelae of acute intoxication (increased oxidative stress, toxic acetaldehyde and aldehydic metabolites, inflammation, chronic glutamate / calcium excitotoxicity, decreased pro-survival factors such as BDNF, decreased neurogenesis) while structural recovery might be due to degeneration stimulated regeneration, global abstinence-stimulated trophic NMDA receptor hyperactivity, or other mechanisms associated with rapid repair and neuro- and glio-genesis (occurring primarily within the first month of abstinence) (Crews & Nixon, 2009). The pre-clinical findings have, however, been difficult to translate into the clinical domain, partly due to the sparse and conflicting evidence describing the progression of AUD-related brain damage and recovery. The capacity for structural recovery of the AUD-related structural brain damage as well as the precise mechanisms associated with alcohol intoxication, AUD-related structural damage, and clinical recovery are not yet fully understood (R. A. Harris et al., 2008; Sutherland et al., 2014b; N. D. Volkow et al., 2017; Zahr & Pfefferbaum, 2017).

Our study has attempted to help address this gap, by documenting longitudinal changes in the white matter microstructure properties in a homogeneous clinical cohort undergoing supervised AUD recovery, compared to matched healthy controls, using magnetic resonance-based diffusion tensor imaging (DTI) and tract-based spatial statistics (TBSS). To the best of our knowledge, approximately thirty-five quantitative DTI studies in AUD have been published to this date. Only 5 of these have compared cross-sectional, mixed-design, or longitudinal differences, analyzing the effect of sustained abstinence on white matter microstructure using comparable techniques to our study (Alhassoon et al., 2012; De Santis et al., 2019; Gazdzinski et al., 2010; Pfefferbaum et al., 2014; Y. Zou et al., 2017).

DTI is a non-invasive quantitative neuroimaging technique which can indirectly assess microstructural integrity of white matter tracts by measuring the directionality of water diffusion in tissue (for review examples, see (Basser & Jones, 2002; Beaulieu, 2002; de Figueiredo, Borgonovi, & Doring, 2011; Soares, Marques, Alves, & Sousa, 2013)). Briefly, DTI can quantify the relative diffusion in different directions in each voxel. The directionality of the diffusion (anisotropy), can thus describe local patterns of restriction on the movement of water molecules, and thus help broadly elucidate the average microstructural properties of the analyzed tissue (which can change in relation to axon diameter, axonal density, fibre tract complexity, integrity of the cell membranes and myelin sheaths, etc.). Water molecules experience random Brownian motion in an unobstructed environment (such as cerebrospinal fluid in the ventricles) and thus on average will not exhibit any directional-dependence in their movement, and would thus be isotropic. On the other hand, tightly packed dense environment of white matter tracts will selectively obstruct the random movement of water molecules perpendicular to the axis of the axons, due to poorly permeable myelin sheaths, cell membranes, and other cellular and extracellular components. The water molecules in the white matter tracts will, therefore, experience a hindered diffusion pattern with greater directionality in parallel rather than perpendicular to the tightly packed axons and thus exhibit large average anisotropy in the analysed voxel. Commonly reported DTI scalars used to summarize the diffusion properties include, axial diffusivity (AD), fractional anisotropy (FA), mean

diffusivity (MD; also referred to as apparent diffusion coefficient), and radial diffusivity (RD). These different measures can help characterize microstructural tissue properties. In comparison to a reference value, they can also help elucidate changes in microstructural tissue integrity such as demyelination or axonal injury (Beaulieu, 2002; Pfefferbaum & Sullivan, 2005). Compared to traditional morphometric techniques, DTI has been also demonstrated to outperform in its sensitivity, detecting patterns of underlying white matter changes before they became apparent to the other techniques (Pfefferbaum & Sullivan, 2002, 2005; Pfefferbaum et al., 2000). In order to facilitate a more robust group-level analysis, this study has selected tract-based spatial statistics (TBSS; (Smith et al., 2006)) to analyze the DTI data. TBSS creates a mean FA skeleton representing the centre of major white matter bundles common to all subjects and projects the average DTI scalar values to the skeleton voxels. This technique should minimize anatomic distortion due to acquisition artifacts, reduce partial volume effects, and thus improve the sensitivity, objectivity, and interpretability of our results, although it also includes several drawbacks such as lack of anatomical specificity of the sample-based skeletons or incorrect characterisation of multi-directional crossing or merging fibres, which are to some extent present in most white matter voxels (M. Bach et al., 2014; Jones, Knösche, & Turner, 2013; Smith et al., 2006).

Our hypotheses were that (1) AUD patients will exhibit a middle to high single percentage drop in FA and AD and increase in MD and RD; 2) longitudinal differences in the AUD group will exhibit a positive middle single digit percentage increase; and 3) the magnitude of the DTI scalar structural damage will correlate to the measures of AUD clinical severity. Although the directionality of changes in FA and MD have been quite extensively documented in both short-term and long-term abstinent AUD patients, their magnitude as well as directionality and magnitude of changes in the other scalars remain poorly documented in the literature with conflicting reports.

2. Materials and Methods

2.1 Subjects

The analysis is based on longitudinal data from 40 recently detoxified adult male alcohol dependent patients (DSM-IV-TR criteria)(American Psychiatric Association, 2000) and matched 51 healthy non-alcohol abusing men. The demographic and clinical overview of the 91 participants is summarized in Table 4.1.

The alcohol dependent participants were recruited from a pool of patients referred to supervised residential treatment programs in Edmonton, Canada and Mannheim, Germany as part of the TRANSALC research project. DSM-IV-TR diagnostic interviews were carried out by a psychiatrist, using the Structured Clinical Interview for the DSM-IV-TR (SCID-I) (First et al., 2002). All of the patients were consistent, steady, heavy drinkers. All of the analyzed patients met the highest Zone IV cut-off score on the Alcohol Use Disorders Identification Test (AUDIT) with an average score of 28 out of 40 (Saunders et al., 1993). The AUD patients exhibited on average an intermediate level of alcohol dependence (second quartile) according to the Alcohol Dependence Scale (ADS) with the average score of 17 out of 47 (Skinner & Allen, 1982). The patients did not abuse non-beverage ethanol or other substances except nicotine. The patients were recruited within the first two weeks of abstinence and underwent longitudinal scanning sessions at two time points: first after approximately two weeks of abstinence (17.82 days on average) and second after approximately one month of abstinence (35.15 days on average). Abstinence was verified at each scanning session in all participants by an alcohol breathalyser (BACtrack S50 Personal Breathalyzer, Portable Breath Alcohol Tester) and a urine drug screen (nal von minden GmbH Drug-Screen® Diptest, Version 1.0).

Controls were recruited concurrently to match the patients' general demographic profile (including sex, age, handedness, general occupation/education background). The controls had no history of alcohol or

drug addiction and consumed alcohol below the Canada's Low-Risk Alcohol Drinking Guidelines (Butt, 2011). Participants in both arms were excluded if they had any history of serious medical (including psychiatric or neurological) complications, brain injury, use of psychotropic medications (other than during the detoxification process), or did not meet magnetic resonance safety criteria for our imaging facilities. The study was approved by the University of Alberta Health Research Ethics Board (study ID: Pro00019424).

Table 4.1: Summary of Key Demographic and Clinical Variables

	AUD Patients (n=40)		Controls (n=51)				
	Mean	**SEM**	**Mean**	**SEM**	**% Δ**	**t-value**	**sig.**
Age	44.65	1.51	42.41	1.43	5	1.07	not sig
Ethanol (grams/day)	265.28	29.60	5.40	0.77	4,813	9.82	***
AUDIT	28.08	0.87	2.62	0.29	972	30.56	***
ADS	17.00	1.31	1.66	0.31	924	12.58	***
OCDS	18.92	1.27	1.34	0.19	1,312	14.77	***
ODS	6.85	0.74	0.19	0.10	3,505	9.59	***
CDS	12.08	0.64	1.15	0.16	950	17.69	***
Abstinence 1 (days)	17.82	1.25	N/A				
Abstinence 2	35.15	1.23	N/A				

*p<0.05, ** p<0.01, *** p<0.001 Bonferroni-corrected; SEM = standard error of mean

2.2 MRI Acquisition

The neuroimaging data was acquired at two clinical sites. Canadian data was acquired using 4.7 Tesla Varian Inova whole-body MRI scanner, located at the University of Alberta, Edmonton. German data was acquired using 3 Tesla Siemens MAGNETOM TRIO whole-body MRI scanner, located at the Central Institute of Mental Health, Mannheim. The scanning protocol included anatomic imaging using T1-weighted magnetization-prepared rapid acquisition echo (MPRAGE) as well as diffusion tensor imaging (DTI) scans. The MPRAGE acquisition parameters were TR 1505.9 ms, inversion time 300.0 ms, relaxation delay time (after readout prior to inversion) 300.0 ms, linear phase encoding, TE 3.71 ms, matrix 240×192×128, field of view 240×192×192 mm^3, 1.0×1.0×1.5 mm^3 voxels, whole brain coverage. Edmonton DTI scans were acquired using echo planar imaging sequence with TR 7.5 ms, TE of 52.31

ms, 30 diffusion-encoding directions with b-value of 996 s/mm^2, 5 non-diffusion-weighted images (b-value 0 s/mm^2), with whole-brain coverage, matrix size 120×120×80, 2 mm^3 isotropic voxels, with 80 slices with no interslice gap. The German DTI scans were acquired using echo planar imaging sequence with TR 14 ms, TE of 84 ms, 41 diffusion-encoding directions with b-value of 1,000 s/mm^2, 1 non-diffusion-weighted images, with whole-brain coverage, matrix size 128×128×64, 2 mm^3 isotropic voxels, with 64 slices with no interslice gap.

All of the scans were visually reviewed by two independent neuroimaging experts for gross abnormalities. None of the subjects exhibited any clinically significant structural abnormalities other than what may be expected from normal aging or prolonged alcohol abuse.

The raw data was also anonymized before any pre-processing and the researchers were blinded to the subject or group label key until the final statistical analysis.

2.3 Diffusion Tensor Preprocessing

Diffusion tensor imaging (DTI) preprocessing was performed using FMRIB Software Library version 6.0 (FSL; https://fsl.fmrib.ox.ac.uk/fsl/fslwiki/FSL; (Jenkinson, Beckmann, Behrens, Woolrich, & Smith, 2012)). The anonymized data was reconstructed and quality checked for imaging artifacts, signal dropout, or partial brain coverage in both anatomical MPRAGE and associated DTI scans. The acceptable raw data was then pre-processed through FSL Diffusion Toolbox (FDT; (Behrens et al., 2003)), where the DTI volumes were corrected for eddy currents and subject motion distortions (EDDY; (J. L. R. Andersson & Sotiropoulos, 2016)), de-skulled (masked based on BET-extracted brain image from the b0 average image (Smith, 2002)), and fitted with voxel-specific diffusion tensors (DTIFIT; (Behrens et al., 2003)). The output of diffusion tensor model included axial diffusivity (AD; output as first eigenvalue L1), fractional anisotropy (FA), mean diffusivity (MD), and radial diffusivity (RD; calculated as the average of 2nd and

3rd eigenvalues). All of the output images were inspected for any abnormalities. Voxelwise statistical analysis of the tensor data was performed using Tract-Based Spatial Statistics toolbox (TBSS; (Smith et al., 2006)).

Using the TBSS toolbox, a two-step normalization was performed using the most-representative FA volume and associated anatomical scan to guide non-linear registration (using FNIRT; (J. L. Andersson, Jenkinson, & Smith, 2007)) to a 1 mm^3 isotropic MNI152 template, to transform all of the DTI scalar images into the standard MNI space. A mean FA image from all of the normalized data was calculated and thinned to create a mean FA skeleton, representing lines of voxels of highest FA values at the centre of all white matter tracts which were common to all of the volumes. Each of the individual normalized FA images was then projected onto this mean FA skeleton. This projection process was repeated for all of the associated AD, MD, and RD images. The skeletonized images should help minimize interscan spatial normalization imperfections between different subjects. Quality assurance checks were performed at each of the TBSS steps. The skeletonized FA, AD, MD, and RD scalars in the MNI space were subsequently fed into voxel-wise group statistical analysis.

2.5 Statistical Analyses

After the quality assurance of the DTI scalar skeletons was complete, the label key was returned to the blinded researcher to allow for group comparison and statistical analysis.

The participant profile summary statistics and group comparison were generated using SPSS (version 20) (IBM Corp, 2011) and MATLAB (version R2018b) (The MathWorks Inc, 2018). The summary statistics included group mean ($\bar{x}$) and standard error of mean (SEM). After verifying validity of the assumptions (including Levene's test of homogeneity), two sample t-tests were used to compare group differences (Δ).

The input data for demographic and clinical summary statistics was not corrected for nuisance variables (such as age).

The neuroimaging group comparison analysis was performed using general linear models and voxel-wise non-parametric permutation tests in FSL (Jenkinson et al., 2012). The linear models included predictors for group status (dummy variables for first and second scans for patients and controls) as well as z-normalized nuisance variables (scanning site, age, and length of abstinence at first scan). The contrasts compared first time point group differences, second time point group differences, as well as interscan longitudinal differences in the AUD group. The group differences were tested using 10,000 permutations in FSL's Randomise algorithm with Threshold-Free Cluster Enhancement (TFCE), using the recommended TBSS skeleton parameters (Winkler, Ridgway, Webster, Smith, & Nichols, 2014).

Post-hoc region-of-interest analysis was performed using normalized data extracted from the significant clusters identified in the neuroimaging group analysis. The significance of the Pearson correlation coefficients to the clinical severity scales was tested using two-tailed t-tests. Anatomical location of the significant clusters was summarized using John Hopkins University DTI-based white matter atlas (Mori, Wakana, Van Zijl, & Nagae-Poetscher, 2005).

For all analyses, the null hypothesis was rejected and group differences were considered as significant at a global alpha threshold of 0.05. The p-values were corrected for multiple comparison using Family-Wise Error (FWE) correction. FWE-correction was estimated either through permutations for neuroimaging data or using Bonferroni method for summary statistics and post-hoc comparisons (Bonferroni, 1936).

3 Results

3.1 Participant profile

The healthy controls were recruited to match the general demographic profile of the AUD patients. As a result, the groups were not significantly different in their general demographic profile. The clinical measures were 9 to 48 times more severe in the AUD group than in the healthy control, as summarized in Table 4.1.

3.2 Longitudinal Differences in the White Matter Microstructure

Detoxified AUD patients have demonstrated significantly lower axial diffusivity (AD) and fractional anisotropy (FA) while significantly greater mean diffusivity (MD) and radial diffusivity (RD) at both 18 days and 35 days, compared to matched healthy controls. The longitudinal interscan comparison during the first month of sustained abstinence did not reveal significant improvement in the AUD group, although a generally positive trend persisted. Figure 4.1 to Figure 4.4 illustrate these changes (red signifying increase while blue signifying decrease).

Table 4.2 provides a summary of the raw diffusion scalars in different groups. Table 4.3 provides a quantitative overview of the average group differences depicted in Figure 4.1 to Figure 4.4. Note the non-significant improvement trend in both increasing AD and FA values as well as decreasing MD and RD values at the follow-up scan. Table 4.4 provides MNI coordinates of peak voxels as well as the cluster as centre-of-gravity (COG). Due to the implementation of skeletonized projections in the statistical analysis and wide-spread clusters, both the peak as well as the centre-of-gravity provide only limited interpretive value. As a result, we have also provided a summary of the anatomical regions through which the significant cluster skeletons have been passing, according to the John Hopkins University DTI-based white matter atlas (Mori et al., 2005) in the following paragraphs.

Clusters of significantly lower axial diffusivity in the AUD patients compared to healthy controls at the first time point included the following regions: cerebellar peduncle (left, right, middle, superior); pontine crossing tract; corpus callosum (body, splenium); corticospinal tract (bilateral); medial lemniscus (left); cerebral peduncle (bilateral); anterior limb of internal capsule (bilateral); posterior limb of internal capsule (bilateral); retrolenticular part of internal capsule (bilateral); anterior corona radiata (left); superior corona radiata (bilateral); posterior corona radiata (bilateral); posterior thalamic radiation (including optic radiation; bilateral); sagittal stratum (including inferior longitudinal fasciculus and inferior fronto-occipital fasciculus; bilateral); external capsule (bilateral); cingulum (right); fornix / stria terminalis (bilateral); superior longitudinal fasciculus (bilateral); and uncinate fasciculus (right). Clusters of significantly lower axial diffusivity in the AUD patients compared to healthy controls at the second time point included the following regions: cerebellar peduncle (middle, right superior, right inferior); pontine crossing tract; corpus callosum (body, splenium); corticospinal tract (bilateral); medial lemniscus (bilateral); inferior cerebellar peduncle (right); superior cerebellar peduncle (right); cerebral peduncle (bilateral); anterior limb of internal capsule (bilateral); posterior limb of internal capsule (bilateral); retrolenticular part of internal capsule (bilateral); superior corona radiata (right); posterior thalamic radiation (including optic radiation; bilateral); sagittal stratum (including inferior longitudinal fasciculus and inferior fronto-occipital fasciculus; bilateral); external capsule (bilateral); cingulum (right); fornix / stria terminalis (bilateral); superior longitudinal fasciculus (bilateral); and tapetum (right). Therefore, at the second time point, axial diffusivity changes in left anterior corona radiata, left superior corona radiata, left posterior corona radiata, as well right uncinate fasciculus were no longer significant. On the other hand, right medial lemniscus, right inferior cerebellar peduncle, and right tapetum showed additional significant decrease of axial diffusivity in the AUD group at the second time point.

Clusters of significantly lower fractional anisotropy in the AUD patients compared to healthy controls at the first time point included the following regions: cerebellar peduncle (middle, left inferior; right

superior); pontine crossing tract; corpus callosum (genu, body, splenium); fornix (column and body of fornix); corticospinal tract (bilateral); cerebral peduncle (bilateral); anterior limb of internal capsule (bilateral); posterior limb of internal capsule (bilateral); retrolenticular part of internal capsule (bilateral); anterior corona radiata (bilateral); superior corona radiata (bilateral); posterior corona radiata (bilateral); posterior thalamic radiation (including optic radiation; bilateral); sagittal stratum (including inferior longitudinal fasciculus and inferior fronto-occipital fasciculus; bilateral); external capsule (bilateral); cingulum (bilateral; left hippocampus); fornix / stria terminalis (bilateral); superior longitudinal fasciculus (bilateral); superior fronto-occipital fasciculus (right); uncinate fasciculus (bilateral); and tapetum (bilateral). Clusters of significantly lower fractional anisotropy in the AUD patients compared to healthy controls at the second time point included the following regions: cerebellar peduncle (middle; bilateral inferior and superior); corpus callosum (genu, body, splenium); fornix (column and body of fornix); corticospinal tract (right); cerebral peduncle (bilateral); anterior limb of internal capsule (bilateral); posterior limb of internal capsule (bilateral); retrolenticular part of internal capsule (bilateral); anterior corona radiata (bilateral); superior corona radiata (bilateral); posterior corona radiata (bilateral); posterior thalamic radiation (include optic radiation; bilateral); sagittal stratum (include inferior longitudinal fasciculus and inferior fronto-occipital fasciculus; bilateral); external capsule (bilateral); cingulum (bilateral); fornix / stria terminalis (bilateral); superior longitudinal fasciculus (bilateral); superior fronto-occipital fasciculus (right); uncinate fasciculus (bilateral); and tapetum (bilateral). Therefore, at the second time point, differences in lower fractional anisotropy in the pontine crossing tract, left corticospinal tract, and left hippocampal portion of cingulum were no longer significant, while cerebellar peduncle and superior cerebellar peduncle showed bilaterally significant changes in the fractional anisotropy.

Clusters of significantly higher mean diffusivity in the AUD patients compared to healthy controls at the first time point included the following regions: corpus callosum (genu, body, splenium); fornix (column and body of fornix); anterior limb of internal capsule (bilateral); posterior limb of internal capsule

(bilateral); retrolenticular part of internal capsule (left); anterior corona radiata (bilateral); superior corona radiata (bilateral); posterior corona radiata (left); posterior thalamic radiation (including optic radiation; left); sagittal stratum (including inferior longitudinal fasciculus and inferior fronto-occipital fasciculus; left); external capsule (bilateral); cingulum (left); fornix / stria terminalis (bilateral); superior longitudinal fasciculus (bilateral); uncinate fasciculus (left); and tapetum (left). Clusters of significantly higher mean diffusivity in the AUD patients compared to healthy controls at the second time point included the following regions: corpus callosum (genu, body, splenium); fornix (column and body of fornix); anterior limb of internal capsule (bilateral); posterior limb of internal capsule (bilateral); retrolenticular part of internal capsule (left); anterior corona radiata (bilateral); superior corona radiata (bilateral); posterior corona radiata (left); posterior thalamic radiation (including optic radiation; left); external capsule (bilateral); cingulum (left); fornix / stria terminalis (right); superior longitudinal fasciculus (bilateral); superior fronto-occipital fasciculus (right); uncinate fasciculus (bilateral); and tapetum (left). Therefore, at the second time point, abnormally high mean diffusivity differences in the left sagittal striatum were no longer significant in the AUD group. On the other hand, abnormally high mean diffusivity in the left fornix, superior fronto-occipital fasciculus, and right uncinate fasciculus reached significance.

Clusters of significantly higher radial diffusivity in the AUD patients compared to healthy controls at the first time point included the following regions: corpus callosum (genu, body, splenium); fornix (column and body of fornix); cerebral peduncle (bilateral); anterior limb of internal capsule (bilateral); posterior limb of internal capsule (left); retrolenticular part of internal capsule (left); anterior corona radiata (bilateral); superior corona radiata (bilateral); posterior corona radiata (bilateral); posterior thalamic radiation (including optic radiation, bilateral); sagittal stratum (including inferior longitudinal fasciculus and inferior fronto-occipital fasciculus, left); external capsule (bilateral); cingulum (left cingulate gyrus and hippocampus); fornix / stria terminalis (bilateral); superior longitudinal fasciculus (bilateral); superior fronto-occipital fasciculus (right); uncinate fasciculus (left); and tapetum (bilateral). Clusters of significantly higher radial diffusivity in the AUD patients compared to healthy controls at the second time

point included the following regions: corpus callosum (genu, body, splenium); fornix (column and body of fornix); anterior limb of internal capsule (bilateral); posterior limb of internal capsule (bilateral); retrolenticular part of internal capsule (bilateral); anterior corona radiata (bilateral); superior corona radiata (bilateral); posterior corona radiata (bilateral); posterior thalamic radiation (including optic radiation; bilateral); sagittal stratum (including inferior longitudinal fasciculus and inferior fronto-occipital fasciculus, bilateral); external capsule (bilateral); cingulum (left cingulate gyrus and hippocampus); fornix / stria terminalis (bilateral); superior longitudinal fasciculus (bilateral); superior fronto-occipital fasciculus (right); uncinate fasciculus (bilateral); and tapetum (bilateral). Therefore, the interscan differences during the first month of sustained abstinence included, lack of significance in abnormally high radial diffusivity of the cerebral peduncle, while posterior limb of internal capsule, retrolenticular part of internal capsule, sagittal striatum, and uncinate fasciculus all showed significant changes across both hemisphere and not just the left hemisphere, as observed in the first set of scans.

Figure 4.1: Longitudinal Changes in Axial Diffusivity (AD) during AUD Recovery

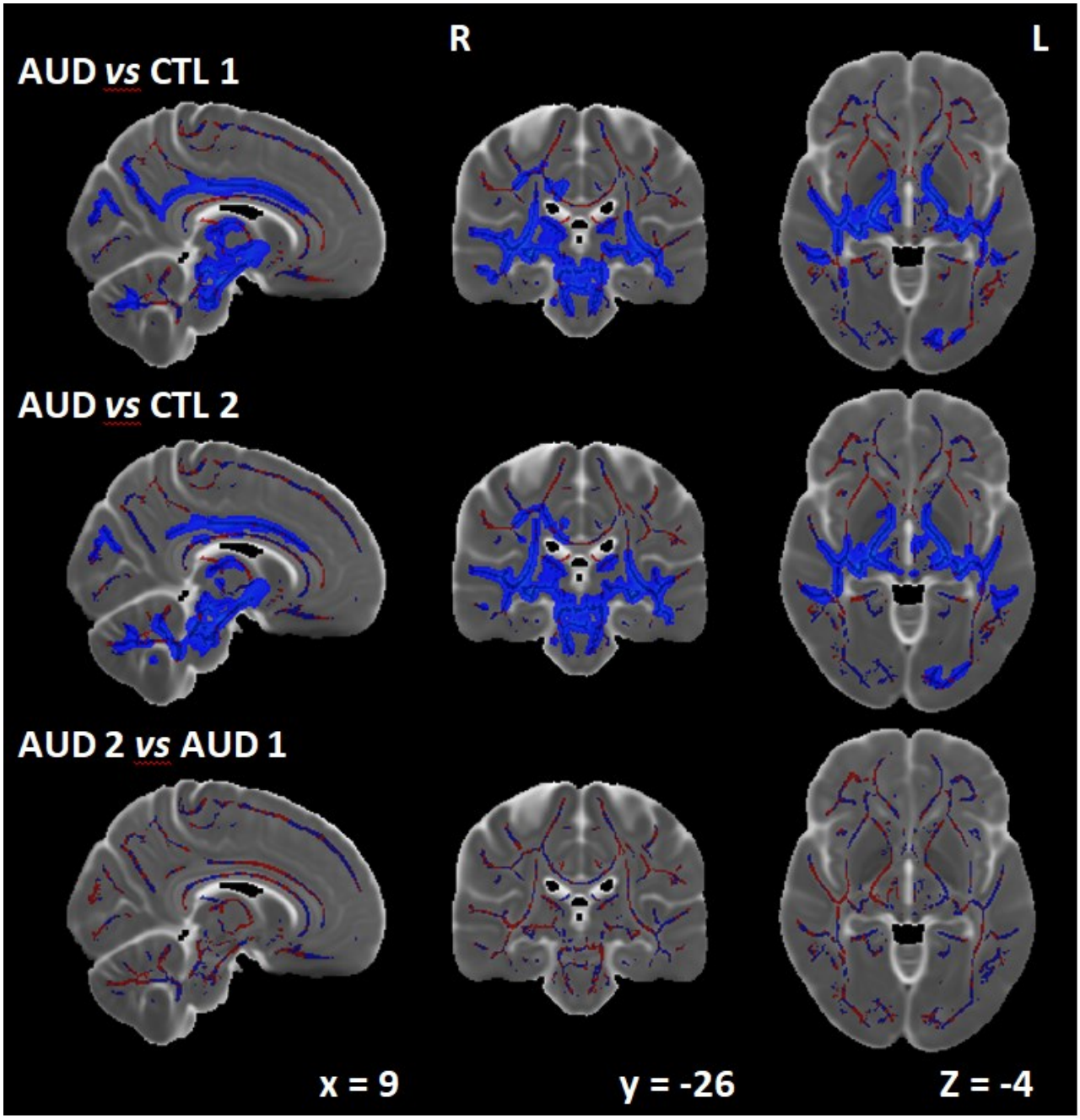

Figure 4.1depicts t-map skeleton projections (blue decrease, red increase) overlayed with filled-in significant p-maps (bright blue indicating significantly lower AD; FWE corrected for multiple comparison) of the longitudinal changes in AD in recovering AUD patients. Top row indicates abnormally low AD at approximately 18 days of abstinence. Middle row depicts persistent abnormally low AD at approximately 35 days of abstinence. Bottom row indicates lack of significant longitudinal interscan changes in the AUD group. Images are projected on HCP1065 template in MNI space. (AD = axial diffusivity; AUD = alcohol use disorder group; CTL = healthy control group)

Figure 4.2: Longitudinal Changes in Fractional Anisotropy (FA) during AUD Recovery

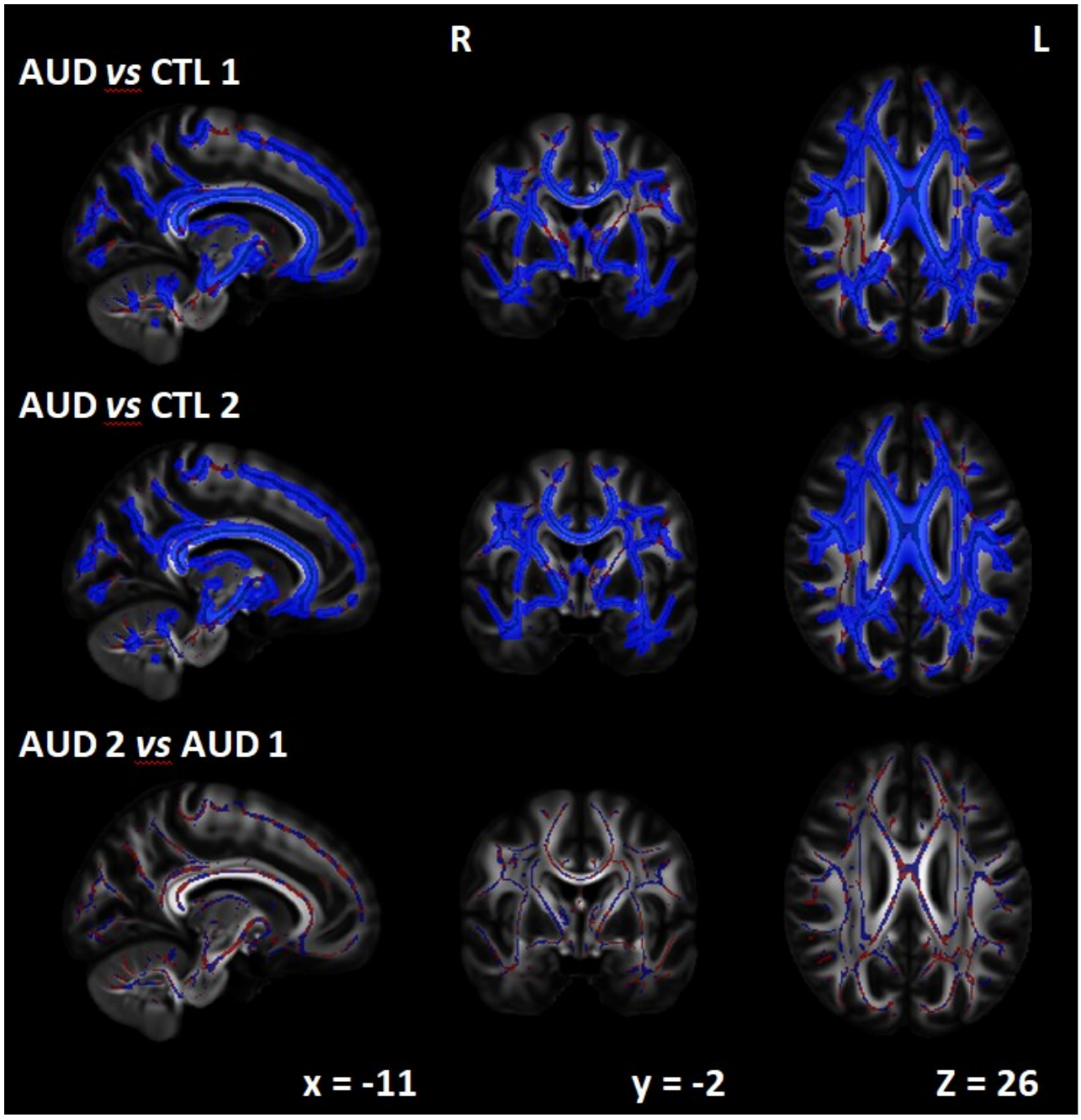

Figure 4.2 depicts t-map skeleton projections (blue decrease, red increase) overlayed with filled-in significant p-maps (bright blue indicating significantly lower FA; FWE corrected for multiple comparison) of the longitudinal changes in FA in recovering AUD patients. Top row indicates abnormally low FA at approximately 18 days of abstinence. Middle row depicts persistent abnormally low FA at approximately 35 days of abstinence. Bottom row indicates lack of significant longitudinal interscan changes in the AUD group. Images are projected on HCP1065 template in MNI space. (FA = fractional anisotropy; AUD = alcohol use disorder group; CTL = healthy control group)

Figure 4.3: Longitudinal Changes in Mean Diffusivity (MD) during AUD Recovery

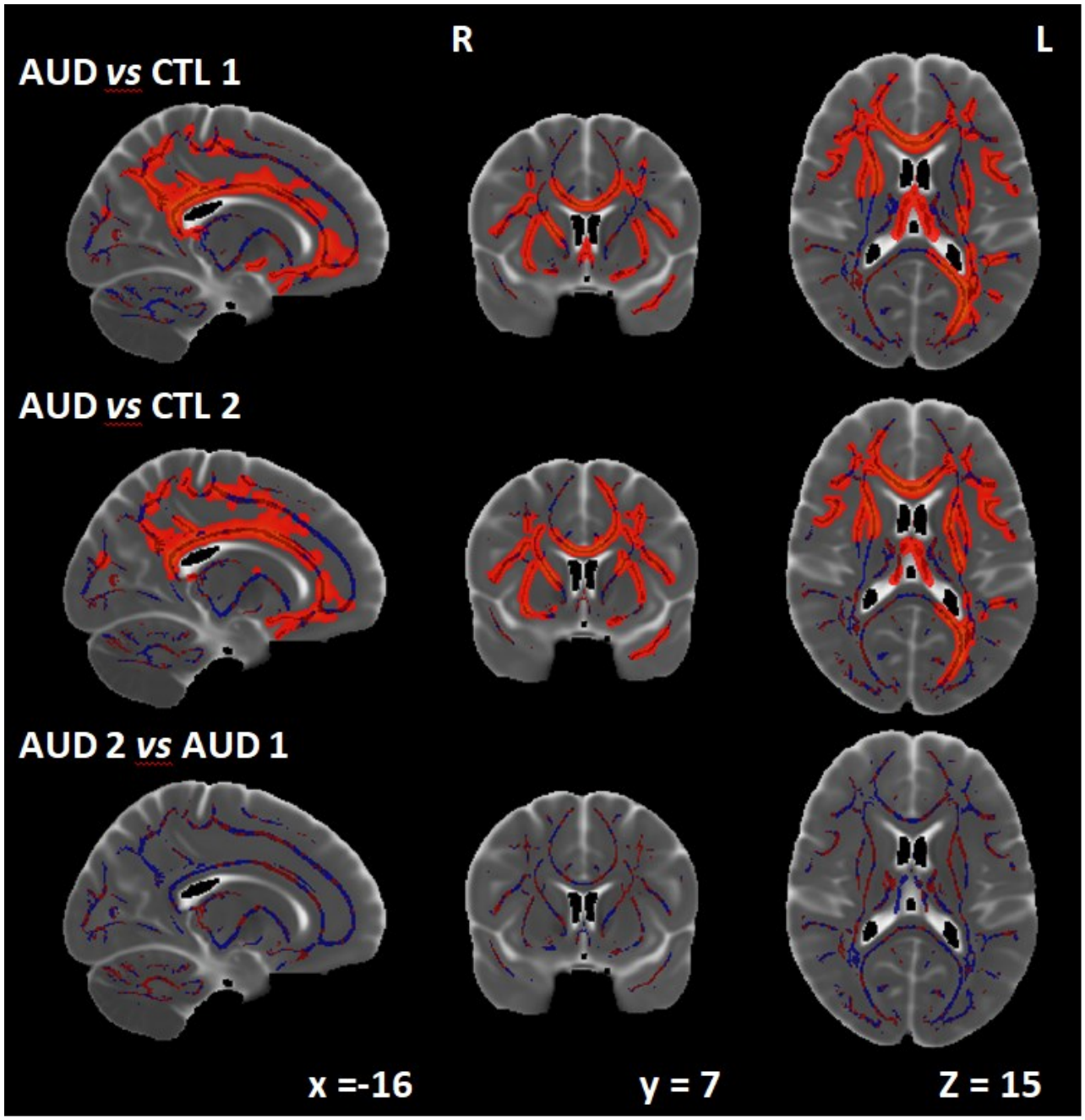

Figure 4.3 depicts t-map skeleton projections (blue decrease, red increase) overlayed with filled-in significant p-maps (bright red indicating significantly higher MD; FWE corrected for multiple comparison) of the longitudinal changes in MD in recovering AUD patients. Top row indicates abnormally high MD at approximately 18 days of abstinence. Middle row depicts persistent abnormally high MD at approximately 35 days of abstinence. Bottom row indicates lack of significant longitudinal interscan changes in the AUD group. Images are projected on HCP1065 template in MNI space. (MD = mean diffusivity; AUD = alcohol use disorder group; CTL = healthy control group)

Figure 4.4: Longitudinal Changes in Radial Diffusivity (RD) during AUD Recovery

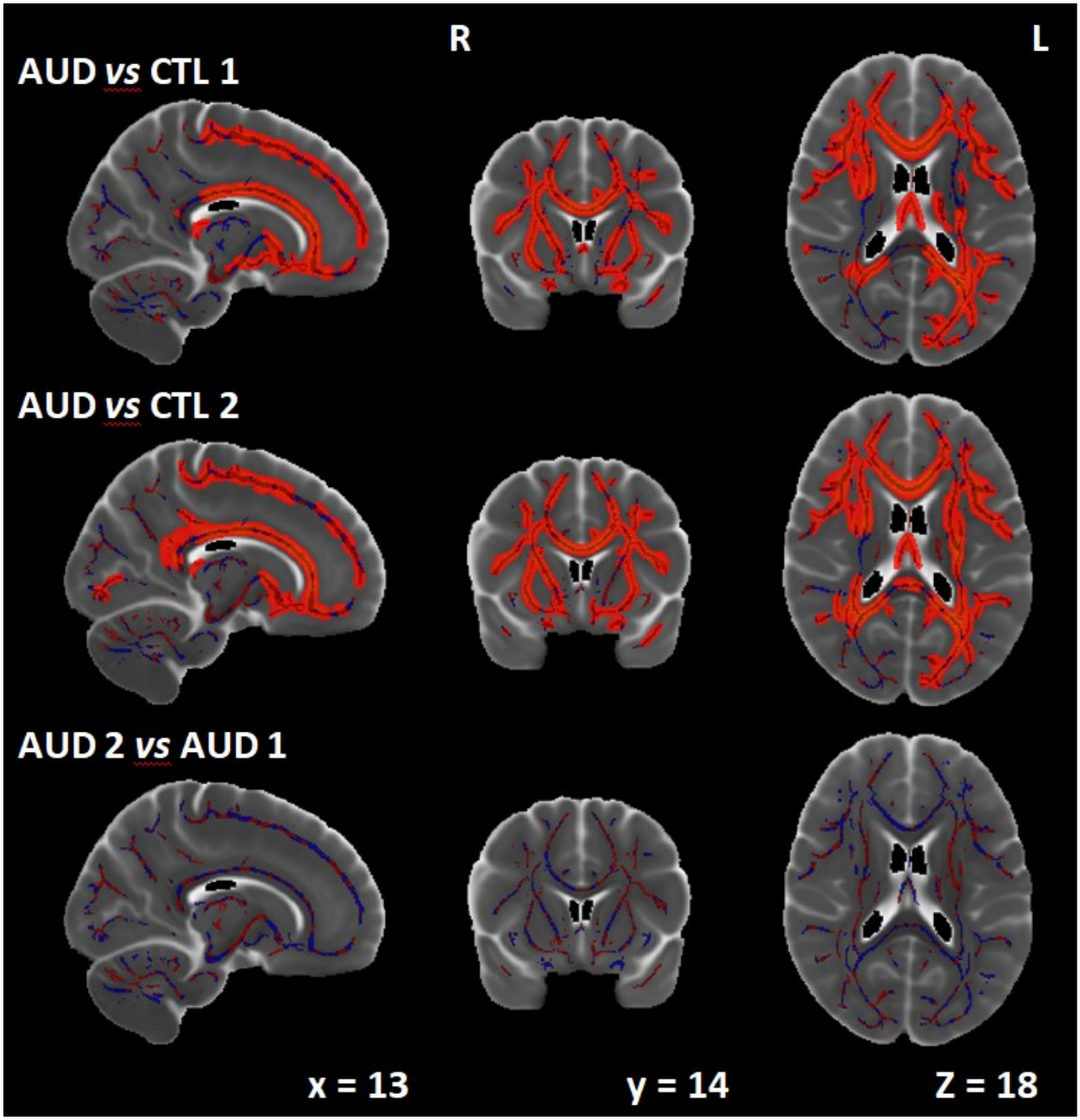

Figure 4.4 depicts t-map skeleton projections (blue decrease, red increase) overlayed with filled-in significant p-maps (bright red indicating significantly higher RD; FWE corrected for multiple comparison) of the longitudinal changes in RD in recovering AUD patients. Top row indicates abnormally high RD at approximately 18 days of abstinence. Middle row depicts persistent abnormally high RD at approximately 35 days of abstinence. Bottom row indicates lack of significant longitudinal interscan changes in the AUD group. Images are projected on HCP1065 template in MNI space. (RD = radial diffusivity; AUD = alcohol use disorder group; CTL = healthy control group)

Table 4.2: Summary of DTI Scalar Longitudinal Values from Significant Regions

	AUD 1		AUD 2		CTL	
	$\bar{x}$	SEM	$\bar{x}$	SEM	$\bar{x}$	SEM
AD	1.06E-03	6.57E-06	1.07E-03	4.31E-06	1.11E-03	4.31E-06
FA	4.19E-01	2.66E-03	4.22E-01	2.50E-03	4.47E-01	2.56E-03
MD	7.99E-04	4.61E-06	7.90E-04	4.31E-06	7.57E-04	3.86E-06
RD	5.77E-04	4.28E-06	5.70E-04	4.00E-06	5.37E-04	3.79E-06

SEM = standard error of mean

Table 4.3: Longitudinal and Group Differences in DTI Scalars in Significant Regions

	AUD vs CTL 1			AUD vs CTL 2			AUD 2 vs AUD 1		
	Δ %	t-value	sig.	Δ %	t-value	sig.	Δ %	t-value	sig.
AD	-4.81	-7.06	***	-3.75	-5.77	***	1.12	1.33	not sig
FA	-6.20	-7.43	***	-5.71	-7.01	***	0.52	0.60	not sig
MD	5.60	7.10	***	4.41	5.77	***	-1.13	-1.43	not sig
RD	7.37	6.93	***	6.09	5.89	***	-1.20	-1.18	not sig

*p<0.05, ** p<0.01, *** p<0.001 Bonferroni-corrected

Table 4.4: MNI Coordinates of Significant Clusters from 1st and 2nd Group Comparisons

Comparison	Voxels	MAX X (mm)	MAX Y (mm)	MAX Z (mm)	COG X (mm)	COG Y (mm)	COG Z (mm)
AD 1	20282	-4	-29	-25	14	-29.2	9.16
	853	26	-51	-37	19.8	-59.5	-32.7
	664	-14	-86	-3	-22.8	-83.5	1.35
	577	-13	-81	20	-15.6	-81.5	22.8
	454	-19	-59	-32	-18.6	-55.9	-34.3
	326	-19	34	26	-18.3	32.1	25.7
	221	18	27	37	18.7	25.2	35.8
	96	-18	-6	42	-18.2	-5.6	42.8
	21	-19	-70	38	-19.1	-69.2	37.1
	9	-24	-2	-12	-24.8	-2.56	-11.1
	4	-27	-82	-8	-26.5	-81.5	-8
	4	-26	-65	27	-25.3	-64.3	27.7
	2	-27	-2	-12	-27.5	-2	-12
	2	-32	-66	3	-32	-66	3.5
AD 2	22876	-6	-26	-30	3.54	-37.7	4.01
	100	-24	-47	-36	-22.8	-52.7	-35
	82	21	-51	23	23.9	-51.8	21.7
	37	52	-29	-12	51.5	-29.7	-11.6
FA 1	61577	-34	-1	-36	-2.09	-14.7	14.8
	2261	23	-60	-21	-2.59	-57.6	-25.1
FA 2	66552	-32	2	-38	0.617	-16.3	15.4
	2906	19	-64	-23	7.69	-58.7	-28.7
	793	-29	-45	-29	-19.3	-51.2	-22.9
	66	-31	-40	49	-31.8	-41.7	49.2
	31	-39	32	6	-37.8	32.6	7.19
MD 1	19558	-20	-50	9	-6.69	-11	23.1
	6570	-24	21	-6	-30.2	4.77	-6.31
	1153	3	1	4	-1.82	-16.3	8.99
	4	-23	-68	0	-23.7	-68	0.25
MD 2	25905	-31	-44	35	-9.02	-3.08	20.1
	364	-2	-14	18	-1.69	-13.2	13.7
	105	20	-35	8	13.4	-30	11.6
	17	-21	-36	6	-19.4	-36.4	6.94
RD 1	45918	14	33	1	-9.45	-9.84	16.9
	162	22	-49	19	23.5	-50.6	19.3
	81	-13	-14	-14	-13	-13.4	-12.5
	63	32	-49	16	32.3	-48.8	17.6
	6	34	-46	12	34	-45.2	12.2
RD 2	49207	33	7	2	-2.04	-12.2	18.1
	598	-2	-15	16	1.06	-18.7	13

COG = centre of gravity

3.3 Correlation between White Matter Microstructural Properties and Clinical Severity

All of the tested clinical severity scales – Alcohol Use Disorders Identification Test (AUDIT), Alcohol Dependence Scale (ADS), Obsessive Compulsive Drinking Scale (OCDS) and its obsessive (ODS) and compulsive (CDS) subscales, as well as average ethanol consumption before detoxification showed positive correlation with increasing MD and RD values and negative correlation with decreasing AD and FA values in a post-hoc analysis. FA and RD showed significant correlation with all clinical severity scales, whole AD only with AUDIT and CDS and MD with all but CDS. The correlation values are summarized in Table 4.5.

Table 4.5: Pearson Correlations of Clinical Severity to DTI Scalar

	AUDIT	ADS	OCDS	ODS	CDS	# Drinks
AD	-0.28 ***	-0.05	-0.15	-0.07	-0.20 **	-0.10
FA	-0.39 ***	-0.27 ***	-0.35 ***	-0.32 ***	-0.35 ***	-0.30 ***
MD	0.39 ***	0.34 ***	0.18 *	0.23 ***	0.13	0.27 ***
RD	0.41 ***	0.49 ***	0.43 ***	0.43 ***	0.39 ***	0.45 ***

*p<0.05, ** p<0.01, *** p<0.001 Bonferroni-corrected

4 Discussion

The objective of this study was to compare longitudinal changes in DTI scalars in white matter of recovering AUD patients between 18 and 35 days of sustained abstinence. Our study has revealed anatomically wide-spread significant changes across both time points in the recovering AUD patients, compared to the matched healthy controls. The most wide-spread deficits were observed in the FA (Figure 4.2) and RD (Figure 4.4), with still wide-spread but less diffused changes in the AD (Figure 4.1) and MD (Figure 4.3). On average, the patients have exhibited -6.20% difference in FA at the first time point and -5.71% difference in FA at the second time point. The interscan change of +0.52% was, however, not significant. Similarly AUD patients exhibited on average -4.81% difference at the first

timepoint and only -3.75% difference at the second time point but the interscan change of 1.12% was also not significant. Unlike FA and AD, the MD and RD have exhibited abnormal increases in their average values. At the first time point, AUD exhibited +5.60% increase which decreased to +4.41% at the second time point, for a non-significant interscan change of -1.13%. RD has exhibited +7.37% increase at first scan, +6.09% at second scan, and a non-significant interscan change of -1.20%. Note, that contrary to our expectations, the anatomical extent of significantly impaired voxels did not always shrink during the interscan period. While the extent of the significant voxels for AD and FA shrunk by 2 and 3% between the first and second time point, for both FA and RD, the number of significantly different voxels has increased by 10 and 8%. Similarly, the overall average whole-skeleton DTI scalar measurements as well as average t-values across all voxels have suggested a non-significant negligible deterioration trend between the two time periods across all white matter DTI scalars. These observations remain to be explained by future studies. Similar results have been recently reported by De Santis *et al.* who have reported decreasing FA and inrceasing RD trend in recovering AUD patients from 2 to 6 weeks (De Santis et al., 2019). However, the consistent overlapping voxels of significant clusters across all scalars in our study as well as between the two time periods for specific scalars support the overall effect of normalizing microstructural deficits between the two time points, compared to both healthy controls and within-group interscan differences in the AUD group. Moreover, the magnitude of the DTI scalar deficits were weakly to moderately correlated with the baseline AUD-related severity scales. FA and RD were correlated across all of the measures while MD was correlated with all except for the Compulsive Drinking Subscale (CDS) and AD was significantly correlated only with CDS and the AUDIT scores. AUDIT scores exhibited the strongest correlation on average across all of the DTI scalars. Although our study has failed to characterize significant longitudinal changes in the white matter microstructural properties, as measured by the four analysed DTI scalars, our results are generally in agreement with our *a priori* hypotheses.

To the best of our knowledge in the past twenty years, approximately thirty-five AUD DTI studies have been published in peer-reviewed English language scientific journals (Alhassoon et al., 2012; De Santis et al., 2019; Durkee, Sarlls, Hommer, & Momenan, 2013; Fortier et al., 2014; Galandra et al., 2020; Gazdzinski et al., 2010; G. J. Harris et al., 2008; Konrad et al., 2012; I. C. Liu et al., 2010; McEvoy et al., 2018; Monnig, Caprihan, et al., 2013; Monnig et al., 2014; Monnig, Tonigan, et al., 2013; Monnig et al., 2015; Muller-Oehring, Schulte, Fama, Pfefferbaum, & Sullivan, 2009; Pandey et al., 2018; Pfefferbaum, Adalsteinsson, & Sullivan, 2006a, 2006b; Pfefferbaum, Rosenbloom, Rohlfing, & Sullivan, 2009; Pfefferbaum, Rosenbloom, Adalsteinsson, & Sullivan, 2007; Pfefferbaum et al., 2014; Pfefferbaum, Rosenbloom, Fama, Sassoon, & Sullivan, 2010; Pfefferbaum & Sullivan, 2002, 2005; Pfefferbaum et al., 2000; Pitel, Chanraud, Sullivan, & Pfefferbaum, 2010; Schulte, Muller-Oehring, Sullivan, & Pfefferbaum, 2012; Schulte, Sullivan, Muller-Oehring, Adalsteinsson, & Pfefferbaum, 2005; Scott F. Sorg et al., 2015; S. F. Sorg et al., 2012; Trivedi et al., 2013; J. J. Wang et al., 2009; Yeh et al., 2009; Zorlu et al., 2013; Zorlu et al., 2014; Y. Zou et al., 2017). They have included 10 to 332 AUD individuals (generally in their forties or fifties on average) and 0 to 88 healthy controls. The duration of abstinence ranged from acute AUD without detoxification to an average of 5.7 years (which included participants with up to 28 years of abstinence). Several studies included large percentage participants with past history or concurrent polysubstance abuse (most frequently cocaine, cannabis, and methamphetamine). The data was acquired on MRI with 1.5T to 4.0T with 6 to 203 different diffusion-weighted gradients. Only five of these studies included a cross sectional, mixed, or longitudinal design, examining different lengths of abstinence (Alhassoon et al., 2012; De Santis et al., 2019; Gazdzinski et al., 2010; Pfefferbaum et al., 2014; Y. Zou et al., 2017). Earlier DTI studies have almost exclusively focused on corpus callosum region-of-interest analyses, while later studies have more commonly deployed TBSS and tract-specific analyses. Although most studies have generally reported lower FA across AUD samples of both short and long term abstinence, the other DTI scalars are less frequently reported and vary in direction (with RD and MD being reported as elevated in AUD compared to controls). The overall reported magnitude of change has also been largely dependent on the measured region – whether reporting an average of a large

region (like corpus callosum or centrum ovale) or just the average across a very specific small significant cluster. Due to frequent disclosure of nuisance-corrected values and figures rather than raw values, the percentage change across different studies has been challenging to summarize and frequently had to be extrapolated from graphs.

From shortest to longest baseline abstinence, the following are quantifiable DTI scalar findings available in the existing literature. At 4.54 days of abstinence, frontal white matter FA was reported to be -3.26% lower in AUD, with subsequent longitudinal improvement within the AUD group by +1.18% from 4.45 to 34 days of abstinence (Gazdzinski et al., 2010). At 6 days of abstinence, AUD compared to light drinkers have exhibited mean differences in significant clusters in the right hemisphere for AD +5.66%, FA -13.46%, MD +12.99%, and RD +16.92% on average while AD +5.98%, FA -11.11%, MD +6.49%, and RD +13.56% in clusters in the left hemisphere (Yeh et al., 2009). Note the opposite direction of AD compared to our study. At approximately 1 week of abstinence, De Santis *et al.* mixed design study reported in AUD compared to healthy controls AD of -9%, FA of -7%, MD of +6%, and RD difference of 11% (De Santis et al., 2019). At the subsequent 2-3 week interval and 4-6 week interval, the within AUD interscan differences revealed continued deterioration of FA by -6% and -7%, slight positive trend in AD +1% and +1%, and continued deterioration in MD with +4% and +4% and in RD with +8% and +9%. The pattern of continued longitudinal deterioration is contradictory to our significant findings, although similar non-significant negligible trends could be observed across the overall averages of entire skeleton DTI scalar values and t-maps. At 10.24 days of abstinence, significant negative change in FA was reported in corpus callosum (-12.90%), right cingulum (-13.46%), right external capsule (-9.44%), and right hippocampus (-17.54%) in a mixed design study (Y. Zou et al., 2017). At second time point of 32.92 days, the same study did not find significant differences in these regions, except for the body of the corpus callosum with interscan FA improvement of +5.09%, +5.07%, +1.40%, and +9.45% in the respective regions. This study also indicated +27 to +61% higher MD values at one month of abstinence, but none of these measures were significant. At approximately 2 weeks of abstinence, longitudinal study

by Alhassoon *et al.* has reported AUD-associated changes in corpus callosum FA or -6.92% (genu), -8.86% (body), and -4.15% (splenium) while increased AD (note the opposite effect to our study) respectively of +6.16%, +2.93%, and +1.49% as well as higher RD respectively of +13.32%, +14.75% and +10.24%. After a 372 day interscan interval, the FA and RD values have demonstrated normalization trend while AD exhibited mixed results. After one year, the FA in AUD was -2.78%, -4.75%, -1.36% lower than in the healthy controls (corresponding to an interscan AUD improvement of +4.45%, +4.50%, +2.91%). RD exhibited +4.06%, +9.33%, and +4.97% difference (AUD interscan improvement of -8.17%, -4.73%, -4.78%). AD was still +4.24%, +2.90% and +2.13% higher in AUD, compared to controls (interscan AUD difference of -1.81%, -0.03%, and +0.63 (Alhassoon et al., 2012). At 15.56 days of abstinence, Durkee *et al.* reported 0 to -25.6% decrease in FA in AUD, however, the AUD group was also 24% older than the controls (Durkee et al., 2013). At median of 17 days of abstinence, Trivedi *et al*. reported decreased FA in the following cluster regions -9.52% in right inferior longitudinal fasciculus, -5.26% in right anterior thalamic radiation, -4.65% in right arcuate fasciculus, -6.25% in fornix, and -6.12% in corpus callosum as well as an abnormally increased MD in fornix +12.12% and corpus callosum +10% (Trivedi et al., 2013). At 17.1 days of abstinence, Zorlu *et al.* reported -10.53% to -14.29% change in FA across different clusters while 9.26% to 15.52% increase in RD and -2.24% to -4.00% decrease in AD in AUD compared to healthy controls (Zorlu et al., 2013). These studies encompassed early average abstinence before or comparable to our first time point. They indicate that AUD-related microstructural damage is detectable within the first few days of abstinence (with sample sizes as small as 10 participants per group) and might experience longitudinal changes during an interscan interval of as little as few weeks to over a year. Note the inconsistent direction of AUD-related AD change in the literature. The calculation of AD and RD especially in pathological conditions might be problematic and the validity of their interpretation in pathological conditions has been questioned in the past (Wheeler-Kingshott & Cercignani, 2009).

Only four studies with short-term average abstinence comparable to the second time-point of study have been reported. These included three above described studies with a second time point (De Santis et al., 2019; Gazdzinski et al., 2010; Y. Zou et al., 2017) and one cross sectional study. At 34.8 days of abstinence, Liu *et al*. reported lower FA in all measured corpus callosum regions (-3.15% to -10.55%), but only the -10.55% decrease in the orbitofrontal regions was significant (I. C. Liu et al., 2010).

The remaining studies have analysed clinical samples with an average and median abstinence length of several months or years. In several instances, the range of abstinence in the AUD cohorts has been extremely heterogeneous, including patients abstinent for days to decades within the same group. At 91.49 days of abstinence, Pfefferbaum *et al*. reported decrease in corpus callosum FA (-10.21% genu, -7.81% body, and -11.31% splenium) and increase in MD (+12.35%, +8.62%, and +10.15% respectively) (Pfefferbaum et al., 2006a). At 113.9 days of abstinence, AUD participants compared to healthy controls have exhibited -1.08% to -6.65% decrease in FA +1.28% to +3.24% increase in AD and +6.82% to +13.92% increase in RD in different transcallosal white matter tracts (Pfefferbaum et al., 2010). At 172 days of abstinence, Pitel *et al.* demonstrated -8.33% decrease in FA and +10% increase in MD in total corpus callosum in elderly AUD (genu -11.36% and +10.00%, body -10.87% and +12.90%, and splenium -7.27% to +10.71%) (Pitel et al., 2010). At 322 median days of abstinence for men and 677 days for women, Pfefferbaum *et al* have reported a decrease in FA of -7.40% in genu of corpus callosum, -3.38% in splenium of corpus callosum, and -6.42% in centrum ovale (Pfefferbaum & Sullivan, 2002; Pfefferbaum et al., 2000). At 847.9 days of abstinence, Zorlu *et al*. have reported elevated diffusivity in significant clusters of +10-18% for RD and +7-10% for AD (Zorlu et al., 2014). Note the opposite effect in AD, compared to results of our own study. At 2081.9 days of abstinence 2 studies have reported significantly lower FA values across several small right hemisphere clusters -36.11% to -44.44% while also reporting significantly lower FA (-6.23% to -1.76% in significant regions), higher MD (+1.74% to +11.10% in significant regions), AD (+3.04% to +9.31% in significant regions), and RD (+2.22% to +12.33% in significant regions) in specific white matter tracts (G. J. Harris et al., 2008; Pfefferbaum et

al., 2009). These long-term abstinent studies document that white matter microstructure might exhibit abnormal diffusivity patterns even after years of sobriety. The evidence of persistent structural deficits is discouraging to our study design of only approximately 17 day interscan interval. This is especially relevant, considering a potential survival bias in cross-sectional studies, especially in long-term abstinent AUD participants. Greater *a priori* integrity of white matter has been associated with better remission outcomes (S. F. Sorg et al., 2012). Given the high relapse rates in AUD (R. H. Moos & Moos, 2006; Walitzer & Dearing, 2006; Witkiewitz, 2011), there is a potential in cross-sectional studies to over-estimate the relative amount of structural recovery due to the gradual drop-out of the most *a priori* structurally compromised patients who are more likely to fail to maintain long-term abstinence. As a result, longitudinal AUD studies are very important in more accurately characterizing the structural trends during the clinical recovery process.

All together, the existing literature has revealed quite consistently lower FA, higher MD, higher RD, and sometimes higher (5/7 studies) and sometimes lower (2/7 studies) AD in AUD compared to healthy controls. These patterns of microstructural deficits have been observed in studies reporting on AUD abstinence of several days as well as multiple years. Overall, there does not appear to be a clear pattern between the magnitude of reported microstructural DTI scalar deficits and the length of abstinence across the varied single time-point studies, although this might be in part due to limitations of heterogeneous abstinence composition of the comparison groups. Significant change in the DTI scalars from weeks to over a year interscan interval in multiple time-point studies have revealed a generally positive trend of low to middle single percentage point towards normalization of the microstructural deficits (but with occasional opposite evidence of continued deterioration during the first few weeks of abstinence). AUD patients who do not maintain their sobriety do not experience a similar normalization trend (Alhassoon et al., 2012; Pfefferbaum et al., 2014; S. F. Sorg et al., 2012). Smoking might also negatively interfere with the white matter microstructural recovery in the abstinent AUD patients (Gazdzinski et al., 2010).

Although most DTI studies have attributed various biological meaning to the changes in the DTI scalars, the interpretation of the microstructural differences should be done with great caution, due to the degenerate nature of the DTI signal, with no particular aspect of tissue microstructure being likely responsible for the observed change (Jones et al., 2013). Despite of the concerns about over-interpretation of DTI changes in the clinical literature, DTI can still serve as a proxy for evaluating microstructural changes in living humans in neurodegenerative disorders with well documented microstructural damage. Both post-mortem pathological evidence and pre-clinical models of AUD have demonstrated extensive evidence of white matter damage (for reviews see: (Crews & Nixon, 2009; Harper et al., 2003; Sutherland et al., 2014b)). The wide-spread alcohol-related overall white matter volume reduction is associated with specific microstructural changes, including demyelination, microtubule disturbance, axonal subtraction, cell body volume reduction, dendritic thinning, and regional neuronal loss (Alling & Boström, 1980; de la Monte, 1988; Harper, 1998; Harper et al., 2003; Harper & Kril, 1989, 1991; Harper, Kril, & Daly, 1987; Jensen & Pakkenberg, 1993; Kashem, Harper, & Matsumoto, 2008; Kril et al., 1997; Lewohl et al., 2000; Mayfield et al., 2002; Paula-Barbosa & Tavares, 1985; Putzke et al., 1998; Tarnowska-Dziduszko, Bertrand, & Szpak, 1995; Wiggins et al., 1988). These pathological microstructural changes may decrease the intracellular and extracellular tract complexity, thus permitting less obstructive water diffusion in the white matter tissue, which can be quantified using DTI. Abstinence-related microstructural recovery has been extensively documented in preclinical models of AUD, which exhibit bursts of axonal remodeling and rapid structural recovery within the first few weeks of sustained abstinence (Crews, 2008). The preclinical alcohol-related deficits as well as longitudinal changes in white matter microstructure have been, furthermore, also validated using DTI and show similar patterns of DTI scalar differences to clinical samples (De Santis et al., 2019; Pfefferbaum, Zahr, Mayer, Rohlfing, & Sullivan, 2015). Magnetic resonance spectroscopy (MRS) in clinical participants has, furthermore, documented metabolic evidence suggesting potential neuronal healing and remyelination associated with sustained abstinence (Bendszus et al., 2001; Durazzo et al., 2006; Ende et al., 2005; Parks et al., 2002; B. C. Schweinsburg et al., 2000).

As a result, it should be reasonable to infer at least broad microstructural biological interpretation of DTI structural changes in AUD given this context.

Fractional anisotropy (FA) describes intravoxel directional coherence of water diffusion along the primary direction of diffusion and is commonly interpreted as a proxy measure of the microstructural white matter integrity (Le Bihan et al., 2001; Pierpaoli & Basser, 1996). Higher FA is interpreted as representing greater white matter structural integrity, while lower FA (as reported in our results) can be associated with degradation of myelin sheaths and axonal membranes, abnormalities in myelination, as well as reduced density of axons in the measured tissue (Gulani, Webb, Duncan, & Lauterbur, 2001; Pierpaoli et al., 2001; S. K. Song et al., 2002; Takahashi et al., 2002; Werring et al., 2000). Axial diffusivity (AD) describes the movement of water parallel to the primary direction of diffusion. Decrease in AD is interpreted as being associated with axonal injury (Ito, Mori, & Melhem, 2002; Lazar et al., 2003; S. K. Song et al., 2003; S. K. Song et al., 2002). Mean diffusivity (MD) describes the overall mean displacement of water molecules in the measured voxel. It is impacted by the cytoarchitectural restrictions in the voxel and can be impacted by cellular density, integrity of cellular membranes, changes in the volume of the intracellular, extracellular and interstitial spaces (Gass, Niendorf, & Hirsch, 2001; Neil et al., 1998; Sotak, 2004). Higher MD could thus represent lower tissue integrity, wider interstitial spaces, or fluid build-up in the measured tissue. Radial diffusivity (RD) describes the movement of water perpendicular to the primary direction of diffusion. Increased RD may represent increased interstitial water movement, potentially reflecting demyelination or dysmyelination (Harsan et al., 2006; S. K. Song et al., 2003; S. K. Song et al., 2002).

All together, the four DTI scalars can describe diffusion patterns associated with different conditions. For example, dense axonal packing would result in high FA, unaffected AD, low MD, and low RD; large axonal diameter and high myelination would result in high FA, high AD, and low RD; axonal degeneration would result in low FA, low AD, high MD, and high RD; demyelination would result in low

FA, unaffected AD, high MD, and high RD (Feldman, Yeatman, Lee, Barde, & Gaman-Bean, 2010). The pattern observed in our study most closely resembles that of axonal degeneration in AUD at both the first and second time point, with a small improvement trend with sustained abstinence. Since the directionality of AD has been inconsistent in the literature, it has been the weakest difference in our data, and it has also been questioned in the past (Wheeler-Kingshott & Cercignani, 2009), the pattern could also resemble that of demyelination, which is also supported by increased RD. The evidence could also describe both since the known pathological changes and preclinical evidence associated with AUD support both possibilities. The DTI signal is only a proxy for changes in water diffusion patterns and thus cannot be directly linked to a specific pathology without additional evidence. Nonetheless, other AUD DTI studies have also generally interpreted their findings as being associated with a loss of tissue integrity due to demyelination or axonal injury (De Santis et al., 2019) with longitudinal recovery during prolonged abstinence thought to be associated with fibre reorganization, myelin repair, remyelination, or glial cell proliferation (Alhassoon et al., 2012; Gazdzinski et al., 2010; Pfefferbaum et al., 2014; Sullivan & Pfefferbaum, 2005; Y. Zou et al., 2017), consistent with our interpretation.

There are several limitations which should be considered when interpreting the findings of our study. DTI is an indirect proxy for microstructural white matter changes with a degenerate signal which could be impacted by a variety of changes (Jones et al., 2013) and should be interpreted with caution, especially in pathological conditions (Wheeler-Kingshott & Cercignani, 2009). DTI scalars used in our study can provide incorrect description of the white matter structural properties in voxels with multi-directional crossing or merging fibres (which have been estimated to be present at least to some extent in most white matter voxels) as well as in voxels impacted by partial volume inhomogeneities (Jones et al., 2013; Pfefferbaum, Adalsteinsson, & Sullivan, 2003; Pierpaoli et al., 2001). TBSS also has limitations beyond those of the DTI itself, including the lack of anatomical specificity, since it is based on data-derived skeleton projections that may not accurately correspond to anatomical tracts. Our study also included several design-related limitations. Although we have tried to mitigate for site- and scanner-specific

variability in our statistical model, our data is based on pooled analysis from two different clinical sites in Canada and Germany. Our data is based only on treatment-seeking male participants with a very homogeneous AUD clinical sample without polysubstance abuse or other comorbidities who were recruited from supervised treatment centres. This makes our sample unrepresentative of the general AUD population or even the typical treatment-seeking patient at the recruitment sites. Furthermore, our study has collected baseline data at an average of 18 days of abstinence with longitudinal follow up after additional 17 days of supervised abstinence. Even though our study was conducted within the early abstinence period which is thought to represent most rapid structural recovery (Crews & Nixon, 2009; Durazzo et al., 2015), it might have missed the very early changes occurring during the first two to three weeks of abstinence (for example (Kühn et al., 2014)) or might have followed-up patients too soon to allow for sufficiently pronounced structural changes to occur in the brain (progenitor cell generation, migration, maturation etc. takes multiple weeks in preclinical models) to be detectable using DTI. Our study also had quite large age heterogeneity with participants ranging from 23 to 64 years old. Although we have tried to account for the age-related structural changes in our statistical design, the age-related within group variability in both patients and controls might have precluded us from detecting stronger effect even in the longitudinal within-subject comparison. Older AUD patients might not experience as large structural recovery following sustained abstinence and age might also negatively exacerbate the alcohol-related structural damage (Pfefferbaum et al., 2006a; Pfefferbaum et al., 1992; Pfefferbaum et al., 2014; Scott F. Sorg et al., 2015; Sullivan et al., 2010; Yeh et al., 2007). Our study relied on self-reported measures of alcohol severity and history. Although we conducted tests for alcohol and drug use, we did not collect independent tests or quantitative assays to test liver health, malnutrition, smoking, or other potential confounding variables which could have impacted structural integrity and recovery in the participants. Our study also did not include any measures of functional neuro-cognitive performance to test the association between microstructural changes and functional improvement.

Future studies should disclose their intentions to analyze clinically-representative samples or homogeneous AUD samples and interpret their findings in the appropriate context. The existing literature includes very heterogeneous clinical cohorts with wide-range of abstinence, frequent polysubstance abuse comorbidities, and cross-sectional designs. In order to better characterize the non-significant but positive trend observed in our study, future studies should consider conducting longitudinal analyses in more homogeneous (i.e. age) samples over multiple intervals spanning both very early abstinence (first few days to weeks) as well as prolonged abstinence and correlating structural differences to functional improvement. Due to high relapse rates in AUD and the need for restrictive recruitment criteria, future studies should aspire for multi-site collaborations and data sharing in order to recruit sufficient numbers of comparable participants to draw more conclusive results.

5 Conclusion

This study has analyzed white matter microstructural changes in recovering AUD patients during the first month of sustained abstinence. The AUD patients in our homogeneous longitudinal sample have exhibited wide-spread microstructural white matter deficits at both 18 and 35 days of abstinence, with a nonsignificant normalization trend. Axial diffusivity (AD) and fractional anisotropy (FA) were significantly lower while radial diffusivity (RD) and mean diffusivity (MD) were significantly higher at both time points. Longitudinal changes in the patients were not significant but described a normalizing trend across all scalars. These changes describe a pattern of (gradually improving) reduced coherence in directional water diffusion in the white matter tissue due to both reduced diffusion along the primary direction of diffusion as well as increased interstitial orthogonal diffusion. These microstructural differences could indirectly represent a pattern of axonal degeneration and/or demyelination, which are both supported by the preclinical and histological evidence as well as the interpretations of other AUD DTI results documented in the literature. Clinical severity of AUD has been weakly to moderately correlated to the magnitude of the microstructural damage. This study alludes to an encouraging trend of

microstructural brain healing process corresponding to the early stages of clinical AUD recovery and is only one of very few existing longitudinal studies investigating microstructural changes during AUD recovery. Future studies with more powerful design will be needed to more conclusively characterize the process of white matter microstructural recovery in AUD during sustained abstinence.

Chapter 5 - Regional Functional Connectivity Changes during First Month of Recovery from Alcohol Use Disorder

Abstract

Alcohol use disorder (AUD) is associated with widespread structural and functional brain pathology, which is at least partially reversible during sustained abstinence. Regional functional connectivity changes during the early recovery period of the first few weeks have not been previously explored. Our study has compared longitudinal changes in amplitude low frequency fluctuations (ALFF), regional homogeneity (ReHo), and degree of centrality (DC) in 41 recently detoxified adult male alcohol dependent patients from 19 to 36 days of abstinence, compared to 50 healthy non-alcohol abusing matched controls. Our analysis has revealed significantly decreased regional functional connectivity in basal ganglia across all measures and persistent at both time points, as well as increased regional functional connectivity in the frontal cortex in the AUD patients compared to the healthy controls. Longitudinal interscan differences within the AUD cohort were not statistically significant, except for a small DC cluster, which exhibited continued longitudinal deterioration. Magnitude of most of the functional changes in the AUD group was weakly to moderately correlated to AUD severity scales. In the context of the existing literature, these findings should be interpreted with caution, potentially providing additional evidence of over-compensatory adaptation in the abstinent AUD patients of decreased reward and increased executive control functional connectivity to help sustain their remission. This was the first longitudinal study to explore regional functional connectivity changes in AUD recovery; the regional functional connectivity study with the largest sample size; and also the first regional functional connectivity study based on a North American and/or European clinical cohort.

Key terms

alcohol use disorder; abstinence; resting state; regional homogeneity; functional magnetic resonance imaging

1. Introduction

Alcohol is one of the most commonly abused and yet one of the most harmful psychoactive substances in the world (Nutt et al., 2010). Excessive chronic alcohol abuse can lead to alcohol use disorder (previously also referred to as alcoholism, alcohol dependence, alcohol addiction, or harmful use of alcohol). Alcohol use disorder (AUD) is a psychiatric disorder characterized by uncontrolled recurrent alcohol abuse despite its significant interference in the individual's mental wellbeing, physical health, and ability to function in their daily lives (American Psychiatric Association & American Psychiatric Association, 2013). The prevalence of alcohol use disorder (AUD) is estimated at 5.1% (2.6% dependence) worldwide in the general population over the age of fifteen (World Health Organization, 2018). Harmful use of alcohol is a leading preventable cause of death (5.9%) and disability (5.1% of global burden of disease) worldwide (World Health Organization, 2018). Even though AUD is a significant, widespread, and costly health problem which has a long pervasive history and well-recognized clinical symptoms, neither the exact mechanism of action of alcohol on the brain nor the mechanism of recovery during prolonged abstinence are fully understood (R. A. Harris et al., 2008; Sutherland et al., 2014b; N. D. Volkow et al., 2017; Zahr & Pfefferbaum, 2017).

Pathological and neuroimaging studies have revealed extensive structural brain damage associated with chronic alcohol abuse (for reviews see (Bühler & Mann, 2011; Fritz et al., 2019; Harper et al., 2003; M. Rosenbloom et al., 2003)). The damage includes gross anatomical structural atrophy as well as region-specific microstructural damage and significant loss in glial cells and neurons. Cross-sectional and longitudinal clinical studies as well as preclinical models have revealed that at least part of this damage is reversible with sustained abstinence (for reviews see (Crews & Nixon, 2009; Fein & Cardenas, 2015; Sullivan & Pfefferbaum, 2005)). The mechanism and precise timeline of structural recovery is not fully understood, but is thought to occur non-linearly, with most rapid recovery during the first few weeks of remission (Durazzo et al., 2015; Gazdzinski et al., 2005; Pfefferbaum et al., 1995; Y. Zou et al., 2017). In

fact, structural recovery might occur up to six times faster (and up to 50% of the total recovery) during the first 3 weeks than during the subsequent year (Charlet et al., 2018; Gazdzinski et al., 2005). The first month of sustained abstinence is, therefore, an especially relevant period to study brain changes associated with AUD recovery. The structural brain changes underlie functional changes which are interlinked with cognitive processing and behavioural changes necessary for a successful addiction remission process.

AUD is also associated with extensive functional deficits. Cognitive, emotional, and behavioural deficits have been all described in AUD (for reviews see (Bernardin, Maheut-Bosser, & Paille, 2014; Le Berre, Fama, & Sullivan, 2017; Oscar-Berman & Marinković, 2007)). Two recent meta-analyses have revealed that cognitive deficits in AUD include significantly poorer performance in speed of processing, executive function, impulsivity, working memory, verbal fluency, verbal learning, and other aspects of learning and memory (Crowe et al., 2019; Stavro et al., 2013). These deficits appear to be at least partially reversible but much of the global functional dysfunction might persist up to the first year of abstinence (Crowe et al., 2019; Stavro et al., 2013). Cognitive improvements can be observed within as early as the first few weeks of abstinence (Mann, Günther, Stetter, & Ackermann, 1999; Oscar-Berman & Marinković, 2007; Petit et al., 2017). Nonetheless, some functional deficits, such as in visuospatial processing or long-term memory, might persist even after several years of sustained sobriety (Brandt, Butters, Ryan, & Bayog, 1983; Fein et al., 2006). The association between structural and functional brain changes and cognitive improvements in recovering AUD have been substantiated by multimodal neuroimaging studies with tissue volume recovery, microstructural integrity, as well as changes in chemical metabolites all being associated with functional improvement (for example see (Alhassoon et al., 2012; Bartsch et al., 2007; Bendszus et al., 2001; Mon et al., 2013; Muuronen et al., 1989; M. J. Rosenbloom et al., 2007; Sullivan, Rosenbloom, Lim, et al., 2000; Yeh et al., 2007)).

Functional neuroimaging and electrophysiological studies have, moreover, revealed that AUD patients exhibit a potentially disorganized inefficient pattern of brain activation with additional recruitment of sometimes far-reaching anatomical regions, in order to compensate for AUD-related impairment (Chanraud & Sullivan, 2014; Sullivan & Pfefferbaum, 2005). For example, AUD patients performing a simple finger-tapping task have exhibited slower performance and yet did not exhibit a proportionate decrease in fronto-cerebellar activation but instead recruited additional cortical regions when completing the task (Parks et al., 2010). Other studies have also revealed that AUD patients recruit additional cortical, subcortical, and cerebellar regions when performing tasks at both worse as well as comparable levels to healthy controls (Chanraud-Guillermo et al., 2009; Gilman & Hommer, 2008; Marinkovic et al., 2009). There is also a growing body of evidence suggesting altered functional connectivity associated with AUD observed at a resting state. Camchong *et al*. have documented what are thought to be adaptive compensatory mechanisms in medium (about 73 days) and long-term (about 2,889 days) abstinent AUD, whereby they appear to exhibit decreased bottom-up reward and greater top-down executive control functional connectivity, potentially compensating for the pathologically reinforced connection developed before remission from the alcohol addiction (for review see (Fein & Cardenas, 2015)). Other studies have reported abnormal patterns of functional connectivity within and between functional networks (Chanraud, Pitel, Pfefferbaum, & Sullivan, 2011; Müller-Oehring, Jung, Pfefferbaum, Sullivan, & Schulte, 2015). The changes in functional connectivity with sustained abstinence, especially at the regional level remain not fully understood.

To the best of our knowledge, there are only 5 AUD studies which have examined regional changes in functional connectivity (H. Kim et al., 2015; R. Liu et al., 2018; X. Luo et al., 2017; Tu, Wang, Liu, & Zheng, 2018; Weng, Chou, Huang, Tyan, & Ho, 2018) in AUD and one which has examined the effect of acute ethanol intoxication in healthy controls (Zheng, Kong, Chen, Zhang, & Zheng, 2015). None of the existing studies have quantified the length of abstinence of their clinical cohort (only Kim *et al.* disclosed at least 2 weeks of abstinence as an inclusion criterion). To the best of our knowledge, there are no

published cross-sectional or longitudinal studies which would explore abstinence-related changes in regional functional connectivity in AUD. There are also no clinical studies from North American or European clinical context.

Our study aimed to address this gap in the literature. We have implemented longitudinal analysis of regional functional connectivity changes in AUD patients during approximately the first month of sustained abstinence compared to matched healthy controls. This study has examined resting state regional functional connectivity changes using indices approximating functional connectivity from the voxel-specific fluctuations to local neighbouring clusters to whole-brain functional connectome in resting state functional magnetic resonance imaging (fMRI) to try to better characterize the pattern of regional functional connectivity and its changes with successful AUD remission.

Functional magnetic resonance imaging (fMRI) is a non-invasive neuroimaging technique which can indirectly approximate changes in the brain activation by measuring changes in magnetic susceptibility contrast due to different properties in oxygenated (diamagnetic) and de-oxygenated (paramagnetic) hemoglobin in response to an increased metabolic load of activated brain tissue (for an overview see (Glover, 2011)). This blood-oxygen-level-dependent (BOLD) signal has been demonstrated to be linearly correlated to simultaneous electrophysiological recordings and thus directly reflects neural activation due to a stimulus (for review see (Logothetis, 2003)). These activation changes occur both due to a specific task-based activation but also due to spontaneous low-frequency (< 0.1Hz) fluctuations in a resting state. Resting state BOLD fluctuations originate (at least partially) due to spontaneous neuronal activity in highly correlated anatomically and functionally linked brain regions, reflecting ongoing functional connectivity at rest (for an overview see (van den Heuvel & Hulshoff Pol, 2010)). Analyzing these spontaneous resting state BOLD fluctuations can, thus, be a robust measure to evaluate functional connectivity between local as well as distant brain regions across the entire brain.

To examine regional functional connectivity changes, several voxel-specific indices are commonly computed, including amplitude low frequency fluctuations (ALFF), regional homogeneity (ReHo), and degree of centrality (DC). ALFF is the most regionally specific measure which quantifies the total power of low frequency oscillation of the BOLD signal within a specific voxel (Y. F. Zang et al., 2007). ReHo measures the BOLD signal synchronization across neighbouring voxels surrounding the specific voxel (Y. Zang, Jiang, Lu, He, & Tian, 2004). DC measures local network connectivity across the entire functional connectome by counting the number of direct connections between all nodes, thus reflecting both local as well as long-distance whole brain functional connectivity (Buckner et al., 2009). Together, these three measures should help us explore both local as well as whole-brain functional connectivity and thus characterize any AUD-related regional functional connectivity changes and their longitudinal progression.

Our *a priori* hypotheses were 1) AUD patients will on average exhibit more diffuse patterns of significantly increased and decreased regional functional connectivity compared to the healthy controls (less efficient organization); 2) abnormal regional functionality connectivity pattern will be associated with abnormal whole-brain functional connectivity (links to compensatory recruitment); 3) longitudinal differences will result in a normalizing trend (functional recovery); and 4) greater magnitude of regional functional connectivity deficits will be correlated to AUD severity measures. This was the first longitudinal study to characterize longitudinal changes during early recovery from AUD.

2. Materials and Methods

2.1 Subjects

The analysis is based on longitudinal data from 41 recently detoxified adult male alcohol dependent patients (DSM-IV-TR criteria)(American Psychiatric Association, 2000) and matched 50 healthy non-

alcohol abusing men. The demographic and clinical overview of the 91 participants is summarized in Table 5.1.

The analysed sample encompasses all of the usable neuroimaging data drawn from a larger dataset consisting of 59 recently detoxified male alcohol dependent patients and 54 matched healthy controls. Unfortunately, 18 patients and 4 controls had to be excluded from the analysis. 4 of the excluded patients and controls had severe imaging artifacts in the first set of scans and 14 of the excluded patients did not have an acceptable second scan (2 had severe second scan artifacts, 2 were too anxious/claustrophobic to undergo or complete the second scanning sequence in its entirety, 5 patients suffered a confirmed relapse, 1 patient died, 1 could not attend the scanning session due to adverse winter weather, 2 confirmed to be unavailable due to out-of-town work by relatives, and the remainder were lost to follow-up and could not be reached or refused to confirm abstinence and participate in the second scanning session). There were no statistically significant differences between the dropped-out participants and the participants included in our longitudinal analysis (also see Figure 5.1).

The alcohol dependent participants were recruited from a pool of patients referred to supervised residential treatment programs in Edmonton, Canada and Mannheim, Germany as part of the TRANSALC research project. DSM-IV-TR diagnostic interviews were carried out by a psychiatrist, using the Structured Clinical Interview for the DSM-IV-TR (SCID-I) (First et al., 2002). All of the patients were consistent, steady, heavy drinkers. All of the analyzed patients met the highest Zone IV cut-off score on the Alcohol Use Disorders Identification Test (AUDIT) with an average score of 28 out of 40 (Saunders et al., 1993). The AUD patients exhibited on average an intermediate level of alcohol dependence (second quartile) according to the Alcohol Dependence Scale (ADS) with the average score of 16 out of 47 (Skinner & Allen, 1982). The patients did not abuse non-beverage ethanol or other substances except nicotine. The patients were recruited within the first two weeks of abstinence and underwent longitudinal scanning sessions at two time points: first after approximately two weeks of

abstinence (18.63 days on average) and second after approximately one month of abstinence (35.76 days on average). Abstinence was verified at each scanning session in all participants by an alcohol breathalyser (BACtrack S50 Personal Breathalyzer, Portable Breath Alcohol Tester) and a urine drug screen (nal von minden GmbH Drug-Screen® Diptest, Version 1.0).

Controls were recruited concurrently to match the patients' general demographic profile (including sex, age, handedness, general occupation/education background). The controls had no history of alcohol or drug addiction and consumed alcohol below the Canada's Low-Risk Alcohol Drinking Guidelines (Butt, 2011). Participants in both arms were excluded if they had any history of serious medical (including psychiatric or neurological) complications, brain injury, use of psychotropic medications (other than during the detoxification process), or did not meet magnetic resonance safety criteria for our imaging facilities. The study was approved by the University of Alberta Health Research Ethics Board (study ID: Pro00019424).

Table 5.1: Summary of Key Demographic and Clinical Variables

	AUD Patients (n=41)		Controls (n=50)				
	Mean	**SEM**	**Mean**	**SEM**	**% Δ**	**t-value**	**sig.**
Age	45.09	1.46	42.17	1.40	7	1.40	not sig
Ethanol (grams/day)	252.78	19.90	5.47	0.55	4,521	13.58	***
AUDIT	27.62	0.65	2.69	0.21	927	39.79	***
ADS	16.49	0.90	1.73	0.22	853	17.15	***
OCDS	18.24	0.88	1.26	0.12	1,348	20.23	***
ODS	6.46	0.50	0.09	0.04	7,078	13.36	***
CDS	11.78	0.46	1.17	0.11	907	23.72	***
Abstinence 1 (days)	18.63	0.82	N/A				
Abstinence 2	35.76	0.80	N/A				

*p<0.05, ** p<0.01, *** p<0.001 Bonferroni-corrected; SEM = standard error of mean

2.2 MRI Acquisition

The neuroimaging data was acquired at two clinical sites. Canadian data was acquired using a 4.7 Tesla Varian Inova whole-body MRI scanner, located at the University of Alberta, Edmonton. German data was

acquired using a 3 Tesla Siemens MAGNETOM TRIO whole-body MRI scanner, located at the Central Institute of Mental Health, Mannheim. The scanning protocol included anatomic imaging using T1-weighted magnetization-prepared rapid acquisition echo (MPRAGE) as well as resting state functional MRI (rs-fMRI) using single-shot, T2*-weighted echo planar imaging (EPI). During rs-fMRI participants were asked to remain still, close their eyes, not fall asleep, and not to think of anything in particular.

Edmonton MPRAGE acquisition parameters were TR 1,505.9 ms, inversion time 300.0 ms, relaxation delay time (after readout prior to inversion) 300.0 ms, linear phase encoding, TE 3.71 ms, matrix 240×192×128, field of view 240×192×192 mm^3, 1.0×1.0×1.5 mm^3 voxels, whole brain coverage. Mannheim MPRAGE acquisition parameters were TR 2,300 ms, inversion time 900 ms, TE 3.03 ms, matrix 256×256×192 with identical field of view, 1.0×1.0×1.0 mm^3 voxels, with whole brain coverage.

Edmonton rs-fMRI EPI scans had acquisition parameters of TR 1500 ms, TE 19 ms, matrix 72×68×36, field of view 216×204×126 mm3, 3×3×3.5 mm3 voxels, whole brain coverage, and with 320 volumes. Mannheim rs-fMRI EPI scans had acquisition parameters of TR 1500 ms, TE 28 ms, matrix 64×64×30, field of view 192×192×120 mm3, 3×3×4 mm3 voxels, whole brain coverage, and with 240 volumes.

All of the scans were visually reviewed by two independent neuroimaging experts for gross abnormalities. None of the subjects exhibited any clinically significant structural abnormalities other than what may be expected from normal aging or prolonged alcohol abuse. Only subjects without severe motion and other noise artifacts in both the first and second fMRI scan were included in the final analysis.

The raw data was also anonymized before any pre-processing and the researchers were blinded to the subject or group label key until the final statistical analysis.

2.3 Neuroimaging Data Preprocessing

The fMRI data was preprocessed using the Data Processing Assistant for Resting-State fMRI Advanced Edition (DPARSFA; version 4.1_160415; http://rfmri.org/DPARSF) (Chao-Gan & Yu-Feng, 2010). Preprocessing steps included: removal of first 10 time points to allow for signal stabilization; slice timing correction; head motion realignment; brain extraction (using BET) (Smith, 2002); nuisance covariate regression (using 2 polynomial trend with Friston 24 head motion parameters as well as white matter and cerebral-spinal fluid regressors based on CompCorr with 6 principal components) (Behzadi, Restom, Liau, & Liu, 2007; Friston, Williams, Howard, Frackowiak, & Turner, 1996); normalization to Montreal Neurological Institute (MNI) space using the default EPI template in a 3×3×3 mm^3 isotropic space; smoothing using a 9 mm isotropic Gaussian kernel (FWHM); and temporal filtering in 0.01 to 0.1 Hz band. The preprocessed data was also masked using a common dataset mask, which included brain voxels common to all scans and was created using FSL (Jenkinson et al., 2012). The order of the preprocessing steps varied based on the type of analysis according to the appropriate reference (for example, Regional Homogeneity and Degree of Centrality measures were calculated on unsmoothed data and the resultant normalized statistical maps were smoothed before group analysis in order to avoid overestimating the voxel-specific measures). Quality assurance steps were undertaken after each preprocessing step.

The preprocessed data was split into equal halves before any subject or group level analysis. The first half was used to calculate regional changes in functional connectivity (see section 2.4). The second half of the preprocessed data was saved for subsequent region of interest (ROI) analysis, which explored long distance whole-brain functional connectivity of the significant clusters, identified by the regional analysis (see section 2.5). This was done to mitigate double-dipping circular analysis error.

2.4 Regional Functional Connectivity Analysis

We have used DPARFSA to calculate three different measures of regional functional connectivity changes: Amplitude of Low Frequency Fluctuations (ALFF), Regional Homogeneity (ReHo), and weighted Degree of Centrality (DC).

ALFF quantifies the total power of low frequency oscillations in the resting state blood-oxygen-level dependent (BOLD) signal in the 0.01 to 0.1 Hz frequency range in the fully preprocessed data (Y. F. Zang et al., 2007). The z-scores of the sum of the amplitudes across the frequency range calculated using DPARFSA were then used for group comparison.

ReHo measures the similarity of signal synchronization across neighbouring voxels by calculating Kendall's coefficient of concordance for each voxel (Y. Zang et al., 2004). The coefficient was calculated based on the surrounding 27 neighbouring voxels (faces, edges and corners) based on the time-series of each unsmoothed preprocessed signal. Standardized z-score maps for each subject calculated using DPARFSA were then smoothed and used for group comparison.

DC measures local network connectivity across the entire functional connectome by counting the number of direct connections between all nodes (Buckner et al., 2009). The connection strength was based on weighted correlation values with a default threshold of 0.25 based on un-smoothed preprocessed data. Standardized z-score maps for each subject calculated using DPARFSA were then smoothed and used for group comparison.

2.5 Region of Interest (ROI) Analysis

Significant clusters from statistical group comparison from section 2.4 were masked, binarized, and used as seeds in region of interest (ROI) analysis. The analysis was conducted on the second half of the fully preprocessed fMRI data from section 2.3 using FMRIB Software Library version 6.0 (FSL; https://fsl.fmrib.ox.ac.uk/fsl/fslwiki/FSL; (Jenkinson et al., 2012)) and its Dual Regression function (Christian F Beckmann, Mackay, Filippini, & Smith, 2009). Briefly, a time course from each of the ROI seed regions was extracted for each subject from the second half of the preprocessed fMRI time-series. These ROI time courses were then regressed into the same fMRI time-series, resulting in a subject-specific spatial map for each ROI. These were then used for statistical group comparison. This analysis evaluated whether regions of abnormal regional functional connectivity were associated also with long-distance whole-brain functional connectivity differences between the different groups.

2.5 Statistical Analyses

After the quality assurance of the fMRI analyses were complete for each subject, the label key was returned to the blinded researcher to allow for group comparison and statistical analysis.

The participant profile summary statistics and group comparison were generated using SPSS (version 20) (IBM Corp, 2011) and MATLAB (version R2018b) (The MathWorks Inc, 2018). The summary statistics included group mean ($\bar{x}$) and standard error of mean (SEM). After verifying validity of the assumptions (including Levene's test of homogeneity), two sample t-tests were used to compare group differences (Δ). The input data for demographic and clinical summary statistics was not corrected for nuisance variables (such as age).

The neuroimaging group comparison analysis was performed using general linear models and voxel-wise non-parametric permutation tests in FSL (Jenkinson et al., 2012). The linear models included predictors for group status (dummy variables for first and second scans for patients and controls) as well z-normalized nuisance variables (scanning site, age, and length of abstinence at first scan). The contrasts compared first time point group differences, second time point group differences, as well as interscan longitudinal differences in the AUD group. For completeness, a separate due diligence analysis was also performed on the usable first-time point neuroimaging data of all of the excluded patients who have dropped out compared to the patients who have remained in the study. The group differences were tested using 10,000 permutations in FSL's Randomise algorithm with Threshold-Free Cluster Enhancement (TFCE), using the recommended parameters (Winkler et al., 2014).

An exploratory post-hoc statistical analysis was also conducted to explore correlations between significant neuroimaging results and clinical severity scales. Significance of the Pearson correlation coefficients was tested using two-tailed t-tests.

For all analyses, the null hypothesis was rejected and group differences were considered as significant at a global alpha threshold of 0.05. The p-values were corrected for multiple comparison using Family-Wise Error (FWE) correction. FWE-correction was estimated either through permutations for neuroimaging data or using Bonferroni method for summary statistics and post-hoc comparisons (Bonferroni, 1936).

3 Results

3.1 Participant profile

The healthy controls were recruited to match the general demographic profile of the AUD patients. As a result, the groups were not significantly different in their general demographic profile. The clinical

measures were 9 to 71 times more severe in the AUD group than in the healthy control, as summarized in Table 5.1.

3.2 Drop-Out Due Diligence

The due diligence comparison of the excluded dropped-out patients compared to the ones included in the longitudinal study revealed that neither the demographic, clinical, nor neuroimaging profile of the clinical subjects was significant. Figure 5.1 illustrates the lack of significant differences in the usable fMRI scans of the 16 dropped-out excluded AUD patients compared to the 41 remaining included AUD patients. The overwhelmingly green t-maps indicate non-significant group differences.

3.3 Amplitude Low-Frequency Fluctuations Differences

Amplitude low-frequency fluctuations (ALFF) analysis has revealed a significant subcortical decrease in recovering AUD patients at 19 days of abstinence compared to controls (as illustrated by bilateral blue clusters in putamen and pallidum in Figure 5.2). This difference has largely persisted at 36 days of abstinence with an additional increase in ALFF in the frontal regions (frontal pole, superior frontal gyrus, inferior frontal gyrus, middle frontal gyrus, cingulate gyrus) and decrease in the thalamus, putamen, occipital lobe and cerebellum compared to the matched healthy controls (as illustrated in red clusters and blue clusters in Figure 5.3). These differences, however, did not survive multiple comparison correction in the interscan longitudinal comparison (even though a positive trend of increasing ALFF can be observed in yellow shade across the t-maps in Figure 5.4). Summary of the average values and corresponding changes are summarized in Table 5.2. Summary of the coordinates of the significant clusters are summarized in Table 5.3.

The above significant regional changes in the ALFF in the first half of the resting state data were associated with both increased and decreased whole-brain region-of-interest functional connectivity changes in the second half of the data. Clusters associated with decreased ALFF in AUD patients at the first time point (putamen and pallidum) were associated with increased whole-brain functional connectivity in bilateral thalamus, right hippocampus, cingulate gyrus and decreased in right parietal lobe (inferior parietal lobule), occipital lobe (middle occipital gyrus), temporal lobe (middle temporal gyrus and inferior temporal gyrus), putamen, and insula in AUD patients compared to healthy controls (as illustrated by the red and blue clusters in the bottom row in Figure 5.2).

At second time point, clusters of significant increased ALFF (frontal lobe) were associated with decreased functional connectivity with clusters in frontal lobe (precentral gyrus, superior frontal gyrus, and middle frontal gyrus) and parietal lobe (postcentral gyrus, and superior parietal lobule). Clusters of significantly decreased ALFF (cerebellum, occipital lobe, and putamen/thalamus) were associated with decreased functional connectivity values in the left cerebellum, occipital lobe, and parietal lobe, primarily within the significant ALFF cluster. These clusters are depicted in red and blue in the third row of Figure 5.3 (seed region is in green).

Summary of the average region-of-interest analysis ALFF values and corresponding changes are summarized in Table 5.4. Summary of the coordinates of the significant clusters are summarized in Table 5.5.

3.4 Regional Homogeneity Differences

Regional homogeneity (ReHo) analysis has revealed similar overall patterns to the ALFF analysis. At the first time point there was a significant ReHo increase in frontal lobe (superior frontal gyrus, middle frontal gyrus, frontal pole, supplementary motor cortex) and parietal lobe (precuneus), with negligible

cluster extending to caudate and thalamus (as indicated in red clusters in the second row of Figure 5.5). On the other hand, bilateral putamen, thalamus, pallidum, and a small extent of frontal orbital cortex have exhibited significant decrease in ReHo in AUD patients at first time point (as illustrated by blue clusters in second row of Figure 5.5). At the second time point, these differences largely persisted, with broader patterns of increased ReHo and more anatomically diffuse patterns of decreased ReHo (as indicated in red and blue clusters in the second row of Figure 5.6). AUD patients at the second time point exhibited increased ReHo in bilateral frontal lobe (anterior superior frontal gyrus, medial frontal gyrus, inferior frontal gyrus, and frontal pole) and parietal lobe (precuneus) and decreased ReHo in cerebellum, bilateral putamen, occipital lobe (lingual gyrus, cuneus), and insula, compared to the matched healthy controls. Even though there was an overall trend of increasing ReHo values with prolonged abstinence, none of these survived multiple comparison correction in the interscan longitudinal comparison. Yellow colour across multiple anatomical regions across the t-maps in Figure 5.7 illustrates this trend. Summary of the average values and corresponding changes are summarized in Table 5.6. Summary of the coordinates of the significant clusters are summarized in Table 5.7.

Region-of-interest whole-brain analysis of the functional connectivity changes associated with the significant differences in regional homogeneity has revealed significant changes at first time point, second time point, but not the within patient interscan comparison. At first time point, the increased ReHo clusters (green clusters in third row of Figure 5.5) in the first half of the data were associated with significant increased functional connectivity (red clusters) in the second half of the data with right putamen and pallidum as well as frontal lobe (superior frontal gyrus) and decreased functional connectivity (blue clusters) in bilateral parietal lobe (post-central gyrus, inferior parietal lobule) and frontal lobe (precentral gyrus). The clusters of decreased ReHo at first time point (green clusters in fourth row of Figure 5.5) were associated with increased functional connectivity with frontal lobe (precentral gyrus) and cerebellum (anterior lobe culmen) and decreased functional connectivity with left temporal lobe (middle temporal gyrus). At second time point, the increased ReHo clusters (green clusters in third

row of Figure 5.6) were associated with significant increased functional connectivity (red clusters) with left frontal lobe (superior frontal gyrus, middle frontal gyrus), occipital lobe (middle occipital gyrus), and right caudate and decreased functional connectivity (blue clusters) in frontal lobe (precentral gyrus) and parietal lobe (post-central gyrus). The clusters of decreased ReHo at second time point (green clusters in fourth row of Figure 5.6) were associated with increased functional connectivity with bilateral cerebellum and occipital lobe as well as decreased functional connectivity with right parietal lobe (angular gyrus, precuneus, inferior parietal lobule). Summary of the average region-of-interest analysis ReHo values and corresponding changes are summarized in Table 5.8. Summary of the coordinates of the significant clusters are summarized in Table 5.9.

3.5 Weighted Degree of Centrality Differences

Weighted degree of centrality (DC) analysis has revealed a significant decrease in bilateral frontal lobe (paracingulate gyrus, cingulate gyrus, and superior frontal gyrus), thalamus, putamen, and pallidum in recovering AUD patients at 19 days of abstinence compared to controls (as illustrated by blue clusters in second row of Figure 5.8). Contrary to our expectations, the difference was further exacerbated at the second time point of 36 days of abstinence. At the second time point, the recovering AUD patients have demonstrated more wide-spread decrease in DC in thalamus, putamen, caudate, and partially occipital lobe and parietal lobe as well as an increase in the frontal lobe (superior frontal gyrus, medial frontal gyrus, and middle frontal gyrus) (as illustrated by blue and red clusters in second row of Figure 5.9). Although comparing extent of the significant cluster changes in Figure 5.8 and Figure 5.9, suggest interscan DC differences primarily in the deep brain tissue and frontal gyrus, the within subject interscan comparison in the recovering AUD patients has only revealed a significant decrease in the left occipital lobe (lingual gyrus), parietal lobe, cerebellum and part of temporal lobe (as illustrated by blue clusters in second row of Figure 5.10). Summary of the average values and corresponding changes are summarized in Table 5.10. Summary of the coordinates of the significant clusters are summarized in Table 5.11.

Region-of-interest whole-brain analysis of the functional connectivity changes associated with the significant differences in degree of centrality, have revealed significant changes at first time point, second time point, as well as within patient interscan comparisons. At the first time point, clusters of significantly decreased DC (in green at the bottom row of Figure 5.8), were associated with increased functional connectivity (in red at the bottom row of Figure 5.8) in left cerebellum and parietal lobe (precuneus, angular gyrus) and decreased functional connectivity (in blue at the bottom row of Figure 5.8) in primarily right frontal lobe (superior frontal gyrus, supplementary motor cortex, precentral gyrus), insula and part of temporal lobe (temporal lobe), as well as putamen in AUD, compared to the healthy controls. At the second time point, significantly increased DC in frontal lobe (in green at third row of Figure 5.9), were associated with increased functional connectivity (in red at the third row of Figure 5.9) in precuneus and cingulate gyrus as well as decreased functional connectivity (in blue at the third row of Figure 5.9) in frontal lobe (superior frontal gyrus, middle frontal gyrus) and parietal lobe (supramarginal frontal gyrus) in AUD, compared to the healthy controls. Significantly decreased DC (in green at the bottom row of Figure 5.9), were associated with increased functional connectivity (in red at the bottom row of Figure 5.9) in right occipital lobe (middle occipital gyrus, inferior occipital gyrus, and fusiform) and cerebellum as well as decreased functional connectivity (in blue at the bottom row of Figure 5.9) in left cerebellum and temporal lobe (fusiform) in AUD, compared to the healthy controls. Clusters of decreased DC interscan AUD differences (in green at the bottom row of Figure 5.10) were associated with decreased functional connectivity (in blue in the bottom row of Figure 5.10) in cerebellum and occipital lobe, substantially overlapping with the significant cluster and extending to the surrounding tissue. Summary of the average region-of-interest analysis DC values and corresponding changes are summarized in Table 5.12. Summary of the coordinates of the significant clusters are summarized in Table 5.13.

3.6 Clinical Severity Correlations

An exploratory post-hoc analysis was conducted on the significantly altered clusters of ALFF, DC, and ReHo and their correlation to the different clinical severity scales. These changes are summarized in Table 5.14. As anticipated, most of the clinical severity scales showed a positive correlation with functional connectivity measures extracted from significant clusters with patient minus control contrast and vice versa. After full Bonferroni correction, Alcohol Use Disorders Identification Test (AUDIT), Compulsive Drinking Subscale (CDS), and Obsessive Compulsive Drinking Scale (OCDS) scores demonstrated the most significant correlation across most of the tested clusters.

Figure 5.1: Differences Between Dropped-Out versus Included Patients at First Time Point

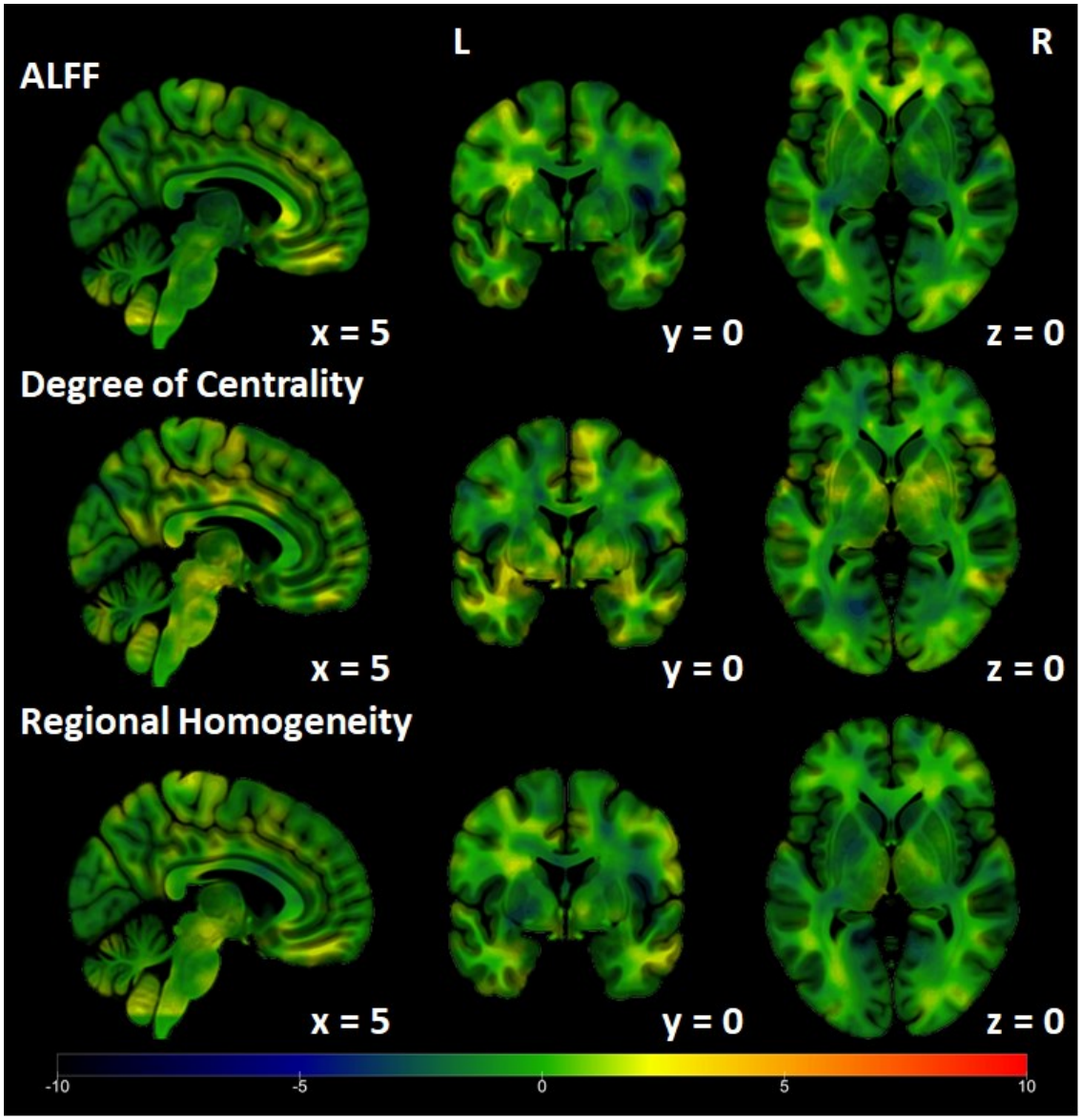

Figure 5.1 depicts t-maps of the group differences in the Amplitude Low Frequency Fluctuations (ALFF), weighted Degree of Centrality, and Regional Homogeneity (ReHo) measures in first time-point scans in patients who dropped out (n=16) compared to the ones who were included in the final, longitudinal analyses (n=41). As indicated by the colour bar, blue indicates decrease, green no differences, and red increased values in the dropped-out patients. None of the changes reached significance. All of the maps are in the MNI space.

Figure 5.2: Amplitude Low Frequency Fluctuations Differences at First Time Point

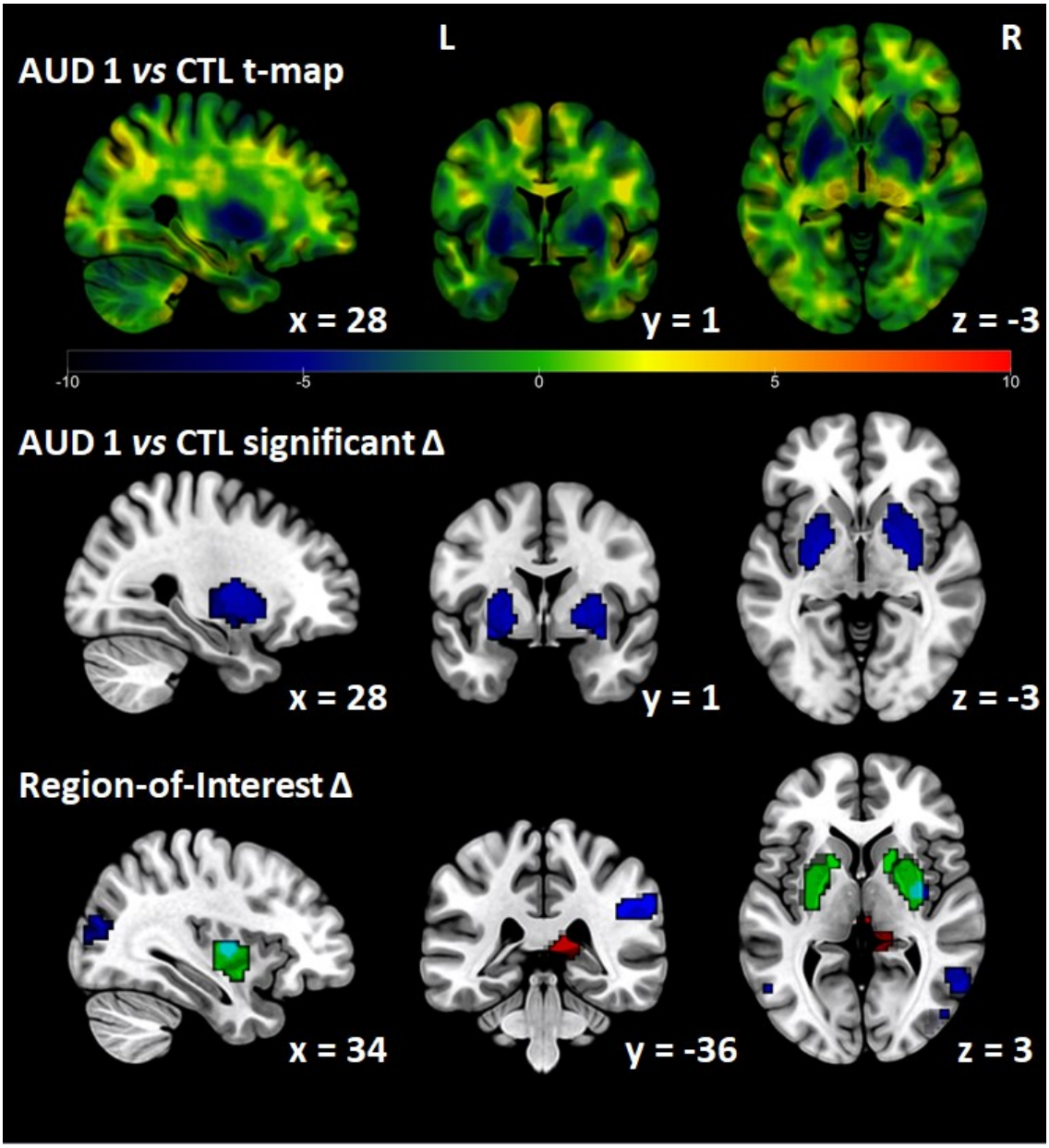

Top row depicts t-map of the group differences in the Amplitude Low Frequency Fluctuations (ALFF) between AUD patients and controls at the first time point (19 days of abstinence). Blue represents decreased ALFF in AUD, green no difference, and red increased ALFF in AUD – as illustrated by the colour bar. The middle row depicts significantly lower clusters in blue. There were no significantly increased clusters which survived Bonferroni multiple comparison correction. Bottom row indicates in green the significantly different ALFF from middle row, which were used as seeds in whole brain region-of-interest analysis. Clusters of significantly lower functional connectivity in AUD group are in blue while those with significantly higher functional connectivity are in red. All of the images are in the MNI space.

Figure 5.3: Amplitude Low Frequency Fluctuations Differences at Second Time Point

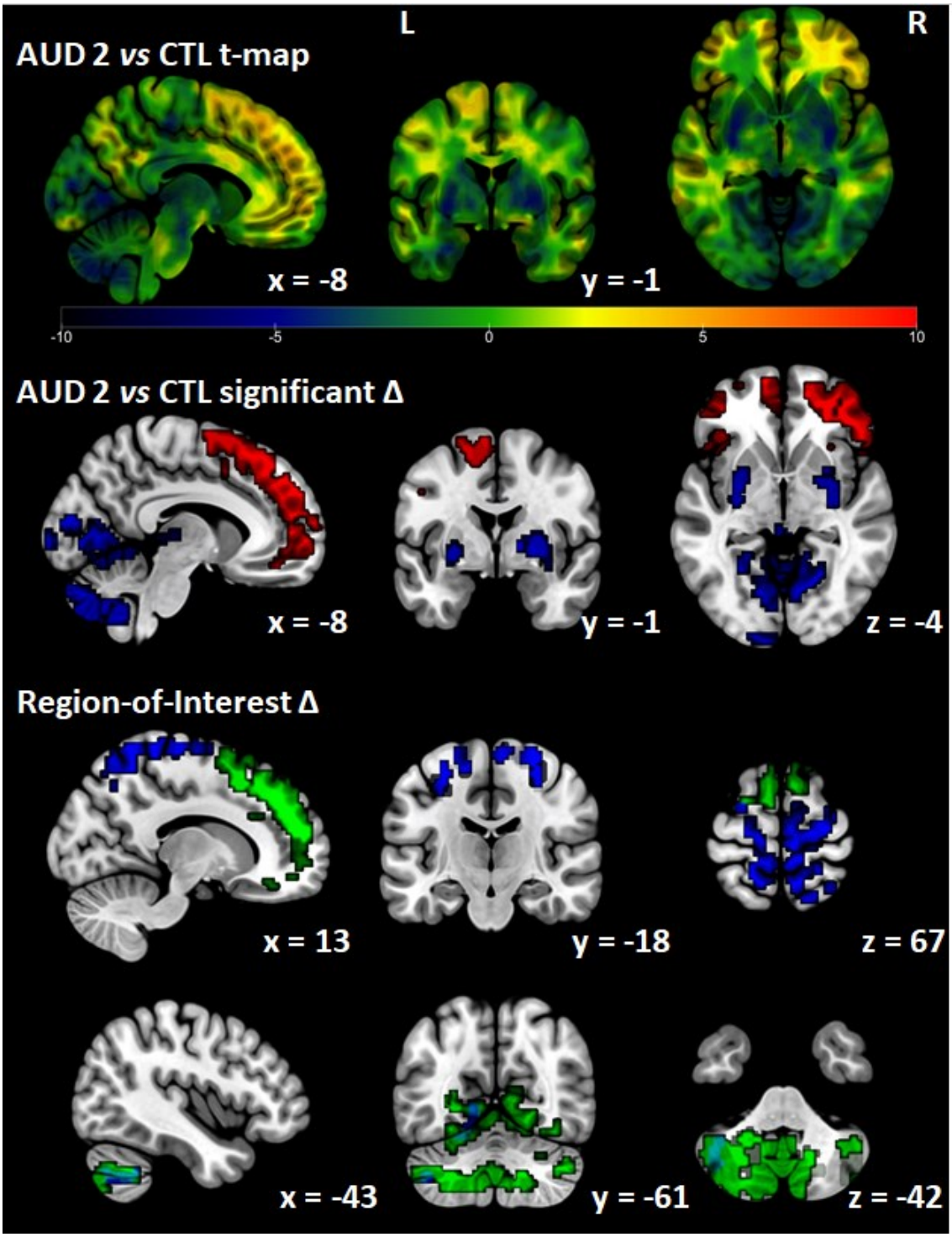

Top row depicts t-map of the group differences in the Amplitude Low Frequency Fluctuations (ALFF) between AUD patients and controls at the second time point (36 days of abstinence) . Blue represents decreased ALFF in AUD, green no difference, and red increased ALFF in AUD – as illustrated by the colour bar. The second row depicts significantly decreased clusters in blue and significantly increased clusters in red. Bottom two rows depict in green the significantly different ALFF from the second row (third row are higher clusters while fourth are lower clusters), which were used as seeds in whole brain region-of-interest analysis and in blue significantly lower and in red significantly higher functional connectivity clusters. Images are all in the MNI space.

Figure 5.4: AUD Interscan Difference s in Amplitude Low Frequency Fluctuations

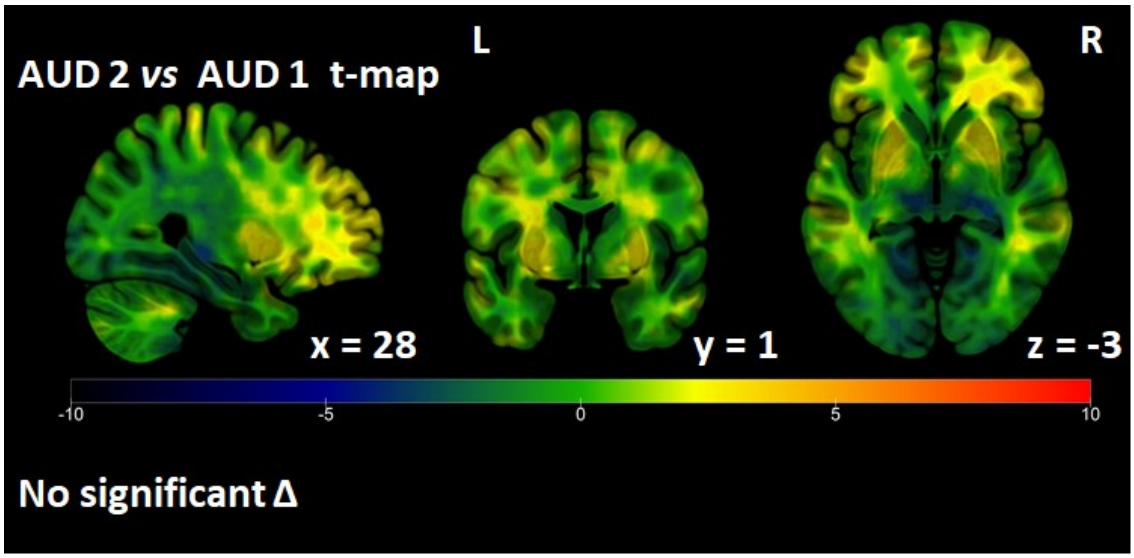

Top row depicts t-map of the interscan longitudinal group differences in the Amplitude Low Frequency Fluctuations (ALFF) between AUD patients (19 versus 36 days of abstinence) . Blue represents decreased ALFF in AUD, green no difference, and red increased ALFF during the interscan interval – as illustrated by the colour bar. None of the differences survived Bonferroni multiple comparison correction. The statistical map is in the MNI space.

Figure 5.5: Regional Homogeneity Differences at First Time Point

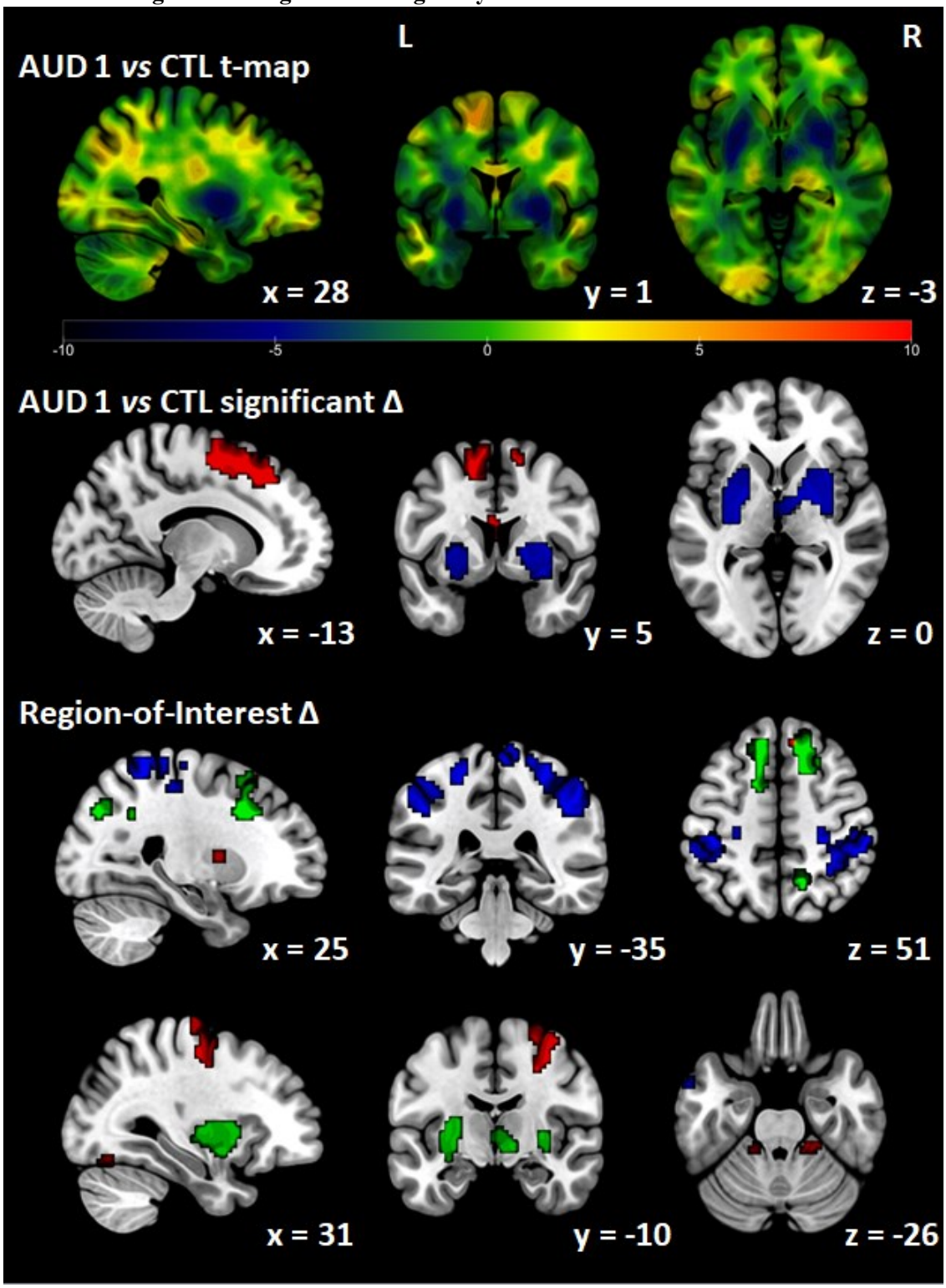

Top row depicts t-map of the group differences in the Regional Homogeneity (ReHo) between AUD patients and control at the first time point (19 days of abstinence) . Blue represents decreased ReHo in AUD, green no difference, and red increased ReHo in AUD – as illustrated by the colour bar. The second row depicts significant clusters (red are higher in AUD while blue are lower in AUD). The bottom two rows represent results of the region-of-interest (ROI) analyses of the second row clusters. The third row used increased ReHo clusters as seeds (green) and shows whole-brain increased functional connectivity clusters in red while decreased in blue. The fourth row depicts the results of the ROI functional connectivity differences between in AUD and controls at first time point using the decreased ReHo clusters as the seed region (green). Similarly red indicates regions of increased whole brain functional connectivity while blue decreased. Images are all in the MNI space.

Figure 5.6: Regional Homogeneity Differences at Second Time Point

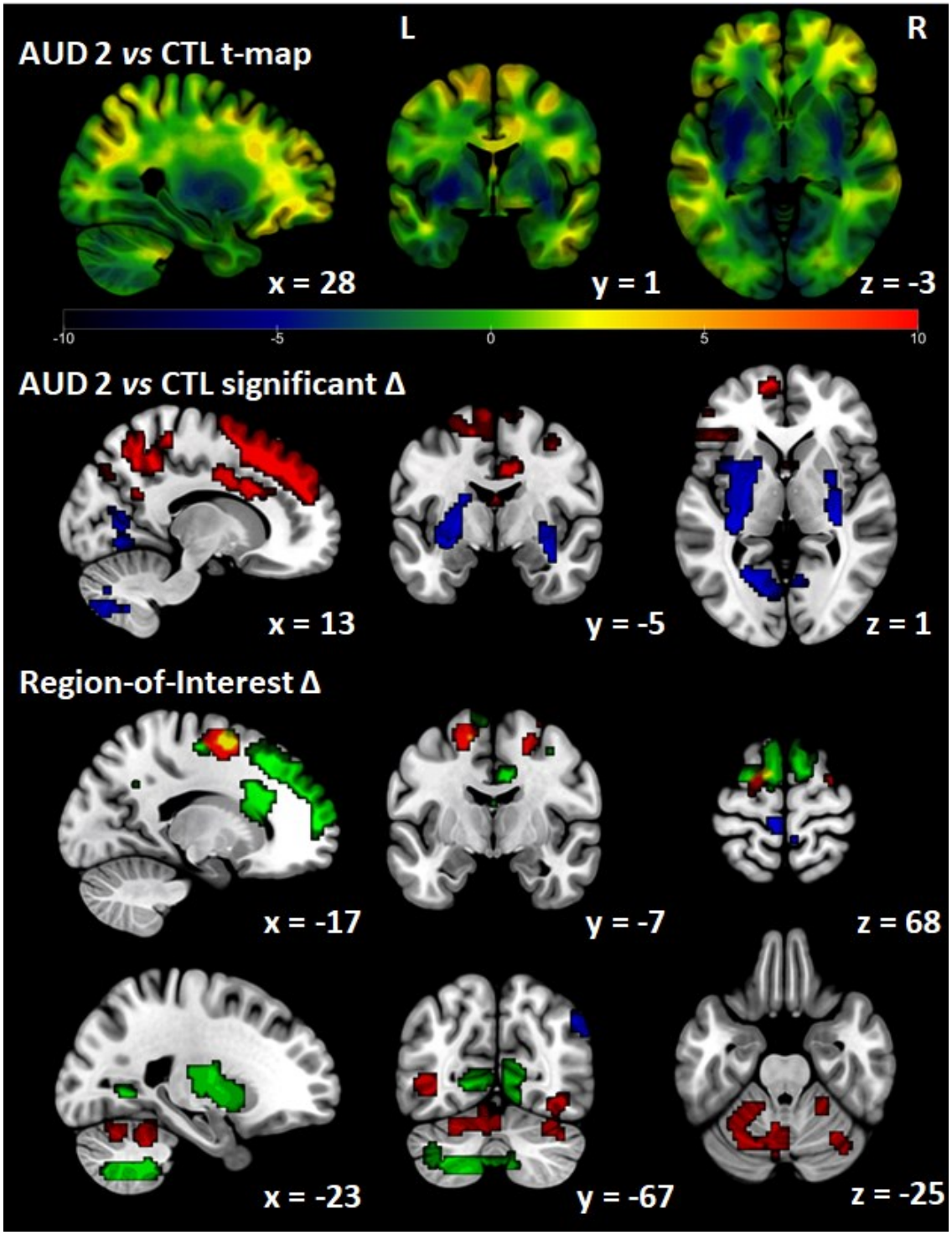

Top row depicts t-map of the group differences in the Regional Homogeneity (ReHo) between AUD patients and control at the second time point (36 days of abstinence) . Blue represents decreased ReHo in AUD, green no difference, and red increased ReHo in AUD – as illustrated by the colour bar. The second row depicts significantly decreased clusters in blue and significantly increased clusters in red. Bottom two rows depict in green the significantly different ReHo clusters from the second row (third row are higher clusters while fourth are lower clusters), which were used as seeds in whole brain region-of-interest analysis. Significantly higher whole-brain functional connectivity in AUD group at the second time point is depicted in blue, while significantly higher in red. Images are all in the MNI space.

Figure 5.7: AUD Interscan Difference s in Regional Homogeneity

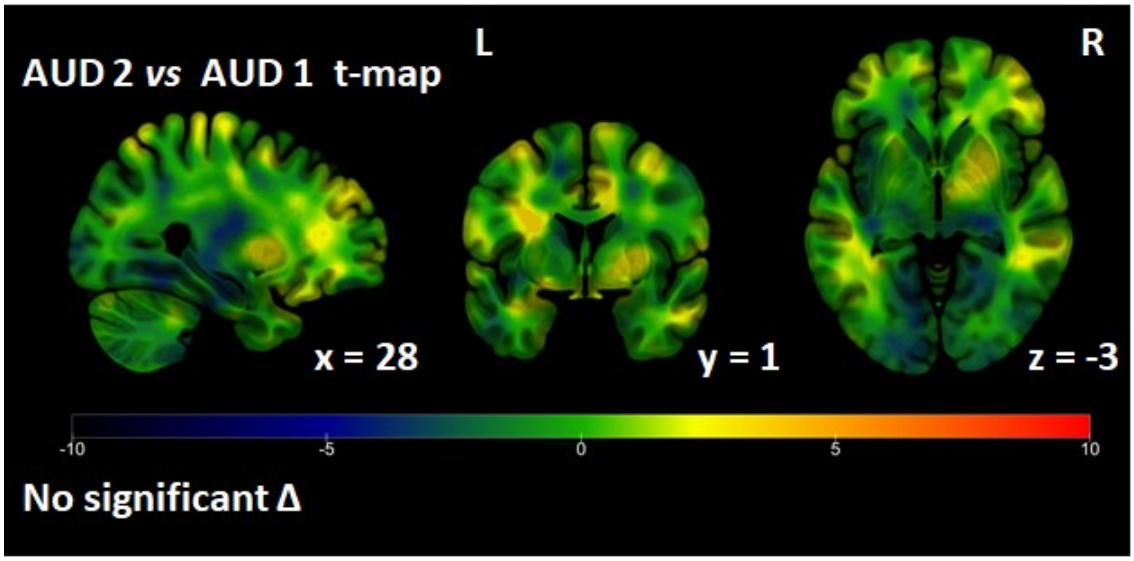

Top row depicts t-map of the interscan longitudinal differences in the Regional Homogeneity (ReHo) between AUD patients (19 versus 36 days of abstinence) . Blue represents decreased ReHo in AUD, green no difference, and red increased ReHo during the interscan interval – as illustrated by the colour bar. None of the differences survived Bonferroni multiple comparison correction. The statistical map is in the MNI space.

Figure 5.8: Degree of Centrality Differences at First Time Point

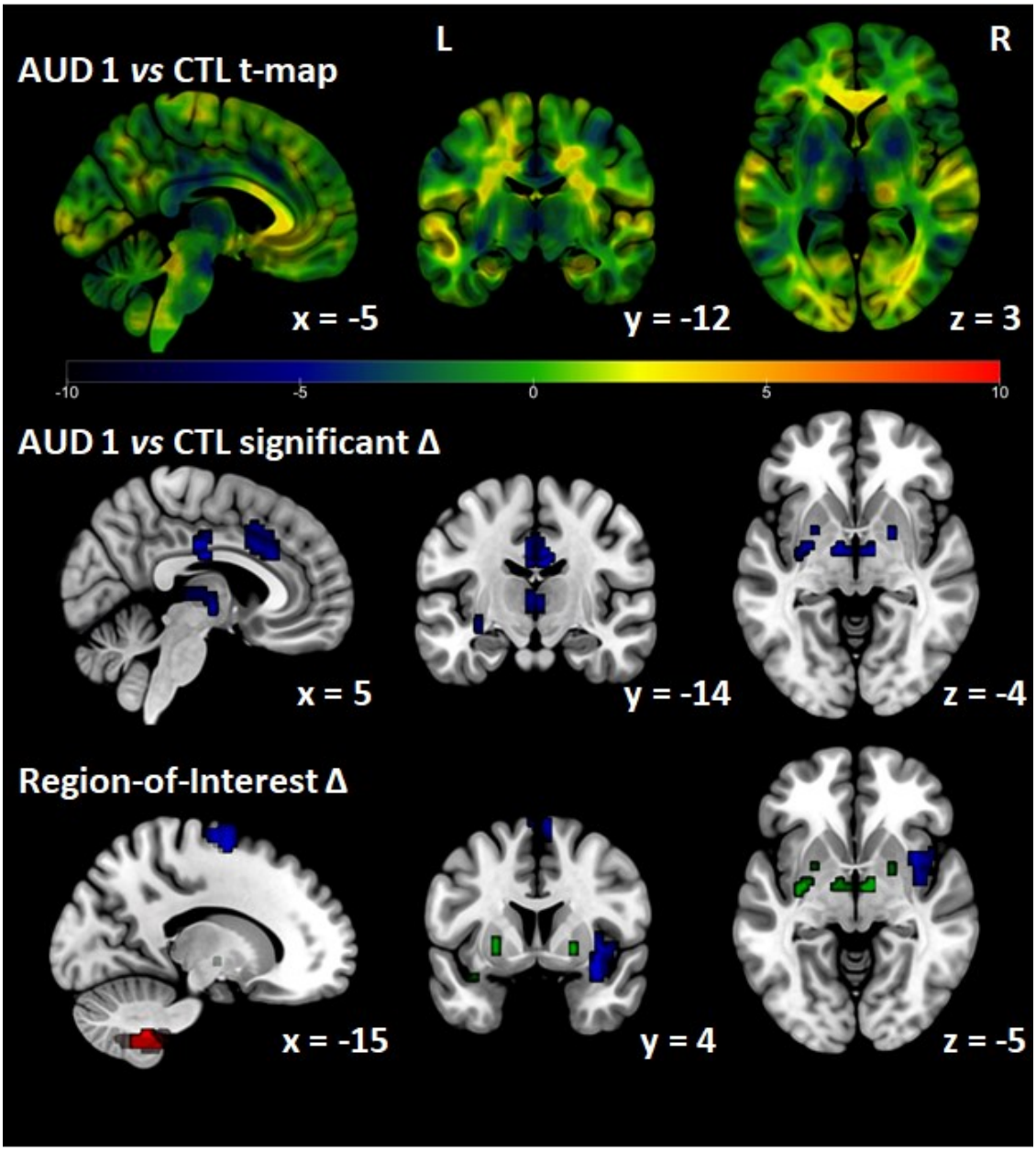

Top row depicts t-map of the group differences in the weighted Degree of Centrality between AUD patients and controls at the first time point (19 days of abstinence) . Blue represents decreased Degree of Centrality in AUD, green no difference, and red increased Degree of Centrality in AUD group – as illustrated by the colour bar. The middle row depicts significantly lower clusters in blue. There were no significantly increased clusters which survived Bonferroni multiple comparison correction. Bottom row indicates in green the significantly different clusters from middle row, which were used as seeds in whole brain region-of-interest analysis and in blue significantly lower and in red significantly higher functional connectivity clusters. Images are all in the MNI space.

Figure 5.9: Degree of Centrality Differences at Second Time Point

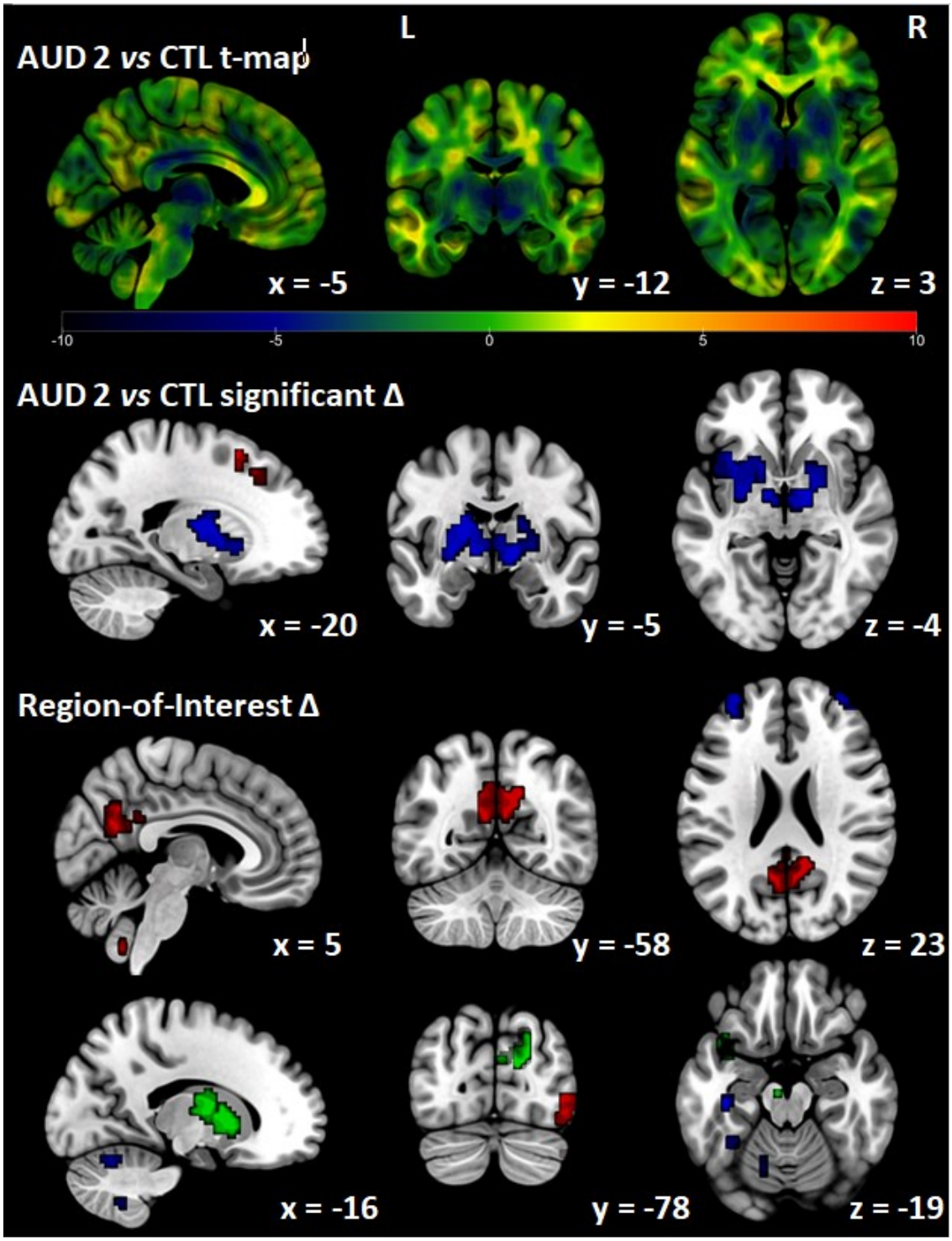

Top row depicts t-map of the group differences in the weighted Degree of Centrality between AUD patients and controls at the second time point (36 days of abstinence) . Blue represents decreased Degree of Centrality in AUD group, green no difference, and red increased group differences in AUD – as illustrated by the colour bar. The second row depicts significantly decreased clusters in blue and significantly increased clusters in red. Bottom two rows depict in green the significantly different clusters from the second row (third row are higher clusters while fourth are lower clusters), which were used as seeds in whole brain region-of-interest analysis and in blue significantly lower and in red significantly higher functional connectivity clusters at the second time point. Images are all in the MNI space.

Figure 5.10: AUD Interscan Difference s in Degrees of Centrality

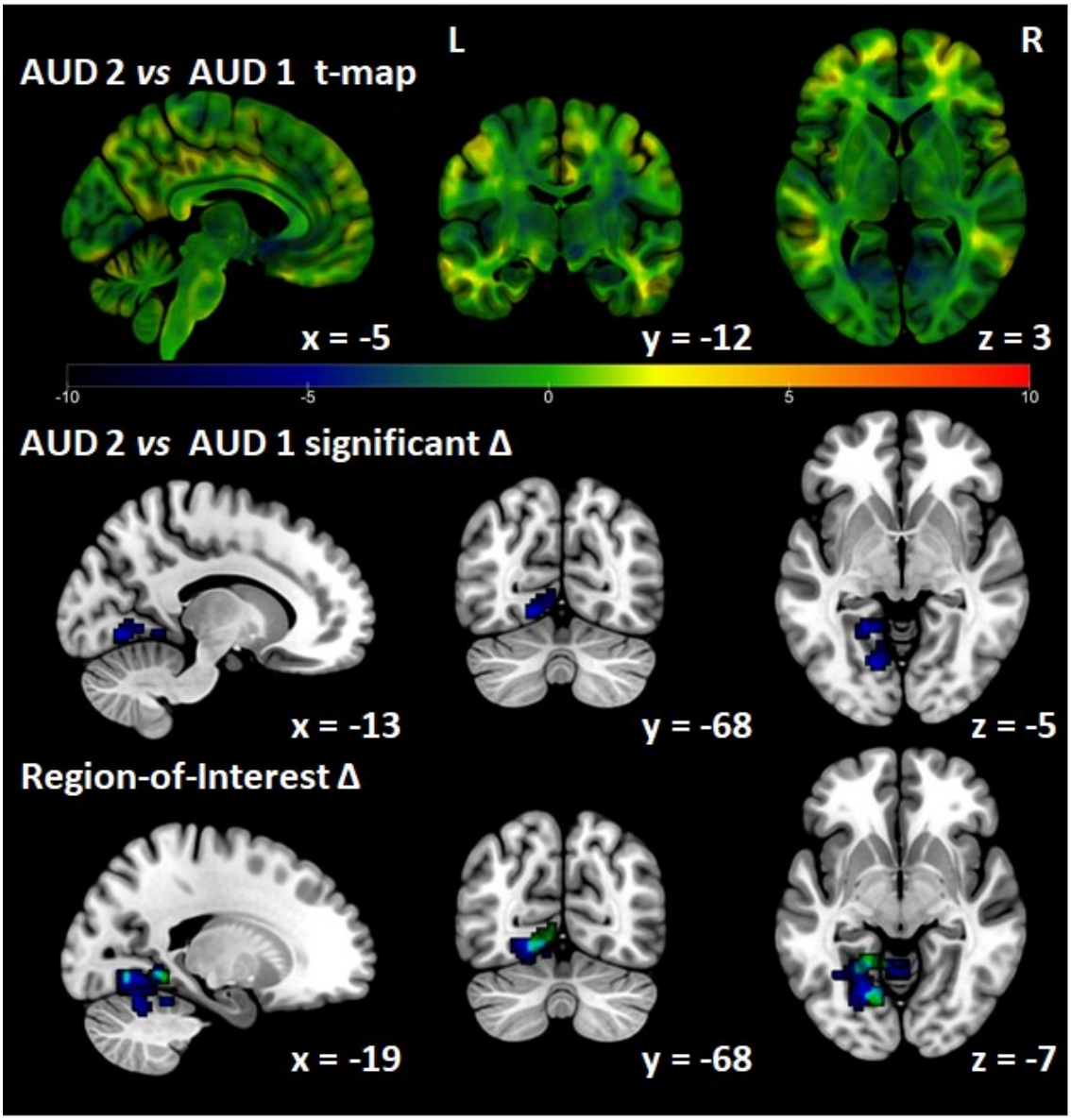

Top row depicts t-map of the group interscan longitudinal differences in the weighted Degree of Centrality between AUD patients (19 versus 36 days of abstinence) . Blue represents decreased Degree of Centrality, green no difference, and red increased Degree of Centrality during the interscan interval – as illustrated by the colour bar. The middle row depicts significant clusters (blue decreased; no significant increased clusters). The bottom row depicts results of whole-brain ROI analysis which used the above clusters as seed regions (green). Blue represents significantly lower functional connectivity at second time point. No clusters associated with increased functional connectivity survived multiple comparison correction. The statistical maps are in the MNI space.

Table 5.2: Summary of Amplitude Low Frequency Fluctuations (ALFF) Differences

ALFF	AUD 1		AUD 2		CTL		AUD1 vs CTL			AUD 2 vs CTL			AUD 2 vs AUD 1		
Clusters	**x̄**	**SEM**	**x̄**	**SEM**	**x̄**	**SEM**	**Δ %**	**t**	**p**	**Δ %**	**t**	**p**	**Δ %**	**t**	**p**
AUD 1 < CTL	0.727	0.009	0.775	0.010	0.850	0.011	**-14.42**	**-8.49**	**8.22E-15**	-8.78	-4.96	1.63E-06	6.59	-3.58	4.58E-04
AUD 2 > CTL	0.988	0.012	1.065	0.012	0.925	0.012	6.81	3.68	3.14E-04	**15.13**	**8.27**	**2.97E-14**	7.79	-4.45	1.57E-05
AUD 2 < CTL	0.976	0.012	0.907	0.012	1.078	0.014	-9.48	-5.61	7.51E-08	**-15.86**	**-9.15**	**1.27E-16**	-7.04	4.08	7.11E-05

Table 5.3: MNI Coordinates of Significant Clusters for ALFF Differences

Contrast	Voxels	MAX X (mm)	MAX Y (mm)	MAX Z (mm)	COG X (mm)	COG Y (mm)	COG Z (mm)
A1 < C	203	21	9	-12	26.3	1.4	-1.05
	194	-27	-6	-15	-26.5	-1.96	-0.82
A2 > C	3481	24	33	-18	-0.645	37.6	23.4
	1	-30	51	0	-30	51	0
A2 < C	2026	9	-75	-51	-2.61	-69.4	-24.6
	129	33	-6	-6	27.2	-5.65	0.954
	72	-3	-30	3	-1.42	-25.9	3.96
	60	-30	-12	-6	-28.3	-6.4	-1.4
	4	45	-24	24	45.7	-24.8	23.3

A1 = Alcohol Use Disorder (AUD) group at first time point; A2 = AUD group at second time point; C = control group; MAX = peak value coordinate; COG = centre of gravity

Table 5.4: Summary of Region of Interest (ROI) Analysis ALFF Differences

ALFF ROI		AUD 1		AUD 2		CTL	
ROI Cluster	Contrast	x̄	SEM	x̄	SEM	x̄	SEM
A1 < C	A1 > C	-0.014	0.026	-0.099	0.026	-0.297	0.035
	A1 < C	0.009	0.015	0.101	0.019	0.219	0.018
A2 > C	A2 < C	-0.202	0.022	-0.308	0.028	-0.097	0.011
A2 < C	A2 < C	0.413	0.03	0.287	0.024	0.488	0.028

Group Differences

ALFF ROI		AUD1 vs CTL			AUD 2 vs CTL			AUD 2 vs AUD 1		
ROI Cluster	Contrast	Δ %	t	p	Δ %	t	p	Δ %	t	p
A1 < C	A1 > C	**-95**	**6.43**	**1.20E-09**	-67	4.56	9.61E-06	586	2.3	2.29E-02
	A1 < C	**-96**	**-3.74**	**1.51E-15**	-54	-4.48	1.34E-05	965	-3.74	2.63E-04
A2 > C	A2 < C	109	3.02	1.33E-10	**218**	**-7.13**	**1.33E-10**	52	3.02	2.95E-03
A2 < C	A2 < C	-15	-1.85	6.64E-02	**-41**	**-5.57**	**9.39E-08**	-31	3.33	1.08E-03

Table 5.5: MNI Coordinates of Significant Clusters for ALFF ROI Analysis

ROI Cluster	Contrast	Voxels	MAX X (mm)	MAX Y (mm)	MAX Z (mm)	COG X (mm)	COG Y (mm)	COG Z (mm)
A1 < C	A1 > C	58	12	-36	6	9.31	-32.7	7.03
	A1 < C	85	60	-30	24	56.4	-33.2	29.7
		76	42	-87	9	40.6	-81.5	12.9
		53	57	-63	-3	55.8	-59.3	-0.453
		14	33	-6	3	33.6	-6.43	4.07
		1	-54	-63	3	-54	-63	3
A2 > C	A2 < C	755	36	-9	54	5.86	-30	64.2
		63	-33	-15	48	-31.4	-19.7	51
		17	33	9	36	31.9	12.7	38.5
A2 < C	A2 < C	30	-21	-63	-15	-16.7	-61.8	-10
		28	-42	-66	-45	-42.8	-61.4	-42.8

A1 = Alcohol Use Disorder (AUD) group at first time point; A2 = AUD group at second time point; C = control group; MAX = peak value coordinate; COG = centre of gravity

Table 5.6: Summary of Regional Homogeneity (ReHo) Differences

ReHo	AUD 1		AUD 2		CTL		AUD1 vs CTL			AUD 2 vs CTL			AUD 2 vs AUD 1		
Clusters	x̄	SEM	x̄	SEM	x̄	SEM	Δ %	t	p	Δ %	t	p	Δ %	t	p
AUD 1 > CTL	1.016	0.011	1.003	0.008	0.906	0.008	**12.13**	**8.17**	**1.06E-13**	10.63	8.33	2.35E-14	-1.34	0.99	3.26E-01
AUD 1 < CTL	0.919	0.010	0.945	0.011	1.038	0.010	**-11.50**	**-8.37**	**1.62E-14**	-8.99	-6.36	1.72E-09	2.84	-1.78	7.74E-02
AUD 2 > CTL	1.032	0.006	1.063	0.006	0.973	0.005	6.00	7.33	8.94E-12	**9.24**	**11.33**	**1.52E-22**	3.06	-3.71	2.84E-04
AUD 2 < CTL	0.935	0.009	0.878	0.010	1.004	0.009	-6.89	-5.49	1.39E-07	**-12.59**	**-9.51**	**1.98E-17**	-6.13	4.19	4.58E-05

Table 5.7: MNI Coordinates of Significant Clusters for ReHo Differences

Contrast	Voxels	MAX X (mm)	MAX Y (mm)	MAX Z (mm)	COG X (mm)	COG Y (mm)	COG Z (mm)
A1 > C	237	21	18	33	17.5	21	48.7
	214	-12	0	57	-11.9	11.1	57.3
	53	0	-3	15	-1.87	3.57	18.2
	25	18	-54	42	14.6	-55	47.5
	15	27	-72	39	25.6	-73.4	37.4
	5	30	-54	33	28.8	-53.4	34.2
A1 < C	270	30	3	-6	21.1	1.73	-3.35
	194	-27	-3	-9	-27	-3.02	-1.01
	17	-36	-72	54	-35.8	-69.7	54
A2 > C	3044	-18	60	9	-5.93	29.7	38.8
	405	9	-51	42	8.16	-57.1	41.5
	27	45	39	18	48.6	37	16.9
	13	-54	-60	15	-53.3	-57.7	15.7
	8	-15	-15	54	-15.7	-15	56.6
	6	45	-63	36	46	-62.5	36.5
	3	33	36	9	33	35	11
	2	27	36	-12	25.5	36	-12
	1	-54	-54	6	-54	-54	6
A2 < C	485	-18	-66	-51	-13.3	-69.6	-45.2
	429	-39	12	-18	-31.1	-3.83	-2.18
	206	-12	-66	3	-2.43	-70.6	5.87
	107	33	-9	-9	31.9	-8.52	-4.35
	18	39	-24	24	38.8	-21.8	24.7
	4	-9	-51	-6	-9	-51	-5.25

A1 = Alcohol Use Disorder (AUD) group at first time point; A2 = AUD group at second time point; C = control group; MAX = peak value coordinate; COG = centre of gravity

Table 5.8: Summary of Region of Interest (ROI) Analysis ReHo Differences

ReHo ROI		AUD 1		AUD 2		CTL	
ROI Cluster	**Contrast**	**x̄**	**SEM**	**x̄**	**SEM**	**x̄**	**SEM**
A1 > C	**A1 > C**	0.143	0.021	0.084	0.015	-0.019	0.012
	A1 < C	0.001	0.029	0.165	0.025	0.229	0.02
A1 < C	**A1 > C**	0.085	0.019	-0.027	0.012	-0.115	0.013
	A1 < C	-0.18	0.036	0	0.023	0.061	0.024
A2 > C	**A2 > C**	0.169	0.02	0.303	0.024	0.057	0.012
	A2 < C	-0.138	0.046	-0.284	0.042	0.093	0.03
A2 < C	**A2 > C**	-0.036	0.012	0.066	0.015	-0.112	0.012
	A2 < C	-0.268	0.038	-0.422	0.045	-0.052	0.03

Group Differences

ReHo ROI		AUD1 vs CTL			AUD 2 vs CTL			AUD 2 vs AUD 1		
ROI Cluster	**Contrast**	**Δ %**	**t**	**p**	**Δ %**	**t**	**p**	**Δ %**	**t**	**p**
A1 > C	**A1 > C**	**-840**	**6.69**	**6.33E-10**	-537	5.38	2.67E-07	-41	2.23	2.73E-02
	A1 < C	**-100**	**-6.48**	**1.24E-09**	-28	-1.98	4.93E-02	27080	-4.3	2.93E-05
A1 < C	**A1 > C**	**-174**	**8.75**	**3.97E-15**	-77	4.92	1.93E-06	-131	5.02	1.54E-06
	A1 < C	**-397**	**-5.62**	**9.30E-08**	-100	-1.85	6.55E-02	-100	-4.27	3.60E-05
A2 > C	**A2 > C**	194	4.76	4.99E-06	**428**	**9.08**	**3.10E-15**	80	-4.25	3.69E-05
	A2 < C	-249	-4.23	4.22E-05	**-406**	**-7.28**	**1.64E-11**	106	2.35	2.01E-02
A2 < C	**A2 > C**	-68	4.56	9.59E-06	**-159**	**9.27**	**1.30E-16**	-285	-5.19	6.42E-07
	A2 < C	418	-4.48	1.38E-05	**715**	**-6.8**	**2.52E-10**	57	2.61	9.97E-03

Table 5.9: MNI Coordinates of Significant Clusters for ReHo ROI Analysis

ROI Cluster	Contrast	Voxels	MAX X (mm)	MAX Y (mm)	MAX Z (mm)	COG X (mm)	COG Y (mm)	COG Z (mm)
A1 > C	**A1 > C**	9	21	3	6	22	2.67	7.67
	A1 < C	375	57	-30	36	35	-38	56.8
		102	-45	-33	39	-46.5	-34.5	47.2
		35	-27	-39	60	-24.6	-35.3	61.1
		3	-21	30	36	-20	30	35
A1 < C	**A1 > C**	82	33	-6	57	31.5	-8.63	60.7
		39	6	-45	-15	-3.69	-43.4	-15.8
		20	48	-24	45	48.6	-24.2	47.1
		15	15	-66	-51	15.2	-68.4	-47.4
		15	36	-72	-15	35.4	-71.8	-16.4
		14	21	-36	-24	20.1	-37.1	-23.6
		12	24	-18	-12	22	-19.2	-11.5
		5	-21	-45	-21	-22.8	-46.2	-19.2
		5	24	-33	-12	24	-34.2	-11.4
		2	24	-24	60	24	-24	61.5
	A1 < C	3	-57	3	-27	-58	4	-27
A2 > C	**A2 > C**	93	-18	-3	63	-17.5	-3.1	60.8
		48	-36	-75	15	-37.6	-72.6	16.4
		45	-3	15	60	-1.13	16.9	59.4
		40	12	15	9	13.1	17.4	13.4
		15	24	-3	57	23.4	-4	56.4
		5	15	0	15	16.2	-0.6	19.2
		4	9	0	-12	9	-0.75	-12.7
		3	27	-3	66	29	-4	68
	A2 < C	109	-3	-33	69	0.742	-30.2	74.7
A2 < C	**A2 > C**	210	-24	-51	-27	-14.6	-59.9	-20.3
		111	24	-45	-21	21.5	-46.1	-11.8
		28	39	-69	-9	39.1	-70.6	-7.5
		25	-39	-69	0	-42.5	-67.7	0.96
		21	36	-69	-27	34.6	-67.1	-25.3
		2	24	-60	-15	22.5	-60	-15
	A2 < C	18	51	-69	39	50.7	-66.7	38.7
		6	12	-57	18	11	-57.5	15
		1	-3	69	21	-3	69	21

A1 = Alcohol Use Disorder (AUD) group at first time point; A2 = AUD group at second time point; C = control group; MAX = peak value coordinate; COG = centre of gravity

Table 5.10: Summary of Weighted Degrees of Centrality (DC) Differences

Weighted DC	AUD 1		AUD 2		CTL		AUD1 vs CTL			AUD 2 vs CTL			AUD 2 vs AUD 1		
Clusters	**x̄**	**SEM**	**x̄**	**SEM**	**x̄**	**SEM**	**Δ %**	**t**	**p**	**Δ %**	**t**	**p**	**Δ %**	**t**	**p**
AUD 1 < CTL	0.965	0.016	0.996	0.016	1.227	0.022	**-21.36**	**-9.54**	**1.36E-17**	-18.80	-8.36	2.01E-14	3.26	-1.36	1.77E-01
AUD 2 > CTL	1.000	0.029	1.059	0.026	0.826	0.021	21.10	4.94	2.00E-06	**28.23**	**7.04**	**5.20E-11**	5.89	-1.53	1.29E-01
AUD 2 < CTL	1.025	0.016	0.950	0.016	1.174	0.018	-12.69	-6.13	5.39E-09	**-19.10**	**-9.30**	**4.89E-17**	-7.34	3.28	1.26E-03
AUD 2 < AUD 1	1.553	0.040	1.249	0.033	1.395	0.023	11.35	3.44	7.71E-04	-10.46	-3.65	3.64E-04	**-19.58**	**5.93**	**1.86E-08**

Table 5.11: MNI Coordinates of Significant Clusters for DC Differences

Contrast	Voxels	MAX X (mm)	MAX Y (mm)	MAX Z (mm)	COG X (mm)	COG Y (mm)	COG Z (mm)
A1 < C	109	0	21	30	1.38	18.9	35
	69	0	-12	3	-1.13	-18.4	2
	45	-3	-15	36	-8.58E-05	-15.3	33.2
	26	-24	-6	3	-26.3	-4.96	0.000664
	4	-36	6	-18	-37.5	7.5	-18
	4	21	3	-3	21	1.5	-1.5
	2	-6	-30	27	-6	-28.5	27
	1	12	-39	54	12	-39	54
	1	9	-45	57	9	-45	57
A2 > C	16	-18	27	42	-15.4	30.7	40.7
	12	-24	15	51	-22.3	15.7	53
A2 < C	671	12	-9	-9	-7.83	-1.36	1.62
	101	18	-69	18	16.8	-75.9	26
	32	-3	-18	27	-0.282	-23.1	27
	2	-6	-18	-21	-6	-18	-19.5
A2 < A1	28	-9	-66	-3	-11.5	-66.5	-3.64
	13	-18	-48	-6	-17.5	-50.3	-6.23
	2	30	-45	-21	31.5	-45	-21

A1 = Alcohol Use Disorder (AUD) group at first time point; A2 = AUD group at second time point; C = control group; MAX = peak value coordinate; COG = centre of gravity

Table 5.12: Summary of Region of Interest (ROI) Analysis DC Differences

DC ROI		AUD 1		AUD 2		CTL	
ROI Cluster	**Contrast**	**x̄**	**SEM**	**x̄**	**SEM**	**x̄**	**SEM**
A1 < C	**A1 > C**	0.022	0.015	-0.088	0.014	-0.165	0.016
	A1 < C	-0.06	0.024	0.081	0.016	0.186	0.018
A2 > C	**A2 > C**	0.202	0.028	0.284	0.037	0.07	0.015
	A2 < C	-0.274	0.034	-0.328	0.031	-0.042	0.021
A2 < C	**A2 > C**	-0.088	0.027	0.103	0.028	-0.144	0.024
	A2 < C	-0.025	0.014	-0.096	0.012	0.067	0.013
A2 < A1	**A2 < A1**	0.596	0.039	0.328	0.024	0.449	0.026

Group Differences

DC ROI		AUD1 vs CTL			AUD 2 vs CTL			AUD 2 vs AUD 1		
ROI Cluster	**Contrast**	**Δ %**	**t**	**p**	**Δ %**	**t**	**p**	**Δ %**	**t**	**p**
A1 < C	**A1 > C**	**-113**	**8.71**	**1.98E-15**	-46	3.6	4.09E-04	-499	5.35	2.96E-07
	A1 < C	**-133**	**-8.23**	**7.02E-14**	-56	-4.33	2.49E-05	-235	-4.89	2.66E-06
A2 > C	**A2 > C**	190	4.22	4.61E-05	**307**	**5.35**	**5.24E-07**	40	-1.75	8.26E-02
	A2 < C	550	-5.73	5.89E-08	**681**	**-7.65**	**2.23E-12**	20	1.19	2.35E-01
A2 < C	**A2 > C**	-39	1.55	1.24E-01	**-171**	**6.64**	**4.15E-10**	-217	-4.88	2.47E-06
	A2 < C	-137	-4.7	5.31E-06	**-244**	**-9.03**	**2.60E-16**	285	3.82	1.91E-04
A2 < A1	**A2 < A1**	33	3.19	1.77E-03	-27	-3.42	7.82E-04	**-45**	**5.89**	**2.89E-08**

Table 5.13: MNI Coordinates of Significant Clusters for DC ROI Analysis

ROI Cluster	Contrast	Voxels	MAX X (mm)	MAX Y (mm)	MAX Z (mm)	COG X (mm)	COG Y (mm)	COG Z (mm)
A1 < C	A1 > C	112	-18	-54	-51	-23.3	-54.6	-50.4
		51	-51	-72	33	-47.5	-69.3	38.4
		1	-36	-57	-12	-36	-57	-12
		1	-9	-45	15	-9	-45	15
	A1 < C	136	36	-3	-15	40	7.19	-12.3
		127	-9	-6	63	-8.22	-4.44	70.3
		11	-33	-12	57	-30.8	-14.2	58.6
		8	39	30	-12	40.5	30.8	-13.1
		8	42	18	3	40.9	16.9	4.12
A2 > C	A2 > C	227	-6	-57	21	-0.978	-54.8	28.4
		72	-30	-36	-9	-27.2	-38.7	-0.292
		5	3	-54	-54	3	-54	-54
		2	-18	33	39	-19.5	33	39
		2	9	39	45	9	40.5	45
	A2 < C	41	-30	45	18	-32.5	52.1	23
		26	42	54	21	37.6	55.5	22.6
		8	66	-39	36	64.1	-37.9	39.4
A2 < C	A2 > C	38	48	-81	-9	46.1	-80.5	-6.87
		14	48	-69	-39	48.6	-68.1	-37.3
	A2 < C	15	-36	-51	-15	-34.6	-50.8	-14.8
		10	-33	-51	-30	-33.6	-49.5	-27.3
		8	-18	-57	-51	-20.6	-57.7	-49.1
		7	-15	-66	-21	-15.4	-64.7	-22.3
		6	-36	-24	-21	-38	-23.5	-20
		1	48	-42	33	48	-42	33
A2 < A1	A2 < A1	202	-21	-60	-21	-16.5	-58.2	-12.2
		1	-3	-39	-9	-3	-39	-9

A1 = Alcohol Use Disorder (AUD) group at first time point; A2 = AUD group at second time point; C = control group; MAX = peak value coordinate; COG = centre of gravity

Table 5.14: Pearson Correlations of Clinical Severity to Functional Connectivity Measures

Correlations	ALFF			ReHo				DC			
Clusters →	A1 < C	A2 > C	A2 < C	A1 > C	A1 < C	A2 > C	A2 < C	A1 < C	A2 > C	A2 < C	A2 < A1
Abstinence	0.11	0.39***	-0.27*	0.06	-0.18	0.31**	-0.17	0.12	-0.11	-0.08	-0.29*
# Drinks	-0.2	0.21	-0.30***	0.38***	-0.17	0.32***	-0.32***	-0.35***	0.34***	-0.38***	0.12
AUDIT	-0.42***	0.28***	-0.42***	0.42***	-0.40***	0.46***	-0.42***	-0.54***	0.44***	-0.5***	0.02
ADS	-0.23**	0.21	-0.35***	0.38***	-0.16	0.35***	-0.44***	-0.45***	0.46***	-0.47***	0.08
OCDS	-0.34***	0.27	-0.45***	0.38***	-0.26**	0.43***	-0.46***	-0.43***	0.46***	-0.45***	-0.04
ODS	-0.27**	0.18	-0.38***	0.34***	-0.17	0.33***	-0.43***	-0.36***	0.42***	-0.37***	-0.01
CDS	-0.37***	0.32***	-0.47***	0.39***	-0.32***	0.48***	-0.44***	-0.44***	0.46***	-0.47***	-0.06

*p<0.05, ** p<0.01, *** p<0.001 Bonferroni-corrected

4 Discussion

The objective of this study was to compare longitudinal changes in regional functional connectivity in recovering AUD patients between 19 and 36 days of sustained abstinence. Our study has revealed substantial decrease across several measures of regional functional connectivity in basal ganglia in AUD patients compared to healthy controls at both time points and a significant increase in superior frontal regions at the second time point. Most of these changes were weakly to moderately correlated to the severity of AUD. Longitudinal interscan changes were not significant across most measures and their interpretation is not intuitive. The changes could be interpreted in the context of compensatory decreased bottom-up and increased executive top-down functional changes associated with addiction recovery (for review of this hypothesis see (Fein & Cardenas, 2015)), although the ROI analysis and deeper investigation of longitudinal changes in overlapping voxels did not provide evidence supporting this interpretation. The longitudinal differences were thus largely contrary to our *a priori* expectations of progressive functional connectivity normalisation with longer AUD remission. The exploratory region-of-interest (ROI) analysis using the significant clusters as seeds has also provided inconsistent differences in the AUD group with both increased and decreased functional connectivity across multiple brain regions. This was also contrary to our expectation of widespread increased compensatory recruitment (and thus broadly increased functional connectivity with the most regionally deficient seed regions) (for review see (Chanraud & Sullivan, 2014; Sullivan & Pfefferbaum, 2005)) and has not revealed additional insights into the functional plasticity associated with early remission from AUD.

This analysis has taken an inside-out approach to our functional connectivity investigation from voxel-specific all the way to the whole brain functional connectome measures. The voxel-specific ALFF analysis has revealed bilateral deficits in low frequency fluctuations in putamen and pallidum in the AUD group at both first and second time points. At the second time point, there was more anatomically wide-spread decrease in putamen and pallidum (less anterior/superior extent and more posterior/inferior) and

much more broader decrease including areas in bilateral thalamus, lingual gyrus and intracalcarine cortex, and bilateral cerebellum (wide-spread across posterior regions). The greater the ALFF deficits, the more severe the clinical correlates across both time points, although the average number of drinks prior to detoxification was only significant at the second time point. Only the second time point ALFF deficit contrast exhibited significant correlation with the length of abstinence. Contrary to our *a priori* expectation, this correlation was negative. At the second time point, there was also a wide-spread ALFF increase in bilateral regions of frontal cortex (frontal pole, frontal orbital cortex, frontal medial cortex, paracingulate gyrus, superior frontal gyrus, middle frontal gyrus, inferior frontal gyrus). These changes were significantly positively correlated to both AUDIT severity as well as compulsive drinking subscale (CDS) score as well the length of abstinence at the first time point. The more severe the compulsive drinking before detoxification and the longer the length of abstinence at the first time point, the greater the ALFF difference in the AUD group compared to controls. These ALFF changes could thus be interpreted as serving as a potential compensatory mechanism for maladaptive addiction-related reinforcement of compulsive functional loops required for sustained remission. 38% of the first time point-voxels were overlapping across both contrasts. The longitudinal interscan differences were not significant, but indicated a positive trend across both the basal ganglia as well as the frontal cortex. The magnitude of differences and the anatomical extent in the contrasts increased from the first to second time point, contrary to our initial normalization hypothesis. However, examining just the average values from the overlapping voxels between the significant contrasts of both scans reveal a positive trend from -15.87% (t -6.09) to -11.34% (t -4.36) with nonsignificant interscan AUD improvement of +5.39% (t +1.67).

The exploratory ROI analysis using the significant ALFF changes clusters on the second half of untested data has also revealed significant whole-brain functional connectivity differences between the AUD patients and healthy controls. At the first time point, the decreased ALFF seed has been associated with an anatomically questionable ROI cluster of increased deep brain functional connectivity which included

thalamus, caudate nucleus but also white matter and lateral ventricles. At the same time, ROI clusters of decreased functional connectivity included right parietal operculum / supramarginal gyrus, right middle temporal gyrus, as well as right putamen and insula. At the second time point, the lower ALFF seed was associated with lower whole-brain functional connectivity with further decrease in cerebellum (left Crus I and II) and left lingual gyrus. The regional clusters of higher ALFF in the frontal cortex were, on the other hand, associated with decreased whole-brain activation in superior frontal regions of the frontal lobe (including postcentral gyrus, precentral gyrus, posterior aspects of superior frontal gyrus) as well as superior aspects of lateral occipital cortex and precuneus.

To the best of our knowledge only two other AUD-related ALFF studies (R. Liu et al., 2018; Weng et al., 2018) and one ALFF study examining acute ethanol intoxication in healthy controls (Zheng et al., 2015) have been published to this date. Liu *et al*. has compared 29 AUD patients of unknown length of abstinence to 29 healthy controls, revealing higher ALFF in right inferior parietal lobule and right supplementary motor area while lower ALFF in left precuneus and bilateral cerebellum posterior lobe. Weng *et al*. has compared 15 AUD (and nicotine dependent) patients of unknown length of abstinence to 17 healthy controls (and 16 betel nut chewers), revealing higher ALFF in the AUD group in the left calcarine sulcus (with cluster size of only 3 voxels). The ALFF results reported in the literature are largely not consistent with each other nor our findings. Our results for the second time point contrast, nonetheless, have some similarities particularly to Liu *et al*. Our study has also revealed higher ALFF partially in the supplementary motor area (but more medially rather than laterally) and lower ALFF in the cuneus rather than in the precuneus (near the parietal-occipital fissure as depicted in Liu's projection) and also in cerebellum (although again not in overlapping regions). Due to substantial spatial smoothing, the precise anatomical location should be considered with caution, especially when reporting findings in boundary regions such as the parietal-occipital fissure. Neither of the ALFF AUD papers has reported significant decrease in the ALFF in the basal ganglia. Interestingly, Zheng *et al*. has reported that acute ethanol intoxication has increased ALFF in the basal ganglia (left caudate and more diffuse cluster across

left basal ganglia) in 32 healthy subjects. Acute intoxication also resulted in increased ALFF in lthe eft hippocampus and left inferior frontal lobe and decreased ALFF in the cerebellum, frontal lobe, and temporal lobe. Chronic, repetitive alcohol intoxication could lead to baseline attenuation of the alcohol-related brain activation to restore relative allostasis during the addiction. This could consequently reflect in decreased baseline ALFF in basal ganglia in the recovering addicted brain. However, this postulation fails to explain decreased ALFF reported in cerebellum both by Zheng *et al.* during acute intoxication as well as in recovering chronic AUD patients in our study. Due to partial volume effects and signal inhomogeneities in regions close to tissue boundaries, the functional differences in cerebellum can be challenging to observe in traditional fMRI scans which focus their field of view primarily on the cortex.

The ReHo analysis, exploring the pattern of Kendall's coefficient of concordance with the neighbouring voxels, has yielded similar results to the voxel-specific ALFF. At the first time point, the AUD group exhibited abnormally lower ReHo in bilateral putamen, pallidum, thalamus (the smoothed cluster extending even past subcortical areas into right subcallosal cortex) and abnormally higher ReHo across bilateral superior frontal gyrus and to a lesser extent also right precuneus, right superior lateral occipital cortex, and right anterior cingulate gyrus. The ReHo deficits were negatively correlated only with AUDIT, OCDS, and CDS scores, while the abnormally increased ReHo was positively correlated with all of the measures except for the length of initial abstinence. Similarly to the ALFF, the second time point results were opposite to our initial expectations and revealed a much broader anatomical extent of both increased and decreased ReHo clusters. At the second time point, the AUD group exhibited a broader anatomical decrease in ReHo, including also bilateral insula (primarily left), bilateral lingual gyrus and intracalcarine and supracalcarine cortices and bilateral cerebellum. At the second time point, the increased ReHo clusters were also more wide-spread, including also bilateral precuneus, and bilateral angular gyrus / lateral occipital cortex. The magnitude of the ReHo deficits was negatively correlated with all of the AUD severity scales except for the length of abstinence at the first time point. The magnitude of the abnormally high ReHo clusters was positively correlated with all of the clinical severity scales and also

the length of initial abstinence, suggesting similarly to the second time point contrast in ALFF a potential compensatory role of the frontal regions. The longitudinal interscan AUD differences in ReHo were similarly to ALFF also not significant but unlike ALFF suggested less uniform trend. 43% of the significant voxels overlapped for the decreased contrast and 79% for the increased contrast. The changes only within the overlapping significant regions have revealed very little change in the average magnitude during the interscan interval. For the lower clusters, the contrasts were -11.86% (t -4.94) to -11.71% (t -4.94) and +0.18% (t +0.00) for interscan, while for the higher clusters were +12.24% (t +4.26), +11.59% (t +4.04) and -0.58% (t -0.22).

The exploratory ROI analysis using the significant ReHo clusters as seeds for whole-brain analysis on the untested second half of the data has revealed different results to the ALFF ROI analysis, even though both ROI analyses were based on broadly similar seed regions (especially in the second time point contrasts). At the first time point, clusters of decreased ReHo in the basal ganglia were associated with increased functional connectivity with the right precentral and postcentral gyri, right occipital fusiform gyrus, and bilateral cerebellum. The only region of significantly decreased functional connectivity with the decreased ReHo seed was located in the temporal lobe and should be considered with caution due to its small cluster size. Increased ReHo seed from the first time point contrast was associated with increased functional connectivity in the AUD group in the right putamen and right superior frontal gyrus and a decreased functional connectivity in the superior precentral gyrus, postcentral gyrus, and supramarginal gyrus (posterior part). Seed clusters from the second time point ReHo contrast revealed different changes in functional connectivity compared to the first time point. The decreased ReHo seed from the second time point contrast was associated with increased functional connectivity with cerebellum, right postcentral gyrus, bilateral lateral occipital cortex (V5), as well as lingual gyrus and temporal-occipital fusiform gyrus. The decreased ReHo cluster was also associated with decreased functional connectivity with right inferior parietal lobule, precuneus, left frontal pole, and brainstem. All of the decreased ROI functional connectivity clusters of decreased ReHo seed were, however, of relatively small size and thus

should be interpreted with caution. The increased ReHo cluster from the second contrast was associated with increased functional connectivity with more widespread increase in bilateral superior frontal gyri, right caudate nucleus, bilateral lateral occipital cortex (inferior parietal lobule, V5) and some non-grey matter regions. Increased ReHo cluster from the second time point contrast was also associated with decreased functional connectivity in bilateral superior aspects of precentral and postcentral gyri. The bigger and less anatomically specific seed regions for the ROI analysis have generally resulted in less significant group differences since the timecourses of the anatomically different clusters averaged out and were thus not strongly correlated to any other specific anatomical region.

To the best of our knowledge, only three AUD-related ReHo studies (H. Kim et al., 2015; Tu et al., 2018; Weng et al., 2018) and one acute ethanol intoxication in healthy controls ReHo study (Zheng et al., 2015) have been published to this date. Kim *et al*. has published ReHo differences between 14 young AUD (average age 29 years) of at least 2 weeks of abstinence (unknown average sobriety length) to 15 healthy controls (and internet gaming subjects), revealing increased ReHo in the right posterior cingulate cortex and to lesser extent also right insula and left middle temporal gyrus while decreased ReHo in the right anterior cingulate cortex. Tu *et al*. has compared 29 AUD patients of unknown length of abstinence to matched 29 controls, revealing wide-spread small clusters of higher ReHo in right superior frontal gyrus, bilateral medial frontal gyrus, and right inferior temporal gyrus while lower ReHo in right cerebellum (posterior and anterior lobes), left rectal gyrus, and right pons. Weng *et al*. has compared 15 AUD (and nicotine dependent) patients of unknown length of abstinence to 17 healthy controls (and 16 betel nut chewers), revealing higher ReHo in the right insula (cluster size of just 2 voxels). None of the above studies reported decreased ReHo in the basal ganglia. Nonetheless, our results overlap to a small extent with the reported literature in reporting lower ReHo in cerebellum and higher ReHo in superior frontal gyrus (both primarily in the second time point contrasts) but also differ, for example, in reporting decreased rather than increased ReHo in the insula in the AUD cohort. Similarly to the ALFF results, Zheng *et al*. has also interestingly reported that 32 healthy volunteers who have been exposed to acute

ethanol intoxication have exhibited increased ReHo in the basal ganglia (spanning left putamen, globus pallidus, and caudate nucleus). Other regions exhibiting increased ReHo included frontal lobe, cerebellum, right internal capsule, left hippocampus, and left precuneus, while lower ReHo was reported in frontal lobe, right temporal lobe, right hippocampus, and left anterior cingulate gyrus. Unlike in the ALFF results, the ReHo results reported by Zheng *et al*. appear to be more consistent with the postulation of allostatic decrease in baseline functional connectivity in recovering AUD brain in response to chronic repetitive alcohol intoxication. The pattern of increased ReHo in basal ganglia and cerebellum while decreased ReHo in frontal lobe and cingulate gyrus during acute ethanol intoxication in healthy controls suggest an inverse trend to the findings reported in the recovering chronic AUD patients in our study.

The Degree of Centrality analysis has explored the most wide-spread functional connectivity patterns during the AUD recovery, comparing the number of direct connections from each voxel to the entire functional connectome of the brain. The DC analysis has revealed the most diverging results from the other analyses, although the negative trend across the basal ganglia has persisted even in DC. This is interesting since DC is especially sensitive for functional connectivity changes in higher association cortices, rather than the subcortical or paralimbic structures (Zuo et al., 2012). At the first time point, the AUD group has exhibited a significantly decreased DC in bilateral putamen, pallidum, and thalamus as well as bilateral cingulate gyrus (anterior, middle) and no significant clusters of increased DC. The magnitude of the DC deficits was significantly negatively correlated with all of the measured clinical severity scales but not with the length of abstinence at the first time point. At the second time point, there was more widespread significant decrease in DC including greater extent of bilateral putamen, pallidum, and thalamus with the smoothed cluster spanning into bilateral caudate nuclei and even into left insula but including less cingulate gyrus. The contrast has also revealed decreased DC in a cluster spanning left cuneus in the occipital cortex. The second time point contrast has also revealed increased DC in the left superior frontal gyrus in the AUD group; however, this should be interpreted with caution due to the small cluster size. The magnitude of DC deficits was negatively correlated and excess DC at the second

time point was positively correlated to all of the clinical severity measures but not to the initial length of baseline abstinence. Unlike in the other two analyses, the interscan AUD differences were significant in DC analysis, revealing a significant decrease in the DC spanning left lingual gyrus and very small cluster in the right occipital fusiform cortex. Contrary to our *a priori* expectations, this suggests continued deterioration in the DC with prolonged abstinence. The significant interscan cluster also falls outside of the significant clusters revealed by the first and second time point AUD minus control contrasts and is only of modest size so should be interpreted with caution. The magnitude of longitudinal DC changes were not significantly correlated to any of the clinical severity scales but was negatively correlated to the baseline length of abstinence. Examining just the overlapping clusters from the two contrasts, we observe 33% overlap and also continued but not significant deterioration from -20.68% (t -4.39) to -22.89% (t -4.81), equivalent to interscan differences of -2.78% (t -0.40).

The ROI analysis based on the DC contrast cluster seeds has similarly to the main contrasts revealed less extensive group differences compared to ALFF and ReHo ROI analyses. The decreased DC at first time point seed region was associated with decreased functional connectivity with superior aspects of bilateral superior frontal and precentral gyri, and right insula (spanning into right orbital frontal cortex and temporal pole) as well as increased functional connectivity with left cerebellum and superior left lateral occipital cortex. The seed region of decreased DC at the second time point was associated with decreased functional connectivity with right posterior supramarginal gyrus, left temporal occipital fusiform cortex, and left cerebellum (but these should be all interpreted with caution due to small cluster size) as well as increased functional connectivity with right lateral occipital cortex and right cerebellum. Because of the questionably small seed region of the increased DC cluster at the second time point, the results of this ROI analysis should be disregarded. This seed region was associated with anatomically unclear regions which included non-grey matter regions and smaller decreased functional connectivity clusters in bilateral frontal pole and increased functional connectivity clusters in bilateral precuneus and smaller clusters in cerebellum, insula, temporal lobe, right superior frontal gyrus. The significant interscan cluster seed was

associated with a decreased functional connectivity with broader clusters extending lingual gyrus, temporal occipital fusiform cortex, and cerebellum at the second time point compared to the first one.

To the best of our knowledge, only one AUD-related DC study has been published to this date (X. Luo et al., 2017). Luo *et al*. compared DC in 24 treatment-naive AUD of unknown length of abstinence to 24 healthy controls, reporting higher DC in AUD in left precentral gyrus, right hippocampus, left orbitofrontal cortex while lower DC in left cerebellum posterior lobe, bilateral secondary visual network (cuneus), and left precuneus. There was no substantial overlap between Luo *et al*. results and the results of our study.

In summary, there does not appear to be a consistent pattern of regional functional connectivity changes across the different measures other than the persistent deficits in basal ganglia and increased regional functional connectivity patterns in superior frontal regions at the second time point. The bilateral resting state functional deficits in the putamen and pallidum are the only regions with overlapping voxels across all of the measures in voxel-specific ALFF activation / fluctuations, ReHo synchrony across neighbouring voxels, as well as DC whole-brain functional connectivity at both time points in the AUD compared to the healthy controls. The anatomical extent of the deficits in the basal ganglia has increased with the prolonged abstinence; however, none of the longitudinal interscan differences were significant in the basal ganglia within the AUD group. The existing literature has reported quite heterogeneous results of altered regional functional connectivity in AUD compared to healthy controls. The reported results only marginally overlapped with our results and did not replicate the main findings of our study. Unlike the existing literature, our study has generally reported larger clusters (or regional groups of clusters) which usually persisted in both hemispheres. Assuming global neurotoxic effect of ethanol and at least partially reversible whole-brain maladaptive processes caused by the chronic recurrent ethanol intoxication (as suggested by preclinical, histological, and neurochemical evidence summarized in the introduction), a bilateral rather than unilateral functional connectivity changes appear to be more likely in the recovering

AUD brain. Our study also consisted of the largest sample size to this date and was the first longitudinal study and has replicated broadly consistent main findings at both time points.

The changes in ALFF and ReHo reported by Zheng *et al*. (2015) during acute ethanol intoxication have, nonetheless, revealed a broadly opposite pattern of regional functional connectivity changes to the differences observed in recovering chronic AUD patients in our study, which could help contextualize our findings. This inverse pattern in acute one-time intoxication versus chronic AUD could be evidence of potential baseline functional attenuation in a recovering addicted brain in regions which have been previously chronically over-activated due to repetitive acute ethanol intoxication. A similar pattern was recently reported in young healthy social drinkers who were scanned before and during intravenous binge-level alcohol intoxication, where participants with heavier baseline alcohol consumption exhibited greater functional connectivity deficits in basal ganglia and where lower impulsivity was associated with impaired pallidum functional connectivity (Fede et al., 2020). Positron emission tomography (PET) studies of glucose metabolism during early recovery from AUD have revealed that detoxified AUD patients exhibit globally decreased glucose metabolism pattern which was especially pronounced and persistent in the basal ganglia (especially in older AUD), while there was a notable increase in glucose metabolism in the frontal lobes, especially within the 16-30 day interval (N. D. Volkow et al., 1994). These metabolic results coincided with the longitudinal window of our study (19 and 36 days of abstinence) and provided similar functional differences as well as longitudinal changes to our resting state functional connectivity findings, further supporting this postulation.

Although the longitudinal difference in our results were largely contrary to our initial expectation of gradual normalization, the decreased regional functional connectivity in basal ganglia and increased regional functional connectivity in frontal cortical regions which at least from anatomical extent became more extensive with longer abstinence could be explained in the context of adaptive lower reward and higher executive control resting state functional activation. This adaptive mechanism of decreased resting

state synchrony in bottom-up reward networks and increased resting state synchrony in top-down executive control networks, which increased in magnitude from medium (73 days) to long-term (2,889 days) abstinence was explored in a series of cross-sectional ROI studies by Camchong *et al*. (Camchong et al., 2013a; J. Camchong, A. Stenger, & G. Fein, 2013b; J. Camchong, V. A. Stenger, & G. Fein, 2013c) and have been reviewed in (Fein & Cardenas, 2015). These functional changes would imply that successful remission from AUD might be associated with an adaptive over-compensatory change rather than a reversal of the addiction-related functional pathology. If this adaptive over-compensatory functional recovery pattern with sustained abstinence in AUD is replicable and correct, it could help guide exciting new opportunities for targeted neurofeedback treatment to complement the existing limited psychosocial and pharmacological interventions. Neuromodulation in addiction and alcohol use disorder has demonstrated encouraging but inconclusive results in pilot studies and case reports (for reviews see (Luigjes, Segrave, de Joode, Figee, & Denys, 2019; Spagnolo & Goldman, 2017)).

In addition to the prototypical reward/executive control addiction interpretation of our results, it is also relevant to consider their context in motor control recovery, even though our research participants were no longer experiencing acute withdrawal symptoms (such as involuntary tremors) as verified using Clinical Institute Withdrawal for Alcohol (CIWA) scale during the structured clinical interview and the anatomical extent of many of the functional changes was exaggerated rather than normalized with increased length of abstinence. Several of the anatomical regions such as cerebellum, primary motor cortex, supplementary motor area, as well as basal ganglia are all involved in motor control and their functional deficits are associated with other neurodegenerative disorders such Parkinson's (which is similarly to addiction associated with impaired dopamine signalling, with estimated over 50% loss in dopaminergic neurons in the substantia nigra and basal ganglia) (Cheng, Ulane, & Burke, 2010). Putamen deficits have been replicated as consistent Parkinson's biomarkers, including decreased ReHo (Pan et al., 2017) as well as abnormal functional connectivity to other motor areas (for example the supplementary

motor area (Yu, Liu, Wang, Chen, & Liu, 2013)). Functional links between motor task performance and regional measures of functional connectivity in AUD should be investigated in future studies.

There are several limitations which need to be considered when interpreting the results of our study. The design of our study was aimed at characterizing AUD-related functional brain changes during early recovery and has thus focused on a very homogeneous clinical sample of all male, chronic, steady treatment-seeking AUD patients within the first few days since detoxification with no psychiatric or neurological comorbidities or history of polysubstance abuse. Similarly the matched control comparison group consisted entirely of healthy men, many of whom have voluntarily abstained from alcohol consumption for multiple years. The results of our study are thus not broadly translatable to the clinical practice since they do not represent typical treatment-seeking patients in the community (who are of both sexes and frequently suffer from complex psychiatric and somatic comorbidities). Despite of the homogeneous clinical profile, our study suffered from several nuisance variable shortcomings including age (range of 23 to 64) and multi-site/scanner study design which were accounted in the statistical models but could have masked more subtle underlying functional changes due to modest signal-to-noise ratio inherent in the resting-state fMRI data. In a previous study, we have also demonstrated iron-related subcortical fMRI signal inhomogeneities in AUD (Juhás et al., 2017), which could have disproportionately distorted the signal in the patient cohort. Since the decreased regional functional connectivity in basal ganglia persisted across all measures (including frequency as well as the correlation based indices), our results should be quite robust. When interpreting our fMRI results one should be mindful that fMRI is an indirect (but well and consistently replicated) measure of neuronal activity and resting state functional connectivity is also an indirect measure of structural connectivity (Logothetis, Pauls, Augath, Trinath, & Oeltermann, 2001; van den Heuvel & Hulshoff Pol, 2010). Changes in large-scale patterns of resting state functional connectivity can, thus, represent diverse direct and indirect excitatory as well as inhibitory changes in functional and structural networks and should be interpreted with caution (Logothetis, 2008). The interpretation should be done especially carefully due to recent

criticism of the validity of neuroimaging results (Button et al., 2013; David et al., 2013; Eklund et al., 2016; Ioannidis, 2011; Woo et al., 2014) due to commonly implemented underpowered study designs as well as too liberal statistical correction with erroneous cluster-based thresholding. Our study has implemented Threshold-Free Cluster Enhancement (TFCE) with 10,000 permutations in addition to Bonferroni correction for multiple contrasts and cautionary interpretation of smaller clusters without anatomical and functional significance in the discussion. TFCE should remain a valid method with greater sensitivity and selectivity even with noise, compared to other voxel and cluster-based threshold correction methods (Han, Glenn, & Dawson, 2019; Pernet, Latinus, Nichols, & Rousselet, 2015; Smith & Nichols, 2009).

Other longitudinal studies aiming to more conclusively characterize functional brain changes associated with early abstinence should aim to recruit larger sample sizes with more uniform demographic cohorts (for example in age) and more and longer interscan intervals. The approximately 2 week interscan interval in our study did not reveal significant interscan changes within the AUD cohort, except for a very small cluster in the DC. This could be potentially due to missing the early functional changes before the first time point (and thus underestimating the initial AUD-related functional connectivity deficits) or due to too short follow-up interval to observe substantially large functional plasticity to be detected by our analysis technique. Inclusion of functional performance tests would also help to more conclusively characterize the significance of the resting state changes beyond speculation based on anatomical location and claims published in other studies.

5 Conclusion

This was the first longitudinal and the largest sample size study to examine regional functional connectivity changes in AUD. Our study has utilized an inside-out approach, examining functional

connectivity changes from voxel-specific to whole-brain connectome measures. Our results have revealed substantial decrease across all measures of regional functional connectivity in the basal ganglia in AUD patients compared to healthy controls at both 19 and 36 days of sustained abstinence. The second time point was also associated with increased regional functional connectivity in frontal regions. Other than a small cluster in one of the measures, the longitudinal interscan differences within the AUD group were not significant. Exploratory ROI analysis also yielded inconclusive and not intuitively interpretable results. The magnitude of functional connectivity changes across most measures was significantly correlated with clinical severity scales. Although these results were largely contrary to our *a priori* expectations of gradual normalization of regional functional connectivity deficits with prolonged abstinence, the results can be interpreted in the context of the existing AUD literature as suggesting decreased reward and increased executive control resting state functional connectivity, which might potentially indicate an over-compensatory adaptation during AUD remission and thus a suitable target for neurofeedback brain modulation therapy. There are only very few regional functional connectivity AUD studies published to this date and their results overlap only marginally. Future studies should thus aim to better characterize not only the regional functional connectivity deficits associated with AUD but also the timeline of functional recovery and its relation to neurocognitive performance.

Chapter 6 - Independent Component Analysis of Functional Connectivity Changes during First Month of Recovery from Alcohol Use Disorder

Abstract

Alcohol use disorder (AUD) is associated with widespread structural and functional brain deficits, which are at least partially reversible with prolonged abstinence. This exploratory study aimed to characterize longitudinal changes in whole-brain resting state functional connectivity in 41 AUD men during early recovery at approximately 19 and 36 days of sustained abstinence, compared to 50 matched healthy controls. We have implemented 15 dimensional independent component analysis (ICA) and hierarchical network analysis. Our study has revealed largely inconsistent results with significant differences across all of the analysed networks. The most consistent differences were observed in the Anterior-Salience / Insula Network, Posterior Default Mode Network, and the Auditory Network. There was an overall normalisation trend of strengthening inter-network communication in the recovering AUD patients, especially in Right Executive Control Network, Mesial-Temporal Network, and Posterior Default Mode Network. Some networks (such as Primary Visual Network, Sensory-Motor Network, and Language Network) also exhibited a diverging pattern, potentially indicating adaptive compensation. Approximately 62% of the significant changes were correlated with at least one AUD severity measure while 36% were correlated with three or more, highlighting the clinical significance of our results. All together, these findings suggest a pattern of global hypoconnectivity in the AUD with encouraging functional connectivity convergence across the plurality of the networks. The results should be considered with caution due to limited spatial and longitudinal reproducibility of the significant clusters. To the best of our knowledge, this was the first longitudinal study which explored resting state functional connectivity changes in recovering AUD patients.

Key terms

alcohol use disorder; abstinence; resting state; independent component analysis; functional magnetic resonance imaging

1. Introduction

Alcohol is one of the most harmful and commonly abused psychoactive substances in the world (Nutt et al., 2010). Harmful use of alcohol is a leading preventable cause of death (5.9%) and disability (5.1% of global burden of disease) worldwide (World Health Organization, 2018). Prevalence of alcohol use disorder (AUD) is estimated at 5.1% (with dependence at 2.6%) worldwide (World Health Organization, 2018). AUD is a chronic relapsing psychiatric disorder characterised by uncontrolled recurrent alcohol abuse despite its significant interference in the individual's mental wellbeing, physical health, and ability to function in their daily lives (American Psychiatric Association & American Psychiatric Association, 2013). AUD under its different historical names (such as drunkenness, disease of the will, alcoholism, *et cetera*) has been documented as a clinical disorder at least since the early 19th century, by which end there was already a growing scientific evidence and clinical understanding of AUD as a disorder of the brain (Marchiafava, 1933; Tabakoff & Hoffman, 2013). Despite of the gradual scientific advancement spanning over 120 years, the precise mechanism of action of alcohol in the brain, AUD-related damage, and brain recovery during sustained abstinence remain not fully understood (R. A. Harris et al., 2008; Sutherland et al., 2014b; N. D. Volkow et al., 2017; Zahr & Pfefferbaum, 2017). Modulation of the pathological changes in the alcohol dependent brain structure and function, nonetheless, remains necessary for cognitive and behavioural recovery in successful AUD remission.

AUD is associated with wide-spread macroscopic as well as microscopic structural brain damage affecting neurons, their connections, as well as glial support cells (for reviews see (Bühler & Mann, 2011; Fritz et al., 2019; Harper et al., 2003; M. Rosenbloom et al., 2003)). This structural damage is at least partially reversible with prolonged abstinence (for reviews see (Crews & Nixon, 2009; Fein & Cardenas, 2015; Sullivan & Pfefferbaum, 2005)). The structural recovery is thought to occur non-linearly, with most rapid recovery during the first few weeks of remission but potentially with some persistent structural deficits (Durazzo et al., 2015; Gazdzinski et al., 2005; Pfefferbaum et al., 1995; Y. Zou et al., 2017). The

first month of abstinence is, therefore, a very important window of time to observe brain changes associated with successful AUD recovery.

Similarly to structural brain damage, AUD is also associated with extensive functional deficits. Cognitive, emotional, and behavioural deficits have been all described in AUD (for reviews see (Bernardin et al., 2014; Le Berre et al., 2017; Oscar-Berman & Marinković, 2007)). These deficits are also at least partially reversible with prolonged abstinence. Some functional improvement has been noted within the first few weeks of sustained abstinence (Mann et al., 1999; Oscar-Berman & Marinković, 2007; Petit et al., 2017), with recent meta-analysis suggesting most global dysfunction should improve within the first year of abstinence (Crowe et al., 2019; Stavro et al., 2013). Some functional deficits, such as in visuospatial processing or long-term memory, however, might persist even after several years of remission (Brandt et al., 1983; Fein et al., 2006). The timeline of functional improvement in the published literature, thus, largely parallels that of the structural improvement.

Multimodal neuroimaging studies have provided evidence linking structural brain changes (tissue morphometry, microstructural integrity, chemical metabolites), functional brain changes (electrophysiology, functional magnetic resonance imaging (fMRI) connectivity, chemical metabolites), and neurocognitive performance in both AUD-related damage as well as recovery with sustained abstinence (for example see (Alhassoon et al., 2012; Bartsch et al., 2007; Bendszus et al., 2001; Mon et al., 2013; Muuronen et al., 1989; M. J. Rosenbloom et al., 2007; Sullivan, Rosenbloom, Lim, et al., 2000; Yeh et al., 2007)). The multimodal results are quite complex and not always in concordance across the different measures and across different studies. Nonetheless, the converging multimodal evidence suggests that there should be substantial underlying structural and functional plasticity in parallel to the successful clinical remission and behavioural recovery during the first few weeks of abstinence. Moreover, these changes should be detectable using the established neuroimaging techniques.

Neuroimaging and electrophysiological evidence of functional brain changes in AUD has generally been more complex than the structural evidence. On average, AUD patients appear to exhibit a less efficient, potentially disorganized pattern of brain activation with additional recruitment of sometimes far-reaching anatomical regions, in order to compensate for AUD-related impairment (Chanraud & Sullivan, 2014; Sullivan & Pfefferbaum, 2005). For example, AUD patients performing a simple finger-tapping task have exhibited increased functional activation with recruitment of additional cortical regions even when completing the task at a slower performance level, which would normally be associated with a proportional decrease within the fronto-cerebellar activation (Parks et al., 2010). Other studies have also revealed that AUD patients recruit additional cortical, subcortical, and cerebellar regions when performing tasks at both worse as well as comparable levels to healthy controls (Chanraud-Guillermo et al., 2009; Gilman & Hommer, 2008; Marinkovic et al., 2009).

There is also a growing body of evidence suggesting aberrant AUD functional connectivity observed in a resting state (when participants are asked to lie awake in a scanner at rest, with eyes opened or closed without thinking of anything in particular or performing any task). Resting state brain fluctuations originate (at least partially) due to spontaneous neuronal activity in highly correlated anatomically and functionally linked brain regions which continue to exhibit robust ongoing functionally connectivity at rest (for an overview see (van den Heuvel & Hulshoff Pol, 2010)). Camchong *et al*. have documented what are thought to be compensatory mechanisms in medium (about 10 weeks) and long-term (about 8 years) abstinent AUD at rest (for review see (Fein & Cardenas, 2015)). Successfully abstinent AUD patients exhibited decreased bottom-up reward and greater top-down executive control resting state functional connectivity, which could represent an excessive functional adaptation to compensate for pathologically reinforced connection developed before remission from AUD. Other studies have reported abnormal patterns of functional connectivity within and between functional networks, decreased network efficiency, global hypoconnectivity, and even abstinence-related compensatory changes (Chanraud et al., 2011; Müller-Oehring et al., 2015; Sjoerds et al., 2017; Vergara, Liu, Claus, Hutchison, & Calhoun, 2017;

Weiland et al., 2014; Zhu, Cortes, Mathur, Tomasi, & Momenan, 2017). To the best of our knowledge, there are no longitudinal fMRI studies documenting functional recovery during sustained abstinence from AUD, even though lack of longitudinal studies has been pointed out as a major limitation in the existing literature (Fede, Grodin, Dean, Diazgranados, & Momenan, 2019; Fein & Cardenas, 2015)

Our study aimed to address this gap in the literature. We have implemented a longitudinal exploratory analysis of functional connectivity changes in AUD patients during early abstinence compared to matched healthy controls. According to both preclinical models as well as neuroimaging studies, the first few weeks of abstinence should be associated with the most rapid brain recovery (Charlet et al., 2018; Crews & Nixon, 2009). This study has, therefore, examined longitudinal changes in functional connectivity at approximately 19 and 36 days of sustained abstinence in a very homogeneous clinical sample of steady, chronic AUD patients compared to matched healthy controls. Our whole-brain analysis has focused on changes in large-scale functional connectivity networks, derived using independent component analysis (ICA) with dual regression (Nickerson, Smith, Öngür, & Beckmann, 2017).

ICA is a powerful data-driven technique which can identify independent component maps common to the sampled data without an *a priori* model (C. F. Beckmann, DeLuca, Devlin, & Smith, 2005). The independent components represent robust and reliable functional connectivity networks, which consist of highly coherent anatomical regions during the resting state (Buckner, Krienen, & Yeo, 2013; van den Heuvel & Hulshoff Pol, 2010). Resting state functional networks are anatomically consistent (Yeo et al., 2011) and reflect task-evoked functional connectivity networks in motor, sensory, and cognitive domains (Crossley et al., 2013; Smith et al., 2009). ICA remains one of the most popular resting state functional connectivity techniques; however, it has several drawbacks including more complex representation of data, which might make interpretation and translation of findings more challenging since it might not correspond to specific anatomical circuits which might be split-up or joined into different networks or sub-networks depending, on ICA's dimensionality and underlying data properties (van den Heuvel & Hulshoff Pol, 2010). ICA has been successfully implemented in AUD or acute alcohol intoxication in

several previous studies, including (Kohno, Dennis, McCready, & Hoffman, 2017; Z. Song, Chen, Wen, & Zhang, 2020; Spagnolli et al., 2013; Vergara et al., 2017; Zhu et al., 2017; Zhu, Du, Kerich, Lohoff, & Momenan, 2018).

This was an exploratory study which main objective was to attempt to characterize the functional connectivity changes in AUD during early recovery. Our *a priori* expectation included: 1) AUD will exhibit decreased functional connectivity globally and within most functional networks (less efficient organization, hypoconnectivity); 2) AUD will exhibit increased functional connectivity to outside clusters (compensatory recruitment); 3) longitudinal differences will result in a normalizing trend (functional recovery); and 4) greater magnitude of functional connectivity deficits will be correlated to AUD severity measures. We, furthermore, anticipated greatest group differences and longitudinal recovery in addiction-related functional networks involved in reward / appetitive drive (such as Basal Ganglia Network) and executive control (such as Executive Control Networks or Anterior Default Mode Network) as suggested by prototypical models of addiction circuits (for reviews see (Fein & Cardenas, 2015; Koob & Volkow, 2010)).

2. Materials and Methods

2.1 Subjects

The analysis is based on longitudinal data from 41 recently detoxified adult male alcohol dependent patients (DSM-IV-TR criteria)(American Psychiatric Association, 2000) and matched 50 healthy non-alcohol abusing men. The demographic and clinical overview of the 91 participants is summarized in Table 6.1.

The analysed sample encompasses all of the usable neuroimaging data drawn from a larger dataset consisting of 59 recently detoxified male alcohol dependent patients and 54 matched healthy controls.

Unfortunately, 18 patients and 4 controls had to be excluded from the analysis. 4 of the excluded patients and controls had severe imaging artifacts in the first set of scans and 14 of the excluded patients did not have an acceptable second scan (2 had severe second scan artifacts, 2 were too anxious/claustrophobic to complete the second scanning sequence in its entirety, 5 patients suffered a confirmed relapse, 1 patient died, 1 could not attend the scanning session due to adverse winter weather, 2 confirmed to be unavailable due to out-of-town work by relatives, and the remainder were lost to follow-up and could not be reached or refused to confirm abstinence and participate in the second scanning session). There were no statistically significant differences between the dropped-out participants and the participants included in our longitudinal analysis (also see Figure 6.1).

The alcohol dependent participants were recruited from a pool of patients referred to supervised residential treatment programs in Edmonton, Canada and Mannheim, Germany as part of the TRANSALC research project. DSM-IV-TR diagnostic interviews were carried out by a psychiatrist, using the Structured Clinical Interview for the DSM-IV-TR (SCID-I) (First et al., 2002). All of the patients were consistent, steady, heavy drinkers. All of the analyzed patients met the highest Zone IV cut-off score on the Alcohol Use Disorders Identification Test (AUDIT) with an average score of 28 out of 40 (Saunders et al., 1993). The AUD patients exhibited on average an intermediate level of alcohol dependence (second quartile) according to the Alcohol Dependence Scale (ADS) with the average score of 16 out of 47 (Skinner & Allen, 1982). The patients did not abuse non-beverage ethanol or other substances except nicotine. The patients were recruited within the first two weeks of abstinence and underwent longitudinal scanning sessions at two time points: first after approximately two weeks of abstinence (18.63 days on average) and second after approximately one month of abstinence (35.76 days on average). Abstinence was verified at each scanning session in all participants by an alcohol breathalyser (BACtrack S50 Personal Breathalyzer, Portable Breath Alcohol Tester) and a urine drug screen (nal von minden GmbH Drug-Screen® Diptest, Version 1.0).

Controls were recruited concurrently to match the patients' general demographic profile (including sex, age, handedness, general occupation/education background). The controls had no history of alcohol or drug addiction and consumed alcohol below the Canada's Low-Risk Alcohol Drinking Guidelines (Butt, 2011). Participants in both arms were excluded if they had any history of serious medical (including psychiatric or neurological) complications, brain injury, use of psychotropic medications (other than during the detoxification process), or did not meet magnetic resonance safety criteria for our imaging facilities. The study was approved by the University of Alberta Health Research Ethics Board (study ID: Pro00019424).

Table 6.1: Summary of Key Demographic and Clinical Variables

	AUD Patients (n=41)		Controls (n=50)				
	Mean	**SEM**	**Mean**	**SEM**	**% Δ**	**t-value**	**sig.**
Age	45.09	1.46	42.17	1.40	7	1.40	not sig
Ethanol (grams/day)	252.78	19.90	5.47	0.55	4,521	13.58	***
AUDIT	27.62	0.65	2.69	0.21	927	39.79	***
ADS	16.49	0.90	1.73	0.22	853	17.15	***
OCDS	18.24	0.88	1.26	0.12	1,348	20.23	***
ODS	6.46	0.50	0.09	0.04	7,078	13.36	***
CDS	11.78	0.46	1.17	0.11	907	23.72	***
Abstinence 1 (days)	18.63	0.82	N/A				
Abstinence 2	35.76	0.80	N/A				

*p<0.05, ** p<0.01, *** p<0.001 Bonferroni-corrected; SEM = standard error of mean

2.2 MRI Acquisition

The neuroimaging data was acquired at two clinical sites. Canadian data was acquired using a 4.7 Tesla Varian Inova whole-body MRI scanner, located at the University of Alberta, Edmonton. German data was acquired using a 3 Tesla Siemens MAGNETOM TRIO whole-body MRI scanner, located at the Central Institute of Mental Health, Mannheim. The scanning protocol included anatomic imaging using T1-weighted magnetization-prepared rapid acquisition echo (MPRAGE) as well as resting state functional MRI (rs-fMRI) using single-shot, T2*-weighted echo planar imaging (EPI). During rs-fMRI participants were asked to remain still, close their eyes, not fall asleep, and not to think of anything in particular.

Edmonton MPRAGE acquisition parameters were TR 1,505.9 ms, inversion time 300.0 ms, relaxation delay time (after readout prior to inversion) 300.0 ms, linear phase encoding, TE 3.71 ms, matrix 240×192×128, field of view 240×192×192 mm^3, 1.0×1.0×1.5 mm^3 voxels, whole brain coverage. Mannheim MPRAGE acquisition parameters were TR 2,300 ms, inversion time 900 ms, TE 3.03 ms, matrix 256×256×192 with identical field of view, 1.0×1.0×1.0 mm^3 voxels, with whole brain coverage.

Edmonton rs-fMRI EPI scans had acquisition parameters of TR 1500 ms, TE 19 ms, matrix 72×68×36, field of view 216×204×126 mm3, 3×3×3.5 mm3 voxels, whole brain coverage, and with 320 volumes. Mannheim rs-fMRI EPI scans had acquisition parameters of TR 1500 ms, TE 28 ms, matrix 64×64×30, field of view 192×192×120 mm3, 3×3×4 mm3 voxels, whole brain coverage, and with 240 volumes.

All of the scans were visually reviewed by two independent neuroimaging experts for gross abnormalities. None of the subjects exhibited any clinically significant structural abnormalities other than what may be expected from normal aging or prolonged alcohol abuse. Only subjects without severe motion and other noise artifacts in both the first and second fMRI scan were included in the final analysis.

The raw data was also anonymized before any pre-processing and the researchers were blinded to the subject or group label key until the final statistical analysis.

2.3 Neuroimaging Data Preprocessing

The fMRI data was preprocessed using the Data Processing Assistant for Resting-State fMRI Advanced Edition (DPARSFA; version 4.1_160415; http://rfmri.org/DPARSF) (Chao-Gan & Yu-Feng, 2010). Preprocessing steps included: removal of first 10 time points to allow for signal stabilization; slice timing correction; head motion realignment; brain extraction (using BET) (Smith, 2002); nuisance covariate

regression (using 2 polynomial trend with Friston 24 head motion parameters as well as white matter and cerebral-spinal fluid regressors based on CompCorr with 6 principal components) (Behzadi et al., 2007; Friston et al., 1996); normalization to Montreal Neurological Institute (MNI) space using the default EPI template in a 3×3×3 mm^3 isotropic space; smoothing using a 9 mm isotropic Gaussian kernel (FWHM); and temporal filtering in 0.01 to 0.1 Hz band. The preprocessed data was also masked using a common dataset mask, which included brain voxels common to all scans and was created using FSL (Jenkinson et al., 2012). Quality assurance steps were undertaken after each preprocessing step.

2.4 Independent Component Analysis

Independent component analysis on the preprocessed data was performed using MELODIC (Multivariate Exploratory Linear Optimized Decomposition into Independent Components) (C. F. Beckmann & Smith, 2004) in FSL (Jenkinson et al., 2012). The number of independent components was limited to 15 and the analysis was performed on multi-session temporally concatenated preprocessed data. The spatial extent of the fifteen independent components is summarized in Figure 6.2.

All of the independent components were then thresholded and binarized into spatial masks, to decrease spatial overlap. These component masks were then processed through Dual Regression to extract subject-specific timecourses based on the group component masks as well as subject-specific spatial maps for each of the components (Christian F Beckmann et al., 2009).

Spatial distribution and timecourse patterns across the concatenated group data as well for each subject were then carefully reviewed and one component (component 05) was excluded because it represented noise. Component number 07 also exhibited some noise-like patterns, but was included in the final analysis since its spatial distribution fell primarily within the mesial-temporal lobe consistently across all

subjects. After quality assurance was concluded, the anonymized subject-specific spatial maps of the fourteen remaining components were then used in statistical analysis.

2.5 Graph Theory Analysis

Functional connectivity patterns and network hierarchy were explored using FSLNets toolbox (https://fsl.fmrib.ox.ac.uk/fsl/fslwiki/FSLNets) in MATLAB. The subject and network-specific timecourses extracted using Dual Regression in the previous analysis step were normalized, full correlation matrices were then calculated, and the networks were sorted based on their correlation patterns. The independent components network hierarchy (based on the healthy control data) is illustrated in Figure 6.2. The between-group differences were also analysed the same way as other neuroimaging data, with same nuisance variables, permutation tests, and full FWE-correction for multiple comparison.

2.6 Statistical Analyses

After the quality assurance of the fMRI analyses were complete for each subject, the label key was returned to the blinded researcher to allow for group comparison and statistical analysis.

The participant profile summary statistics and group comparison were generated using SPSS (version 20) (IBM Corp, 2011) and MATLAB (version R2018b) (The MathWorks Inc, 2018). The summary statistics included group mean ($\bar{x}$) and standard error of mean (SEM). After verifying validity of the assumptions (including Levene's test of homogeneity), two sample t-tests were used to compare group differences (Δ). The input data for demographic and clinical summary statistics was not corrected for nuisance variables (such as age).

The neuroimaging analysis of group differences was performed using general linear models and voxel-wise non-parametric permutation tests in FSL (Jenkinson et al., 2012). The linear models included predictors for group status (dummy variables for first and second scans for patients and controls) as well z-normalized nuisance variables (scanning site, age, and length of abstinence at first scan). The contrasts compared first time point group differences, second time point group differences, as well as interscan longitudinal differences in the AUD group. For completeness, a separate due diligence analysis was also performed on the usable first-time point neuroimaging data of all of the excluded patients who have dropped out compared to the patients who have remained in the study (see Figure 6.1 for summary of t-maps). The group differences were tested using 10,000 permutations in FSL's Randomise algorithm with Threshold-Free Cluster Enhancement (TFCE), using the recommended parameters (Winkler et al., 2014).

An exploratory post-hoc statistical analysis was also conducted to explore correlations between significant neuroimaging results and clinical severity scales. Significance of the Pearson correlation coefficients was tested using two-tailed t-tests.

For all analyses, the null hypothesis was rejected and group differences were considered as significant at a global alpha threshold of 0.05. The p-values were corrected for multiple comparison using Family-Wise Error (FWE) correction. FWE-correction was estimated either through permutations for neuroimaging data and/or using Bonferroni method for summary statistics and post-hoc comparisons (Bonferroni, 1936).

3 Results

3.1 Participant profile

The healthy controls were recruited to match the general demographic profile of the AUD patients. As a result, the groups were not significantly different in their general demographic profile. The clinical measures were 9 to 71 times more severe in the AUD group than in the healthy control, as summarized in Table 6.1.

3.2 Drop-Out Due Diligence

The due diligence comparison of the excluded dropped-out patients compared to the ones included in the longitudinal study revealed that neither the demographic, clinical, nor neuroimaging profile of the clinical subjects was significant. Figure 6.1 illustrates the lack of significant differences in the usable fMRI scans of the 16 dropped-out excluded AUD patients compared to the 41 remaining included AUD patients. The overwhelmingly green t-maps indicate non-significant group differences (green on colour bar indicates t-value of 0).

Figure 6.1: No Significant Difference between Dropped-Out and Included Patients at First Time Point

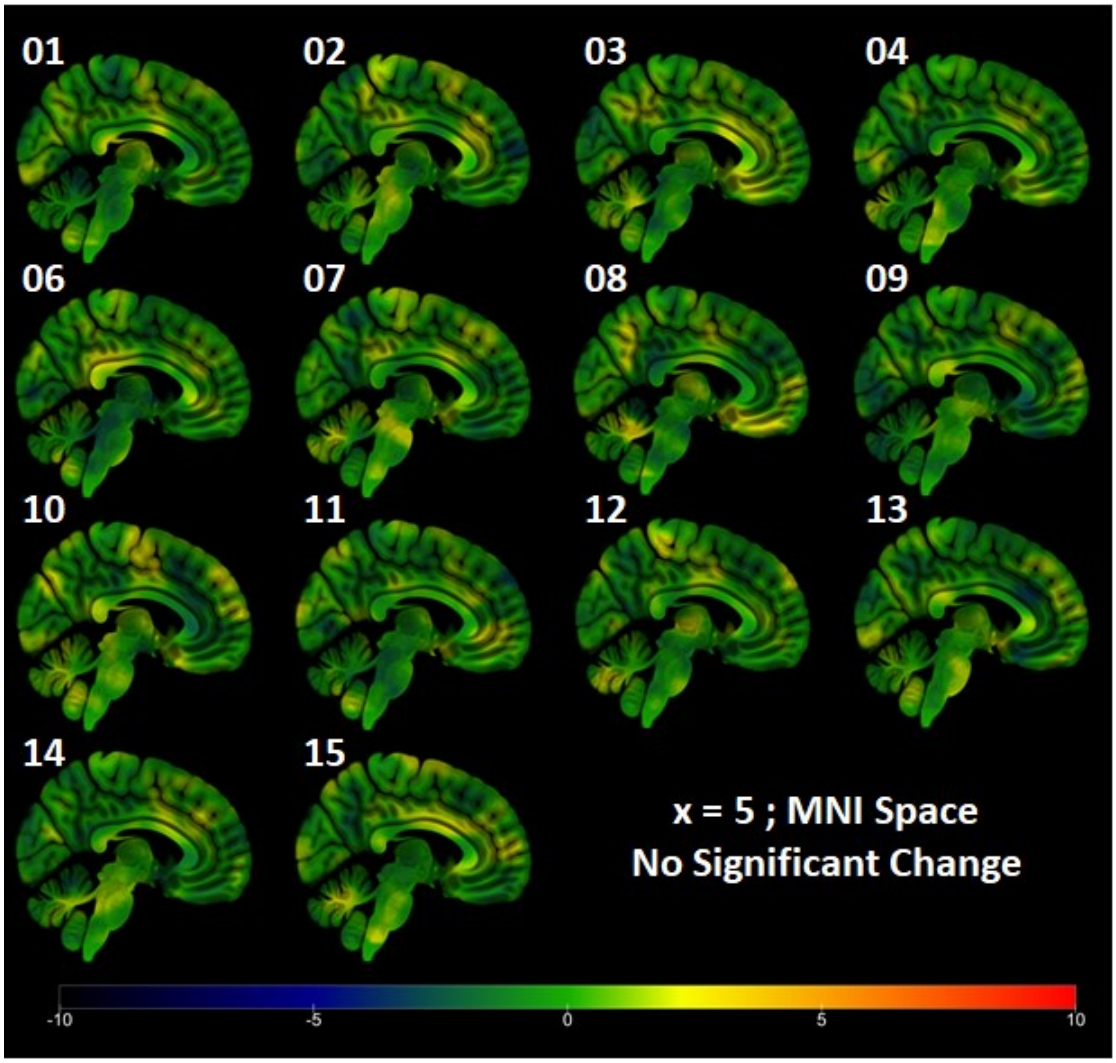

Figure 6.1 depicts t-maps of the group differences between patients who dropped out (n=16) compared to the ones who have been included in the longitudinal analysis (n=41) for each of the independent components used in this analysis. As indicated by the colour bar, green depicts no differences while blue indicates decreased functional connectivity in the dropped out group and red increased functional connectivity in the dropped out group. None of the differences were statistically significant. The sagittal slices were taken at x = 5 in MNI space.

3.3 Independent Component Analysis Networks

Independent component analysis in this study was restrained to 15 components. We have experimented with higher and lower component numbers on partial datasets during the recruitment process. Restricting the algorithm to 15 components provided the best compromise between specificity and sensitivity (i.e. reasonable number of statistical tests, which would not necessitate unreasonable Bonferroni-corrected thresholds on the permuted p-values, given our modest sample size).

The fifteen independent components consisted of the following anatomical regions: component 01: Basal Ganglia / Deep Gray Matter Network (spanning thalamus, putamen, caudate nucleus, brainstem, a little bit of temporal lobe); component 02: Cerebellum Network (spanning cerebellum and minimum of occipital and temporal lobes); component 03: Primary Visual Network (spanning occipital lobe and little of cerebellum, parietal, and temporal lobes); component 04: Anterior Default Mode Network (spanning frontal lobe and a little parietal lobe); component 05: Noise (excluded from analysis); component 06: Posterior Default Mode Network (spanning primarily parietal lobe with a little occipital lobe); component 07: Mesial-Temporal Network (partially noise; spanning temporal lobe and also including small parts of frontal lobe, cerebellum, insula, occipital lobe, putamen, caudate, parietal lobe and thalamus); component 08: Sensory-Motor Network (spanning frontal and parietal lobe); component 09: Auditory Network (spanning temporal lobe and insula with a little parietal lobe, frontal lobe and minimum putamen); component 10: Visual Network – Lingual Gyrus (spanning occipital lobe, parietal lobe, cerebellum, little of temporal, frontal, and thalamus); component 11: Language Network (spanning parietal and temporal lobe, with little frontal and occipital lobes); component 12: Right Executive Control Network (spanning right parietal and frontal lobes with minimum of temporal lobe); component 13: Precuneus Network (spanning parietal lobe and occipital lobe with a little frontal and temporal lobes); component 14: Left Executive Control Network (spanning left frontal lobe and parietal lobe with a little temporal and

occipital lobes); and component 15: Anterior-Salience (Insula) Network (spanning frontal lobe with a little parietal, temporal lobe, insula and minimum of putamen and occipital lobe).

The fourteen retained functional connectivity networks represented 88% of the brain space analysed in this study (which already excluded non-brain tissue, ventricles, and dominant white matter regions based on the average smoothed tissue probability maps). 60% of the voxels included in the independent components were unique to each functional network and did not overlap, 23% voxels overlapped with one other network, 7% with 2 other networks, and 2% with 3 networks, at the threshold level depicted in the figures. The overlapping regions included several functional hubs such as precuneus, posterior cingulate cortex, and bilateral angular gyri which are commonly associated with the default mode network and exhibit increased resting-state brain activity. The spatial extent of the different functional networks varied: 01 Basal Ganglia Network represented 7% of the analysed voxels, 02 Cerebellum Network spanned 10% of the voxels, 03 Primary Visual Network 11%, 04 Anterior Default Mode Network 10%, 06 Posterior Default Mode Network 7%, 07 Mesial-Temporal Network 11%, 08 Sensory-Motor Network 12%, 09 Auditory Network 10%, 10 Visual Network – Lingual Gyrus 7%, 11 Language Network 8%, 12 Right Executive Control Network 9%, 13 Precuneus Network 8%, 14 Left Executive Network 9%, and 15 Anterior Salience (Insula) Network spanning 8% of the analysed brain space.

Figure 6.2: Independent Components Hierarchy

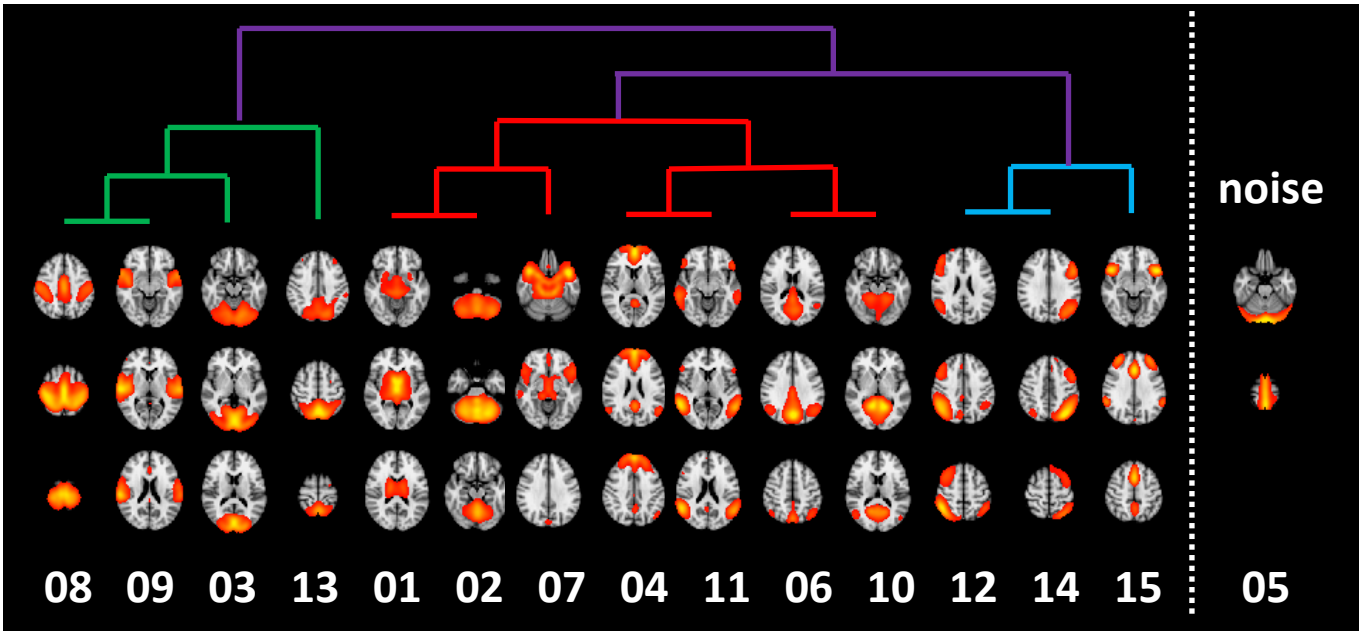

Figure 6.2 summarizes the spatial extent of the independent component resting state networks and their relative activation hierarchy.

3.4 Group ICA Differences

The results of the significant differences between AUD patients at first scan, at second scan, as well as interscan patient differences are summarized in Table 6.2 (group averages and differences) and Table 6.3 (significant cluster coordinates) and depicted in Figure 6.3 to Figure 6.16 (independent components in green and significantly increased clusters in red and decreased in blue). All of the significant clusters survived Bonferroni correction by factor of 84 (14 networks with 3 sets of up and down contrasts) on the FWE permutation corrected values ($p < 0.000595$).

For component 1 (Basal Ganglia / Deep Gray Matter Network), there were significant differences across all three sets of contrasts (as depicted in Figure 6.3). AUD patients at first time point (19 days of abstinence), have shown a bilateral increase in insula and temporal lobe (planum polare, Heschl's gyrus, lateral superior temporal gyrus) functional connectivity and a left cerebellum decrease, spanning a little into left fusiform gyrus of temporal lobe (Brodmann area 20 and 37), compared to the healthy controls. At

second time point (36 days of abstinence), decrease in cerebellum (posterior cerebellum and cerebellar tonsil), occipital lobe (area around lingual gyrus), frontal lobe (anterior cingulate and paracingulate gyrus) and parietal lobe (post-central gyrus / primary somatosensory cortex), compared to healthy controls. Longitudinal interscan differences within the AUD group were associated with increased functional connectivity with cerebellum (left anterior lobe) and decrease in frontal lobe (bilateral paracingulate, cingulate, and superior frontal gyri as well as frontal pole), with prolonged abstinence.

For component 2 (Cerebellum Network), both first and second time-point were associated with decreased functional connectivity largely within the cerebellum (as illustrated in Figure 6.4). Even though the extent of the decrease has lowered with prolonged abstinence, none of the interscan differences survived multiple comparison correction. At the first time point, the AUD patients have exhibited a diffuse decrease in bilateral cerebellar functional connectivity, largely within the independent component, in comparison to the healthy controls. At the second time point, the AUD patients have shown decreased functional connectivity in cerebellum (left culmen and tonsil), largely within the independent component but to a lesser extent than during the first time-point.

For component 3 (Primary Visual Network), both the first and second time point were associated with significantly increased functional connectivity in the AUD group, compared to the healthy controls (as illustrated in Figure 6.5). There were no significant interscan changes associated with prolonged abstinence within the AUD group. At first time point, the AUD group exhibited an increase in frontal lobe (left supplementary motor cortex and also bilateral cingulate and superior frontal gyri and right posterior cingulate gyrus) functional connectivity, compared to the healthy controls. At second time point, the AUD group has shown increase in frontal lobe (right superior frontal gyrus and supplementary motor cortex) and occipital lobe (pole, lateral inferior, and fusiform gyri – primarily in the right hemisphere) but a decrease in functional connectivity in cerebellum (posterior right tonsil). Unexpectedly, the increased

functional connectivity with supplementary motor cortex was in the opposite hemisphere at the second time point compared to the first.

For component 4 (Anterior Default Mode Network), there were significant differences between patients and controls at both time points (as illustrated by Figure 6.6), but there were no significant longitudinal differences within the AUD group. At the first time point, AUD patients exhibited increase in functional connectivity in left parietal lobe (post-central gyrus, inferior parietal lobule / supramarginal gyrus) and small part of frontal lobe (pre-central gyrus) and a decrease in functional connectivity in frontal lobe (right precentral gyrus) and bilateral thalamus. At the second time point, AUD patients exhibited increased functional connectivity in left temporal lobe (middle and superior temporal gyri) and a small part of left parietal lobe (angular and supramarginal gyri) and decreased functional connectivity in left occipital lobe (cuneus) and parietal lobe (precuneus).

Component 5 (Noise) was excluded from analysis.

For component 6 (Posterior Default Mode Network), there were significant functional connectivity differences between AUD patients and healthy controls at first time point but not at second time point (as illustrated by Figure 6.7). At the first time point, the AUD patients exhibited increased functional connectivity with a cluster in right frontal lobe (spanning frontal pole as well as inferior and middle frontal gyri) and decreased functional connectivity in right occipital lobe (inferior occipital gyrus and fusiform gyrus), compared to the healthy controls. At the second time point, none of these changes remained significant. Interscan longitudinal comparison in the AUD group has also revealed decreased functional connectivity in the right frontal lobe (middle cingulate gyrus).

For component 7 (Mesial-Temporal Network), all three sets of contrasts were associated with significant changes in functional connectivity (as illustrated by Figure 6.8). At first time point, the AUD group had

increased functional connectivity in insula, temporal lobe (temporal pole and superior temporal gyrus), and frontal lobe (orbital frontal cortex) and decreased functional connectivity in clusters across right temporal lobe, (superior temporal gyrus, planum polare) frontal lobe (right precentral gyrus), right insula, occipital lobe (fusiform), and cerebellum (right posterior lobe), compared to the healthy controls. At second time point, the AUD group exhibited increased functional connectivity in parietal lobe (post-central gyrus, precuneus) and frontal lobe (left pre-central gyrus) and decreased connectivity in right temporal lobe with small extent into insula, parietal lobe, and frontal lobe surrounding right operculum. Interscan comparison within the AUD group has also revealed increased functional connectivity in the left brainstem (pons and midbrain), associated with prolonged abstinence.

For component 8 (Sensory-Motor Network), all three sets of contrasts were associated with significant changes in functional connectivity (as illustrated by Figure 6.9). At first time point, the AUD group had increased functional connectivity in left parietal (precuneus, inferior and superior parietal lobules), temporal lobe (superior temporal gyrus, middle temporal gyrus, and transverse temporal gyrus), and insula and decreased functional connectivity in frontal lobe (frontal pole, superior frontal gyrus, middle frontal gyrus, precentral gyrus, and cingulate gyrus) and a little bit of parietal lobe (postcentral gyrus). At the second time point, the AUD group exhibited increased functional connectivity in the parietal lobe (superior parietal lobule, postcentral gyrus, and supramarginal gyrus). Interscan AUD comparison has revealed significant increase in functional connectivity in the right cerebellum.

For component 9 (Auditory Network), all three sets of contrasts were associated with significant changes in functional connectivity (as illustrated by Figure 6.10). At the first time point, the AUD group had increased functional connectivity in frontal lobe (middle frontal gyrus), parahippocampal gyrus, and brainstem (pons and midbrain), compared to the healthy controls. At the second time point, the AUD group had increased functional connectivity in right temporal lobe (superior temporal gyrus, middle temporal gyrus) and decreased in left temporal lobe (fusiform cortex, inferior temporal gyrus,

parahippocampal gyrus), spanning partially into cerebellum. The longitudinal interscan AUD comparison has revealed decreased functional connectivity in the left temporal lobe (inferior temporal gyrus and fusiform cortex).

For component 10 (Visual Network – Lingual Gyrus), all three sets of contrasts were associated with significant changes in functional connectivity (as illustrated by Figure 6.11). At first time point, the AUD group exhibited increased functional connectivity in cerebellum and small parts of parietal lobe (precuneus) as well as decreased functional connectivity in the right frontal lobe (precentral gyrus, medial frontal gyrus), insula, and parietal lobe (supramarginal gyrus, operculum). At second time point, the AUD group demonstrated increased functional connectivity in frontal lobe (cingulate gyrus), parietal lobe, temporal lobe, and brainstem and decreased functional connectivity in cerebellum, parietal lobe (superior parietal lobule, supramarginal gyrus), and frontal lobe (frontal pole). Longitudinal interscan differences within the AUD group included increased functional connectivity in parietal lobe, frontal lobe (posterior cingulate gyrus), and temporal lobe as well as decreased functional connectivity in left cerebellum and bilateral parietal lobe (precuneus).

For component 11 (Language Network), all three sets of contrasts were associated with significant changes in functional connectivity (as illustrated by Figure 6.12). At the first time point, the AUD group exhibited increased functional connectivity in the left temporal lobe (temporal pole, superior temporal gyrus) and frontal lobe (frontal orbital cortex, inferior frontal gyrus). At the second time point, the AUD group exhibited decreased functional connectivity in the right parietal lobe (supramarginal gyrus, angular gyrus, and operculum). Longitudinal interscan differences within the AUD group included increased functional connectivity in the left frontal lobe (supplementary motor cortex, cingulate gyrus).

For component 12 (Right Executive Control Network), all three sets of contrasts were associated with significant changes in functional connectivity (as illustrated by Figure 6.13). At first time point, the AUD

group exhibited increased functional connectivity in frontal lobe (precentral gyrus, superior frontal gyrus), parietal lobe (postcentral gyrus) as well as insula and temporal lobe while decreased functional connectivity in left frontal lobe (supplementary motor cortex, precentral gyrus, medial frontal gyrus, and superior frontal gyrus). At the second time point, the AUD group demonstrated increased functional connectivity in frontal lobe (paracingulate gyrus and cingulate gyrus) and parietal lobe (post-central gyrus, precuneus) and decreased functional connectivity in left parietal lobe (precuneus). The AUD group has exhibited both increased functional connectivity in the frontal lobe (precentral gyrus, paracingulate gyrus, supplementary motor cortex) as well as decreased functional connectivity frontal lobe (superior frontal gyrus) between the two scanning sessions.

For component 13 (Precuneus Network), all three sets of contrasts were associated with significant changes in functional connectivity (as illustrated by Figure 6.14). At the first time point, the AUD group exhibited increased functional connectivity in the left temporal lobe (temporal pole, superior temporal gyrus, middle temporal gyrus) and decreased functional connectivity in right temporal lobe (superior temporal gyrus and middle temporal gyrus). At second time point, the AUD group compared to the healthy controls has demonstrated increased functional connectivity in left parietal lobe (superior parietal lobule, supramarginal gyrus, and angular gyrus) and decreased functional connectivity in temporal lobe (superior temporal gyrus) and a little part of insula and amygdala. The interscan AUD comparison has revealed decreased functional connectivity in the right temporal lobe (fusiform cortex, superior temporal gyrus, middle temporal gyrus, and inferior temporal gyrus).

For component 14 (Left Executive Control Network), all three sets of contrasts were associated with significant changes in functional connectivity (as illustrated by Figure 6.15). At the first time point, the AUD group exhibited decreased functional connectivity in the left temporal lobe (superior temporal gyrus). At the second time point, the AUD group exhibited increased functional connectivity in the right

occipital lobe (cuneus) and brainstem (midbrain and pons) and also decreased functional connectivity in the occipital lobe, compared to the healthy control group. The interscan longitudinal comparison in the AUD group revealed increased functional connectivity in the occipital lobe, parietal lobe, and thalamus and decreased functional connectivity in the frontal lobe (frontal pole, middle frontal gyrus).

For component 15 (Anterior-Salience / Insula Network), there was only one significant group difference which survived multiple comparison correction. Comparison of the AUD group to the healthy controls at first time point has revealed increased functional connectivity in left frontal lobe (supplementary motor cortex / medial frontal gyrus) within the extent of the independent component.

Table 6.2: Summary of Significant Differences in Functional Connectivity for Each Component

		AUD 1		AUD 2		CTL		AUD1 vs CTL		AUD 2 vs CTL		AUD 2 vs AUD 1	
Component	**Contrast**	**x̄**	**SEM**	**x̄**	**SEM**	**x̄**	**SEM**	**Δ**	**t**	**Δ**	**t**	**Δ**	**t**
01	**AUD 1 > CTL**	1.04	0.07	0.82	0.07	0.49	0.06	**0.56**	**5.85*****	0.33	3.64*	0.23	2.28
	AUD 1 < CTL	-0.1	0.06	0.01	0.05	0.25	0.07	**-0.35**	**-3.95****	-0.24	-2.83	-0.11	-1.37
	AUD 2 < CTL	0.06	0.02	-0.05	0.03	0.33	0.03	-0.27	-7.63***	**-0.37**	**-8.54*****	0.11	2.64
	AUD 2 > AUD 1	-0.05	0.06	0.08	0.05	0	0.06	-0.05	-0.562	0.08	1.01	**-0.13**	**-1.65**
	AUD 2 < AUD 1	0.1	0.07	-0.12	0.08	0.13	0.06	-0.03	-0.378	-0.25	-2.59	**0.22**	**2.13**
02	**AUD 1 < CTL**	1.65	0.05	1.72	0.05	2.04	0.05	**-0.38**	**-5.23*****	-0.31	-4.44**	-0.07	-0.94
	AUD 2 < CTL	0.9	0.06	0.74	0.07	1.12	0.05	-0.22	-2.822	**-0.39**	**-4.44****	0.17	1.89
03	**AUD 1 > CTL**	0.33	0.06	0.23	0.04	-0.14	0.04	**0.47**	**6.13*****	0.37	6.37***	0.1	1.32
	AUD 2 > CTL	1.29	0.05	1.29	0.05	0.94	0.03	0.35	6.36***	**0.35**	**6.19*****	0	0
	AUD 2 < CTL	-0.19	0.05	-0.38	0.06	-0.07	0.04	-0.13	-1.941	**-0.31**	**-4.27****	0.18	2.42
04	**AUD 1 > CTL**	0.23	0.06	0.03	0.06	-0.19	0.04	**0.42**	**5.53*****	0.22	3.12	0.21	2.44
	AUD 1 < CTL	-0.22	0.06	0.07	0.06	0.28	0.06	**-0.5**	**-6.23*****	-0.21	-2.45	-0.29	-3.41
	AUD 2 > CTL	0.28	0.08	0.45	0.05	-0.06	0.05	0.34	3.71*	**0.51**	**6.93*****	-0.17	-1.87
	AUD 2 < CTL	-0.32	0.05	-0.31	0.05	0.22	0.05	-0.54	-7.43***	**-0.53**	**-7.4*****	-0.01	-0.11
06	**AUD 1 > CTL**	0.09	0.07	0.05	0.07	-0.24	0.05	**0.33**	**4.03****	0.29	3.55*	0.04	0.42
	AUD 1 < CTL	-0.58	0.08	-0.2	0.08	0.02	0.07	**-0.6**	**-5.76*****	-0.22	-2.1	-0.38	-3.44
	AUD 2 < AUD 1	0.49	0.06	0.2	0.06	0.33	0.05	0.16	2.11	-0.13	-1.75	**0.29**	**3.46**
07	**AUD 1 > CTL**	2.13	0.11	2	0.08	1.5	0.07	**0.63**	**4.91*****	0.5	4.74***	0.13	0.96
	AUD 1 < CTL	0.01	0.04	0.17	0.04	0.46	0.04	**-0.45**	**-8.37*****	-0.29	-5.06***	-0.16	-2.66
	AUD 2 > CTL	-0.12	0.04	0.02	0.04	-0.46	0.05	0.34	5.54***	**0.47**	**7.45*****	-0.13	-2.54
	AUD 2 < CTL	0.22	0.05	0.09	0.05	0.64	0.05	-0.42	-6.12***	**-0.55**	**-8.29*****	0.13	1.92
	AUD 2 > AUD 1	1.62	0.1	1.97	0.12	1.78	0.1	-0.16	-1.101	0.2	1.28	**-0.35**	**-2.25**
08	**AUD 1 > CTL**	0.51	0.05	0.38	0.04	0.12	0.04	**0.4**	**6.74*****	0.26	4.80***	0.13	2.21
	AUD 1 < CTL	0.23	0.05	0.3	0.04	0.5	0.04	**-0.27**	**-4.57*****	-0.21	-3.78*	-0.07	-1.03
	AUD 2 > CTL	1.96	0.06	2	0.06	1.47	0.05	0.49	6.06***	**0.53**	**6.59*****	-0.04	-0.43
	AUD 2 > AUD 1	-0.02	0.06	0.22	0.05	-0.04	0.05	0.02	0.295	0.26	3.68*	**-0.24**	**-3.17**

Table 6.2 continues on the next page.

Table 6.2(continued): Summary of Significant Differences in Functional Connectivity for Each Component

		AUD 1		AUD 2		CTL		AUD1 vs CTL		AUD 2 vs CTL		AUD 2 vs AUD 1	
Component	**Contrast**	**x̄**	**SEM**	**x̄**	**SEM**	**x̄**	**SEM**	**Δ**	**t**	**Δ**	**t**	**Δ**	**t**
9	**AUD 1 > CTL**	0.37	0.05	0.08	0.05	-0.03	0.04	**0.39**	**6.22*****	0.11	1.72	0.29	4.35**
	AUD 2 > CTL	1.66	0.11	2.01	0.09	1.27	0.06	0.38	3.03	**0.74**	**6.76*****	-0.36	-2.47
	AUD 2 < CTL	-0.01	0.04	-0.08	0.04	0.17	0.03	-0.18	-3.71*	**-0.25**	**-4.71*****	0.07	1.24
	AUD 2 < AUD 1	0.1	0.04	-0.09	0.05	0.07	0.04	0.02	0.38	-0.16	-2.38	**0.18**	**2.78**
10	**AUD 1 > CTL**	0	0.06	-0.07	0.05	-0.27	0.03	**0.28**	**4.38****	0.21	3.58**	0.07	0.98
	AUD 1 < CTL	0.04	0.06	0.12	0.05	0.38	0.05	**-0.34**	**-4.60*****	-0.26	-3.87**	-0.08	-1.04
	AUD 2 > CTL	0.06	0.06	0.36	0.05	-0.05	0.04	0.11	1.62	**0.41**	**6.03*****	-0.29	-3.86*
	AUD 2 < CTL	-0.1	0.04	-0.29	0.03	0.15	0.03	-0.26	-5.37***	**-0.44**	**-9.56*****	0.19	3.85*
	AUD 2 > AUD 1	-0.1	0.05	0.18	0.05	-0.07	0.04	-0.03	-0.4	0.25	3.88*	**-0.28**	**-3.71***
	AUD 2 < AUD 1	0.91	0.1	0.45	0.11	0.5	0.08	0.41	3.12	-0.06	-0.41	**0.47**	**3.03**
11	**AUD 1 > CTL**	1.23	0.13	0.9	0.09	0.49	0.11	**0.73**	**4.36****	0.41	2.97	0.33	2.05
	AUD 2 < CTL	0.66	0.08	0.62	0.09	1.25	0.09	-0.6	-4.79***	**-0.64**	**-4.96*****	0.04	0.32
	AUD 2 > AUD 1	-0.41	0.07	-0.04	0.06	-0.15	0.05	-0.26	-2.98	0.11	1.42	**-0.38**	**-3.83***
12	**AUD 1 > CTL**	0.45	0.05	0.2	0.04	-0.05	0.04	**0.5**	**8.02*****	0.25	4.09**	0.25	3.91*
	AUD 1 < CTL	-0.23	0.06	-0.15	0.07	0.08	0.05	**-0.31**	**-3.91***	-0.23	-2.65	-0.08	-0.85
	AUD 2 > CTL	0.39	0.07	0.73	0.04	0.29	0.05	0.11	1.26	**0.44**	**6.56*****	-0.33	-4.31**
	AUD 2 < CTL	0.04	0.09	-0.27	0.09	0.24	0.09	-0.2	-1.52	**-0.52**	**-4.02****	0.32	2.51
	AUD 2 > AUD 1	-0.07	0.05	0.25	0.04	0.09	0.03	-0.16	-2.77	0.15	3.08	**-0.31**	**-5.32*****
	AUD 2 < AUD 1	0.37	0.07	0.12	0.07	0	0.06	0.38	3.90*	0.12	1.3	**0.26**	**2.56**
13	**AUD 1 > CTL**	0.48	0.05	0.2	0.05	0.12	0.03	**0.36**	**5.67*****	0.08	1.45	0.28	3.88*
	AUD 1 < CTL	-0.18	0.07	-0.06	0.06	0.06	0.07	**-0.24**	**-2.54**	-0.12	-1.35	-0.12	-1.36
	AUD 2 > CTL	1.24	0.1	1.75	0.1	0.92	0.09	0.32	2.36	**0.83**	**6.43*****	-0.51	-3.6*
	AUD 2 < CTL	0.06	0.06	0.13	0.07	0.37	0.05	-0.31	-4.00**	**-0.24**	**-2.83**	-0.07	-0.82
	AUD 2 < AUD 1	0.32	0.04	0.08	0.04	0.07	0.02	0.25	4.94***	0.01	0.27	**0.24**	**3.93***
14	**AUD 1 < CTL**	0.07	0.08	0.48	0.08	0.86	0.08	**-0.79**	**-7.03*****	-0.38	-3.3	-0.4	-3.51*
	AUD 2 > CTL	0.11	0.04	0.23	0.04	-0.13	0.04	0.24	4.14**	**0.36**	**6.57*****	-0.12	-2.14
	AUD 2 < CTL	0.03	0.03	-0.12	0.04	0.21	0.04	-0.19	-3.82*	**-0.34**	**-6.56*****	0.15	3.04
	AUD 2 > AUD 1	-0.54	0.06	-0.19	0.05	-0.33	0.04	-0.21	-3.08	0.14	2.23	**-0.36**	**-4.70*****
	AUD 2 < AUD 1	-0.1	0.05	-0.36	0.06	-0.18	0.05	0.08	1.06	-0.18	-2.19	**0.25**	**3.14**
15	**AUD 1 > CTL**	1.33	0.09	1.2	0.08	0.98	0.07	**0.35**	**3.03**	0.22	2.09	0.13	1.06

*p<0.05, ** p<0.01, *** p<0.001 Bonferroni-corrected; SEM = standard error of mean

Table 6.3: MNI Coordinates of Significant Clusters for Each Component

Component	Contrast	Voxels	MAX X (mm)	MAX Y (mm)	MAX Z (mm)	COG X (mm)	COG Y (mm)	COG Z (mm)
01	AUD 1 > CTL	95	42	-6	-3	44.1	-3.57	-4.64
		51	-42	-9	-9	-44.5	-4.65	-5.47
		3	-36	15	6	-35	15	5
	AUD 1 < CTL	75	-36	-51	-30	-38.2	-48.1	-27.4
	AUD 2 < CTL	142	21	-84	-3	21.9	-75.6	3.51
		111	39	-66	-57	26	-60.7	-51.4
		101	-15	-42	54	-19.6	-41.6	61.9
		56	6	39	21	-0.107	40.9	23.9
		43	-33	-60	-57	-28.7	-57.3	-52.8
		16	33	-15	-9	29.6	-15.9	-5.06
		8	33	3	-15	34.1	3.37	-11.6
	AUD 2 > AUD 1	38	-27	-57	-30	-24.9	-54	-29.4
	AUD 2 < AUD 1	69	3	42	24	0.826	44.6	25
02	AUD 1 < CTL	479	-33	-69	-54	-9.73	-70.1	-35.3
		96	39	-72	-51	36.4	-68.3	-44
	AUD 2 < CTL	76	-45	-51	-42	-42.4	-46.1	-31.4
03	AUD 1 > CTL	54	-9	-6	57	-7.72	-3.11	61.6
		15	6	-42	21	7.8	-44	20.6
	AUD 2 > CTL	63	42	-87	-15	36.9	-84.2	-7.05
		24	12	6	57	9.37	11.6	59.1
		17	-27	-81	9	-26.6	-80.5	11.3
	AUD 2 < CTL	18	15	-51	-48	14.5	-52.3	-44.5
04	AUD 1 > CTL	78	-69	-24	21	-66.4	-20.3	29.6
		32	-63	-39	42	-61.4	-39.5	42.3
	AUD 1 < CTL	66	27	-21	69	28.3	-17	70.2
		9	-3	-15	9	2	-11.3	11.7
	AUD 2 > CTL	41	-63	-51	3	-64.8	-49	4.39
		12	-12	57	-9	-13.5	58.5	-7.5
	AUD 2 < CTL	290	-18	-72	15	-22.7	-71.1	28.3
		16	0	60	36	-1.31	59.1	36
06	AUD 1 > CTL	66	39	39	6	40.8	42.7	7.23
		1	-33	-93	21	-33	-93	21
	AUD 1 < CTL	10	30	-87	-18	32.4	-88.8	-16.5
	AUD 2 < AUD 1	15	9	-3	33	8.2	-5.2	35.6
07	AUD 1 > CTL	139	33	12	-24	38.4	15.8	-16.5
	AUD 1 < CTL	91	54	-6	0	52.2	-4.65	3.96
		47	39	-69	-30	40.3	-66.6	-25.2
		15	33	-84	-21	33.2	-83.6	-19
		7	-42	24	36	-42	23.6	36.4
		4	12	-39	-12	11.3	-38.2	-11.2
	AUD 2 > CTL	39	-12	-54	15	-15.3	-55.9	17.7
		33	-63	-3	33	-60.9	-7.73	35.5
		10	-63	-21	24	-65.4	-19.5	24.6
	AUD 2 < CTL	169	60	-6	-6	55.2	-11.1	2.96
		17	15	-48	63	13.9	-46.6	65.5
	AUD 2 > AUD 1	6	-9	-27	-21	-10	-24.5	-19

Table 6.3 (continued): MNI Coordinates of Significant Clusters for Each Component

Component	Contrast	Voxels	MAX X (mm)	MAX Y (mm)	MAX Z (mm)	COG X (mm)	COG Y (mm)	COG Z (mm)
08	AUD 1 > CTL	71	-45	-39	9	-42.1	-38.6	16.4
		25	-30	-51	42	-28.4	-51.7	46.2
		3	-27	-30	15	-27	-29	17
		1	15	-51	45	15	-51	45
	AUD 1 < CTL	68	21	24	36	18.1	31.3	39.1
		8	-27	-27	69	-26.3	-25.9	68.6
	AUD 2 > CTL	175	39	-51	48	28.5	-45.2	51.7
		21	-33	-51	45	-32.9	-50.9	48.6
		14	42	-27	27	45	-21.9	26.6
	AUD 2 > AUD 1	5	24	-66	-39	20.4	-66	-40.2
09	AUD 1 > CTL	36	6	-27	-24	12	-25.3	-16.2
		12	27	39	-6	28.5	39.7	-7.25
		2	-21	-24	-12	-21	-24	-10.5
	AUD 2 > CTL	42	63	-33	6	62.3	-32.7	7.14
		8	0	-63	0	-1.5	-61.5	-1.5
	AUD 2 < CTL	66	-51	-39	-27	-40.3	-35.1	-25.5
		11	-51	-18	-36	-49.9	-16.4	-35.5
	AUD 2 < AUD 1	39	-51	-39	-27	-49.7	-37.9	-22.3
10	AUD 1 > CTL	73	-30	-72	-57	-22.9	-66.7	-53.3
		8	3	-57	39	1.13	-55.1	39.7
	AUD 1 < CTL	31	3	-21	72	2.13	-19	72.3
		19	45	-39	21	43.7	-37.7	24.8
	AUD 2 > CTL	279	6	-42	27	3.82	-26.9	36.6
		19	3	-9	-18	0.947	-9.16	-15
		13	-21	-3	-30	-22.4	-3.23	-26.5
	AUD 2 < CTL	192	9	-57	-42	7.12	-55.3	-34.4
		92	-33	-54	48	-38.7	-50	53.2
		58	3	57	18	-3.78	60.9	19.3
		28	-51	-3	27	-52.8	-3.32	30.6
	AUD 2 > AUD 1	314	9	-36	27	4.45	-23.9	35.3
		36	-18	-3	-33	-20.3	-1.33	-28.7
		32	45	-42	21	45.6	-38.3	25.5
		10	-30	-96	6	-30.9	-95.1	8.7
	AUD 2 < AUD 1	13	-3	-57	39	-3.46	-55.4	42.9
11	AUD 1 > CTL	19	-48	18	-15	-48	19.7	-15
	AUD 2 < CTL	6	48	-42	27	47.5	-41.5	28.5
	AUD 2 > AUD 1	45	-3	-3	54	-8	-3.6	56.1

Table 6.3 (continued): MNI Coordinates of Significant Clusters for Each Component

Component	Contrast	Voxels	MAX X (mm)	MAX Y (mm)	MAX Z (mm)	COG X (mm)	COG Y (mm)	COG Z (mm)
12	AUD 1 > CTL	129	0	30	60	4.77	17.7	67.4
		80	42	-9	-21	41.7	-0.413	-15.4
		68	-51	-18	57	-37.7	-19.5	67
	AUD 1 < CTL	19	-9	-15	66	-7.58	-12.6	66.5
	AUD 2 > CTL	97	0	21	36	2.2	22.9	37.7
		17	9	-45	69	7.59	-43.2	67.9
		16	24	-78	54	24.4	-75.2	54
	AUD 2 < CTL	8	-6	-69	39	-7.5	-67.5	40.5
	AUD 2 > AUD 1	196	-3	9	30	-2.37	14.8	39.2
		162	12	-33	60	7.04	-24.4	66.1
	AUD 2 < AUD 1	147	6	21	66	4.9	12.4	69.3
13	AUD 1 > CTL	90	-54	0	-15	-55.1	4.1	-11.5
		7	15	-45	-57	15	-42.4	-55.3
	AUD 1 < CTL	18	63	-12	-6	60.7	-10.2	-3.67
	AUD 2 > CTL	40	-42	-51	54	-41.9	-51.2	58.1
	AUD 2 < CTL	18	39	-3	-24	38.7	-2.5	-21
		19	-57	0	-12	-57.5	4.74	-11.7
	AUD 2 < AUD 1	16	36	-3	-48	31.3	-0.75	-46.7
14	AUD 1 < CTL	24	-39	18	-39	-39.8	17.7	-35.5
	AUD 2 > CTL	55	6	-24	-21	4.75	-19.7	-19.5
		44	21	-87	15	21.4	-85.2	20.2
	AUD 2 < CTL	93	-33	-33	-33	-33.1	-38	-18.4
		38	-21	-69	-21	-20.2	-68.5	-18.4
		20	18	-72	-18	16.4	-72.3	-15.9
		12	-30	-60	-45	-33.2	-60	-39
	AUD 2 > AUD 1	16	9	-33	9	9.19	-32.8	9.94
		4	-21	-96	0	-22.5	-96	3
	AUD 2 < AUD 1	11	33	39	9	33.8	42.3	9.55
15	AUD 1 > CTL	3	-9	-3	57	-9	-2	58

MAX = peak value coordinate; COG = centre of gravity

Figure 6.3: Independent Component 01 - Basal Ganglia / Deep Gray Matter Network

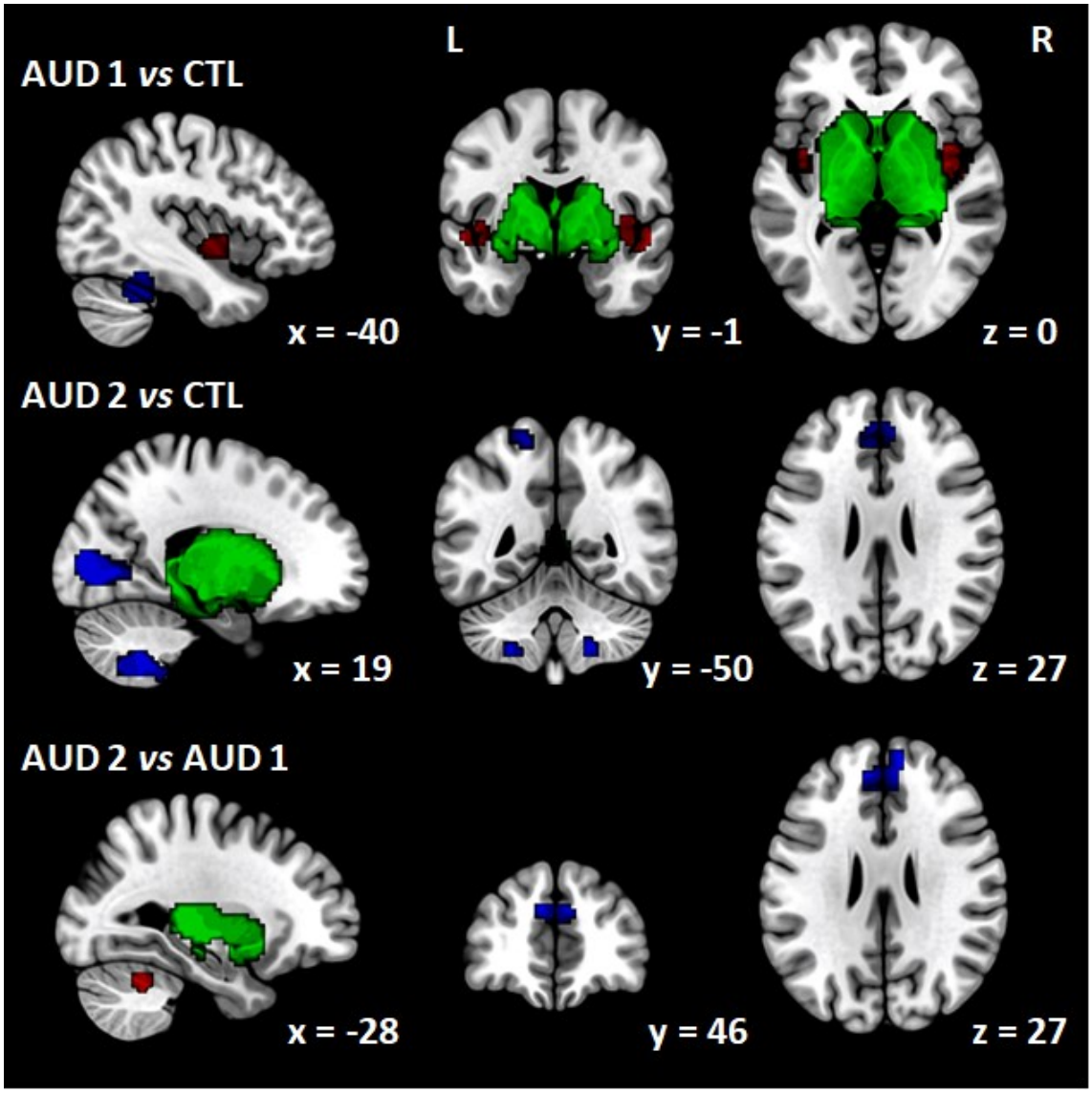

Independent component 01 is illustrated in green. Clusters of significantly lower functional connectivity are in blue while those with significantly higher functional connectivity are in red. Top row illustrates results for comparison of AUD patient group and healthy controls at first time point. Middle row depicts results for comparison of AUD patient group and healthy controls at second time point. Bottom row summarizes the results for the longitudinal differences between second and first time point in the AUD group. All of the images are in the MNI space. The same format is used for all subsequent Independent Component figures (Figure 6.3 to Figure 6.16).

Figure 6.4: Independent Component 02 - Cerebellum Network

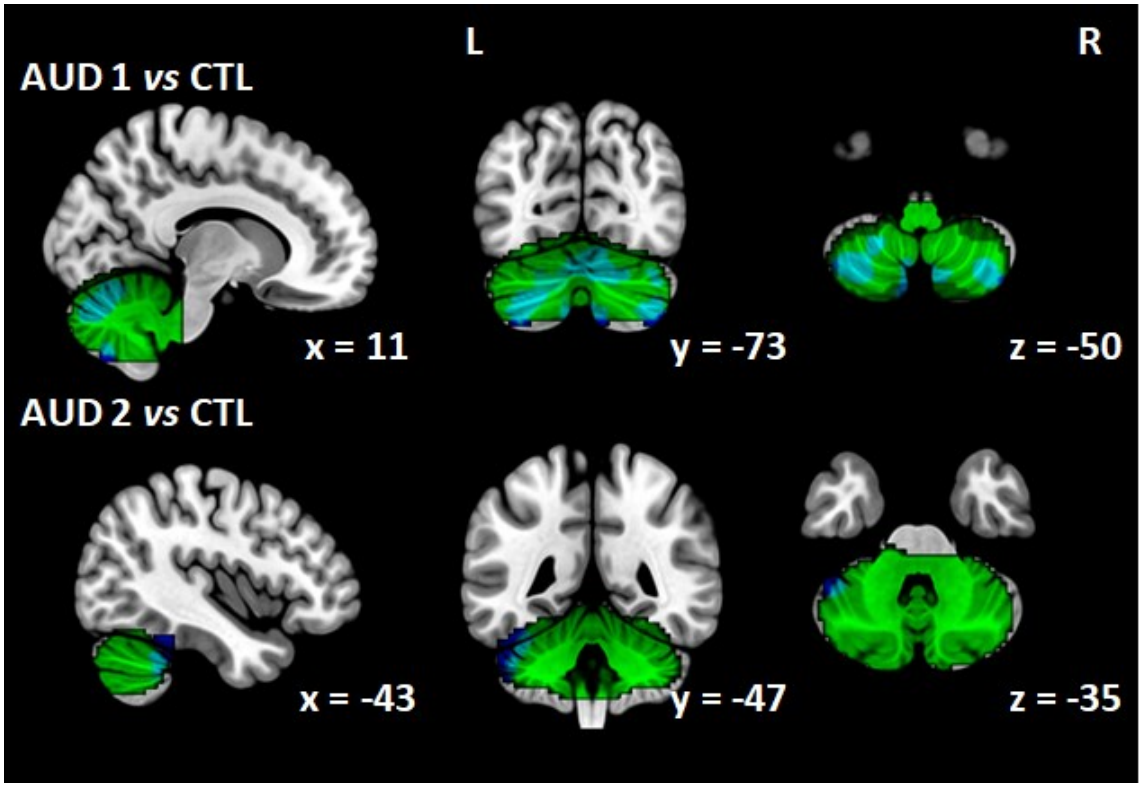

Figure 6.5: Independent Component 03 - Primary Visual Network

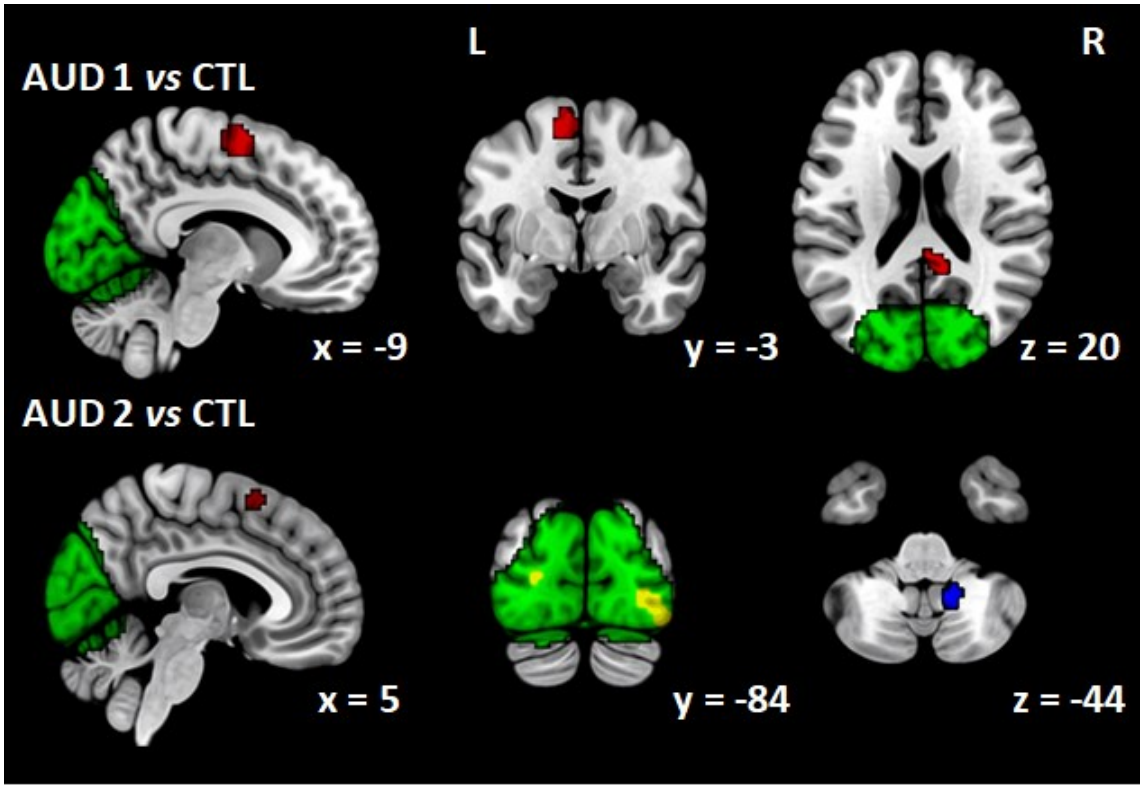

Figure 6.6: Independent Component 04 - Anterior Default Mode Network

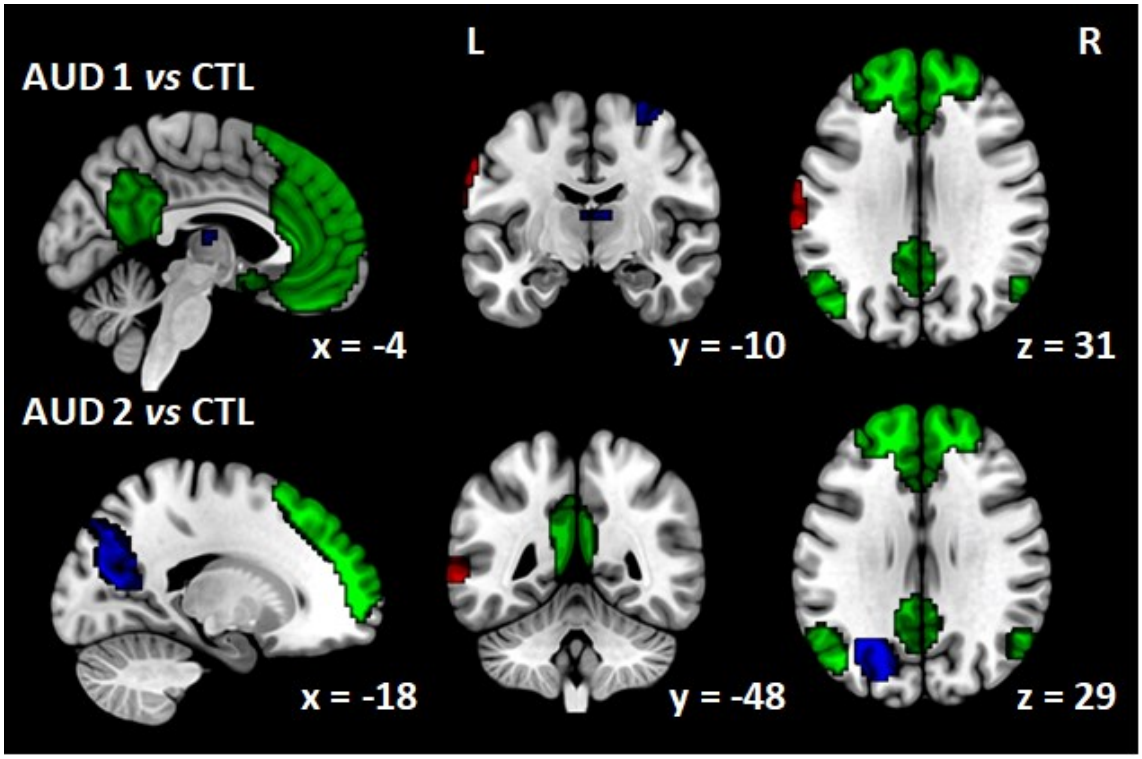

Figure 6.7: Independent Component 06 - Posterior Default Mode Network

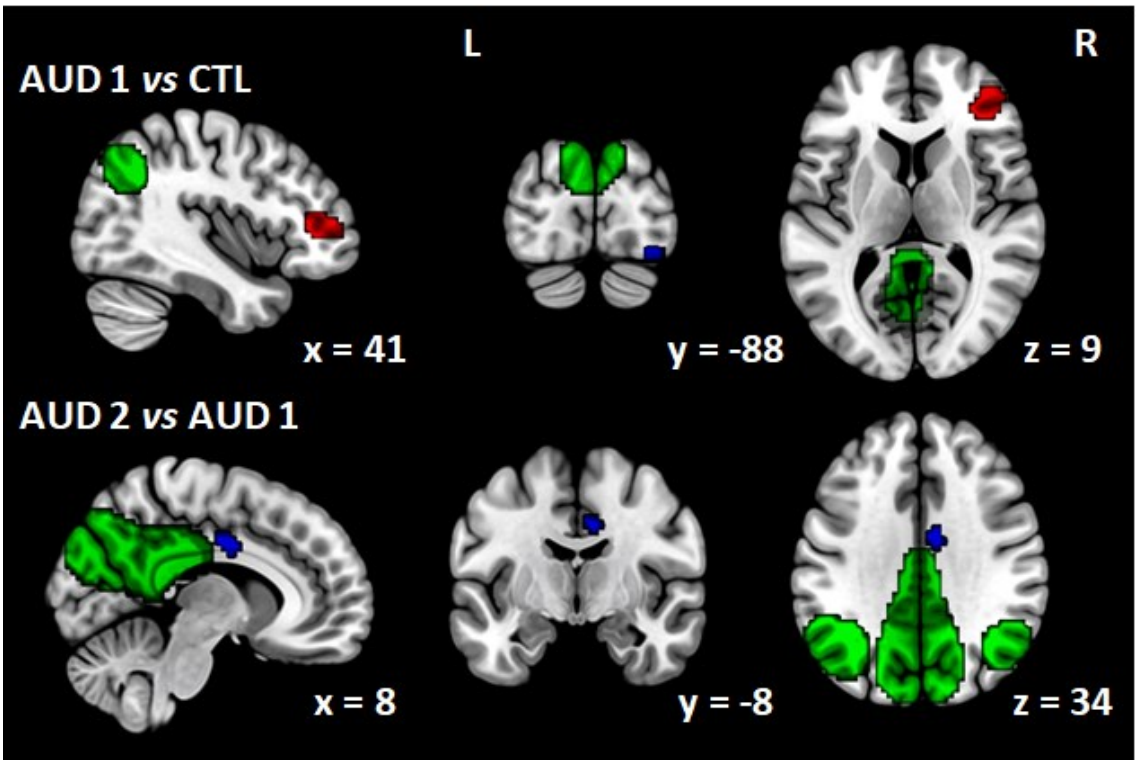

Figure 6.8: Independent Component 07 Mesial-Temporal Network

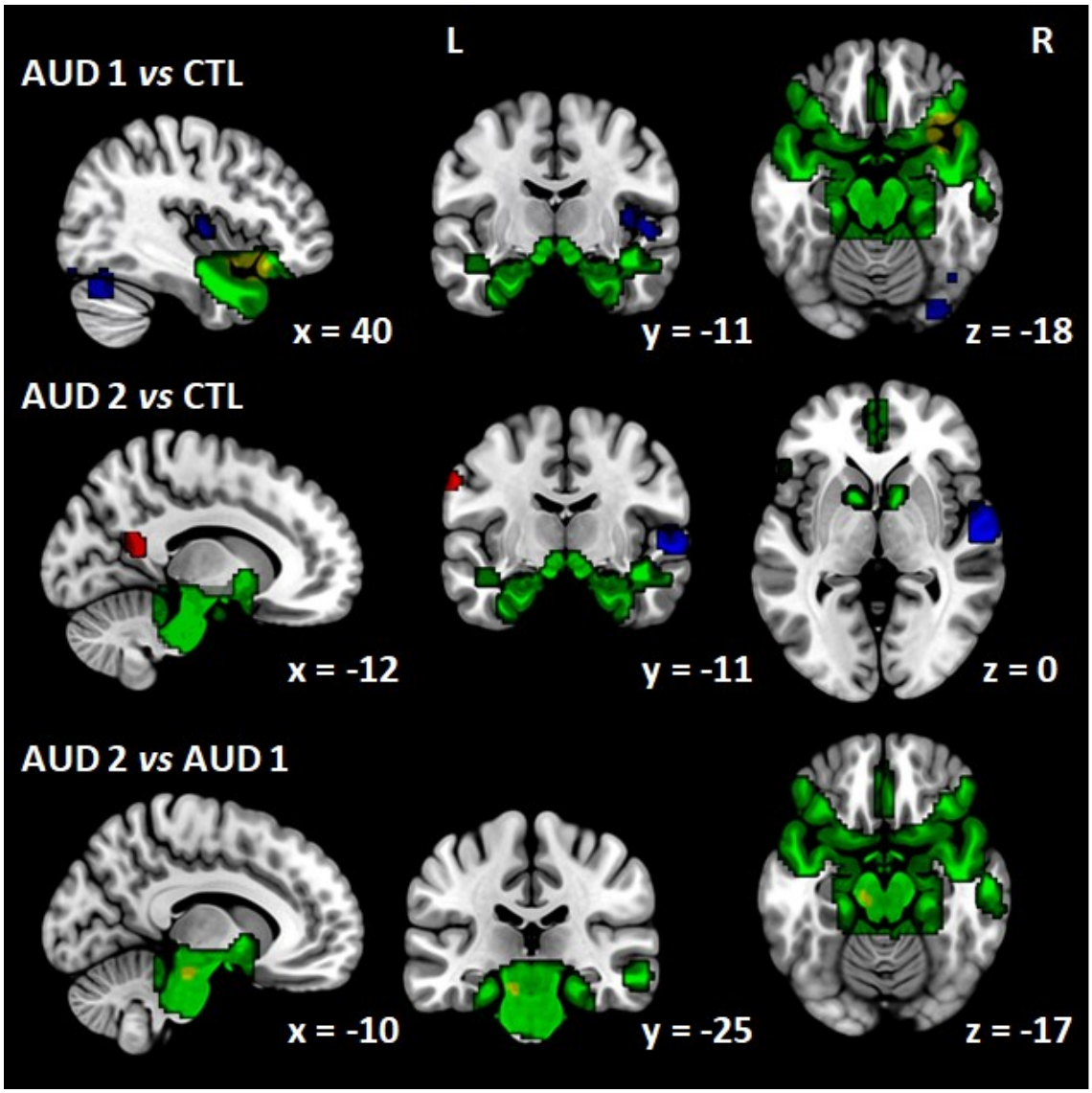

Figure 6.9: Independent Component 08 - Sensory-Motor Network

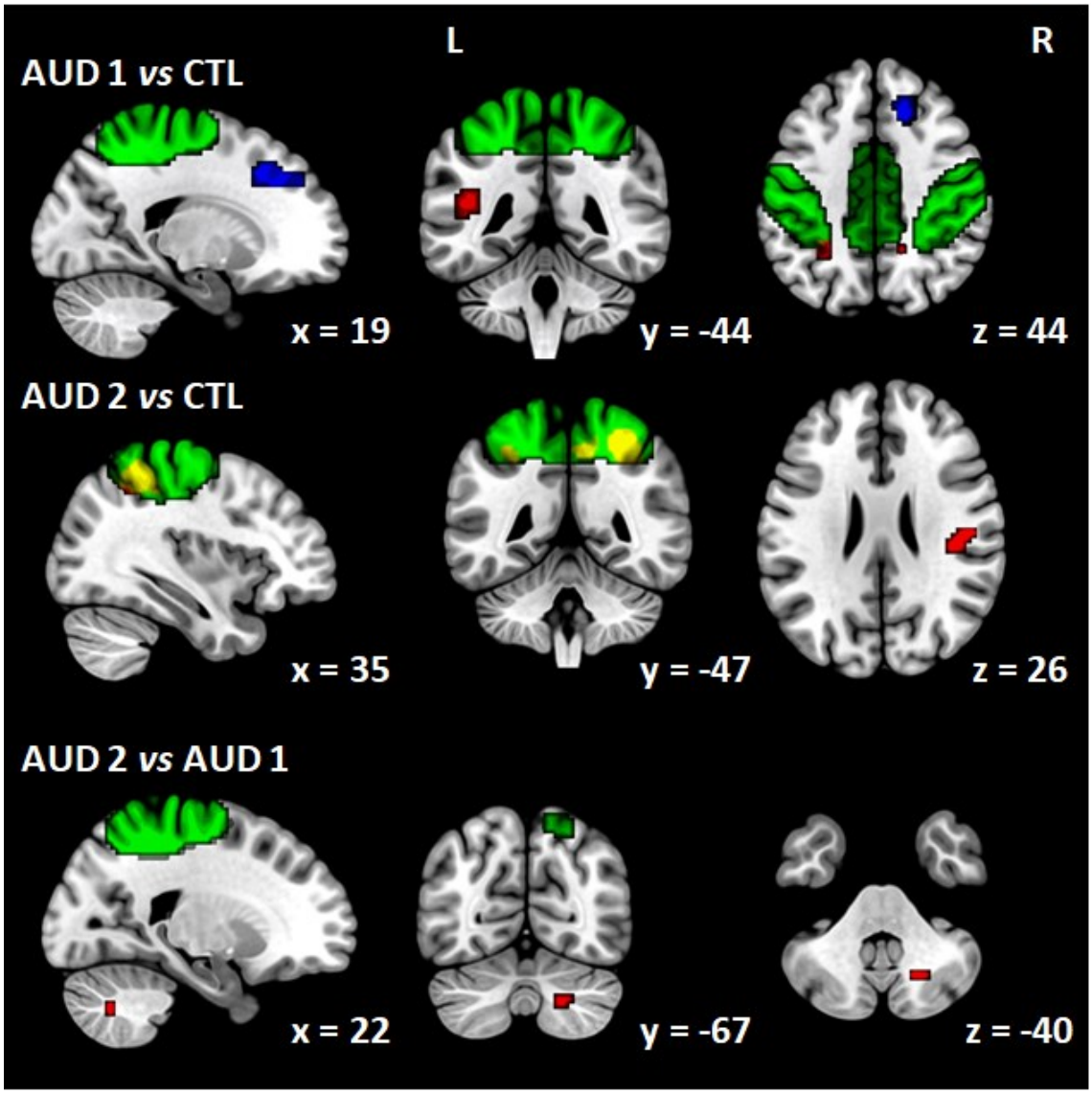

Figure 6.10: Independent Component 09 - Auditory Network

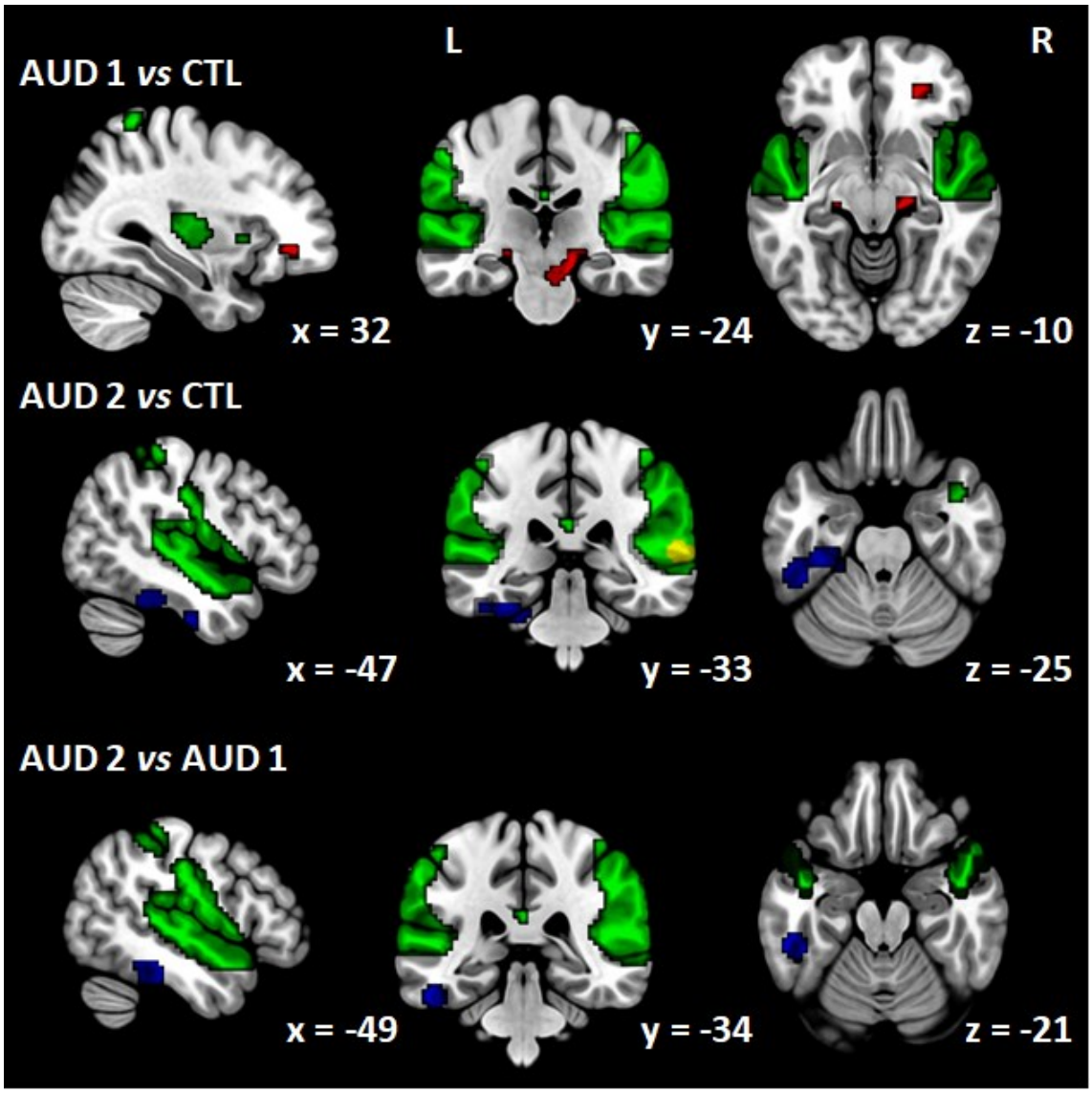

Figure 6.11: Independent Component 10 - Visual Network – Lingual Gyrus

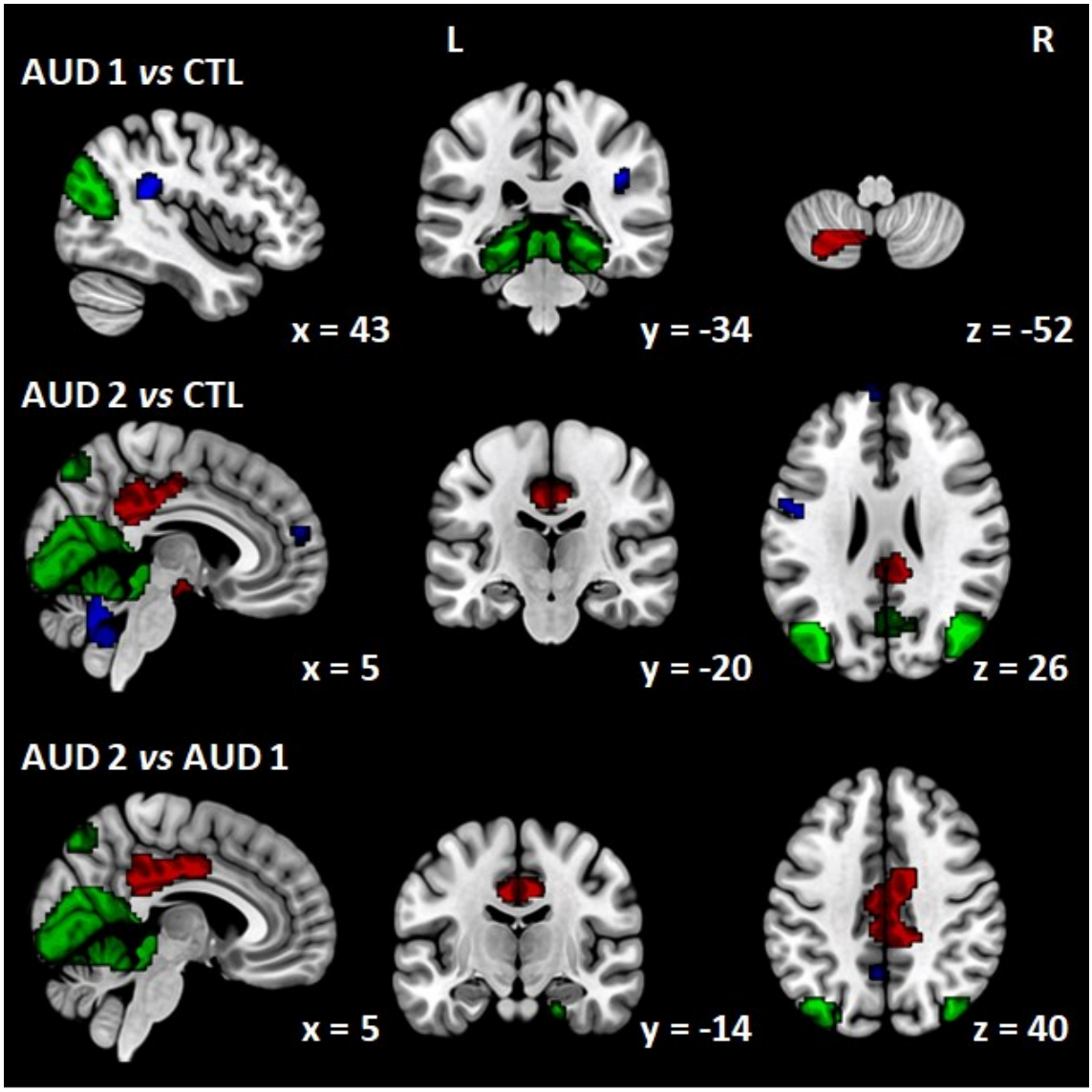

Figure 6.12: Independent Component 11 - Language Network

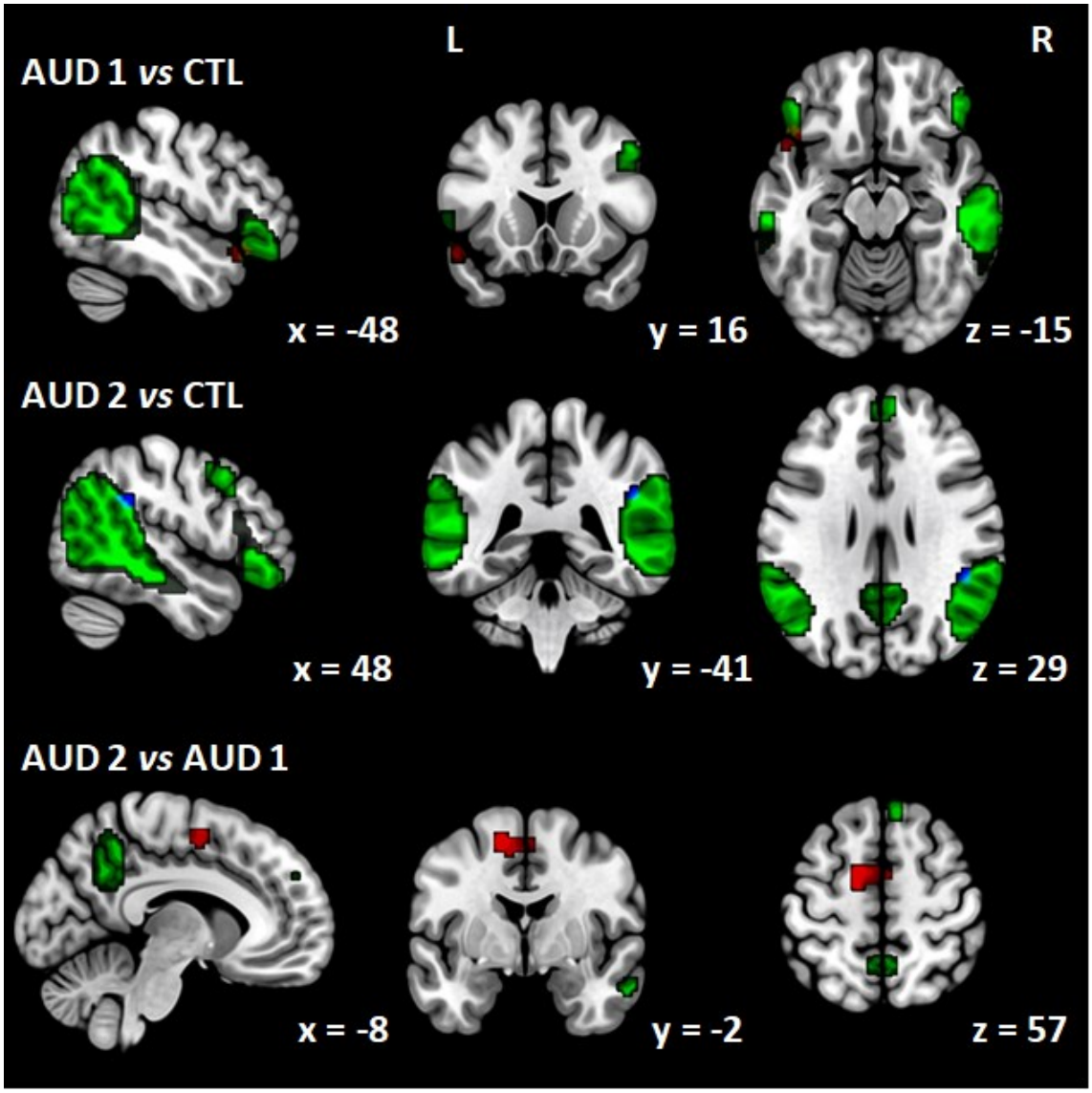

Figure 6.13: Independent Component 12 - Right Executive Control Network

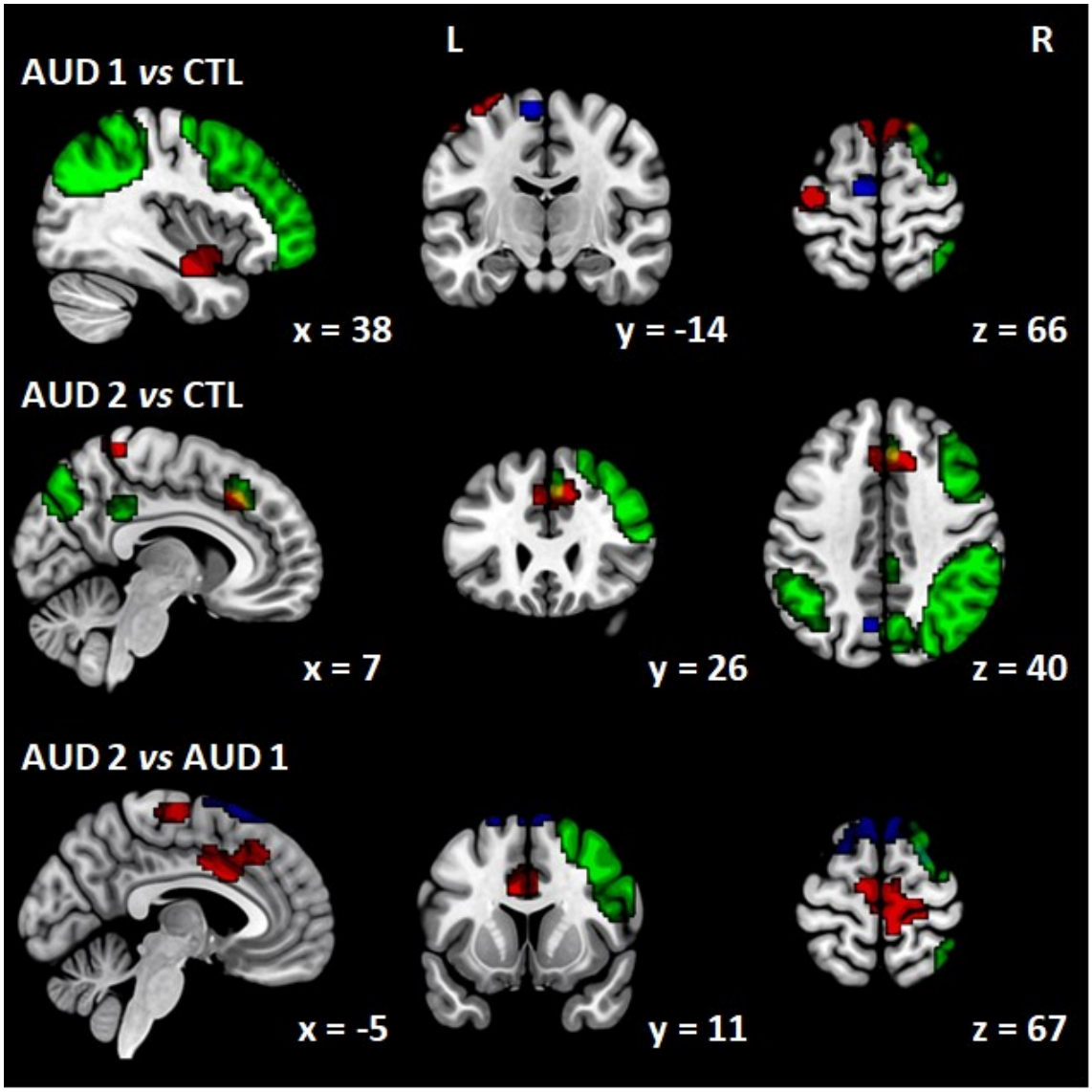

Figure 6.14: Independent Component 13 - Precuneus Network

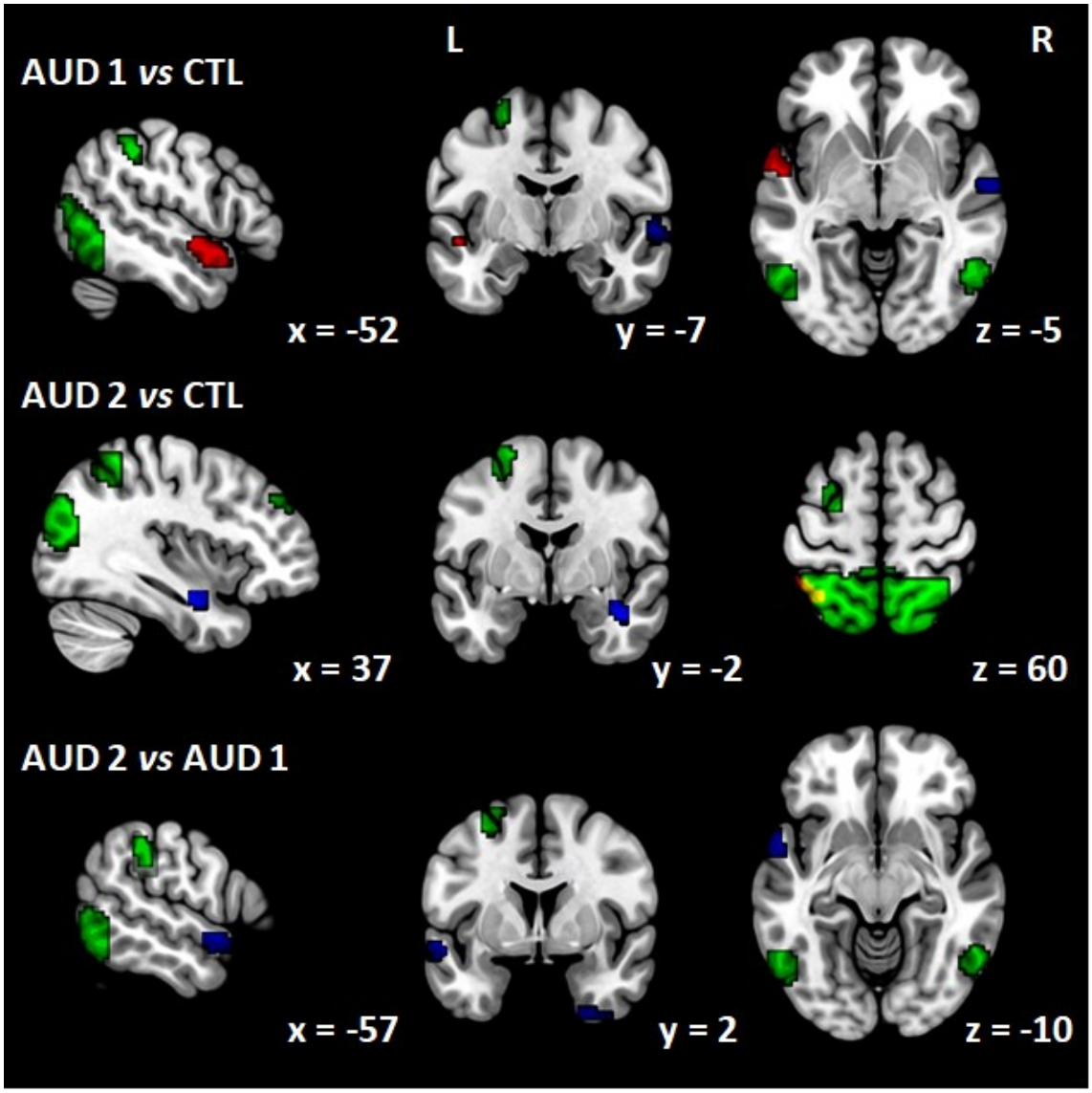

Figure 6.15: Independent Component 14 - Left Executive Control Network

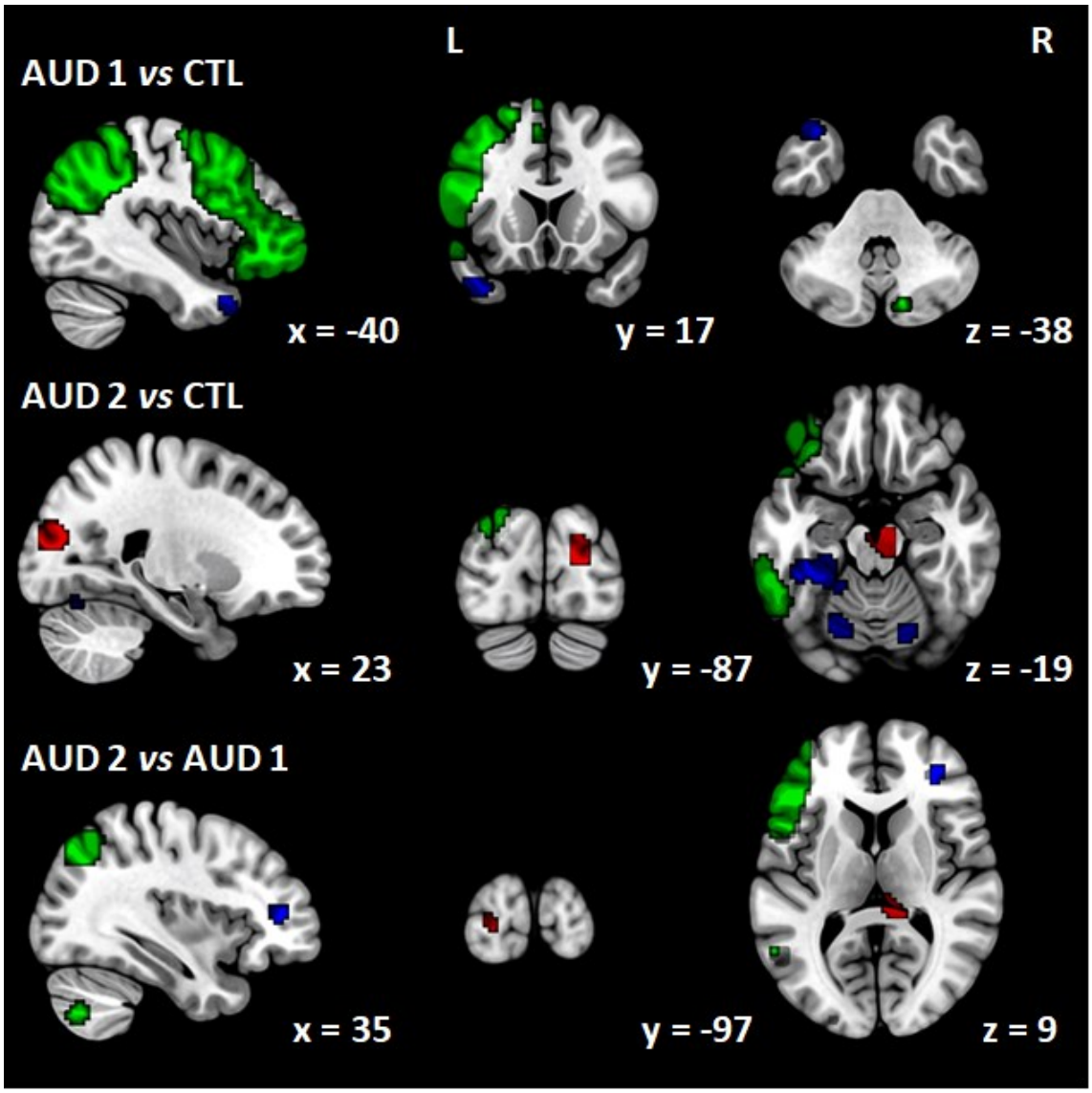

Figure 6.16: Independent Component 15 - Anterior-Salience / Insula Network

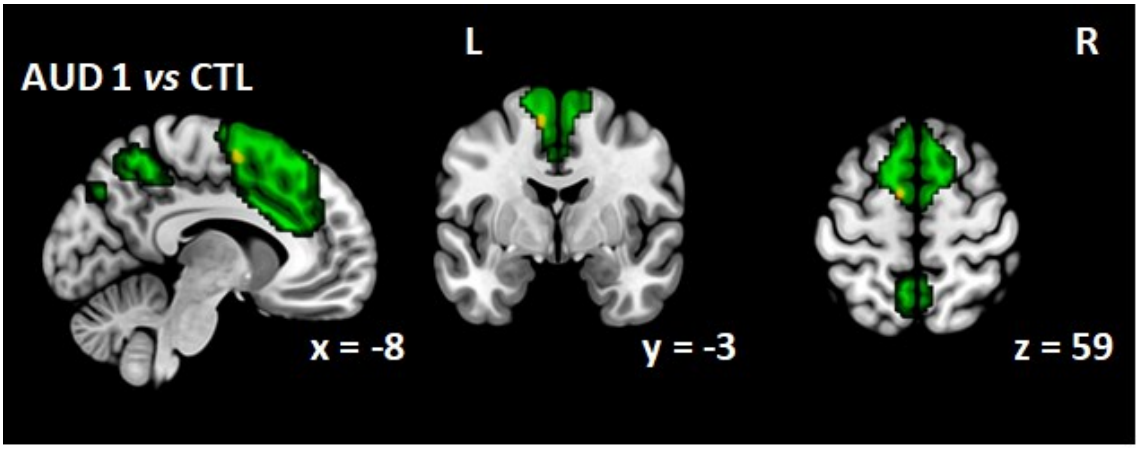

3.5 Clinical Severity Correlations

An exploratory post-hoc analysis was conducted on the significantly different clusters revealed by the ICA group analysis and their correlation to different clinical severity scales. These changes are summarized in Table 6.4. As anticipated, clusters which showed increased functional connectivity in the AUD patient group compared to the healthy control group were associated with significant positive correlation and *vice versa*. 20 clusters from 84 contrasts tested in our analysis have demonstrated a consistent significant correlation with at least three different clinical severity measures, after full multiple-comparison correction. All of these were from comparisons of the AUD group to the healthy control at first, second, or both time points. None of the longitudinal interscan differences within the AUD group showed a consistent track record of significant correlation with the clinical severity scales. Only a cluster of increased cerebellar functional connectivity of component 8 (Sensory-Motor Network) showed a significant positive correlation with any of the collected clinical severity scales (Obsessive Compulsive Drinking Scale and its Obsessive Drinking Subscale) for the interscan comparisons.

The 20 clusters which showed at least three sets of significant correlation with clinical scale included: Component 1 AUD 2 < CTL, Component 2 AUD 1 < CTL, Component 2 AUD 2 < CTL, Component 3 AUD 2 > CTL, Component 4 AUD 2 > CTL, Component 4 AUD 2 < CTL, Component 7 AUD 1 < CTL, Component 7 AUD 2 > CTL, Component 7 AUD 2 < CTL, Component 8 AUD 2 > CTL, Component 9 AUD 2 > CTL, Component 9 AUD 2 < CTL, Component 10 AUD 1 > CTL, Component 10 AUD 2 < CTL, Component 11 AUD 2 < CTL, Component 12 AUD 2 > CTL, Component 13 AUD 2 < CTL, Component 14 AUD 1 < CTL, Component 14 AUD 2 > CTL, and Component 14 AUD 2 < CTL.

The clinical severity scale which was most commonly correlated with the significant clusters was AUDIT at 52%, followed by CDS at 39%, ADS at 38%, OCDS at 38%, number of standard drinks typically consumed before detoxification at 34%, ODS at 27%, and length of abstinence at just 2% (only in the AUD 2 > CTL in Component 3).

Table 6.4: Pearson Correlations of Clinical Severity to Functional Connectivity Measures

Component	Contrast	Abstinence	# Drinks	AUDIT	ADS	OCDS	ODS	CDS
01	AUD 1 > CTL	0.14	0.09	**0.25***	0.03	0.21	0.09	**0.29****
	AUD 1 < CTL	0.04	-0.21	**-0.25***	**-0.27****	-0.17	-0.15	-0.17
	AUD 2 < CTL	0.08	**-0.42*****	**-0.51*****	**-0.44*****	**-0.45*****	**-0.37*****	**-0.47*****
	AUD 2 > AUD 1	0	0.04	0.01	-0.06	-0.05	-0.08	-0.01
	AUD 2 < AUD 1	0.17	-0.22	-0.17	-0.21	-0.13	-0.15	-0.1
02	AUD 1 < CTL	-0.13	**-0.31*****	**-0.35*****	**-0.30*****	**-0.36*****	**-0.33*****	**-0.35*****
	AUD 2 < CTL	0.13	**-0.33*****	**-0.34*****	**-0.31*****	**-0.32*****	**-0.27***	**-0.33*****
03	AUD 1 > CTL	0.05	0.23	**0.28****	0.22	0.24	0.18	**0.27***
	AUD 2 > CTL	**-0.35****	**0.40*****	**0.48*****	**0.50*****	**0.51*****	**0.43*****	**0.52*****
	AUD 2 < CTL	0.03	-0.13	**-0.26***	-0.2	-0.1	-0.04	-0.14
04	AUD 1 > CTL	0.02	0.11	**0.27****	0.15	0.13	0.1	0.15
	AUD 1 < CTL	-0.02	-0.21	-0.2	-0.12	-0.15	-0.13	-0.15
	AUD 2 > CTL	-0.13	0.16	**0.36*****	**0.31*****	**0.38*****	**0.34*****	**0.39*****
	AUD 2 < CTL	0.2	**-0.25***	**-0.49*****	**-0.43*****	**-0.31*****	**-0.26***	**-0.33*****
06	AUD 1 > CTL	0.16	0.21	0.23	0.19	0.16	0.14	0.17
	AUD 1 < CTL	0.08	-0.11	**-0.26***	-0.18	-0.14	-0.11	-0.16
	AUD 2 < AUD 1	0.07	-0.05	0	-0.03	0.01	-0.01	0.02
07	AUD 1 > CTL	0.3	0.05	**0.25***	0.07	0.12	0.08	0.15
	AUD 1 < CTL	-0.04	**-0.35*****	**-0.38*****	**-0.37*****	**-0.36*****	**-0.27****	**-0.40*****
	AUD 2 > CTL	0.02	**0.36*****	**0.47*****	**0.38*****	**0.38*****	**0.30****	**0.42*****
	AUD 2 < CTL	-0.05	**-0.32*****	**-0.43*****	**-0.41*****	**-0.38*****	**-0.28****	**-0.42*****
	AUD 2 > AUD 1	-0.03	0.04	0.11	0.07	0.09	0.12	0.06
08	AUD 1 > CTL	0.06	0.23	**0.29****	0.23	**0.25***	0.21	**0.26***
	AUD 1 < CTL	-0.17	-0.12	-0.17	-0.1	-0.05	0.02	-0.1
	AUD 2 > CTL	-0.09	**0.39*****	**0.38*****	**0.27***	**0.27****	0.25	**0.27****
	AUD 2 > AUD 1	-0.04	0.13	0.18	0.23	0.25*	0.26*	0.23

Table 6.4 continues on the next page.

Table 6.4 (continued): Pearson Correlations of Clinical Severity to Functional Connectivity Measures

Component	Contrast	Abstinence	# Drinks	AUDIT	ADS	OCDS	ODS	CDS
09	AUD 1 > CTL	-0.06	0.21	0.19	0.15	0.1	0.07	0.12
	AUD 2 > CTL	-0.07	**0.26***	**0.38*****	**0.42*****	**0.45*****	**0.41*****	**0.44*****
	AUD 2 < CTL	0.23	**-0.35*****	**-0.31*****	**-0.28****	**-0.28****	-0.21	**-0.32*****
	AUD 2 < AUD 1	0.14	-0.17	-0.13	-0.13	-0.12	-0.1	-0.13
10	AUD 1 > CTL	0.16	0.18	0.24	**0.28****	**0.29****	**0.31*****	**0.26***
	AUD 1 < CTL	-0.25	-0.07	-0.22	-0.19	-0.25	-0.24	-0.23
	AUD 2 > CTL	0.06	0.24	**0.25***	0.2	0.12	0.07	0.15
	AUD 2 < CTL	0.03	**-0.42*****	**-0.46*****	**-0.35*****	**-0.44*****	**-0.40*****	**-0.44*****
	AUD 2 > AUD 1	-0.02	0.18	0.15	0.14	0.04	0.02	0.06
	AUD 2 < AUD 1	0	0	0.09	0.08	0.07	0.1	0.03
11	AUD 1 > CTL	0	**0.25***	0.24	0.23	0.21	0.23	0.17
	AUD 2 < CTL	0.06	-0.23	**-0.27****	**-0.25***	**-0.26***	-0.21	**-0.28****
	AUD 2 > AUD 1	0.03	-0.02	-0.02	-0.05	-0.05	-0.07	-0.03
12	AUD 1 > CTL	0.1	0.14	**0.31*****	0.17	0.16	0.07	0.22
	AUD 1 < CTL	-0.22	-0.09	-0.12	-0.1	-0.1	0	-0.17
	AUD 2 > CTL	-0.06	**0.27****	**0.33*****	**0.34*****	**0.41*****	**0.37*****	**0.41*****
	AUD 2 < CTL	0.08	**-0.26***	-0.15	**-0.27****	-0.2	-0.15	**-0.22**
	AUD 2 > AUD 1	-0.05	0.13	0.07	0.11	0.22	0.23	0.19
	AUD 2 < AUD 1	0.16	-0.02	0.12	0.01	-0.03	-0.08	0.02
13	AUD 1 > CTL	-0.02	0.1	0.17	0.12	0.07	-0.01	0.12
	AUD 1 < CTL	-0.07	-0.1	-0.13	-0.17	-0.13	-0.12	-0.13
	AUD 2 > CTL	0.26	**0.28****	0.25	0.22	0.2	0.18	0.2
	AUD 2 < CTL	0.3	**-0.30*****	**-0.30****	**-0.30*****	**-0.28****	-0.23	**-0.30*****
	AUD 2 < AUD 1	0.04	0.07	0.14	0.09	0.08	0.02	0.12
14	AUD 1 < CTL	0.1	**-0.29*****	**-0.30*****	-0.22	-0.18	-0.13	-0.2
	AUD 2 > CTL	-0.05	**0.28****	**0.36*****	**0.31*****	**0.35*****	**0.27****	**0.37*****
	AUD 2 < CTL	-0.02	-0.14	**-0.35*****	**-0.30*****	**-0.33*****	-0.24	**-0.38*****
	AUD 2 > AUD 1	0.02	0.08	0	0.09	0.09	0.11	0.07
	AUD 2 < AUD 1	0.03	-0.18	-0.02	-0.02	-0.11	-0.1	-0.11
15	AUD 1 > CTL	0.22	0.17	0.1	0.08	0.05	0.03	0.06

3.6 Graph Theory and Network Hierarchy

A simple full correlation analysis of all of the independent component networks has revealed the relative functional connectivity hierarchy of the networks, as depicted at the top of Figure 6.2. Table 6.5 also summarized the correlations between the independent component networks in the healthy subjects, with the full simple correlation on the lower left corner and the standard error of mean in the upper right corner. Table 6.6 summarizes the relative group differences in the correlations between the healthy control group and the AUD patient group at both first and second time points. In general, the controls have exhibited stronger positive and negative correlations across most networks.

Interestingly, Component 01 (Basal Ganglia / Deep Gray Matter Network) and 10 (Visual Network - Lingual) were positively correlated in the AUD group at both time points but negatively correlated in the control group (the differences were statistically significant after full Bonferroni correction). Similar but non-significant trend was also observed between Component 01 (Basal Ganglia / Deep Gray Matter Network) and 09 (Auditory Network). The inverse trend of negative correlation at first AUD time point, negative correlation at the second AUD time point, while positive in the healthy control reference group was observed in correlations between Component 02 (Cerebellum Network) and Component 15 (Anterior-Salience / Insula Network) as well as Component 10 (Visual Network – Lingual Gyrus) and Component 13 (Precuneus Network) (although neither reached significance). There was also a trend of normalizing correlations/anti-correlations between networks between Component 06 (Posterior Default Mode Network) and 07 (Mesial-Temporal Network) of negative at first time point, positive at second time point, and positive in controls (also not significant). There were also groups of edges which exhibited deterioration of the correlation trends. Positive at first time point, negative at second time point, while controls exhibited positive correlation occurred between Components 03 (Primary Visual Network) and 10 (Visual Network - Lingual) (only the difference between healthy control group and AUD group at the

second time point survived multiple comparison correction). A similar non-significant trend occurred also between Components 04 (Anterior Default Mode Network) and 07 (Mesial-Temporal Network); 02 (Cerebellum Network) and 10 (Visual Network – Lingual Gyrus); 08 (Sensory-Motor Network) and 13 (Precuneus Network). An inverse trend in continued deterioration from negative at first time point to positive at second time point, compared to negative reference correlation in the control group occurred between Components 2 (Cerebellum Network) and 10 (Visual Network – Lingual Gyrus) (only the difference between healthy control group and AUD group at the second time point survived multiple comparison correction). A similar non-significant trend also occurred between Components 04 (Anterior Default Mode Network) and 10 (Visual Network – Lingual Gyrus); 06 (Posterior Default Mode Network) and 13 (Precuneus Network); 07 (Mesial-Temporal Network) and 08 (Sensory-Motor Network); and 08 (Sensory-Motor Network) and 11 (Language Network).

Beyond just correlation and anti-correlations trends between the functional networks, the longitudinal differences between AUD group and healthy control group converged across 52 edges (57%) and diverged across 42 edges (43%). Examining these differences in greater detail reveals that there is a wide divergence between the patterns observed across different functional networks. The longitudinal convergence varied from overwhelmingly normalizing in Component 12 (Right Executive Control Network) with 85% of edges converging to predominantly diverging in Components 03 (Primary Visual Network) and 08 (Sensory-Motor Network) with only 31% of edges converging with prolonged abstinence. Longitudinal convergence across the networks was the following Component 12 (85%), Component 07 (77%), Component 06 (69%), Component 01 (62%), Component 09 (62%), Component 13 (62%), Component 13 (62%), Component 14 (62%), Component 02 (54%), Component 04 (54%), Component 10 (54%), Component 11 (54%), Component 15 (46%), Component 03 (31%), and Component 08 (31%). Overall, these results suggest a trend of normalization across the resting state functional connectivity with strengthening inter-network communication with prolonged abstinence in the recovering AUD patients. 33% of the edges were more correlated at first time point while 38% at second time point, with 41% networks increasing interscan in the AUD group. Increasing divergence across

several networks involving the Primary Visual Network (Component 03), Sensory-Motor Network (Component 08), and the Language Network (Component 11), nonetheless, suggests a possibility of an adaptive mechanism rather than "healing" of the abnormal addiction-related connectivity pattern as well. These diverging networks, however, do not include prototypical addiction-related anatomical regions nor prototypical pattern of excess top-down executive control and deficit bottom-up reward over-compensatory adaptive changes, as reviewed by (Fein & Cardenas, 2015).

Table 6.5: Healthy Independent Component Correlations Hierarchy

		Standard Error of Mean													
	Component	**1**	**2**	**3**	**4**	**6**	**7**	**8**	**9**	**10**	**11**	**12**	**13**	**14**	**15**
Nuisance-Corrected Mean Correlation Z-Stat	**1**		0.14	0.12	0.13	0.13	0.11	0.15	0.12	0.15	0.13	0.13	0.12	0.11	0.11
	2	1.66		0.20	0.14	0.13	0.14	0.17	0.12	0.14	0.14	0.12	0.12	0.13	0.15
	3	-1.84	-0.44		0.13	0.15	0.10	0.17	0.17	0.17	0.13	0.14	0.14	0.13	0.16
	4	0.06	-0.67	-1.26		0.18	0.15	0.14	0.16	0.17	0.14	0.15	0.13	0.12	0.15
	6	1.07	-0.03	-1.51	1.86		0.12	0.14	0.15	0.16	0.15	0.16	0.13	0.14	0.17
	7	0.45	-0.20	-0.98	0.18	0.12		0.12	0.13	0.12	0.13	0.11	0.11	0.13	0.13
	8	-1.70	-1.54	1.35	-1.39	-1.21	-0.40		0.16	0.16	0.12	0.15	0.13	0.13	0.15
	9	-0.14	-0.85	0.76	-2.97	-1.91	0.54	1.98		0.16	0.13	0.14	0.16	0.14	0.17
	10	-0.11	-0.69	0.77	-0.42	1.67	-0.18	0.95	-0.17		0.15	0.14	0.13	0.14	0.16
	11	-0.08	-0.39	-0.03	1.11	0.74	0.05	-0.51	-0.34	0.17		0.14	0.14	0.12	0.12
	12	-0.53	0.13	-1.50	0.33	-0.21	-0.94	-1.46	-1.21	-1.55	-0.37		0.15	0.17	0.13
	13	-1.08	0.14	1.05	-1.88	-0.29	-0.83	0.28	0.68	0.01	-1.58	0.52		0.13	0.15
	14	-0.42	0.21	-1.11	0.58	-0.43	-1.14	-0.96	-1.70	-1.33	0.25	1.99	-0.73		0.14
	15	1.29	0.25	-1.99	-0.21	-0.16	-0.05	-0.90	1.04	-1.15	0.66	1.20	-1.08	0.74	

Table 6.6: Significant Network Correlation Differences

Component	AUD1		AUD2		CTL		AUD 1 *vs* CTL		AUD 2 *vs* CTL		AUD 2 *vs* AUD 1	
	x̄	SEM	x̄	SEM	x̄	SEM	% Δ	t	% Δ	t	% Δ	t
1 & 2	0.86	0.16	1.06	0.12	1.66	0.14	**-48**	**-4.02**	-36	-3.02	23	0.95
1 & 3	-1.11	0.13	-0.98	0.17	-1.84	0.12	**-40**	**3.77**	-47	4.43	-12	0.63
1 & 8	-1.04	0.14	-0.65	0.17	-1.70	0.15	-39	3.06	**-62**	**4.88**	-38	1.73
1 & 10	0.69	0.14	0.85	0.14	-0.11	0.15	**-718**	**3.95**	**-862**	**4.74**	23	0.76
1 & 13	-1.20	0.15	-0.47	0.17	-1.08	0.12	12	-0.63	-56	3.03	**-61**	**3.49**
1 & 15	0.46	0.14	0.44	0.13	1.29	0.11	**-64**	**-4.60**	**-66**	**-4.74**	-6	-0.14
2 & 8	-0.50	0.17	-0.36	0.20	-1.54	0.17	**-68**	**4.21**	**-77**	**4.78**	-28	0.54
2 & 10	-0.46	0.17	0.00	0.12	-0.69	0.14	-33	1.12	**-101**	**3.40**	-101	2.18
3 & 10	0.40	0.16	-0.33	0.20	0.77	0.17	-48	-1.49	**-143**	**-4.45**	-182	-2.82
3 & 14	-1.25	0.14	-0.52	0.14	-1.11	0.13	13	-0.76	-53	3.06	**-58**	**3.64**
8 & 9	1.49	0.17	2.43	0.16	1.98	0.16	-25	-2.14	22	1.92	**63**	**3.87**
11 & 15	1.05	0.17	1.41	0.17	0.66	0.12	58	1.83	**112**	**3.53**	34	1.62

Bolded numbers are significant.

4 Discussion

The objective of this study was to compare longitudinal changes in large-scale resting state functional networks in recovering AUD patients between 19 and 36 days of sustained abstinence. Our study has revealed a rich but very complex set of results which are not intuitive to interpret. In order to facilitate our understanding, we will discuss our findings from a macroscopic perspective of the functional networks themselves.

Component 1 (Basal Ganglia / Deep Gray Matter Network) was one of the most addiction-relevant resting state functional networks because it encompasses most appetitive drive-related anatomy of the limbic system and is thus sometimes also referred to as the reward network or core reward network (Hobkirk, Bell, Utevsky, Huettel, & Meade, 2019). Anatomical constituents of 01 Basal Ganglia Network have been involved in reward, risk-taking, and drug-cue event-related functional connectivity changes (along with other regions of extended reward network such as dorso-lateral prefrontal cortex and anterior cingulate cortex) (G. Di Chiara & Bassareo, 2007; Koob & Volkow, 2016; McClure, Laibson, Loewenstein, & Cohen, 2004; Rao, Korczykowski, Pluta, Hoang, & Detre, 2008). Laird *et al.* have demonstrated association between Basal Ganglia Network and especially reward tasks but also thermal stimulation, interoceptive function (such as hunger, thirst, sexuality, etc), as well as emotional processing (anxiety) and cognitive processing (motor, pain, somatosensory) (Laird et al., 2011). Our study revealed hierarchical organization of the 01 Basal Ganglia Network in the same branch as 02 Cerebellum Network and adjacent to 07 Mesial-Temporal Network with some positive correlation to the default-mode network branch and opposite to the sensory and motor branch as well as the executive control and salience branch, as illustrated in Figure 6.2.

At first time point, 01 Basal Ganglia Network was associated with decreased functional connectivity with 02 Cerebellum Network and increased functional connectivity with insula and temporal operculum regions within 09 Auditory Network as well as a small part of 07 Mesial-Temporal Network. The correlation between 01 and 02 was positive and longitudinally convergent towards stronger healthy interconnectivity, in agreement with the negative cluster. 01 was also positively correlated to 07 and 09 in AUD but exhibited excessive correlation trend compared to the healthy controls, also in agreement with the positive cluster. The negative clusters were negatively correlated to the AUDIT as well as ADS scores while the positive clusters were positively correlated with AUDIT score as well as CDS sub-score.

At the second time point, 01 Basal Ganglia Network exhibited decreased functional connectivity with 02 Cerebellum Network (in non-overlapping regions compared to the first time point), itself (putamen), as well as 03 Primary Visual Network and 10 Visual Network – Lingual Gyrus (lingual gyrus), 04 Anterior Default Mode Network (anterior cingulate cortex), and 08 Sensory-Motor Network (post-central gyrus) while no increased functional connectivity. 01 was negatively correlated with 03 but more weakly than in healthy controls with a converging trend. 01 was positively correlated with 10 with a diverging pattern while it was negatively correlated in controls. 01 was almost not correlated with 04 in both AUD as well as healthy controls, with a converging longitudinal trend. 01 and 08 were negatively correlated with a diverging trend towards increasingly weaker correlation compared to the healthy controls. The negative clusters at the second time point exhibited substantially stronger negative correlation with all of the clinical severity measures (amount of alcohol consumer prior detoxification, AUDIT, ADS, OCDS, ODS, and CDS) compared to the first time point negative clusters.

Interscan AUD differences in 01 Basal Ganglia Network included decreased functional connectivity with 04 Anterior Default Mode Network (paracingulate / superior frontal gyri) and increased 02 Cerebellum Network in region partially overlapping with the deficits observed at the first time point. Both of these changes coincided with a convergent correlation inter-network connectivity pattern. None of the interscan

differences were significantly correlated to any of the AUD severity scales and should, thus, be interpreted with caution. The differences in functional connectivity between 01 Basal Ganglia Network and 02 Cerebellum Network remain persistent across all of the contrasts, even without anatomical overlap. The decreased longitudinal activation between 01 and 04 Anterior Default Mode Network (in the clusters spanning anterior cingulate / prefrontal cortex) could be interpreted as supporting the adaptive, decreased bottom-up reward connectivity reviewed by (Fein & Cardenas, 2015) and be associated with changes in higher order cognitive and motivational processing, including attenuation of craving experience (Goldstein & Volkow, 2002). Other studies grouped 01 with parts of 04, which have included the significant negative clusters, as part of the same extended reward independent component network in AUD (Müller-Oehring et al., 2015).

Component 02 (Cerebellum Network) has been traditionally considered as motor structure. Smith *et al.* have accordingly demonstrated association between resting state Cerebellum Network and functional activation in action-execution as well as perception-somesthesis-pain BrainMap domains (Laird et al., 2011; Smith et al., 2009). Growing body of evidence has, however, implicated cerebellum also in cognitive and affecting processing and its importance in addiction as a potential intermediary between motor and higher order cognitive control, reward, and motivation domains (for review see (Moulton et al., 2014)). AUD also leads to substantial structural damage to cerebellum (Harper et al., 2003) and cerebellar functional deficits such as ataxia, impaired movement and speed, as well as impaired postural stability and balance (J. Luo, 2015). The hierarchy of 02 Cerebellum Network was closest to 01 Basal Ganglia as described above. The results of our study revealed that 02 exhibited decreased functional connectivity within itself at both the first and second time point in the AUD group, although to a smaller anatomical extent at the second time point. Both sets of negative clusters were significantly negatively correlated with all of the clinical severity measures and the amount of alcohol consumption before detoxification. The within group interscan differences were not significant. Even though cerebellum exhibited significant

functional connectivity differences with numerous other functional networks in our analysis, it did not exhibit reciprocal relationship, instead revealing primarily within-network differences. Longitudinally, cerebellum has exhibited less extensive functional connectivity at the second time point suggesting a potential underlying (but not significant) pattern of functional recovery.

Component 03 (Primary Visual Network) consisted of visual processing regions of the occipital lobe, spanning what are sometimes reported as several visual networks in the resting state literature and beyond just the V1 primary visual cortex. Smith and Laird have accordingly demonstrated association between the resting state visual networks corresponding to our Primary Visual Network and visual stimuli and tasks during paradigms such as cognition–language–orthography and cognition–space (including basic visual stimuli, higher order visual processing, reading) (Laird et al., 2011; Smith et al., 2009). The hierarchical organization of 03 was closest to the common branch between 08 (Sensory-Motor Network) and 09 (Auditory Network) as well as branch of 13 (Precuneus Network), as indicated in Figure 6.2. Interestingly, 10 (Visual Network – Lingual Gyrus) was more closely associated with the default-mode network branch than 03, despite of their close anatomical relationship.

At the first time point, 03 did not exhibit decreased functional connectivity with any networks. Nonetheless, two sets of clusters exhibited increased functional connectivity with a region overlapping 15 (Anterior-Salience / Insula Network) and 08 (Sensory-Motor Network) in the left supplementary motor cortex and also with 06 (Posterior Default Mode Network) in the right posterior cingulate cortex. These differences showed only limited positive correlation with the clinical severity as measured with AUDIT and CDS. 03 was positively correlated to 08 but negatively correlated to 15 with both correlations suggesting a non-significant trend of weaker magnitude at the first time point compared to the healthy controls.

At the second time point, the AUD group exhibited decreased functional connectivity between 03 and 02 (Cerebellum Network) which were weakly negatively correlated (with a diverging trend of weaker correlation compared to controls) and showed significant negative correlation only with the AUDIT score. There were also several clusters of increased functional connectivity including the superior frontal gyrus, which fell primarily within 15 (Anterior-Salience / Insula Network) as well as V3/4 occipital lobe within itself. These positive clusters exhibited very significant positive correlation with AUD severity scales as well as significant negative correlation with the length of abstinence at the first time point (as the only cluster in our study). The positive superior frontal gyrus cluster from the second contrast did not overlap with the positive cluster in the contralateral supplementary motor area in the first contrast but they both were located partially in Brodmann area 6 and overlapped the most with 15 out of our resting state networks. 03 and 15 were negatively correlated in both AUD as well as healthy controls with a weaker, divergent trend in the magnitude in the AUD patients. These differences suggest that these changes might be associated with a compensatory adaptive mechanism which might become stronger with prolonged abstinence, potentially in the ventral object recognition stream (via the greater functional recruitment of V3/V4 cluster). Our study did not include any visual performance measures or any other neurocognitive to better contextualize these resting state results. Several studies have, nonetheless, reported impaired visual processing function and poorer visual learning, visual memory, and visuospatial abilities in abstinent AUD patients, which sometimes persisted even after long term remission of several years (for meta-analysis see (Stavro et al., 2013)).

Component 04 (Anterior Default Mode Network) was also of particular interest since it included anatomical regions such as orbito-frontal cortex, prefrontal cortex, subgenual anterior cingulate cortex, and posterior cingulate cortex, which are all pivotal components involved in executive control and to lesser extent also appetitive drive in addiction (Fein & Cardenas, 2015; Koob & Volkow, 2010). Smith *et al.* did not isolate a single network comparable to our 04 Anterior Default Mode Network in their ICA.

Our network is a combination of Smith's executive control (8) and default mode (4) networks, which were related to action–inhibition, emotion, perception–somesthesis–pain and several other cognitive paradigms for executive control network and negative cognitive paradigm contrasts for the default mode component (Smith et al., 2009). Laird *et al.* similarly did not isolate a single comparable network, with best match to their ICN2 spanning anterior cingulate and orbitofrontal cortex, which was associated with reward and thirst tasks as well as olfaction, gustation, and emotion (Laird et al., 2011). Hierarchically, 04 Anterior Default Mode Network was most closely related to 11 Language Network within the same branch and then to the second branch consisting of 06 Posterior Default Mode Network and 10 Visual Network – Lingual Gyrus, as illustrated in Figure 6.2. Complex data representation as evident in this pattern can make interpretation of ICA findings challenging (van den Heuvel & Hulshoff Pol, 2010).

At first time point, the AUD group exhibited abnormally low 04 Anterior Default Mode Network functional connectivity in the precentral gyrus within the 08 (Sensory-Motor Network) as well as in thalamus within 01 (Basal Ganglia / Deep Gray Matter Network). There was also excess functional connectivity in the left parietal lobe which was within 09 (Auditory Network) but also partially in 14 (Left Executive Control Network) and 15 (Anterior-Salience / Insula Network). The inter-network correlation between 04 and 08 was negative and diverging in the AUD group while the correlation between 04 and 01 was positive and converging to a weaker magnitude. 04 and 09 exhibited very strong negative correlation which was divergently strengthening with abstinence while the edges between 04 and both 14 and 15 were converging and increasing in magnitude, although 14 was positive while 15 was negative in correlation. The positive clusters at first time point were only marginally positively correlated with clinical severity (only AUDIT). The negative clusters were not correlated to any of the clinical severity measures and should, thus, be considered with caution.

At the second time point, the AUD group exhibited decreased functional connectivity between 04 and 06 (Posterior Default Mode Network) in the lateral occipital cortex and also in a potentially noisy cluster in

the frontal pole within the 04 network itself. There was also excessive functional connectivity between 04 and 11 (Language Network) in middle temporal gyrus and in the frontal pole (Brodmann area 10) within the 04 itself. The negative clusters were significantly negatively correlated with all AUD severity measures (especially AUDIT and ADS) while the positive clusters were positively correlated with most of the AUD severity measures (except for the average daily amount of alcohol consumed prior to detoxification). 04 and 06 were positively correlated with a diverging longitudinal pattern of strengthening excess correlation while 04 and 11 were also positively correlated but with converging strengthening patter of less deficient edge correlation with prolonged abstinence. There was no overlap in the longitudinal contrasts between AUD and healthy controls and also no significant interscan differences within the AUD group. Lack of converging evidence makes interpretation of these results challenging.

Component 06 (Posterior Default Mode Network) was also of a significant *a priori* interest. Posterior Default Mode Network is the prototypical resting-state functional network and thus also likely the best studied resting state network. Posterior Default Mode Network also spans several important addiction-related anatomical regions, including the middle cingulate gyrus associated with executive control and the posterior cingulate gyrus associated with appetitive drive (Fein & Cardenas, 2015; Koob & Volkow, 2010). Because default mode network is associated with rest and is thus deactivated during most event-related tasks, it is not usually associated with any specific task other than as a negative contrast during mostly cognitive tasks (Smith et al., 2009). Nonetheless, default mode network is still relatively strongly associated with social cognition and theory of mind paradigms as well as fixation, episodic recall, imagined scenes, and delayed discounting (Laird et al., 2011). Some studies have implicated Posterior Default Mode Network (06) in future-oriented reflection while Anterior Default Mode Network (04) more on present (Xu, Yuan, & Lei, 2016). Several AUD studies have reported aberrant default mode network functional connectivity (Chanraud et al., 2011; Müller-Oehring et al., 2015; Z. Song et al., 2020; Zhu et al., 2017) but some also reported no significant default mode network abnormalities (S. Kim, Im, Lee, &

Lee, 2017). Hierarchically, 06 Posterior Default Mode Network was associated the most closely with 10 Visual Network – Lingual Gyrus and a branch including 04 Anterior Default Mode Network and 11 Language Network, as illustrated in Figure 6.2.

Contrary to our expectations, the functional connectivity pattern of 06 Posterior Default Mode Network remained largely conserved within the AUD group with clusters which were not significant and/or not correlated to clinical severity measures (with exception of negative cluster from first contrast and AUDIT). Even though the reported clusters were statistically significant, they are on balance of probabilities unlikely to be associated with AUD if they are not related to any AUD-related clinical severity measures and might be due to other, unknown variables.

At the first time point, AUD exhibited decreased functional connectivity between 06 and the 03 (Primary Visual Network) in the lateral occipital cortex as well as excessive functional connectivity between 06 and 12 (Right Executive Control Network) in the right frontal pole / inferior frontal gyrus. 06 and 03 were negatively correlated with diverging trend of weakening correlation while 06 and 12 were initially weakly positively and then weakly negatively correlated with a converging negative correlation pattern. There were no significant differences in functional connectivity of 06 at the second time point, suggesting a normalization trend. The interscan within-AUD differences involved decreased functional connectivity in the middle cingulate gyrus in a boundary between several independent components but with largest overlap with 08 (Sensory-Motor Network). This interscan difference consisted only of a small cluster size which was also not significantly correlated to any clinical severity measures and should thus be interpreted with caution. 06 and 08 exhibit negative correlation with a converging trend which went from weaker to excess negative magnitude in comparison to the healthy controls.

Component 07 (Mesial-Temporal Network) was a somewhat problematic component due to its noisy character and inclusion of non-gray matter regions spanning multiple complex tissue boundaries at the base of the brain. It was of significant interest due to its inclusion of addiction-related areas, including basal ganglia reward-related regions (caudate nucleus, putamen, thalamus) and also parts of orbitofrontal cortex (preoccupation/anticipation) as well as insula (cravings and relapse) (Koob & Volkow, 2010). There was no comparable resting state network reported by Smith *et al*. (2009). Nonetheless, ICN 1 (limbic and medial-temporal areas) reported by Laird *et al*. substantially overlapped with 07 Mesial-Temporal Network in our study (Laird et al., 2011). This resting state functional network was strongly associated with tasks involving discrimination of emotional faces and pictures (especially fear, happiness, humour) and interoceptive processing during air-hunger (breathlessness) as well as olfactory and gustatory stimuli (Laird et al., 2011). Hierarchically, 07 Mesial-Temporal Network was most closely associated with a branch containing 01 Basal Ganglia Network and 02 Cerebellum Network, as illustrated in Figure 6.2. The complex anatomical extent of this component has resulted in complex functional connectivity differences.

At the first time point, 07 Mesial-Temporal Network exhibited excess functional connectivity within itself in the right insula in the AUD group. At the same time, 07 in AUD group also exhibited decreased connectivity with 09 (Auditory Network) in the right operculum / superior temporal gyrus / Heschl's gyrus / insula cluster as well as 15 (Anterior-Salience / Insula Network) in middle frontal gyrus, which has also partially overlapped with 14 (Left Executive Control Network), and clusters in cerebellum and occipital lobe within the 02 (Cerebellum Network) and 03 (Primary Visual Network), as well as some smaller noisy clusters in complex locations between networks. 07 and 09 were positively correlated with a converging trend of strengthening correlation. 07 and 15 were negatively correlated with a converging trend of weakening correlation. 07 and 02 as well as 03 were negatively correlated with a converging trend of strengthening inverse correlation. The increased cluster in the first contrast consisted only of a few clusters and was only correlated with one clinical severity measure (AUDIT) and should, thus, be

interpreted with caution. The decreased clusters exhibited very significant negative correlation with all of the clinical severity measures.

At the second time point, AUD group exhibited decreased functional connectivity between 07 and 09 (Auditory Network) in the right operculum as well as 08 (Sensory-Motor Network) in the right post-central gyrus. The AUD group also exhibited excess functional connectivity between 07 and left pre/post central gyrus cluster which spanned across both 08 (Sensory-Motor Network) and 09 (Auditory Network) and also a cluster in precuneus which mostly overlapped with 06 (Posterior Default Mode Network). Both positive and negative clusters were very significantly correlated with all measures of clinical severity. The correlation between 07 and 09 was positive and converging as described above. 07 and 08 exhibited a diverging correlation from weakly negative to stronger positive compared to stronger positive in healthy controls. 07 and 06 had a converging correlation trend from weakly negative to marginally positive compared to weakly positive in controls.

Interscan differences within the AUD group in 07 were associated with increased connectivity within the network itself in the brainstem area. This area is also overlapping with 01 (Basal Ganglia / Deep Gray Matter Network). These differences were not correlated to any clinical severity measures and should, thus, be considered with caution, especially since the underlying average reference signal from 07 was from a less uniform anatomical area than in the other components.

The only consistent trend in the Mesial-Temporal Network analysis included decreased functional connectivity between 07 and 09 in a cluster spanning the right temporal lobe and insula, which was strongly correlated to all of the clinical severity measures (with strongest correlation to CDS and AUDIT). Insula has been implicated as a potential neural locus influencing compulsive and impulsive behaviour, including addiction (especially in reward or anxiety states) and has been demonstrated to also exhibit reduced structural integrity as well as altered function in patients suffering from compulsive

disorders as well as their siblings (Belin-Rauscent et al., 2016). The positive converging trend of strengthening correlation between the two networks suggest a potential normalisation / recovery trend, although it did not reach significance on the interscan contrast. This could potentially reflect decreased alcohol cravings or compulsive urges with sustained abstinence during the remission process.

Component 08 (Sensory-Motor Network) is one of the most dominant and the first resting state functional networks that was identified (Biswal, Yetkin, Haughton, & Hyde, 1995). It is associated with action–execution and perception–somesthesis paradigms corresponding especially to hand movements tasks (finger tapping, grasping, pointing, tactile or electrical finger stimulation) (Laird et al., 2011). Hierarchically, 08 Sensory-Motor Network was most closely associated with 09 Auditory Network and then branch 03 Primary Visual Network and then another branch 13 Precuneus Network, as illustrated in Figure 6.2.

Component 08 (Sensory-Motor Network) was associated with decreased functional connectivity in the AUD group at the first time point within itself in left precentral gyrus as well as with 04 (Anterior Default Mode Network) in the right paracingulate / superior frontal gyri. At the same time, 08 was associated with increased functional connectivity with 09 (Auditory Network) in the left parietal operculum and within itself (and partially 13) in the left superior parietal lobule. The negative clusters were not significantly correlated to any clinical severity measures and should, thus, be considered with caution while the positive clusters were positively correlated with AUDIT, OCDS, and CDS. 08 and 04 were negatively correlated with a diverging trend of increasingly negative correlation. 08 and 09 were positively correlated with a converging trend in excess of the controls.

At the second time point, component 08 was associated with excess functional connectivity in several clusters within itself and a cluster in right parietal operculum / insula in 09 (Auditory Network). These

differences were positively correlated with all clinical severity measures, except for ODS. The two networks were positively correlated with a converging trend, as described above.

Interscan differences within the AUD group included increased functional connectivity between 08 and 02 (Cerebellum Network). Although this difference was significant and positively correlated with some clinical severity scales (OCDS and ODS), it constituted of only a very small cluster and should, thus, be considered with caution. Although no significant interscan differences were observed in 08, both first and second time point contrasts have revealed significantly increased functional connectivity within the network itself, with an increasing anatomical extent. This persistent excess activation could suggest an over-compensatory adaptive mechanism, as suggested in the executive control regions in long-term abstinent AUD patients (Fein & Cardenas, 2015). The clinical severity measures suggest that the more severe the AUD, the more pronounced this effect was at both time points. Given the anatomical composition outside of the prototypical addiction circuits, these changes might reflect compensatory changes in motor-sensory function since even long-term abstinent AUD patients can exhibit motor deficits (such as decreased speed and efficiency in motor tasks) even after several years of remission (Sullivan et al., 2010). The Sensory-Motor Network (together with 03 Primary Visual Network) has exhibited the greatest functional connectivity divergence out of all of the networks in our study, with more than 2 edges diverging for every converging edge, suggesting such aberrant compensatory changes might increase during early abstinence from AUD.

Component 09 (Auditory Network) spanned across primarily the auditory cortex, but also included several addiction-related regions including putamen, insula, frontal lobe. The resting state Auditory Network corresponds to event-related activation in action–execution–speech, cognition–language–speech, and perception–audition paradigms which include tone and pitch discrimination, music, speech, phonological discrimination, and oddball discrimination (Laird et al., 2011; Smith et al., 2009).

Hierarchically, 09 Auditory Network was most closely associated with 08 Sensory-Motor Network with more extended association with 03 Primary Visual Network and then 13 Precuneus Network, as illustrated in Figure 6.2.

Component 09 functional connectivity differences between AUD and the healthy controls for the first time point should be considered with caution and most likely disregarded. The small clusters fall largely outside of gray matter tissue close to tissue boundaries and are not correlated to any clinical severity scales. The clusters are located in regions spanning both 01 (Basal Ganglia / Deep Gray Matter Network) and 07 (Mesial-Temporal Network).

More pronounced differences were revealed at the second time point contrast. 09 was associated with decreased connectivity in the left inferior temporal gyrus mostly outside of the other independent components, partially overlapping 07 (Mesial-Temporal Network) and 14 (Left Executive Control Network) in the AUD group. At the same time, increased functional connectivity in right superior temporal gyrus was within 09 and partially 11 (Language Network). A small positive cluster between cerebellum and lingual gyrus overlapped with 10 (Visual Network – Lingual Gyrus). Both the positive and negative second time-point clusters were associated with very significant correlation with almost all of the clinical severity measures (negative cluster excluded ODS). Correlation between 09 and 07 was positive and converging as described previously. Correlation between 09 and 14 was negative and diverging to a weaker correlation. Same trend was observed between 09 and 11. Correlation between 09 and 10 was negative and diverged from weaker to excessively negative compared to the healthy controls.

Interscan differences for 09 were associated with decreased functional connectivity in the left inferior temporal gyrus (Brodmann area 20) which fell outside of most independent components but was close to 14 (Left Executive Control Network) and overlapping with the down cluster from the second time point comparison. These differences were, however, not correlated to the length of abstinence at the first time

point or any of the clinical severity scales and should, thus, be considered with caution. Other than the overlap in the inferior temporal gyrus, there did not appear to be a consistent trend in the functional connectivity changes between 09 and the other networks.

Component 10 (Visual Network – Lingual Gyrus) is an atypical resting state functional network, which was not reported in the behavioural and functional literature by Smith *et al* (2009) or Laird *et al* (2011). Hierarchically, 10 Visual Network – Lingual Gyrus is most closely associated with 06 Posterior Default Mode Network, constituting its functional extension into the occipital and temporal lobes. 10 was also associated with 04 Anterior Default Mode Network and 11 Language Network which were clustered at a parallel branch, as illustrated in Figure 6.2.

At first time-point, the AUD group exhibited functional connectivity deficits between 10 and 08 (Sensory-Motor Network) in precentral gyrus as well as in a cluster in parietal operculum outside of most independent components but closest to 09 (Auditory Network). These negative clusters should be interpreted with caution since they were not significantly correlated with any of the clinical severity measures. At the first time point, there was also increased functional connectivity in the AUD group between 10 and 02 (Cerebellum Network) in cerebellum and also in precuneus, which overlapped several functional networks, including 13 (Precuneus Network), 11 (Language Network), 6 (Posterior Default Mode Network), and 4 (Anterior Default Mode Network). These positive clusters were all positively correlated with ADS, OCDS, ODS, and CDS. Inter-network correlation between 10 and 08 was positive and weaker and diverging compared to controls. 10 and 09 correlation was negative and diverging, as described previously. 10 and 02 correlation was negative and diverging from weak to no correlation. The correlations between 10 and 13, 11, 6, and 04 did not show a uniform pattern. Correlations between 10 and 11 as well as 06 were positive while for 13 and 04 were negative. 13, 11, and 06 were all converging

while 4 was diverging. The interpretation of the positive precuneus cluster as part of 04 is most consistent with these results, although functionally problematic to contextualize.

At the second time point, AUD exhibited functional connectivity deficits between 10 and 14 (Left Executive Control Network), 13 (Precuneus Network), 02 (Cerebellum Network), 04 (Anterior Default Mode Network), and in a cluster in precentral gyrus across multiple networks including 14 (Left Executive Control Network), 09 (Auditory Network), and 08 (Sensory-Motor Network). The negative clusters were very significantly correlated with all clinical measures. There was also excessive functional connectivity between 10 and 06 in the posterior cingulate and smaller cluster falling within 01 or 07 which might be disregarded as possible noise. These positive clusters were not significantly correlated with any clinical severity measures and should thus be interpreted with caution. The pattern of inter-network correlations of 10 was already discussed above.

Interscan comparison within the AUD group revealed functional deficits between 10 and precuneus which overlapped several networks including 06 (Posterior Default Mode Network), 11 (Language Network), and 13 (Precuneus Network) while excess connectivity in posterior cingulate clusters which overlapped primarily within 06 (Posterior Default Mode Network) but partially also 12 (Right Executive Control Network), parietal operculum in 12 (Right Executive Control Network) and 09 (Auditory Network), small occipital cluster in 03 (Primary Visual Network), and right hippocampal gyrus / amygdala in 07 (Mesial-Temporal Network). Neither the positive nor negative clusters showed significant correlation to any clinical severity scales or the length of abstinence at the first time point and should, thus, be considered with caution. The inter-network correlation patterns were described above and do not show a common positive or converging network trend. Other than potential overlap of decreased functional connectivity between 10 and different anatomical portions of 08 and/or 09 (in regions spanning multiple components) across both time point contrasts, there did not appear to be a consistent trend in the observed longitudinal changes in Component 10.

Component 11 (Language Network) is also a less commonly reported resting state functional network which was not functionally characterized by Smith *et al* (2009) or Laird *et al* (2011). Nonetheless, a similar language network has been reported in resting state data by other authors and is included in Dr. Greicius's 90 functional region of interest atlas (Shirer, Ryali, Rykhlevskaia, Menon, & Greicius, 2012). Hierarchically, 11 Language Network is most closely associated with 04 Anterior Default Mode Network and then with at a parallel branch with 06 Posterior Default Mode Network and 10 Visual Network – Lingual Gyrus, as illustrated in Figure 6.2. Component 11 did not substantially spatially overlap with anatomical regions reported in prototypical addiction circuits (Fein & Cardenas, 2015; Koob & Volkow, 2010).

Functional connectivity analysis of Component 11 in AUD has revealed only relatively small differences. 11 has also only seldom exhibited significant functional connectivity differences with the other networks. At the first time point, AUD group exhibited excess functional connectivity in the left temporal pole within the network itself but also overlapping with 07 (Mesial-Temporal Network) and close to boundaries of 09 (Auditory Network). At the second time point, the AUD group exhibited deficits in supramarginal gyrus / parietal lobe within the Language Network itself. Longitudinal interscan comparison within the AUD group revealed significant increase in functional connectivity with bilateral premotor cortex (Brodmann area 6) within 08 (Sensory-Motor Network) which also partially overlapped with 15 (Anterior-Salience / Insula Network). The first time point positive cluster was only significantly positively correlated to the amount of alcohol consumed prior to detoxification. The second time point negative cluster was negatively correlated with most clinical severity measures (AUDIT, ADS, OCDS, and CDS). The interscan differences were not significantly correlated to any clinical measures or the length of abstinence at the first time point. Although significant after full correction, the results of component 11 should be considered with caution due to their small cluster size and lack of clinical

correlation for the interscan cluster. Most of the differences spanned within the network itself. Inter-network correlation between 11 and 08 changed from weakly negative to marginally positive compared to stronger negative correlation in the healthy controls, suggesting a diverging pattern and in accord with the positive cluster observed in the interscan comparison. These results suggest that the pattern of resting state functional connectivity in the Language Network in AUD remains largely intact without significant compensatory recruitment from other anatomical regions. Overall, however, the Language Network has still exhibited decreased correlation with more networks than increased correlation, with mixed but still longitudinally converging trends.

Component 12 (Right Executive Control Network) is also commonly referred to as fronto-parietal network is largely a mirror image of the Component 14 Left Executive Control Network and both share high relevance to AUD due to the involvement of dorsolateral prefrontal cortex in inhibitory control which is disrupted in addiction and might undergo adaptive compensatory change in medium and long-term abstinent AUD (Fein & Cardenas, 2015; Koob & Volkow, 2010). Executive Control Networks are associated with several cognitive processes, including reasoning, attention, inhibition, memory, as well as language (Laird et al., 2011). While the right-lateralized network has been described to map stronger perception–somesthesis–pain paradigms, the left-lateralized network corresponded stronger to cognition–language paradigms (Smith et al., 2009). Hierarchically, 12 Right Executive Control Network has been most strongly associated with 14 Left Executive Control Network and then with 15 Anterior-Salience (Insula) Network, as illustrated in Figure 6.2.

At the first time point, AUD exhibited decreased functional connectivity between 12 and 08 (Sensory-Motor Network) in the premotor cortex while increased connectivity to 08 (Sensory-Motor Network) in pre/post central gyri as well as 15 (Anterior-Salience / Insula Network) in the superior frontal gyrus, and 07 (Mesial-Temporal Network) and/or 09 (Auditory Network) in an overlapping region in the right insula

/ temporal lobe. The negative cluster was not correlated to any clinical severity scales and should, thus, be interpreted with caution. The positive cluster was significantly positively correlated only with AUDIT. Inter-network correlation between 12 and 08 was negative and converging to more negative correlation in excess of the healthy controls in agreement with the negative cluster premotor results but contradictory to the positive cluster in pre/post motor gyri. Correlation between 12 and 15 was positive and converging to weaker correlation more comparable to the controls contradictory to the excess connectivity in the superior frontal cluster. Correlation between 12 and 07 was negative and remained comparable at all times with a small converging trend. Correlation between 12 and 09 was negative and weaker in AUD with only a small converging trend. Neither 07 nor 09 correlations thus advanced our understanding of the significance of the increased functional connectivity in the right insula / temporal lobe cluster.

At the second time point, AUD exhibited decreased functional connectivity between 12 and left precuneus which was located within both 14 (Left Executive Control Network) and 13 (Precuneus Network). At the same time, the AUD patients exhibited excessive functional connectivity between 12 and 15 (Anterior-Salience / Insula Network) in the anterior cingulate / paracingulate cortex but also partially overlapping within itself and 04 (Anterior Default Mode Network), potentially suggesting broader compensatory recruitment. Other significant positive clusters also included postcentral gyrus cluster which falls within 08 (Sensory-Motor Network) and also partially 13 (Precuneus Network) as well as superior lateral occipital cortex cluster which falls within 14 (Left Executive Control Network) and also 13 (Precuneus Network). Both the positive and negative clusters at the second time point were significantly correlated to the clinical severity scales, with the positive clusters being positively correlated with all measures while the negative clusters being negatively correlated only with the amount of alcohol consumed prior to detoxification and the ADS score. Moreover, the negative cluster only consisted of a modest number of voxels and should, thus, be interpreted with caution. Inter-network correlation between 12 and 14 was positive and diverging to become weaker with time compared to the controls, in agreement with the negative precuneus cluster. Correlation between 12 and 13 was also positive and diverging to

become weaker also in agreement with the negative precuneus cluster which is overlapping both anatomical extent of 14 and 13. 12 and 15 positive converging trend of weaker correlation is contradictory to the positive cluster in the anterior cingulate. 12 and 04 exhibit a converging trend from positive to negative in excess of the controls which would be also contrary to the positive anterior cingulate cluster. Correlation between 12 and 08 was negative and converging to more negative correlation in excess of the healthy controls contrary to the postcentral positive cluster. 12 and 13 correlation described above is also contrary to the changes observed in the postcentral positive cluster. The superior lateral occipital positive cluster exhibited an opposite trend to the 12 and 14 as well as 12 and 13 correlations described above.

The interscan comparison revealed decreased functional connectivity between 12 and 15 (Anterior-Salience / Insula Network) in superior frontal gyrus and increased connectivity between 12 and 15 in the middle and anterior cingulate / paracingulate gyri which partially spanned into 09 (Auditory Network) as well as increased connectivity between 12 and 08 (Sensory-Motor Network) in the precentral gyrus. None of these changes were correlated with any of the clinical severity scales or the length of abstinence at the first time point. The 12 and 15 inter-network correlation pattern described above is in agreement with the negative superior frontal cluster but contrary to the positive anterior cingulate cluster. Increased functional connectivity in the precentral positive cluster was also contrary to the inter-network correlation trends between 12 and 08 described above. In summary, only positive clusters of differences between AUD and controls at the first and second time point were correlated to clinical severity and also had larger cluster sizes to be considered interpretable. Only the functional connectivity differences with 15 and 8 appear to be at least partially consistent differences observed in our analysis of the Right Executive Control Network changes during AUD recovery.

Component 13 (Precuneus Network) is not a commonly reported resting state functional network since it anatomically overlaps with the Posterior Default Mode Network. It has been similarly to 11 also reported in Dr. Greicius's 90 functional region of interest atlas (Shirer et al., 2012). Hierarchically, 13 Precuneus Network was most closely associated with 03 and then 08 and 09, as illustrated in Figure 6.2. The visuospatial processing function related to 03 and 08 rather than self-reflection and self-consciousness functions related to 06 are thus more likely dominant in our Component 13.

At the first time point, AUD exhibited decreased functional connectivity between 13 and 09 (Auditory Network) in the right superior temporal gyrus while increased functional connectivity with 07 (Mesial-Temporal Network) and/or 09 (Auditory Network) in an overlapping region in the left temporal pole. These differences should be considered with caution since none of them was significantly correlated to any of the clinical measures. Inter-network correlations between 13 and 09 exhibited a positive converging trend of decreasing correlation in agreement with the above negative cluster. 13 and 07 exhibited a converging negative correlation of stronger negative correlation contrary to the positive cluster.

At the second time point, 13 exhibited decreased functional connectivity with 07 (Mesial-Temporal Network) close to the edge of 09 (Auditory Network) and increased functional connectivity within itself and/or possibly 14 (Left Executive Control Network) and/or possibly 12 (Right Executive Control Network) in an overlapping region in the left superior parietal lobule. The negative cluster was correlated with all clinical severity measures, except for ODS. The positive cluster exhibited significant correlation only with the amount of alcohol consumed prior to detoxification. Inter-network correlations between 13 and 07 exhibited a converging negative correlation as described above. This was in agreement with the negative cluster in AUD at the second time point. 13 and 14 exhibited negative correlation with a converging trend of strengthening correlation, in agreement with the positive cluster. 13 and 12 exhibited positive correlation with a converging trend of a weakening correlation, which was also in support of the

positive cluster. The absence of a positive cluster in the first time point contrast, however, was contrary to the converging trend observed in the inter-network correlation patterns which would suggest decreasing rather than increasing significance with time in anatomical regions associated with the observed change.

Interscan comparison within the AUD group was associated with decreased functional connectivity between 13 and a cluster in right temporal fusiform gyrus, which was located largely outside of most of the independent components but closest to 07 (Mesial-Temporal Network) and a cluster in left temporal pole, which overlapped most with 09 (Auditory Network) and also 07 (Mesial-Temporal Network). These negative longitudinal clusters were not correlated to any clinical severity measures and also constituted of only small size. As described above, inter-network correlations between 13 and 07 exhibited converging negative correlation of increasingly negative correlation, in agreement with the above results. 13 and 09 exhibited a positive converging trend of decreasing correlation which was also in agreement with the second negative cluster. The interscan negative difference in 09 substantially overlapped with the positive cluster from the first time point comparison, which supports its absence in the second contrast. Both of these differences were not correlated to AUD severity and thus might be associated with non-AUD related functional differences. Other than the changes in connectivity with 09, there did not appear to be a unified trend in the observed results for the Precuneus Network.

Component 14 (Left Executive Control Network) is largely the mirror image of Component 12 (Right Executive Control Network) which was introduced above. Although similar, some functional differences were reported between the lateralized networks, including stronger association with language and some memory tasks in the left network (Laird et al., 2011; Smith et al., 2009).

At the first time point, AUD exhibited decreased functional connectivity between 14 and 07 (Mesial-Temporal Network) in the left temporal pole. This difference was significantly correlated to the amount of

alcohol consumed prior to detoxification as well as the AUDIT score. The size of the cluster was, however, only modest and should be considered with caution. Inter-network correlation between 14 and 07 exhibited a positive converging trend of stronger correlation, in accord with the functional connectivity deficit observed at the first time point.

At the second time point, the AUD group exhibited decreased functional connectivity between 14 and 02 (Cerebellum Network) in several cerebellar clusters as well as with 10 (Visual Network – Lingual Gyrus) in the temporal fusiform cortex. At the same time, the AUD group exhibited excess functional connectivity with 03 (Primary Visual Network) in the right superior lateral occipital pole and 01 (Basal Ganglia / Deep Gray Matter Network) and/or 07 (Mesial-Temporal Network) in the brainstem. The negative clusters were significantly negatively correlated to AUDIT, ADS, OCDS, and CDS measures of clinical severity. The positive clusters were significantly positively correlated to all of the measures of clinical severity. Inter-network correlation between 14 and 02 was positive and diverging from smaller positive no correlation, in agreement with the cerebellar negative clusters. 14 and 10 exhibited weaker negative correlation with a diverging trend, which was also in agreement with the fusiform negative cluster. 14 and 03 exhibited a diverging pattern in negative correlation which changed from more negative to less negative than in the healthy controls, in accord with the positive cluster in the occipital pole. 14 and 01 as well as 14 and 07 have exhibited smaller negative correlation at the second time point compared to the controls, however, 07 exhibited converging while 01 diverging trend. The positive brainstem cluster was thus more consistent with the 01 than 07 since it was not present at the first time point.

Interscan comparison within the AUD revealed decreased functional connectivity between 14 and 12 (Right Executive Control Network) in the right frontal pole / inferior frontal gyrus. The AUD patients also exhibited increased functional connectivity at the second time point between 14 and 03 (Primary Visual Network) in the left occipital pole and 01 (Basal Ganglia / Deep Gray Matter Network) in the right thalamus. The interscan differences should be interpreted with caution since none of them were

significantly correlated to any of the clinical severity measures or the length of abstinence prior to detoxification and only included small clusters. Inter-network correlation between 14 and 12 was positive and diverging by becoming weaker than in the healthy controls, in agreement with the negative interscan cluster. 14 and 03 exhibited a diverging pattern in negative correlation which changed from more negative to less negative than in the healthy controls, in agreement with the positive interscan cluster in the left occipital pole. 14 and 01 exhibited a diverging trend of increased correlation from more negative to less negative than in the healthy controls, in agreement with the interscan positive cluster in the brainstem.

Overall, there did not appear to be a consistent trend in functional connectivity differences during the sustained recovery from AUD in the Left Executive Control Network. Both time points involved altered functional connectivity with 07 but in different directions and different anatomical regions with no interscan overlap. The pattern observed in the Left Executive Control Network (14) was also not similar or contralateral to that of the Right Executive Control Network (12) despite of the quite consistent mirror anatomical extent and partial anatomical overlap between the two functional networks. The diverging longitudinal pattern of inter-network correlation between these two components in the recovering AUD patients was also contrary to our *a priori* expectations of normalisation (converging trend) or adaptive compensation (diverging in the opposite direction) functional connectivity changes.

Component 15 (Anterior-Salience / Insula Network) is a resting state functional network which is not commonly reported in the literature and sometimes is constituted of different anatomical extent. Laird *et al* have reported that an insula network (largely consistent with our Component 15) was associated with a complex set of heterogeneous paradigms (language, executive function, affective, auditory, pain, gustatory, and interoceptive) across a great variety of tasks, suggesting this network might link cognition with emotion and interoception as a transitional intermediary (Laird et al., 2011). Component 15 was relevant to AUD due to involving insula, cingulate cortex, and also small parts of the basal ganglia

(putamen) which are all important components of addiction circuits (Koob & Volkow, 2010). Hierarchically, 15 Anterior-Salience (Insula) Network was most closely associated with 12 Right Executive Control Network and 14 Left Executive Control Network, as illustrated in Figure 6.2.

At first time point, AUD exhibited increased functional connectivity within the Anterior-Salience / Insula Network itself in the left supplementary motor area. This cluster also overlapped with 08 (Sensory-Motor Network). This positive cluster was not correlated to any clinical severity measures and consisted of only negligible cluster size and should, thus, be interpreted with great caution. Inter-network correlation between 15 and 08 exhibited weaker negative correlation at both time points with a diverging trend compared to the controls, in agreement with the positive cluster. There were no significant changes at the second time point or interscan longitudinal comparison within the AUD group. Although five of the other functional networks have reported significant clusters across eight different contrasts within the Anterior-Salience (Insula) Network, the network itself remained quite resilient in AUD and did not exhibit large-scale resting state functional connectivity differences.

Altogether, our study has revealed a rich set of complex results. The significant results did not substantially overlap between the different contrasts, even from a macroscopic network-level perspective. Concerningly, only very few of the functional differences remained consistent even within the same subjects during the repeat longitudinal scanning in reference to the same healthy control baseline (at broader network and not cluster level, including only 02, 03, 07 and 08), contrary to our *a priori* expectation. The significant differences in functional connectivity also did not appear to be reciprocal between different networks, suggesting a more complex indirect modulation between the networks. The significant clusters from all 84 contrasts have altogether spanned only 8.96% of the analysed brain space. 7.75% of the brain voxels were unique to just one contrast (not replicated), 1.21% voxels were

significantly different at least in 2 contrasts, 0.02% voxels were significant in at least 3 contrasts, and none in more than 3 contrasts.

The clusters of significant differences in the AUD group compared to the healthy controls were not uniformly distributed throughout the different functional networks. 19% of all significant voxels fell into 02 Cerebellum Network (spanning 17% of the network); 17% in 08 Sensory-Motor Network (13% of the network); 15% in 09 Auditory Network (14% of network); 11% in 15 Anterior Salience / Insula Network (spanning 12% of the network); 10% in 03 Primary Visual Network (8% of network); 9% in 07 Mesial Temporal Network (8% of network); 8% in 06 Posterior Default Mode Network (11% of network); 8% in 13 Precuneus Network (9% of network); 8% of 14 Left Executive Control Network (8% of network); 7% in 04 Anterior Default Mode Network (6% of network); 6% of 12 Right Executive Control Network (6% of network); 4% in 10 Visual Network – Lingual Gyrus (5% of network); 3% in 11 Language Network (3% of network); and 2% in 01 Basal Ganglia / Deep Gray Matter Network (3% of network). The voxels spanning overlapping significant clusters were also not uniformly distributed, falling 16% within 15 Anterior-Salience (Insula) Network; 14% within 06 Posterior Default Mode Network; 13% within 09 Auditory Network; 12% within 04 Anterior Default Mode Network; 11% within 08 Sensory-Motor Network; 7% within 02 Cerebellum Network; 7% within 12 Right Executive Control Network; 6% within 14 Left Executive Control Network; 6% within 07 Mesial-Temporal Network; 5% within 13 Precuneus Network; 1% within 01 Basal Ganglia / Deep Gray Matter Network; 1% within 11 Language Network; and 0% within both 03 Primary Visual Network and 10 Visual Network – Lingual Gyrus. The most widely affected functional networks did not exhibit the most consistent abnormal pattern of functional activation. The results should, therefore, be interpreted more conservatively when extrapolating functional or clinical significance of the observed resting state fMRI differences. The most replicably different anatomical brain regions included anterior/middle cingulate and paracingulate gyri; insula and temporal lobe; parietal operculum; supplementary motor area; and superior parietal lobule. These regions did not provide a consistent over-arching functional or anatomical insight into the functional deficits associated

with AUD and subsequent early recovery. Overall, there was a positive normalizing trend of converging inter-network correlations (similar to the normalization trends observed in functional connectivity clusters in 02, 06, or 07) but several networks exhibited increased divergence (similar to adaptive compensatory changes observed in clusters in 01 or 08), as summarized in the Graph Theory section in the Results.

Existing AUD literature has provided single time point neuroimaging evidence which has consistently reported a general global trend of hypoconnectivity and less efficient functional network organization (Sjoerds et al., 2017; Vergara et al., 2017), with some region-specific compensatory connectivity changes (Fein & Cardenas, 2015). These patterns of aberrant functional connectivity were reported both in multiple large scale networks (S. Kim et al., 2017; Müller-Oehring et al., 2015; Zhu et al., 2017) as well as specific networks such as Basal Ganglia Network (Alba-Ferrara, Müller-Oehring, Sullivan, Pfefferbaum, & Schulte, 2016; Kohno et al., 2017), Central Executive Control (Galandra et al., 2019; Kohno et al., 2017; Weiland et al., 2014), and Default Mode Network (Chanraud et al., 2011; Z. Song et al., 2020). Functional connectivity changes associated with AUD remission have not been explored beyond cross-sectional differences between medium and very long term abstinent AUD patients (reviewed by (Fein & Cardenas, 2015)) and some post-hoc exploratory analyses which have explored correlations between significant clusters or network edges and the length of abstinence, such as Chanraud *et al* (2011), who suggested an abstinence-related compensatory change between posterior cingulate and cerebellar lobules. The results of our study should thus provide additional evidence of the changes associated with early recovery from AUD which have not yet been characterised and help further elucidate the complex pattern of AUD-related functional connectivity.

Our study had several limitations, which need to be considered when interpreting our findings. The objective of our study was to characterize AUD-related functional brain plasticity during early recovery from AUD. As a result, our study was based on a very homogeneous clinical sample of all male, working

age, steady chronic alcohol dependent treatment seeking patients who were recruited within the first few days since detoxification and had no psychiatric or neurological comorbidities or history of polysubstance abuse. Similarly the matched control comparison group consisted entirely of healthy men, many of whom have voluntarily abstained from alcohol consumption for multiple years. The results of our study are thus not broadly translatable to the general population or clinical practice, which includes patients of both sexes with various levels of AUD and with frequent complex psychiatric and somatic comorbidities. Our results also cannot conclusively explain the cause of the observed aberrant functional connectivity since it only observed group differences especially at the first time point. A growing body of evidence suggests structural and functional abnormalities in individuals with family history of AUD (Acheson, Robinson, Glahn, Lovallo, & Fox, 2009; Andrews et al., 2011; Cservenka, Herting, & Nagel, 2012; Herting, Schwartz, Mitchell, & Nagel, 2010; Kareken et al., 2010; Mackiewicz Seghete, Cservenka, Herting, & Nagel, 2013; Meyerhoff et al., 2004; A. D. Schweinsburg et al., 2004; Spadoni, Norman, Schweinsburg, & Tapert, 2008). A family history of AUD can not only predispose individuals to higher likelihood of developing AUD but also exhibit similar neuroimaging deficits (including aberrant bottom-up reward and top-down executive functional connectivity) even in absence of addiction or excessive alcohol exposure. Future studies should consider evaluating family history loading to isolate the effect of AUD, especially when considering brain changes associated with successful remission. Our analysis also did not differentiate between AUD-related changes due to repeat neurotoxic ethanol exposure (in both the brain and the body) and maladaptive plasticity due to the reinforced addiction behaviour. We have conducted exploratory post-hoc correlation to the average amount of alcohol consumed per day prior to detoxification but not to lifetime alcohol consumption (since we were unable to reliably collect this information from our participants). Our exclusion criteria also included any neurological disorders (including those due to nutritional or neurotoxic deficits due to chronic AUD, such as Wernicke-Korsakoff syndrome). Despite of the homogeneous clinical profile, our study suffered from several nuisance variable shortcomings, including broad age range (23 to 64) and multi-site/scanner study design. These were both included in the statistical models but the additional variability could have masked more

subtle underlying functional changes due to modest signal-to-noise ratio inherent in the resting-state fMRI data (resting state fluctuations were originally considered as background noise and still are in task-based paradigms). ICA also has several limitations, including its data-driven functional network decomposition, which will vary in different studies due to data variability as well as different dimensionalities of ICA. This might impact the translatability and comparability of our results to the literature. Moreover, although functional connectivity differences have been traditionally considered as robust and reliable, diverging evidence suggesting poor reliability of functional connectivity has been emerging in the recent past (Noble et al., 2019). The poor reliability reported in this meta-analysis could help contextualize the limited overlap in the functional connectivity differences observed in our longitudinal results. Lastly, it is important to be mindful that fMRI is an indirect (but very well and consistently replicated) measure of neuronal activity and resting state functional connectivity is also an indirect measure of structural connectivity (Logothetis et al., 2001; van den Heuvel & Hulshoff Pol, 2010). Significant results in a functional connectivity contrast can thus represent a diverse direct as well as indirect excitatory as well as inhibitory changes in functional and structural networks and should be interpreted with caution (Logothetis, 2008). The lack of reciprocity in the functional differences across the different functional networks in our study points to the complex, indirect modulation underlying these functional dynamics.

Future studies should aim to collect additional evidence of longitudinal differences to more conclusively characterize functional brain changes associated with AUD recovery. To expand on our findings, future studies should aim to recruit larger sample sizes with more uniform demographic cohorts (for example in age) and more and longer interscan intervals. The approximately 2 week interscan interval in our study detected only marginal overlapping results (for example in 02, 03, 07, and 08) and did not reveal consistent functional connectivity trends across the different networks. This could be potentially explained due to potentially too short follow-up interscan interval for sufficient functional plasticity to take place and/or due to underestimating the initial AUD-related functional due to not recruiting participants until approximately 17 days after detoxification. Future studies should also aspire to include

multiple scanning time points for their healthy controls to better account for natural interscan variability in their results (performing [A2-A1]-[C2-C1] contrast rather than just [A2-A1]). Moreover, inclusion of a neurocognitive test battery could help future studies more conclusively characterize the functional significance of their results beyond speculation of extrapolated anatomical function reported in the literature.

5 Conclusion

In summary, our study has revealed significant functional connectivity changes spanning approximately 9% of the voxels across approximately 65% of the contrasts. The functional connectivity results were generally inconsistent both between networks and longitudinally within the same networks. Even at a macroscopic level of functional networks, there was only little overlap in the functional dynamics. Most of the functional connectivity changes spanned 02 (Cerebellum Network), 08 (Sensory-Motor Network), and 09 (Auditory Network) while the least commonly affected were 01 (Basal Ganglia / Deep Gray Matter Network), 11 (Language Network), and 10 (Visual Network – Lingual Gyrus). The networks with the most overlapping changes were different and included 15 (Anterior-Salience / Insula Network), 06 (Posterior Default Mode Network), 09 (Auditory Network). Even though some networks such as 02 (Cerebellum Network), 15 (Anterior-Salience / Insula Network) and 11 (Language Network) were associated with aberrant connectivity changes in other functional networks, their own functional connectivity pattern remained quite resilient and restricted primarily to internal within network differences. Analysis of the network properties of the different functional networks has revealed a normalisation trend of strengthening inter-network communication with prolonged abstinence in the recovering AUD patients, especially in 12 (Right Executive Control Network), 07 (Mesial-Temporal Network), and 06 (Posterior Default Mode Network). Some networks also exhibited a diverging pattern, potentially indicating an adaptive compensation trend, however, these included mostly functional

networks not prototypically associated with addictions, such as 03 (Primary Visual Network), 08 (Sensory-Motor Network), and 11 (Language Network). Approximately 62% of the significant changes were correlated with at least one AUD severity measure while 36% were correlated with three or more, highlighting the clinical significance of our results. All together, these findings suggest a pattern of global hypoconnectivity in the AUD with an encouraging pattern of converging functional connectivity across the plurality of the networks. The results should, nonetheless, be considered with caution due to limited spatial and longitudinal reproducibility of the significant clusters. To the best of our knowledge, this was the first longitudinal study which explored resting state functional connectivity changes in recovering AUD patients and also one of very few studies to holistically analyze AUD-related functional connectivity changes across functional networks spanning the entire brain.

Chapter 7 - Deep Grey Matter Iron Accumulation in Alcohol Use Disorder

Abstract

The purpose of this study was to evaluate brain iron accumulation in alcohol use disorder (AUD) patients compared to controls using quantitative susceptibility mapping (QSM). QSM was performed retrospectively by using phase images from resting state functional magnetic resonance imaging (fMRI). 20 male AUD patients and 15 matched healthy controls were examined. Susceptibility values were manually traced in deep grey matter regions including caudate nucleus, combined putamen and globus pallidus, combined substantia nigra and red nucleus, dentate nucleus, and a reference white matter region in the internal capsule. Average susceptibility values from each region were compared between the patients and controls. The relationship between age and susceptibility was also explored. The AUD group exhibited increased susceptibility in caudate nucleus (+8.5%, p=0.034), combined putamen and globus pallidus (+10.8%, p=0.006), and dentate nucleus (+14.9%, p=0.022). Susceptibility increased with age in two of the four measured regions - combined putamen and globus pallidus (p=0.013) and combined substantia nigra and red nucleus (p=0.041). AUD did not significantly modulate the rate of susceptibility increase with age in our data. Retrospective QSM computed from standard fMRI datasets provides new opportunities for brain iron studies in psychiatry. Substantially elevated brain iron was found in AUD subjects in the basal ganglia and dentate nucleus. This was the first human AUD brain iron study and the first retrospective clinical fMRI QSM study.

Key terms

brain iron, alcohol use disorder, quantitative susceptibility mapping, deep grey matter, echo-planar imaging, resting state fMRI

1. Introduction

Alcohol use disorder (AUD) is a chronic relapsing disease characterized by recurrent compulsive alcohol abuse despite significant alcohol-related behavioural, cognitive, physiological, and social problems (American Psychiatric Association, 2013). AUD can be considered the world's biggest addiction problem. Harmful use of alcohol is estimated to lead to 5.9% of all deaths, 5.1% of the global burden of disease, and has been demonstrated to have a causal relationship with over 200 adverse health conditions (World Health Organization, 2014). This makes AUD one of the most damaging preventable causes of illness in the world. When considering the total harm of AUD including its societal costs, alcohol is by a wide margin the most harmful drug in the western world (Nutt et al., 2010). Neurobiological mechanisms driving adaptive changes during alcohol abuse and subsequent recovery are not fully understood and continue to be of scientific interest (Fein & Cardenas, 2015; Seo & Sinha, 2015). Previous evidence suggests that chronic alcohol abuse can lead to abnormally high systemic iron levels (Duane, Raja, Simpson, & Peters, 1992; Y. Kohgo et al., 2005; Milman & Kirchhoff, 1996; Whitfield, Zhu, Heath, Powell, & Martin, 2001) which might be associated with increased brain iron concentration (Nordmann, Ribiere, & Rouach, 1987; Rouach, Houze, Gentil, Orfanelli, & Nordmann, 1994, 1997; Rouach et al., 1990). A wide range of neural disorders is associated with brain iron abnormalities (Zecca, Youdim, Riederer, Connor, & Crichton, 2004), thus increased brain iron may contribute to commonly observed brain damage and atrophy in AUD.

Quantitative susceptibility mapping (QSM) is an emerging magnetic resonance imaging (MRI) technique developed for quantifying tissue magnetic susceptibility (Haacke et al., 2015; C. Liu, Li, Tong, Yeom, & Kuzminski, 2015; Y. Wang & Liu, 2015). QSM can be used to measure iron content in deep grey matter brain structures and has been extensively validated to be able to identify altered deep grey matter iron in normal aging as well as many neurological disorders (Bartzokis et al., 1999; Bilgic, Pfefferbaum, Rohlfing, Sullivan, & Adalsteinsson, 2012; Haacke et al., 2015; Li et al., 2014; C. Liu et al.,

2015; Stuber, Pitt, & Wang, 2016). Our team has recently developed a means to extract QSM from previously acquired echo planar imaging (EPI) scans (Sun & Wilman, 2015), as well as traditional functional MRI (fMRI) studies (Sun, Seres, & Wilman, 2016). Provided the phase or raw signal is available, this method enables retrospective examination of brain iron from existing fMRI studies. Here, using an existing AUD resting state fMRI dataset, we applied this unique QSM method to examine brain iron deposition in clinical cases with AUD to test the hypothesis whether AUD is associated with increased deep grey matter iron concentration. To the best of our knowledge this is the first AUD QSM study and the first clinical study to use retrospective QSM from functional MRI. Our findings provide important technological advances in MRI application that allow examination of novel aspects of brain tissue alterations, and may be useful for developing highly needed biomarkers for neurological and psychiatric disorders at various stages of progression and treatment.

2. Materials and Methods

2.1 Subjects

Twenty recently detoxified male alcohol dependent patients (DSM-IV-TR criteria) (American Psychiatric Association, 2000) and 15 matched healthy non-alcohol abusing men were recruited for the AUD and control groups, respectively. The DSM-IV-TR diagnostic investigations were carried out by a psychiatrist, using the Structured Clinical Interview for the DSM-IV-TR (SCID-I) (First et al., 2002). The demographic and clinical overview of the participants is summarized in Table 7.1. The alcohol dependent participants were recruited from a pool of patients referred to a supervised residential treatment program from all addiction treatment facilities in the Edmonton area between 2012 and 2015 as part of the international TRANSALC project. The patients were consistent, steady, heavy drinkers (mean duration of alcohol dependence of 16.0+/-2.7 years, standard error of mean). All of the patients met the highest Zone IV cut-off score on the Alcohol Use Disorders Identification Test (AUDIT) with the average score of 30

out of 40 (Saunders et al., 1993). The AUD patients exhibited on average a substantial level of alcohol dependence (third quartile) according to the Alcohol Dependence Scale (ADS) with the average score of 25.5 out of 47 (Skinner & Allen, 1982). The patients did not abuse non-beverage ethanol or other substances except nicotine. The patients were recruited between 6 to 12 days of abstinence. Abstinence at the time of scanning was verified in all participants by an alcohol breathalyser (BACtrack S50 Personal Breathalyzer, Portable Breath Alcohol Tester) and a urine drug screen (nal von minden GmbH Drug-Screen® Diptest, Version 1.0). The patients were not provided with any prescription medications including adjuvant pharmacotherapy for prevention of relapse such as Naltrexone or Disulfiram during this time. Controls were recruited concurrently to match the patients' general demographic profile (including sex, age, handedness, general occupation/education background). The controls had no history of alcohol or drug addiction and consumed alcohol below the Canada's Low-Risk Alcohol Drinking Guidelines (Butt, 2011). Participants in both arms were excluded if they had any history of serious medical (including psychiatric or neurological) complications, brain injury, use of psychotropic medications (other than during the detoxification process), or did not meet magnetic resonance safety criteria for our imaging facility. The study was approved by the University of Alberta Health Research Ethics Board (study ID: Pro00019424).

Table 7.1: Demographic and Clinical Profile of Subjects

	AUD Patients (n=20)				Controls (n=15)				
	$\bar{x}$	SEM†	Min	Max	$\bar{x}$	SEM†	Min	Max	p-value
Age	43.05	2.38	23.98	60.88	44.61	2.72	29.79	58.60	0.667
Years of Education	12.85	0.55	9.00	18.00	12.13	0.48	9.00	16.00	0.351
Edinburgh Handedness Inventory (Oldfield, 1971)	0.56	0.15	0.00	1.00	0.43	0.13	0.09	1.00	0.516
AUDIT[o] Score (Saunders et al., 1993)	30.00	1.03	20.00	37.00	1.67	0.36	0.00	6.00	0.000*
ADS[1] Score (Skinner & Allen, 1982)	25.50	1.95	6.00	38.00	0.87	0.32	0.00	4.00	0.000*
Standard Drinks per Day[2]	21.72	2.50	9.88	54.89	0.22	0.06	0.00	0.81	0.000*
Days of Abstinence	9.11	0.46	6.00	12.00	N/A	N/A	N/A	N/A	N/A

[o] Alcohol Use Disorders Identification Test
[1] Alcohol Dependence Scale
[2] Canadian standard drink constitutes of 17.24 mL or 13.6g of ethanol.

† Standard Error of Mean
* Significant at *a priori* α level of P<0.05.

2.2 MRI Acquisition

Neuroimaging data were acquired using 4.7 Tesla Varian Inova whole-body MRI scanner, located at the University of Alberta. The scanning protocol included anatomic imaging using T1-weighted magnetization-prepared rapid acquisition echo (MPRAGE) and resting state functional MRI (rs-fMRI) using single-shot, T2*-weighted echo planar imaging (EPI). During rs-fMRI participants were asked to remain still, close their eyes, not fall asleep, and not to think of anything in particular. The acquisition parameters for MPRAGE were: TR 1505.9 ms, inversion time 300.0 ms, relaxation delay time (after readout prior to inversion) 300.0 ms, linear phase encoding, TE 3.71 ms, matrix 240×192×128, field of view 240×192×192 mm^3, 1.0×1.0×1.5 mm^3 voxels, whole brain coverage. The acquisition parameters for EPI were: TR 1500 ms, TE 19 ms, matrix 72×68×36, field of view 216×204×126 mm^3, 3×3×3.5 mm^3 voxels, whole brain coverage, and with 320 volumes.

The anatomical scans were visually reviewed by two independent neuroimaging experts for gross abnormalities. None of the subjects exhibited any clinically significant structural abnormalities other than what may be expected from normal aging or prolonged alcohol abuse.

2.3 Quantitative Susceptibility Mapping (QSM)

The quantitative susceptibility maps were generated retrospectively from the phase component of the raw resting-state fMRI signal to test feasibility of the method previously described by Sun *et al.* (Sun et al., 2016; Sun & Wilman, 2015). Briefly, the multi-channel complex phase signal was combined using an adaptive method (Walsh, Gmitro, & Marcellin, 2000). Brain volume mask was generated using Brain Extraction Tool of FMRIB software library (FSL) (Smith, 2002). Phase images were unwrapped using the Phase Region Expanding Labeller for Unwrapping Discrete Estimates (PRELUDE) in FSL (Jenkinson,

2003). Slowly varying dominant background phase due to air-tissue interfaces or imperfect shimming was removed using the Regularization Enabled Sophisticated Harmonic Artifact Reduction for Phase data (RESHARP) method (Sun & Wilman, 2014). The field map was normalized by the main magnetic field strength to parts-per-million (ppm). Dipole fields were inversed using a total variation technique (Wu, Li, Guidon, & Liu, 2012) with regularization in the L1-norm form of derivatives cost function, yielding QSM images (Sun & Wilman, 2015). Magnitude rs-fMRI images were then motion corrected using rigid-body transformation using FMRIB's Linear Registration Tool (FLIRT) (Jenkinson & Smith, 2001). The same transformation matrix was applied to matching QSM images with tri-linear interpolation. Re-aligned 320 QSM volumes for each subject's scanning session were averaged to minimize noise, resulting in one QSM three-dimensional volume for each original four-dimensional reconstructed raw rs-fMRI file. Although our study was conducted at a high field of 4.7 Tesla and signal to noise ratio improves with field strength, the susceptibility contrast is field independent and EPI-QSM has been validated at 1.5 Tesla (Sun & Wilman, 2015). Therefore, provided that the raw phase images are saved, this technique should work on EPI from standard clinical systems.

2.4 Data Analysis

The analysis protocol consisted of data anonymization, map normalization, manual tracing, and statistical comparison. The data were inspected visually for quality assurance purposes at each step of the analysis.

First, the data were anonymized to blind the researcher from the subjects' alcoholic/control status using a randomly assigned numbered code. The key was withheld from the researcher until completion of region of interest tracing and quality assurance.

Second, the anonymized files were normalized to the MNI-152 template using the standard FLIRT protocol with an anatomical image intermediate to help guide the transformation matrix for the rs-fMRI

magnitude image (Greve & Fischl, 2009; Jenkinson, Bannister, Brady, & Smith, 2002). The same transformation matrix was subsequently applied to the QSM maps derived from the identical EPI rs-fMRI signal.

Third, the normalized subject-specific QSM volumes were all averaged to create a QSM group template. Manual tracing of all regions of interest was then completed on this template. The *a priori* regions of interest included caudate nucleus, putamen, globus pallidus, internal capsule, thalamus, red nucleus, substantia nigra, and the dentate nucleus. Except for the internal capsule, all of these brain regions are known to contain a high concentration of protein-bound ferric iron (Hallgren & Sourander, 1958; Sun et al., 2015). Due to the modest resolution of our resting state fMRI images ($3\times3\times3.5$ mm^3), we could not clearly discern the boundaries of some of the *a priori* regions of interest in our dataset. As a result, thalamus was excluded from the analysis and two sets of regions of interest - the putamen / globus pallidus; substantia nigra / red nucleus - were included each as a single, combined region. Manual tracing was, therefore, done to delineate the caudate nucleus; the combined putamen and globus pallidus region; combined region including substantia nigra and red nucleus (most likely including also part of the subthalamic nucleus located between these two regions); the dentate nucleus; and the internal capsule (as the background signal reference), in both left and right hemispheres. Ventral striatum (i.e. nucleus accumbens) and ventral tegmental area, which belong to the basal ganglia and are of high research interest in AUD, could not be confidently traced in our data due to their unclear anatomical boundaries on the QSM images alone. Once the reference set of 3-D traces was completed on the averaged QSM mask in FSL-VIEW, region of interest (ROI) masks were manually modified to fit each subject's specific anatomy, creating subject-specific manual ROI masks within the same reference boundary space. Figure 7.1 illustrates the traced regions from a representative 43-year-old subject. The average intensity values from each of these subject-specific ROI masks were extracted and tabulated for statistical analysis.

The fourth step was ROI signal intensity analysis. Mean ROI susceptibility values for each subject were normalized by subtracting the average background white matter intensity of the internal capsule ROI. This subtraction standardized the results since susceptibility from dipole inversion is a relative as opposed to an absolute measure (Sun & Wilman, 2015). The data were subsequently de-anonymized and split into patient and control groups for comparison. The literature indicates that both systemic and brain iron levels increase with heavy alcohol exposure (Duane et al., 1992; Y. Kohgo et al., 2005; Milman & Kirchhoff, 1996; Nordmann et al., 1987; Robinson, Godfrey, Denne, & Cox, 1998; Rouach et al., 1994; Rouach, Houze, et al., 1997; Rouach et al., 1990; Skikne, Flowers, & Cook, 1990; Whitfield et al., 2001). Therefore, our *a priori* hypothesis was that we would observe increased iron concentration in the AUD patients in all of the traced areas of interest. To test this hypothesis for each region, we conducted Levene's test of homogeneity and subsequently a one-tailed t-test testing the significance of the increases in the mean QSM intensity in the different regions for patients *versus* controls. False discovery rate (FDR) correction was used to correct for multiple comparisons across the four brain regions (Benjamini & Hochberg, 1995).

We also conducted a secondary comparison of QSM intensity to participant age in an attempt to try to replicate a weak positive trend between age and brain iron accumulation published about working-age adults in the literature (Acosta-Cabronero, Betts, Cardenas-Blanco, Yang, & Nestor, 2016; Bilgic et al., 2012; Hallgren & Sourander, 1958). For each of the four anatomical regions (caudate nucleus, putamen/globus pallidus, red nucleus/substantia nigra, dentate nucleus), a general linear model analysis was done, including predictors for group status (patient *vs.* control) as well as age (modelled separately for patients and controls). Two-tailed t-tests were conducted to test the relationship between age and susceptibility for patients *vs.* controls (*i.e.* slope of age regressed against susceptibility for patients *vs.* controls) as well as the relationship between age and susceptibility independent of group status. These tests were done for illustration purposes only. Based on the literature, we were aiming to replicate a small positive relationship between age and QSM, and this particular comparison was not part of the primary

investigation of the study. Therefore, tests of the relationship between age and QSM scores were not corrected for multiple comparisons.

Figure 7.1: Representative Region-of-Interest Traces

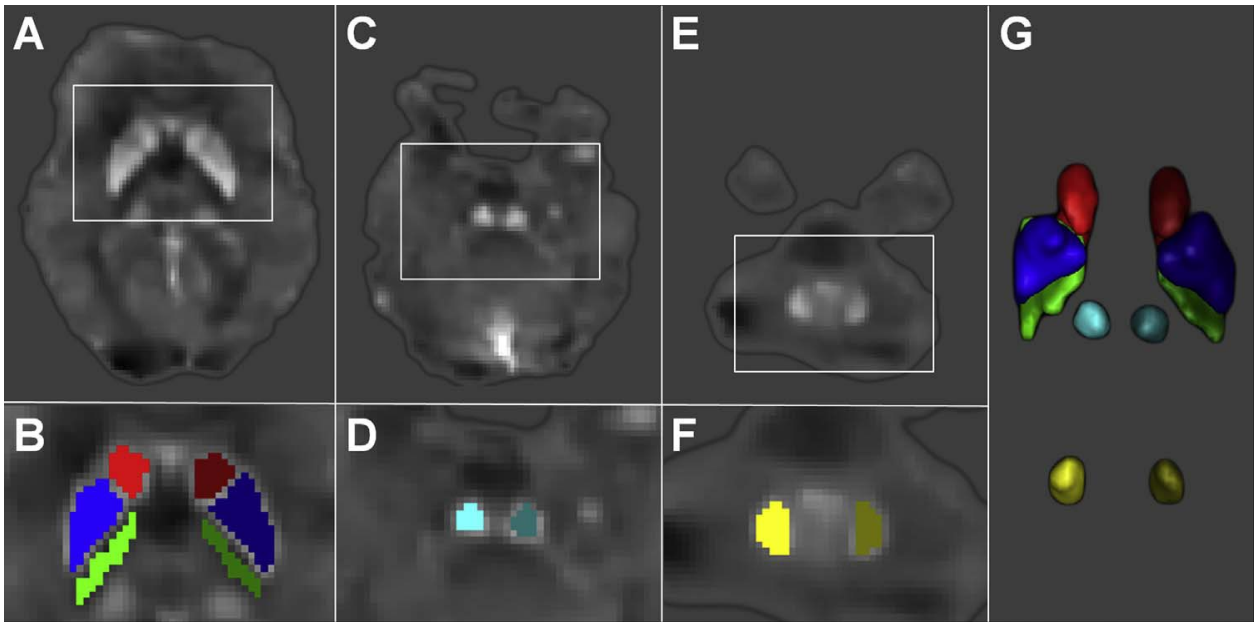

Panes A, C and E depict axial slices of a representative averaged EPI-QSM contrast in fMRI of a 43-year old male thresholded at -0.10 to 0.20 ppm in standard MNI space. Panes B, D, and F depict corresponding traces on the above slices. Pane G depicts a rendering of the three-dimensional manual traces in this subject. Caudate nucleus region of interest is red; putamen & globus pallidus is blue; substantia nigra and red nucleus is in cyan, dentate nucleus is in yellow. The white matter signal reference region of internal capsule is green

3. Results

The alcohol-dependent subjects exhibited an apparently consistent increase in all of the tested deep grey matter regions - although only the differences in caudate nucleus, combined putamen / globus pallidus, and dentate nucleus were significant. This evidence of increased QSM intensity in deep grey matter brain regions, suggesting increased iron deposition, supported our *a priori* hypothesis. The increase ranged from 7% to 15%. Figure 7.2 depicts the average bilateral susceptibility values with standard errors of mean. Table 7.2 summarizes the quantitative values, including significance. The putamen / globus pallidus combined region showed the highest susceptibility in both controls and patients, the largest

absolute AUD increase, and the most significant group difference. Contrary to our expectations, the largest relative difference was not seen in the putamen / globus pallidus but was observed in the dentate nucleus, which is a deep cerebellar cluster of neurons involved primarily in the movement of skeletal muscles.

As part of our quality assurance, the reference signal from the internal capsule white matter ROI was compared between controls and patients, and there was no statistically significant difference. This observation suggests that the internal capsule provided a set of reasonable reference values for standardizing the results of our analysis.

Table 7.2: Average AUD-related group differences in QSM intensity

Anatomical Area	AUD Patients (n=20)				Controls (n=15)				Difference		p-value
	$\bar{x}$	SEM†	Min	Max	$\bar{x}$	SEM†	Min	Max			
Caudate Nucleus	0.096	0.003	0.076	0.115	0.089	0.003	0.072	0.115	0.007	8.52%	0.034*
Putamen / Globus Pallidus	0.142	0.003	0.123	0.173	0.128	0.004	0.101	0.154	0.014	10.85%	0.006*
Substantia Nigra / Red Nucleus	0.117	0.004	0.082	0.146	0.109	0.004	0.084	0.143	0.008	7.06%	0.101
Dentate Nucleus	0.096	0.004	0.075	0.124	0.084	0.005	0.059	0.118	0.012	14.92%	0.022*

† Standard Error of Mean

***** Significant at *a priori* α level of P<0.05, FDR corrected.

Figure 7.2: Bilateral AUD-Related Quantitative Susceptibility Differences

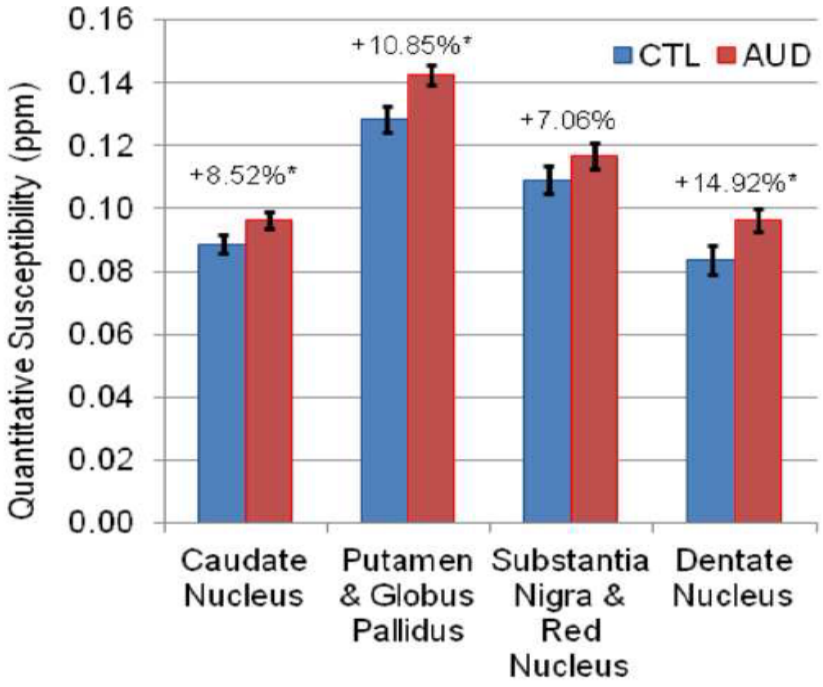

* Significant at *a priori* α level of 0.05. AUD=alcohol dependent patients; CTL=healthy controls

As part of our post-hoc secondary analysis, our general linear model comparison revealed a positive trend between the susceptibility of each of the grey matter regions of interest and the age of the subjects, independent of group status (patient *vs.* control). The relationship of age to QSM scores was significant in putamen / globus pallidus (p=0.013) and red nucleus / substantia nigra (p=0.041). The relationship was not significant in caudate nucleus (p=0.583) or dentate nucleus (p=0.085). The putamen / globus pallidus region showed the greatest separation of values and also the steepest age-related increase in susceptibility as illustrated in Figure 7.3.

Although we observed significant group differences in susceptibility in three of the four measured regions, testing whether susceptibility increased at a different rate with age in the AUD patients compared to the controls did not yield statistically significant results (two-tailed t-tests: caudate nucleus p=0.966; putamen / globus pallidus p=0.360; red nucleus / substantia nigra p=0.631; dentate nucleus p=0.746). Our

data, therefore, does not suggest age-related interaction in iron accumulation exacerbation in working-age alcohol-dependent adults.

Figure 7.3: Quantitative Susceptibility Increases with Age in Both Patients and Controls

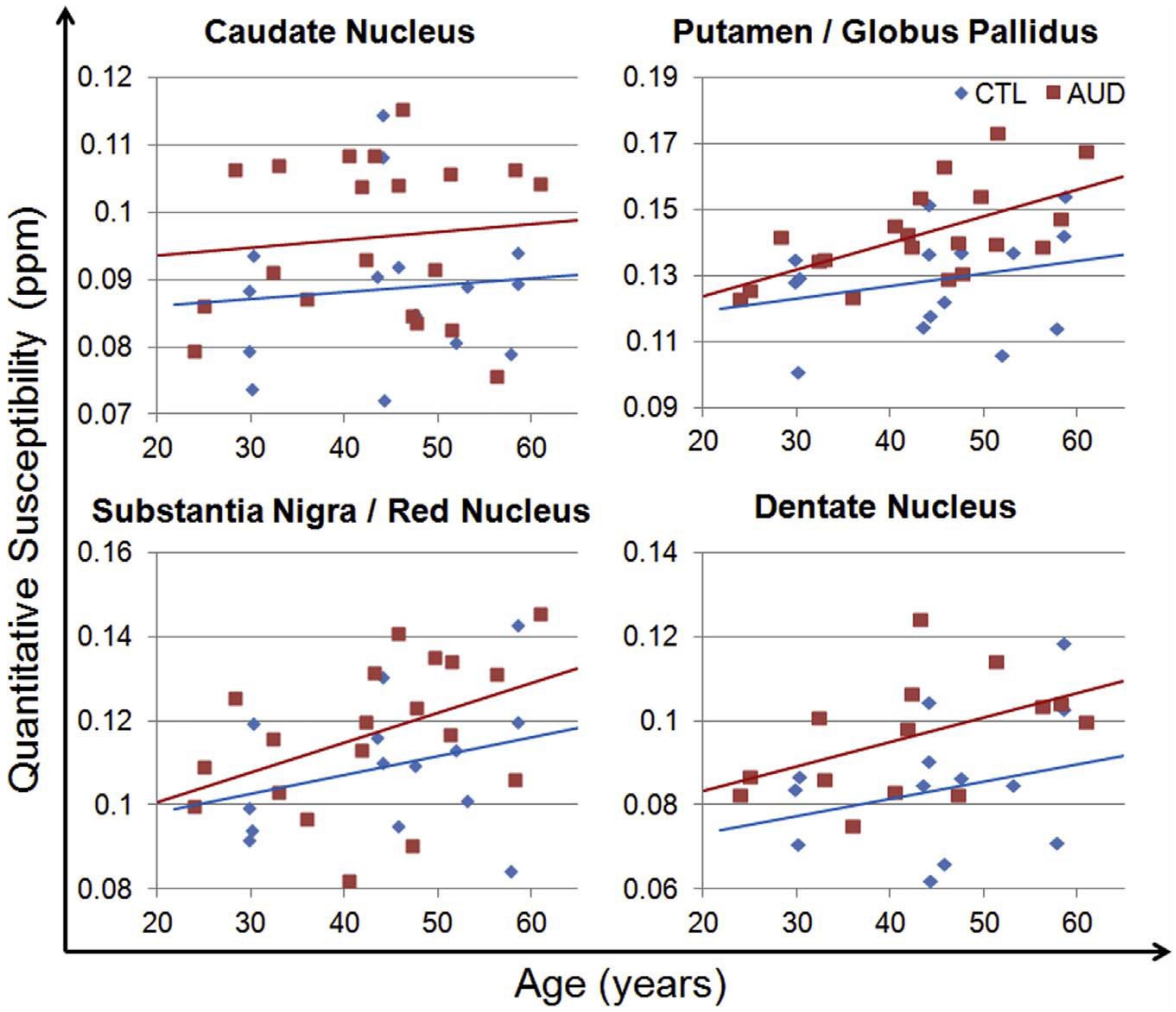

4. Discussion

Iron is an essential mineral that is vitally important for normal human development and physiological functions (Ganz, 2013; Radlowski & Johnson, 2013). Iron requirements in brain are high due to its high metabolic rate as well as many specialized functions requiring iron as an enzymatic co-factor, including catecholamine synthesis and myelination (Beard & Connor, 2003; Connor & Menzies, 1996; Finney &

O'Halloran, 2003; Hallgren & Sourander, 1958; Todorich, Pasquini, Garcia, Paez, & Connor, 2009; Wong-Riley, 1989). Chemical properties which make iron an essential mineral can also make it very harmful due to the tendency of iron ions to catalyze creation of reactive oxygen and nitrogen species. Iron is, therefore, very tightly controlled *in vivo* and usually sequestered in protein-bound forms for storage (ferritin and hemosiderin) or transport (transferrin). Ferritin-bound stored iron is the primary source of the QSM contrast (Hallgren & Sourander, 1958; Langkammer et al., 2012; Sun et al., 2015). Tight mechanisms for *in vivo* sequestration/control of iron are also important for avoiding systemic iron overload (such as in hereditary hemochromatosis) because there are no known active mechanisms for systemic iron elimination (Hunt, Zito, & Johnson, 2009; Yutaka Kohgo, Ikuta, Ohtake, Torimoto, & Kato, 2008).

Because the blood-brain-barrier normally prevents passive passage of hydrophilic transferrin, the brain is dependent primarily on transferrin receptor-mediated transport of iron (unique in the brain luminal capillary endothelial cells) and forms its own local brain iron pool which is protected from systemic iron fluctuations (T. Moos, 2002; T. Moos, Rosengren Nielsen, Skjorringe, & Morgan, 2007). The distribution of iron in the brain is heterogeneous, primarily localized in deep grey matter basal ganglia - where it can reach concentrations as high as those occurring in the liver (N. Singh et al., 2014) which is the body's primary iron storage site. Brain iron concentrations increase with age (Bilgic et al., 2012; Gelman et al., 1999; Hallgren & Sourander, 1958; Zecca et al., 2004). Both the heterogeneous accumulation of brain iron as well as its increase with normal aging are still not fully understood and remain an active area of research (Koeppen, 2003). Several hypotheses propose that the deep grey matter of brain might serve as a central nervous system iron reservoir (similar to the liver for the whole body) or be involved in white matter myelination (Connor & Menzies, 1996; Rouault, 2013). As with systemic iron, there is only very limited brain iron export or elimination. Some data hint at the presence of a limited export mechanism (T. Moos et al., 2007) most likely via cerebrospinal fluid transferrin-mediated return of iron into subarachnoid circulation (T. Moos & Morgan, 1998) or physical removal by macrophages during severe

inflammation (Hua et al., 2006; T. Moos et al., 2007). Nonetheless, current evidence suggests that once non-heme iron has entered the brain, it largely remains there.

There is a growing body of evidence associating a wide range of disorders with brain iron abnormalities, including: Alzheimer's disease, Parkinson's disease, multiple sclerosis, congenital aceruloplasminemia, Friedreich's ataxia, neuroferritinopathy, neurodegeneration with brain iron accumulation, amyotrophic lateral sclerosis, and restless leg syndrome (Zecca et al., 2004). Most of these disorders are associated with excess iron accumulation. It is of interest that several of these disorders share similar features to chronic alcohol abuse such as motor and/or memory deficits, altered dopamine signalling, and immune system dysfunction. It is possible to draw on existing related alcohol abuse literature and parallels to other disorders to try to explain the abnormally high concentration of iron in our alcohol dependent patients. We propose three possible explanations which alone or in combination could explain our findings. These include: 1) systemic iron overload, 2) excess dopaminergic activity, and 3) tissue damage associated with inflammation and leaky brain.

4.1 Systemic iron overload in AUD

Alcohol abuse is associated with increased uncontrolled intestinal iron absorption (Duane et al., 1992), increased iron in alcohol-damaged liver (Y. Kohgo et al., 2005), and related abnormal hepcidin signalling (Y. Kohgo et al., 2005; Y. Kohgo et al., 2008), which could all contribute to systemic iron overload that is well documented in 20-30% of alcohol abusers (Duane et al., 1992; Whitfield et al., 2001). Population-based studies suggest that even social drinking of a moderate amount of alcohol (2-3 drinks per day) is associated with increased indirect measures of iron stores which can be considered as acceptable markers of overall body iron stores (Milman & Kirchhoff, 1996; Robinson et al., 1998; Skikne et al., 1990; Whitfield et al., 2001). Studies of both acute and chronic alcohol exposure in animal models of alcohol abuse also report systemic iron overload, further reporting associated increases in brain iron accumulation

(Nordmann et al., 1987; Rouach, Fataccioli, et al., 1997; Rouach et al., 1994; Rouach et al., 1990). Consequently, the evidence for systemic iron overload in AUD humans may be related to our novel *in vivo* finding of increased brain iron. Excess alcohol-related systemic iron could overload normal iron metabolism which lacks any mechanisms for substantial elimination of excess iron from the body or the brain, thus causing abnormal brain iron accumulation in AUD patients.

The increased iron stores in the brain combined with alcohol's suppression of antioxidant defences (such as levels of α-tocopherol, glutathione, and cytosolic superoxide dismutase) could potentially lead to increased reactive oxygen and nitrogen species which could contribute to the increased lipid peroxidation and cellular damage observed in animal models (Nordmann et al., 1987; Nordmann, Ribiere, & Rouach, 1990; Rouach et al., 1994). Iron chelating agents in animal AUD models have minimized the alcohol's oxidative brain damage (Bondy & Orozco, 1994). This evidence could potentially implicate iron in the etiology of alcohol-related structural atrophy and functional deficiencies commonly associated with AUD (for an overview of AUD brain pathology, refer to Harper *et al.*, 2003) (Harper et al., 2003). Oxidative damage (Crews & Nixon, 2009) is often offered as the most plausible explanation of alcohol-abuse-related brain damage, particularly of white matter which is most vulnerable to chronic alcohol abuse. The high metabolic need of the brain combined with a large amount of easily oxidizable substrates (such as polyunsaturated fats and catecholamines) and low activity of some of the cellular antioxidant protective mechanisms might contribute to such a high vulnerability (Nordmann et al., 1990). Iron-mediated oxidative damage has been already implicated as a key factor associated with alcohol-related liver damage (Y. Kohgo et al., 2005). Alcohol-related liver damage could also impede proper iron regulation and signalling (Y. Kohgo et al., 2005; Y. Kohgo et al., 2008). A recent susceptibility-weighted brain imaging study of severely cirrhotic patients (primarily from hepatic cirrhosis) reported increased iron accumulation in brain structures which was correlated to cognitive deficiencies (S. Xia et al., 2015).

Although most human and animal evidence supports our assertion of excess alcohol-related systemic and brain accumulation, two rat studies indicate no significant changes or mixed evidence (Jurczuk, Brzoska, Rogalska, & Moniuszko-Jakoniuk, 2003; J. Xia, Simonyi, & Sun, 1999). One rabbit study also claimed folic acid dietary deficiency rather than alcohol as a potential cause of AUD-related excess iron accumulation (Celada, Rudolf, & Donath, 1979).

4.2 Excess aggregate dopaminergic activity in AUD

AUD is associated with excessive activation of dopamine signalling pathways during acute intoxication and cue exposure (Boileau et al., 2003; Nora D. Volkow, Wang, Fowler, Tomasi, & Telang, 2011). Acute ingestion of alcohol results in substantially higher dopamine surge compared to natural rewards or baseline conditions (G Di Chiara & Imperato, 1988). Increased dopamine activity is also observed in protracted abstinence after chronic alcohol exposure (Hirth et al., 2016). Thus, AUD patients have experienced aggregate excess dopaminergic activity despite a transient down-regulation and resultant hypodopaminergic milieu during acute withdrawal from alcohol (Heinz et al., 1996; Koob & Volkow, 2010; Rossetti, Melis, Carboni, & Gessa, 1992). Iron is an important co-factor in the rate-limiting step of dopamine synthesis, and there is an emerging body of evidence associating dopamine signalling and brain iron accumulation which could potentially link excessive dopamine signalling in AUD to abnormally high brain iron concentrations.

Excess dopamine signalling, as observed for example in methamphetamine-exposed monkeys, is associated with abnormally high brain iron accumulation which is comparable to monkeys 2-3 times older (Berman, O'Neill, Fears, Bartzokis, & London, 2008; Melega, Lacan, Harvey, & Way, 2007). On the other hand, potential deficits in dopamine metabolism might be associated with abnormally low brain iron levels as observed in medication-naïve patients with attention-deficit hyperactivity (ADHD) (Adisetiyo & Helpern, 2015; Adisetiyo et al., 2014; Cortese, Angriman, Lecendreux, & Konofal, 2012; Cortese, Azoulay, et al., 2012; Picchietti, 2007; Soto-Insuga et al., 2013). Treatment of ADHD patients with

traditional dopaminergic psychostimulants may normalize brain iron levels (Adisetiyo et al., 2014). Animal studies also revealed that dopamine-receptor-blocking antipsychotics such as haloperidol alter brain iron metabolism (Ben-Shachar, Livne, Spanier, Zuk, & Youdim, 1993; Ben-Shachar & Youdim, 1990). Evidence from Parkinson's disease studies further indicate a potential interplay between brain iron and dopamine in redox toxicity and neurodegeneration (Hare & Double, 2016). This could explain why male methamphetamine abusers who have physiologically higher iron levels than their female counterparts exhibit greater white matter damage (S. C. Bae et al., 2006; Chung et al., 2007) and may also help to explain the brain atrophy associated with chronic alcohol abuse.

4.3 Inflammation, tissue damage, and leaky brain in AUD

AUD is associated with chronic inflammation (Crews et al., 2006; Crews & Nixon, 2009; Kelley & Dantzer, 2011; H. J. Wang, Zakhari, & Jung, 2010). As an antibacterial defence mechanism, inflammation triggers the body to sequester and absorb excess iron (Wessling-Resnick, 2010). Chronic alcohol abuse also disrupts the blood-brain-barrier (Cornford, Braun, Oldendorf, & Hill, 1982; Elmas, Kucuk, Kalayci, Cevik, & Kaya, 2001; Haorah et al., 2005; Haorah, Knipe, Gorantla, Zheng, & Persidsky, 2007; A. K. Singh, Jiang, Gupta, & Benlhabib, 2007). Increased systemic iron in combination with impaired transit control and increased iron sequestering signalling could lead to abnormally high iron accumulation in the leaky brain.

A related explanation can be also drawn from parallels between AUD and neurodegenerative disorders associated with brain iron dysregulation, such as multiple sclerosis. Iron is required to help maintain integrity of oligodendrocytes and myelin (LeVine & Macklin, 1990; Stephenson, Nathoo, Mahjoub, Dunn, & Yong, 2014). Iron-containing enzymes are required for both myelination and remyelination following injury. Recurrent white matter damage in multiple sclerosis results in waves of iron liberation from dying oligodendrocytes and increased iron turnover which may cause further damage. Active multiple sclerosis white matter lesions are associated with increased iron loads (Hametner et al., 2013).

Alcohol is toxic and particularly damaging to white matter integrity. Chronic cycles of fluctuating toxic levels of alcohol in AUD, may lead to recurrent cycles of white matter damage and repair which may not only lead to excess extracellular iron release from widespread tissue damage but also signal increased iron demand for remyelination and repair. Even in better characterised neurodegenerative disorders, however, it is still not known whether observed excess brain iron is the cause or the outcome of cell damage (Rouault, 2013).

In summary, there is a range of possible inter-linked explanations for brain iron accumulation in AUD. The literature provides collateral evidence which may link the observed deep grey matter siderosis to alcohol mediated systemic iron overload, excess brain dopamine activity, and chronic inflammation and brain cellular damage. These processes could interact to support the premature aging hypothesis in AUD (Noonberg, Goldstein, & Page, 1985; Oscar-Berman & Marinkovic, 2003; Ryan & Butters, 1984; Sanhueza, Garcia-Moreno, & Exposito, 2011; Spencer & Hutchison, 1999). Our analysis indicated a positive relationship between age and susceptibility (brain iron) levels in all four regions of interest tested (Figure 7.3), though this relationship was significant only in putamen / globus pallidus and red nucleus / substantia nigra. The interaction between group status (patients *vs.* control) and the relationship of age to QSM levels was not significant in our working-age adults.

This study has some limitations in relation to sample size and data resolution. This was a proof-of-concept, retrospective, case-controlled analysis of an existing dataset which was optimized for high temporal resolution and not high spatial resolution. As a result, we were unable to clearly delineate all of the *a priori* regions of interest, leading to two combined regions and to potential partial volume artifacts. This was particularly problematic for the substantia nigra / red nucleus ROI which likely included part of the subthalamic nucleus due to its anatomical proximity. Higher resolution studies would be preferred using more standard QSM methods that do not rely on EPI; however, the use of EPI-QSM enables initial

studies from existing fMRI data. The modest sample size with a broad age range has also precluded us from drawing more concrete conclusion about the interaction of alcohol use disorder and aging on the trajectory of brain iron accumulation. FDR correction was used for multiple comparisons, and this is less stringent than family-wise error correction. Lastly, because only adult male patients were included in our study, the conclusions of our study might not be generalizable to the overall population of patients suffering from alcohol use disorder. The strengths of our study are in the stringent recruitment criteria (which excluded all interested participants with history of polysubstance abuse or comorbid disorders) as well as the robust blinded analysis using 3D manual tracing.

5 Conclusion

To the best of our knowledge, this is the first study exploring QSM in the alcohol dependent brain, the first human alcohol-related brain iron study, and the first retrospective study to apply the new EPI-QSM technique to an existing clinical rs-fMRI dataset. Our study demonstrated that retrospective QSM may unlock hidden value in existing and future fMRI datasets, multiplying the data yield for the same amount of scanning time and money. This could help advance our understanding of iron metabolism or calcification in psychiatric disorders such as AUD. This could also help revitalize research in iron dysregulation and oxidative damage in psychiatric disorders as well as catalyze identification of potential diagnostic and prognostic biomarkers for complex brain disorders as solicited by the NIMH Research Domain Criteria initiative. Future prospective or retrospective studies should aim to replicate our findings with higher resolution and larger sample sizes. The EPI-QSM technique would be especially valuable to the emerging field of high resolution (Sun et al., 2016). The positive relationship between alcohol abuse and brain iron should be further explored in a broader range of AUD severity in both sexes since our sample included only very heavy male drinkers.

Chapter 8 - Discussion and Conclusions

This is a paper-based thesis, which included respective discussion of the results and their interpretation in each of the relevant chapters. As a result, we will succinctly summarize the most important findings and focus on the overall limitations and lessons for future studies.

The aim of this exploratory study was to characterize multimodal neuroimaging differences associated with AUD and its early recovery between approximately 2 weeks and one month of sustained abstinence. Our overall *a priori* expectations included significant wide-spread structural and functional deficits at both time points, which would show a positive recovery trend with sustained abstinence. We also hypothesized that the magnitude of neuroimaging deficits would correlate to the clinical severity measures. Our analyses succeeded in characterizing significant AUD-related changes generally in agreement with our *a priori* expectations but failed to detect significant longitudinal differences during the interscan interval in most modalities, despite of generally encouraging converging trends. The persistent failure to detect significant longitudinal differences could be due to too short interscan interval (too little time to accumulate sufficient microscopic changes to be detectable on the macroscopic MRI scale), missing very early brain deficits prior to our baseline scan (underestimating the AUD-related deficits), or too great inter-subject variability for our sample size (within group natural interscan variability and nuisance variables such as age, multiple scanning sites, *et cetera* could noise out a weaker between group contrast signal). The functional independent component analysis has been especially complex with largely inconsistent results. Our inability to more conclusively characterize the abstinence-related neuroimaging dynamics has, unfortunately, substantially impaired our ability to draw functional or clinical interpretations of our findings and precluded us from realizing the full potential of our analyses.

The most important findings from each of the six sets of analyses included the following:

1) **Voxel and Surface Based Morphometry** revealed a broad high single digit decrease in global gray and white matter densities in AUD at the first time point, which persisted in mid-single digit at the second time point, exhibiting a positive but non-significant structural integrity improvement with sustained abstinence. AUD group also exhibited a persistent low single digit decrease in global cortical thickness, which persisted during both time points. Clinical severity scales were weakly to moderately correlated to the magnitude of the structural atrophy. To the best of our knowledge, our analysis was only the third surface-based longitudinal AUD study (with abstinence window between the two other studies) and the first based on a North American clinical cohort (P. Bach et al., 2020; G. Y. Wang et al., 2016).

2) **Region-Based Morphometry** revealed wide-spread high single digit decrease in region-specific cortical, subcortical, and cerebellar regions which showed significant correlation to the clinical severity, especially in the most affected regions. Longitudinal interscan differences associated with sustained abstinence did not survive multiple comparison correction but indicated a positive recovery trend. To the best of our knowledge, this was only the second longitudinal region-based morphometry study to analyze hippocampal subfields (Kühn et al., 2014) and the first study to analyze structural dynamics of cerebellar lobules during AUD recovery.

3) **White Matter Microstructure DTI Analysis** revealed aberrant diffusion tensor imaging (DTI) scalar pattern consistent with wide-spread neuronal and/or myelin injury in AUD at both time points. Magnitude of the scalar's impairment was in most cases correlated to the clinical severity measures. The longitudinal differences were not significant but alluded to a pattern of microstructural healing during the early AUD recovery. Although the existing literature has reported quite extensively directionality of both fractional anisotropy (FA) and mean diffusivity (MD) in both short-term and long-term abstinent AUD, their magnitude as well the changes in other less commonly reported scalars remain poorly documented with conflicting reports. Our

study was one of only very few longitudinal DTI analyses which documented microstructural changes during AUD remission. To the best of our knowledge, only five other longitudinal, cross-sectional, and mixed design studies have explored the effect of sustained abstinence on white matter microstructure using comparable techniques to our study (Alhassoon et al., 2012; De Santis et al., 2019; Gazdzinski et al., 2010; Pfefferbaum et al., 2014; Y. Zou et al., 2017).

4) **Regional Functional Connectivity Analysis** revealed AUD-related decrease in regional functional connectivity indices in basal ganglia which persisted during both time points, as well as aberrant increase in functional connectivity in the frontal cortex in the AUD patients. Longitudinal differences were mostly not significant. Magnitude of most of the functional deficits was correlated to the AUD clinical severity measures. The longitudinal changes should be considered with caution but might potentially provide evidence of over-compensatory adaptation in the abstinent AUD. To the best of our knowledge, this was the first longitudinal study to explore regional functional connectivity changes in AUD recovery; the regional functional connectivity study with the largest sample size to this date; and also the first regional functional connectivity study based on a North American and/or European clinical cohort.

5) **Independent Component and Hierarchical Analysis of Functional Connectivity** revealed a largely inconsistent complex set of differences in the resting state functional networks, which exhibited only very limited spatial and longitudinal reproducibility across the different contrasts. The overall findings, nonetheless, still suggested a global pattern of hypoconnectivity in AUD, with encouraging converging trend in functional connectivity across plurality of the networks (most notably Right Executive Control Network, Mesial-Temporal Network, and Posterior Default Mode Network). Most of the significant changes were correlated with at least one measure of AUD severity. To the best of our knowledge, this was the first longitudinal study

which has attempted to characterize longitudinal differences in resting state functional connectivity in recovering AUD patients across large-scale functional networks.

6) **Quantitative Susceptibility (QSM) Analysis** has demonstrated high single to low teen percentage increase in iron accumulation in deep brain gray matter in AUD. We have postulated three possible explanations for these differences including systemic iron overload, excess dopaminergic activity, and tissue damage associated with inflammation and leaky brain. To the best of our knowledge, this was the first study exploring QSM in the alcohol dependent brain, the first human alcohol-related brain iron study, and the first retrospective study to apply the new EPI-QSM technique to an existing clinical fMRI dataset. Our study has demonstrated a new analysis paradigm for non-invasive brain iron measurements which could retrospectively derive additional insights about a wide variety of psychiatric and neurological conditions from existing neuroimaging datasets. Some relevant disorders include addictions, obsessive-compulsive disorder, attention-deficit hyperactivity disorder, Alzheimer's disease, Parkinson's disease, multiple sclerosis, congenital aceruloplasminemia, Friedreich's ataxia, neuroferritinopathy, neurodegeneration with brain iron accumulation, amyotrophic lateral sclerosis, and restless leg syndrome. Since its publication, this study has been cited by at least 11 other publications.

Although our analysis was unable to fulfill its main objective of comprehensive characterization of abstinence-related structural and functional neuroimaging dynamics during the early AUD remission, our project has made a substantial contribution to the existing literature, expanding our current understanding of AUD-related brain changes as well as providing first longitudinal AUD results for multiple neuroimaging modalities. Even the non-significant longitudinal observation should provide valuable insights to future researchers who might attempt to replicate similar analyses in the future.

The most important lesson from this study which was not discussed in the individual chapters has been the enormous difficulty in recruitment, retention, and patient follow-up. The recruitment for this study has taken over three years. In the Edmonton node alone, our team has screened and interviewed over 1,123 AUD patients from all of the city's detoxification and addiction treatment centres and over 668 healthy controls to enroll 28 eligible patients and 18 matched healthy controls, out of which only 14 patients and 12 controls completed both longitudinal scans. In other words, we had to interview over 80 patients to be able to collect a single data point. Because of these difficulties, the initial design of this project had to be substantially reduced, we had to pool our data with our German collaborators, and we were still unable to detect significant longitudinal differences to fully characterize the brain changes during early recovery across most modalities. These recruitment statistics, nonetheless, highlight the value and importance of the contribution of our analyses to the existing literature as well as document a common practical reason why true longitudinal neuroimaging studies with clinically homogeneous recruitment criteria remain quite rare in the literature.

Another related observation is pertaining to aspects of our study which could not be realized due to the recruitment difficulties. One aspect of the initial study design aimed to compare functional brain changes and treatment outcomes to pharmacological intervention with naltrexone (in relation to the μ-opioid receptor OPRM1 allele profile). We were unable to fully explore this aspect of our project due to insufficient sample size. Nonetheless, the preliminary results have suggested a very interesting pattern, whereby 10 out of 12 randomly assigned patients taking naltrexone completed all follow-up sessions while only 4 out of 12 in treatment as usual group completed the follow-up. Future studies might want to consider exploring these observations in greater detail, especially due to recent neuroimaging evidence suggesting naltrexone may help ameliorate AUD-related functional abnormalities (Elton, Dove, Spencer, Robinson, & Boettiger, 2019; Morris et al., 2018).

Future studies should also consider other aspects when trying to more conclusively characterize neuroimaging changes associated with AUD recovery which were discussed in the individual chapters. These included, for example, increasing sample size, decreasing heterogeneity of the sample (due to large age range or multiple scanning sites), increasing number of time-points, collecting an earlier baseline AUD scan, increasing the interscan interval, collecting longitudinal data also in the controls (to allow for contrast which will account for normal interscan variability and decrease likelihood of spurious results), accounting for smoking interaction with AUD and smoking disparity between controls and patients, accounting for family history of AUD (to account for possible inherent predispositions), and collecting neurocognitive performance data to allow for more reliable functional interpretation of possible functional connectivity results. Although longitudinal studies with restrictive inclusion and exclusion criteria are quite challenging to complete, they provide unique insights into the progression of AUD which cannot be readily replicated by other designs. Difficulties in completing such studies highlight the importance of multi-site collaboration projects and data sharing between research groups which might be necessary in order to collect sufficiently large dataset in a reasonable time period.

In conclusion, our exploratory study has documented AUD-related structural and functional brain differences in patients undergoing early remission between approximately the first two weeks and the first month of sustained abstinence. Our results revealed an encouraging but not statistically significant trend of longitudinal brain recovery. Several of our studies have provided first or one of very few longitudinal observations of structural and functional changes during early AUD recovery. Our study has also documented clinical application of a novel retrospective analysis for detecting iron accumulation from existing fMRI datasets, widely applicable to many psychiatric and neurological disorders. Although our study was unable to exhaustively characterize the longitudinal neuroimaging differences in early AUD recovery, it has still provided very valuable new evidence which was very challenging to collect and is thus quite unique in the context of the existing literature.

Beyond its scientific merits, our study also had a meaningful impact on both personal and clinical level in the greater community outside of academia. Treatment seeking and recovering AUD patients have to often navigate and overcome many obstacles and stigma associated with AUD and its limited treatment options. Even though the patients are guided through their recovery journey by dedicated work of their clinical team and supported by their network of sponsors, friends and families in the greater community, remaining engaged and committed to the recovery process can be very challenging.

The encouraging findings from our study have anecdotally helped to strengthen patient engagement, therapeutic alliance, and mutual confidence in the therapeutic process in the participating treatment centres. Although our results might not have been as exhaustive as we initially aspired to, our project still provided tangible evidence of structural and functional changes associated with early remission from AUD. The results have objectively demonstrated that even a few weeks of sustained abstinence and psychosocial intervention in the real-world public addiction treatment facilities in our communities can meaningfully alter some of the aberrant brain changes caused by the chronic alcohol abuse.

Our research team has received an overwhelmingly positive feedback from the patients, their families, and clinicians involved in the study. It is our hope that other researchers can be encouraged by our own experience to pursue and persevere with clinical research even in very challenging cohorts or with more complex longitudinal designs.

References

Acheson, A., Robinson, J. L., Glahn, D. C., Lovallo, W. R., & Fox, P. T. (2009). Differential activation of the anterior cingulate cortex and caudate nucleus during a gambling simulation in persons with a family history of alcoholism: studies from the Oklahoma Family Health Patterns Project. *Drug Alcohol Depend, 100*(1-2), 17-23. doi:10.1016/j.drugalcdep.2008.08.019

Acosta-Cabronero, J., Betts, M. J., Cardenas-Blanco, A., Yang, S., & Nestor, P. J. (2016). In Vivo MRI Mapping of Brain Iron Deposition across the Adult Lifespan. *J Neurosci, 36*(2), 364-374. doi:10.1523/jneurosci.1907-15.2016

Adisetiyo, V., & Helpern, J. A. (2015). Brain iron: a promising noninvasive biomarker of attention-deficit/hyperactivity disorder that warrants further investigation. *Biomark Med, 9*(5), 403-406. doi:10.2217/bmm.15.9

Adisetiyo, V., Jensen, J. H., Tabesh, A., Deardorff, R. L., Fieremans, E., Di Martino, A., . . . Helpern, J. A. (2014). Multimodal MR imaging of brain iron in attention deficit hyperactivity disorder: a noninvasive biomarker that responds to psychostimulant treatment? *Radiology, 272*(2), 524-532. doi:10.1148/radiol.14140047

Agartz, I., Brag, S., Franck, J., Hammarberg, A., Okugawa, G., Svinhufvud, K., & Bergman, H. (2003). MR volumetry during acute alcohol withdrawal and abstinence: a descriptive study. *Alcohol Alcohol, 38*(1), 71-78. doi:10.1093/alcalc/agg020

Alba-Ferrara, L., Müller-Oehring, E. M., Sullivan, E. V., Pfefferbaum, A., & Schulte, T. (2016). Brain responses to emotional salience and reward in alcohol use disorder. *Brain Imaging Behav, 10*(1), 136-146. doi:10.1007/s11682-015-9374-8

Alhassoon, O. M., Sorg, S. F., Taylor, M. J., Stephan, R. A., Schweinsburg, B. C., Stricker, N. H., . . . Grant, I. (2012). Callosal white matter microstructural recovery in abstinent alcoholics: a longitudinal diffusion tensor imaging study. *Alcohol Clin Exp Res, 36*(11), 1922-1931. doi:10.1111/j.1530-0277.2012.01808.x

Alling, C., & Boström, K. (1980). Demyelination of the mamillary bodies in alcoholism. A combined morphological and biochemical study. *Acta Neuropathol, 50*(1), 77-80. doi:10.1007/BF00688539

American Psychiatric Association. (2000). *Diagnostic and statistical manual of mental disorders : DSM-IV-TR*. Washington, DC: American Psychiatric Association.

American Psychiatric Association. (2013). *Diagnostic and statistical manual of mental disorders : DSM-5*. Washington, D.C.: American Psychiatric Association.

Andersson, J. L., Jenkinson, M., & Smith, S. (2007). Non-linear registration aka Spatial normalisation FMRIB Technial Report TR07JA2.

Andersson, J. L. R., & Sotiropoulos, S. N. (2016). An integrated approach to correction for off-resonance effects and subject movement in diffusion MR imaging. *Neuroimage, 125*, 1063-1078. doi:10.1016/j.neuroimage.2015.10.019

Andrews, M. M., Meda, S. A., Thomas, A. D., Potenza, M. N., Krystal, J. H., Worhunsky, P., . . . Pearlson, G. D. (2011). Individuals family history positive for alcoholism show functional magnetic resonance imaging differences in reward sensitivity that are related to impulsivity factors. *Biol Psychiatry, 69*(7), 675-683. doi:10.1016/j.biopsych.2010.09.049

Artmann, H., Gall, M. V., Hacker, H., & Herrlich, J. (1981). Reversible enlargement of cerebral spinal fluid spaces in chronic alcoholics. *AJNR Am J Neuroradiol, 2*(1), 23-27.

Ashburner, J. (2007). A fast diffeomorphic image registration algorithm. *Neuroimage, 38*(1), 95-113.

Ashburner, J., Barnes, G., Chen, C., Daunizeau, J., Flandin, G., Friston, K., . . . Moran, R. (2014). SPM12 manual. *Wellcome Trust Centre for Neuroimaging, London, UK*.

Ashburner, J., & Friston, K. J. (2005). Unified segmentation. *Neuroimage, 26*(3), 839-851. doi:10.1016/j.neuroimage.2005.02.018

Bach, M., Laun, F. B., Leemans, A., Tax, C. M., Biessels, G. J., Stieltjes, B., & Maier-Hein, K. H. (2014). Methodological considerations on tract-based spatial statistics (TBSS). *Neuroimage, 100*, 358-369. doi:10.1016/j.neuroimage.2014.06.021

Bach, P., Koopmann, A., Bumb, J. M., Vollstädt-Klein, S., Reinhard, I., Rietschel, M., . . . Kiefer, F. (2020). Leptin predicts cortical and subcortical gray matter volume recovery in alcohol dependent patients: A longitudinal structural magnetic resonance imaging study. *Horm Behav, 124*, 104749. doi:10.1016/j.yhbeh.2020.104749

Bae, S., Kang, I., Lee, B. C., Jeon, Y., Cho, H. B., Yoon, S., . . . Choi, I. G. (2016). Prefrontal Cortical Thickness Deficit in Detoxified Alcohol-dependent Patients. *Exp Neurobiol, 25*(6), 333-341. doi:10.5607/en.2016.25.6.333

Bae, S. C., Lyoo, I. K., Sung, Y. H., Yoo, J., Chung, A., Yoon, S. J., . . . Renshaw, P. F. (2006). Increased white matter hyperintensities in male methamphetamine abusers. *Drug Alcohol Depend, 81*(1), 83-88. doi:10.1016/j.drugalcdep.2005.05.016

Bartsch, A. J., Homola, G., Biller, A., Smith, S. M., Weijers, H. G., Wiesbeck, G. A., . . . Bendszus, M. (2007). Manifestations of early brain recovery associated with abstinence from alcoholism. *Brain, 130*(Pt 1), 36-47. doi:10.1093/brain/awl303

Bartzokis, G., Cummings, J. L., Markham, C. H., Marmarelis, P. Z., Treciokas, L. J., Tishler, T. A., . . . Mintz, J. (1999). MRI evaluation of brain iron in earlier- and later-onset Parkinson's disease and normal subjects. *Magn Reson Imaging, 17*(2), 213-222.

Basser, P. J., & Jones, D. K. (2002). Diffusion-tensor MRI: theory, experimental design and data analysis - a technical review. *NMR Biomed, 15*(7-8), 456-467. doi:10.1002/nbm.783

Beard, J. L., & Connor, J. R. (2003). Iron status and neural functioning. *Annu Rev Nutr, 23*, 41-58. doi:10.1146/annurev.nutr.23.020102.075739

Beaulieu, C. (2002). The basis of anisotropic water diffusion in the nervous system - a technical review. *NMR Biomed, 15*(7-8), 435-455. doi:10.1002/nbm.782

Beck, A., Wüstenberg, T., Genauck, A., Wrase, J., Schlagenhauf, F., Smolka, M. N., . . . Heinz, A. (2012). Effect of brain structure, brain function, and brain connectivity on relapse in alcohol-dependent patients. *Arch Gen Psychiatry, 69*(8), 842-852. doi:10.1001/archgenpsychiatry.2011.2026

Beckmann, C. F., DeLuca, M., Devlin, J. T., & Smith, S. M. (2005). Investigations into resting-state connectivity using independent component analysis. *Philos Trans R Soc Lond B Biol Sci, 360*(1457), 1001-1013. doi:10.1098/rstb.2005.1634

Beckmann, C. F., Mackay, C. E., Filippini, N., & Smith, S. M. (2009). Group comparison of resting-state FMRI data using multi-subject ICA and dual regression. *Neuroimage, 47*(Suppl 1), S148.

Beckmann, C. F., & Smith, S. M. (2004). Probabilistic independent component analysis for functional magnetic resonance imaging. *IEEE Trans Med Imaging, 23*(2), 137-152. doi:10.1109/TMI.2003.822821

Behrens, T. E., Woolrich, M. W., Jenkinson, M., Johansen-Berg, H., Nunes, R. G., Clare, S., . . . Smith, S. M. (2003). Characterization and propagation of uncertainty in diffusion-weighted MR imaging. *Magn Reson Med, 50*(5), 1077-1088. doi:10.1002/mrm.10609

Behzadi, Y., Restom, K., Liau, J., & Liu, T. T. (2007). A component based noise correction method (CompCor) for BOLD and perfusion based fMRI. *Neuroimage, 37*(1), 90-101. doi:10.1016/j.neuroimage.2007.04.042

Belin-Rauscent, A., Daniel, M. L., Puaud, M., Jupp, B., Sawiak, S., Howett, D., . . . Belin, D. (2016). From impulses to maladaptive actions: the insula is a neurobiological gate for the development of compulsive behavior. *Mol Psychiatry, 21*(4), 491-499. doi:10.1038/mp.2015.140

Ben-Shachar, D., Livne, E., Spanier, I., Zuk, R., & Youdim, M. B. (1993). Iron modulates neuroleptic-induced effects related to the dopaminergic system. *Isr J Med Sci, 29*(9), 587-592.

Ben-Shachar, D., & Youdim, M. B. (1990). Neuroleptic-induced supersensitivity and brain iron: I. Iron deficiency and neuroleptic-induced dopamine D2 receptor supersensitivity. *J Neurochem, 54*(4), 1136-1141.

Bendszus, M., Weijers, H. G., Wiesbeck, G., Warmuth-Metz, M., Bartsch, A. J., Engels, S., . . . Solymosi, L. (2001). Sequential MR imaging and proton MR spectroscopy in patients who underwent recent detoxification for chronic alcoholism: correlation with clinical and neuropsychological data. *AJNR Am J Neuroradiol, 22*(10), 1926-1932.

Benjamini, Y., & Hochberg, Y. (1995). Controlling the False Discovery Rate: A Practical and Powerful Approach to Multiple Testing. *jroyastatsocise2 Journal of the Royal Statistical Society. Series B (Methodological), 57*(1), 289-300.

Bergouignan, L., Chupin, M., Czechowska, Y., Kinkingnéhun, S., Lemogne, C., Le Bastard, G., . . . Fossati, P. (2009). Can voxel based morphometry, manual segmentation and automated segmentation equally detect hippocampal volume differences in acute depression? *Neuroimage, 45*(1), 29-37. doi:10.1016/j.neuroimage.2008.11.006

Berman, S., O'Neill, J., Fears, S., Bartzokis, G., & London, E. D. (2008). Abuse of amphetamines and structural abnormalities in the brain. *Ann N Y Acad Sci, 1141*, 195-220. doi:10.1196/annals.1441.031

Bernardin, F., Maheut-Bosser, A., & Paille, F. (2014). Cognitive impairments in alcohol-dependent subjects. *Front Psychiatry, 5*, 78. doi:10.3389/fpsyt.2014.00078

Bilgic, B., Pfefferbaum, A., Rohlfing, T., Sullivan, E. V., & Adalsteinsson, E. (2012). MRI estimates of brain iron concentration in normal aging using quantitative susceptibility mapping. *Neuroimage, 59*(3), 2625-2635. doi:10.1016/j.neuroimage.2011.08.077

Biswal, B., Yetkin, F. Z., Haughton, V. M., & Hyde, J. S. (1995). Functional connectivity in the motor cortex of resting human brain using echo-planar MRI. *Magn Reson Med, 34*(4), 537-541. doi:10.1002/mrm.1910340409

Boileau, I., Assaad, J. M., Pihl, R. O., Benkelfat, C., Leyton, M., Diksic, M., . . . Dagher, A. (2003). Alcohol promotes dopamine release in the human nucleus accumbens. *Synapse, 49*(4), 226-231. doi:10.1002/syn.10226

Bondy, S. C., & Orozco, J. (1994). Effects of ethanol treatment upon sources of reactive oxygen species in brain and liver. *Alcohol Alcohol, 29*(4), 375-383.

Bonferroni, C. E. (1936). *Teoria statistica delle classi e calcolo delle probabilit `a*. Retrieved from

Brandt, J., Butters, N., Ryan, C., & Bayog, R. (1983). Cognitive loss and recovery in long-term alcohol abusers. *Arch Gen Psychiatry, 40*(4), 435-442. doi:10.1001/archpsyc.1983.01790040089012

Buckner, R. L., Krienen, F. M., & Yeo, B. T. (2013). Opportunities and limitations of intrinsic functional connectivity MRI. *Nat Neurosci, 16*(7), 832-837. doi:10.1038/nn.3423

Buckner, R. L., Sepulcre, J., Talukdar, T., Krienen, F. M., Liu, H., Hedden, T., . . . Johnson, K. A. (2009). Cortical hubs revealed by intrinsic functional connectivity: mapping, assessment of stability, and relation to Alzheimer's disease. *J Neurosci, 29*(6), 1860-1873. doi:10.1523/JNEUROSCI.5062-08.2009

Butt, P. (2011). Alcohol and health in Canada a summary of evidence and guidelines for low-risk drinking. In. Ottawa, Ont. :: Canadian Centre on Sustance Abuse.

Button, K. S., Ioannidis, J. P., Mokrysz, C., Nosek, B. A., Flint, J., Robinson, E. S., & Munafò, M. R. (2013). Power failure: why small sample size undermines the reliability of neuroscience. *Nat Rev Neurosci, 14*(5), 365-376. doi:10.1038/nrn3475

Bühler, M., & Mann, K. (2011). Alcohol and the human brain: a systematic review of different neuroimaging methods. *Alcohol Clin Exp Res, 35*(10), 1771-1793. doi:10.1111/j.1530-0277.2011.01540.x

Camchong, J., Stenger, A., & Fein, G. (2013a). Resting-state synchrony during early alcohol abstinence can predict subsequent relapse. *Cereb Cortex, 23*(9), 2086-2099. doi:10.1093/cercor/bhs190

Camchong, J., Stenger, A., & Fein, G. (2013b). Resting-state synchrony in long-term abstinent alcoholics. *Alcohol Clin Exp Res, 37*(1), 75-85. doi:10.1111/j.1530-0277.2012.01859.x

Camchong, J., Stenger, V. A., & Fein, G. (2013c). Resting-state synchrony in short-term versus long-term abstinent alcoholics. *Alcohol Clin Exp Res, 37*(5), 794-803. doi:10.1111/acer.12037

Canadian Substance Use Costs and Harms Scientific Working Group. (2018). *Canadian substance use costs and harms (2007–2014)*. Ottawa: Canadian Centre on Substance Use and Addiction.

Cardenas, V. A., Studholme, C., Gazdzinski, S., Durazzo, T. C., & Meyerhoff, D. J. (2007). Deformation-based morphometry of brain changes in alcohol dependence and abstinence. *Neuroimage, 34*(3), 879-887. doi:10.1016/j.neuroimage.2006.10.015

Carlen, P. L., & Wilkinson, D. A. (1980). Alcoholic brain damage and reversible deficits. *Acta Psychiatr Scand Suppl, 286*, 103-118. doi:10.1111/j.1600-0447.1980.tb08058.x

Carlen, P. L., Wilkinson, D. A., Wortzman, G., & Holgate, R. (1984). Partially reversible cerebral atrophy and functional improvement in recently abstinent alcoholics. *Can J Neurol Sci, 11*(4), 441-446. doi:10.1017/s0317167100045972

Carlen, P. L., Wortzman, G., Holgate, R. C., Wilkinson, D. A., & Rankin, J. C. (1978). Reversible cerebral atrophy in recently abstinent chronic alcoholics measured by computed tomography scans. *Science, 200*(4345), 1076-1078. doi:10.1126/science.653357

Celada, A., Rudolf, H., & Donath, A. (1979). Effect of experimental chronic alcohol ingestion and folic acid deficiency on iron absorption. *Blood, 54*(4), 906-915.

Chanraud, S., Pitel, A. L., Pfefferbaum, A., & Sullivan, E. V. (2011). Disruption of functional connectivity of the default-mode network in alcoholism. *Cereb Cortex, 21*(10), 2272-2281. doi:10.1093/cercor/bhq297

Chanraud, S., & Sullivan, E. V. (2014). Compensatory recruitment of neural resources in chronic alcoholism. *Handb Clin Neurol, 125*, 369-380. doi:10.1016/B978-0-444-62619-6.00022-7

Chanraud-Guillermo, S., Andoh, J., Martelli, C., Artiges, E., Pallier, C., Aubin, H. J., . . . Reynaud, M. (2009). Imaging of language-related brain regions in detoxified alcoholics. *Alcohol Clin Exp Res, 33*(6), 977-984. doi:10.1111/j.1530-0277.2009.00918.x

Chao-Gan, Y., & Yu-Feng, Z. (2010). DPARSF: A MATLAB Toolbox for "Pipeline" Data Analysis of Resting-State fMRI. *Front Syst Neurosci, 4*, 13. doi:10.3389/fnsys.2010.00013

Charlet, K., Rosenthal, A., Lohoff, F. W., Heinz, A., & Beck, A. (2018). Imaging resilience and recovery in alcohol dependence. *Addiction, 113*(10), 1933-1950. doi:10.1111/add.14259

Cheng, H. C., Ulane, C. M., & Burke, R. E. (2010). Clinical progression in Parkinson disease and the neurobiology of axons. *Ann Neurol, 67*(6), 715-725. doi:10.1002/ana.21995

Chung, A., Lyoo, I. K., Kim, S. J., Hwang, J., Bae, S. C., Sung, Y. H., . . . Renshaw, P. F. (2007). Decreased frontal white-matter integrity in abstinent methamphetamine abusers. *Int J Neuropsychopharmacol, 10*(6), 765-775. doi:10.1017/s1461145706007395

Connor, J. R., & Menzies, S. L. (1996). Relationship of iron to oligodendrocytes and myelination. *Glia, 17*(2), 83-93. doi:10.1002/(SICI)1098-1136(199606)17:2<83::AID-GLIA1>3.0.CO;2-7

Cornford, E. M., Braun, L. D., Oldendorf, W. H., & Hill, M. A. (1982). Comparison of lipid-mediated blood-brain-barrier penetrability in neonates and adults. *Am J Physiol, 243*(3), C161-168.

Cortese, S., Angriman, M., Lecendreux, M., & Konofal, E. (2012). Iron and attention deficit/hyperactivity disorder: What is the empirical evidence so far? A systematic review of the literature. *Expert Rev Neurother, 12*(10), 1227-1240. doi:10.1586/ern.12.116

Cortese, S., Azoulay, R., Castellanos, F. X., Chalard, F., Lecendreux, M., Chechin, D., . . . Konofal, E. (2012). Brain iron levels in attention-deficit/hyperactivity disorder: a pilot MRI study. *World J Biol Psychiatry, 13*(3), 223-231. doi:10.3109/15622975.2011.570376

Coupé, P., Manjón, J. V., Fonov, V., Pruessner, J., Robles, M., & Collins, D. L. (2011). Patch-based segmentation using expert priors: application to hippocampus and ventricle segmentation. *Neuroimage, 54*(2), 940-954. doi:10.1016/j.neuroimage.2010.09.018

Crews, F. T. (2008). Alcohol-related neurodegeneration and recovery: mechanisms from animal models. *Alcohol Res Health, 31*(4), 377-388.

Crews, F. T., Bechara, R., Brown, L. A., Guidot, D. M., Mandrekar, P., Oak, S., . . . Zou, J. (2006). Cytokines and alcohol. *Alcohol Clin Exp Res, 30*(4), 720-730. doi:10.1111/j.1530-0277.2006.00084.x

Crews, F. T., & Nixon, K. (2009). Mechanisms of neurodegeneration and regeneration in alcoholism. *Alcohol Alcohol, 44*(2), 115-127. doi:10.1093/alcalc/agn079

Crossley, N. A., Mechelli, A., Vértes, P. E., Winton-Brown, T. T., Patel, A. X., Ginestet, C. E., . . . Bullmore, E. T. (2013). Cognitive relevance of the community structure of the human brain functional coactivation network. *Proc Natl Acad Sci U S A, 110*(28), 11583-11588. doi:10.1073/pnas.1220826110

Crowe, S. F., Cammisuli, D. M., & Stranks, E. K. (2019). Widespread Cognitive Deficits in Alcoholism Persistent Following Prolonged Abstinence: An Updated Meta-analysis of Studies That Used Standardised Neuropsychological Assessment Tools. *Arch Clin Neuropsychol*. doi:10.1093/arclin/acy106

Cservenka, A., Herting, M. M., & Nagel, B. J. (2012). Atypical frontal lobe activity during verbal working memory in youth with a family history of alcoholism. *Drug Alcohol Depend, 123*(1-3), 98-104. doi:10.1016/j.drugalcdep.2011.10.021

Dahnke, R., Yotter, R. A., & Gaser, C. (2013). Cortical thickness and central surface estimation. *Neuroimage, 65*, 336-348. doi:10.1016/j.neuroimage.2012.09.050

David, S. P., Ware, J. J., Chu, I. M., Loftus, P. D., Fusar-Poli, P., Radua, J., . . . Ioannidis, J. P. (2013). Potential reporting bias in fMRI studies of the brain. *PLoS One, 8*(7), e70104. doi:10.1371/journal.pone.0070104

de Figueiredo, E. H., Borgonovi, A. F., & Doring, T. M. (2011). Basic concepts of MR imaging, diffusion MR imaging, and diffusion tensor imaging. *Magn Reson Imaging Clin N Am, 19*(1), 1-22. doi:10.1016/j.mric.2010.10.005

de la Monte, S. M. (1988). Disproportionate atrophy of cerebral white matter in chronic alcoholics. *Arch Neurol, 45*(9), 990-992. doi:10.1001/archneur.1988.00520330076013

De Santis, S., Bach, P., Pérez-Cervera, L., Cosa-Linan, A., Weil, G., Vollstädt-Klein, S., . . . Canals, S. (2019). Microstructural White Matter Alterations in Men With Alcohol Use Disorder and Rats With Excessive Alcohol Consumption During Early Abstinence. *JAMA Psychiatry, 76*(7), 749-758. doi:10.1001/jamapsychiatry.2019.0318

Demirakca, T., Ende, G., Kammerer, N., Welzel-Marquez, H., Hermann, D., Heinz, A., & Mann, K. (2011). Effects of alcoholism and continued abstinence on brain volumes in both genders. *Alcohol Clin Exp Res, 35*(9), 1678-1685. doi:10.1111/j.1530-0277.2011.01514.x

Deshmukh, A., Rosenbloom, M. J., De Rosa, E., Sullivan, E. V., & Pfefferbaum, A. (2005). Regional striatal volume abnormalities in schizophrenia: effects of comorbidity for alcoholism, recency of alcoholic drinking, and antipsychotic medication type. *Schizophr Res, 79*(2-3), 189-200. doi:10.1016/j.schres.2005.04.025

Desikan, R. S., Ségonne, F., Fischl, B., Quinn, B. T., Dickerson, B. C., Blacker, D., . . . Killiany, R. J. (2006). An automated labeling system for subdividing the human cerebral cortex on MRI scans into gyral based regions of interest. *Neuroimage, 31*(3), 968-980. doi:10.1016/j.neuroimage.2006.01.021

Di Chiara, G., & Bassareo, V. (2007). Reward system and addiction: what dopamine does and doesn't do. *Curr Opin Pharmacol, 7*(1), 69-76. doi:10.1016/j.coph.2006.11.003

Di Chiara, G., & Imperato, A. (1988). Drugs abused by humans preferentially increase synaptic dopamine concentrations in the mesolimbic system of freely moving rats. *Proceedings of the National Academy of Sciences, 85*(14), 5274-5278.

Duane, P., Raja, K. B., Simpson, R. J., & Peters, T. J. (1992). Intestinal iron absorption in chronic alcoholics. *Alcohol Alcohol, 27*(5), 539-544.

Durazzo, T. C., Gazdzinski, S., Rothlind, J. C., Banys, P., & Meyerhoff, D. J. (2006). Brain metabolite concentrations and neurocognition during short-term recovery from alcohol dependence: Preliminary evidence of the effects of concurrent chronic cigarette smoking. *Alcohol Clin Exp Res, 30*(3), 539-551. doi:10.1111/j.1530-0277.2006.00060.x

Durazzo, T. C., & Meyerhoff, D. J. (2019). Changes of frontal cortical subregion volumes in alcohol dependent individuals during early abstinence: associations with treatment outcome. *Brain Imaging Behav*. doi:10.1007/s11682-019-00089-5

Durazzo, T. C., Mon, A., Gazdzinski, S., & Meyerhoff, D. J. (2017). Regional brain volume changes in alcohol-dependent individuals during early abstinence: associations with relapse following treatment. *Addict Biol, 22*(5), 1416-1425. doi:10.1111/adb.12420

Durazzo, T. C., Mon, A., Gazdzinski, S., Yeh, P. H., & Meyerhoff, D. J. (2015). Serial longitudinal magnetic resonance imaging data indicate non-linear regional gray matter volume recovery in abstinent alcohol-dependent individuals. *Addict Biol, 20*(5), 956-967. doi:10.1111/adb.12180

Durazzo, T. C., Nguyen, L. C., & Meyerhoff, D. J. (2020). Medical Conditions Linked to Atherosclerosis Are Associated With Magnified Cortical Thinning in Individuals With Alcohol Use Disorders. *Alcohol Alcohol, 55*(4), 382-390. doi:10.1093/alcalc/agaa034

Durazzo, T. C., Tosun, D., Buckley, S., Gazdzinski, S., Mon, A., Fryer, S. L., & Meyerhoff, D. J. (2011). Cortical thickness, surface area, and volume of the brain reward system in alcohol dependence: relationships to relapse and extended abstinence. *Alcohol Clin Exp Res, 35*(6), 1187-1200. doi:10.1111/j.1530-0277.2011.01452.x

Durkee, C. A., Sarlls, J. E., Hommer, D. W., & Momenan, R. (2013). White matter microstructure alterations: a study of alcoholics with and without post-traumatic stress disorder. *PloS one, 8*(11), e80952-e80952. doi:10.1371/journal.pone.0080952

Eklund, A., Nichols, T. E., & Knutsson, H. (2016). Cluster failure: Why fMRI inferences for spatial extent have inflated false-positive rates. *Proc Natl Acad Sci U S A, 113*(28), 7900-7905. doi:10.1073/pnas.1602413113

Elmas, I., Kucuk, M., Kalayci, R. B., Cevik, A., & Kaya, M. (2001). Effects of profound hypothermia on the blood-brain barrier permeability in acute and chronically ethanol treated rats. *Forensic Sci Int, 119*(2), 212-216.

Elton, A., Dove, S., Spencer, C. N., Robinson, D. L., & Boettiger, C. A. (2019). Naltrexone Acutely Enhances Connectivity Between the Ventromedial Prefrontal Cortex and a Left Frontoparietal Network. *Alcohol Clin Exp Res, 43*(5), 965-978. doi:10.1111/acer.13999

Ende, G., Welzel, H., Walter, S., Weber-Fahr, W., Diehl, A., Hermann, D., . . . Mann, K. (2005). Monitoring the effects of chronic alcohol consumption and abstinence on brain metabolism: a longitudinal proton magnetic resonance spectroscopy study. *Biol Psychiatry, 58*(12), 974-980. doi:10.1016/j.biopsych.2005.05.038

Fede, S. J., Abrahao, K. P., Cortes, C. R., Grodin, E. N., Schwandt, M. L., George, D. T., . . . Momenan, R. (2020). Alcohol effects on globus pallidus connectivity: Role of impulsivity and binge drinking. *PLoS One, 15*(3), e0224906. doi:10.1371/journal.pone.0224906

Fede, S. J., Grodin, E. N., Dean, S. F., Diazgranados, N., & Momenan, R. (2019). Resting state connectivity best predicts alcohol use severity in moderate to heavy alcohol users. *Neuroimage Clin, 22*, 101782. doi:10.1016/j.nicl.2019.101782

Fein, G., & Cardenas, V. A. (2015). Neuroplasticity in Human Alcoholism: Studies of Extended Abstinence with Potential Treatment Implications. *Alcohol Res, 37*(1), 125-141.

Fein, G., & Fein, D. (2013). Subcortical volumes are reduced in short-term and long-term abstinent alcoholics but not those with a comorbid stimulant disorder. *Neuroimage Clin, 3*, 47-53. doi:10.1016/j.nicl.2013.06.018

Fein, G., Torres, J., Price, L. J., & Di Sclafani, V. (2006). Cognitive performance in long-term abstinent alcoholic individuals. *Alcohol Clin Exp Res, 30*(9), 1538-1544. doi:10.1111/j.1530-0277.2006.00185.x

Feldman, H. M., Yeatman, J. D., Lee, E. S., Barde, L. H., & Gaman-Bean, S. (2010). Diffusion tensor imaging: a review for pediatric researchers and clinicians. *J Dev Behav Pediatr, 31*(4), 346-356. doi:10.1097/DBP.0b013e3181dcaa8b

Finney, L. A., & O'Halloran, T. V. (2003). Transition Metal Speciation in the Cell: Insights from the Chemistry of Metal Ion Receptors. *Science, 300*(5621), 931-936. doi:10.1126/science.1085049

First, M. B., Spitzer, R. L., Gibbon, M., & Williams, J. B. W. (2002). Structured Clinical Interview for DSM-IV-TR Axis I Disorders (SCID-I), Research Version, Alcohol Dependence - Module E.4. In. New York: Biometric Research, New York State Psychiatric Institute.

Fortier, C. B., Leritz, E. C., Salat, D. H., Lindemer, E., Maksimovskiy, A. L., Shepel, J., . . . McGlinchey, R. E. (2014). Widespread effects of alcohol on white matter microstructure. *Alcohol Clin Exp Res, 38*(12), 2925-2933. doi:10.1111/acer.12568

Fortier, C. B., Leritz, E. C., Salat, D. H., Venne, J. R., Maksimovskiy, A. L., Williams, V., . . . McGlinchey, R. E. (2011). Reduced cortical thickness in abstinent alcoholics and association with alcoholic behavior. *Alcohol Clin Exp Res, 35*(12), 2193-2201. doi:10.1111/j.1530-0277.2011.01576.x

Friston, K. J., Williams, S., Howard, R., Frackowiak, R. S., & Turner, R. (1996). Movement-related effects in fMRI time-series. *Magn Reson Med, 35*(3), 346-355. doi:10.1002/mrm.1910350312

Fritz, M., Klawonn, A. M., & Zahr, N. M. (2019). Neuroimaging in alcohol use disorder: From mouse to man. *J Neurosci Res*. doi:10.1002/jnr.24423

Galandra, C., Basso, G., Manera, M., Crespi, C., Giorgi, I., Vittadini, G., . . . Canessa, N. (2019). Abnormal fronto-striatal intrinsic connectivity reflects executive dysfunction in alcohol use disorders. *Cortex, 115*, 27-42. doi:10.1016/j.cortex.2019.01.004

Galandra, C., Crespi, C., Basso, G., Manera, M. R., Giorgi, I., Poggi, P., & Canessa, N. (2020). Decreased information processing speed and decision-making performance in alcohol use disorder: combined neurostructural evidence from VBM and TBSS. *Brain Imaging Behav*. doi:10.1007/s11682-019-00248-8

Ganz, T. (2013). Systemic iron homeostasis. *Physiol Rev, 93*(4), 1721-1741. doi:10.1152/physrev.00008.2013

Gaser, C. (2019). TFCE Toolbox for SPM12 (Version r186). Retrieved from http://www.neuro.uni-jena.de/tfce/

Gaser, C., & Dahnke, R. (2016). *CAT-a computational anatomy toolbox for the analysis of structural MRI data*. Paper presented at the HBM 2016.

Gass, A., Niendorf, T., & Hirsch, J. G. (2001). Acute and chronic changes of the apparent diffusion coefficient in neurological disorders--biophysical mechanisms and possible underlying histopathology. *J Neurol Sci, 186 Suppl 1*, S15-23. doi:10.1016/s0022-510x(01)00487-7

Gazdzinski, S., Durazzo, T. C., & Meyerhoff, D. J. (2005). Temporal dynamics and determinants of whole brain tissue volume changes during recovery from alcohol dependence. *Drug Alcohol Depend, 78*(3), 263-273. doi:10.1016/j.drugalcdep.2004.11.004

Gazdzinski, S., Durazzo, T. C., Mon, A., Yeh, P. H., & Meyerhoff, D. J. (2010). Cerebral white matter recovery in abstinent alcoholics--a multimodality magnetic resonance study. *Brain, 133*(Pt 4), 1043-1053. doi:10.1093/brain/awp343

Gelman, N., Gorell, J. M., Barker, P. B., Savage, R. M., Spickler, E. M., Windham, J. P., & Knight, R. A. (1999). MR imaging of human brain at 3.0 T: preliminary report on transverse relaxation rates and relation to estimated iron content. *Radiology, 210*(3), 759-767. doi:10.1148/radiology.210.3.r99fe41759

Gilman, J. M., & Hommer, D. W. (2008). Modulation of brain response to emotional images by alcohol cues in alcohol-dependent patients. *Addict Biol, 13*(3-4), 423-434. doi:10.1111/j.1369-1600.2008.00111.x

Glover, G. H. (2011). Overview of functional magnetic resonance imaging. *Neurosurg Clin N Am, 22*(2), 133-139, vii. doi:10.1016/j.nec.2010.11.001

Goldstein, R. Z., & Volkow, N. D. (2002). Drug addiction and its underlying neurobiological basis: neuroimaging evidence for the involvement of the frontal cortex. *Am J Psychiatry, 159*(10), 1642-1652. doi:10.1176/appi.ajp.159.10.1642

Greve, D. N., & Fischl, B. (2009). Accurate and robust brain image alignment using boundary-based registration. *Neuroimage, 48*(1), 63-72. doi:10.1016/j.neuroimage.2009.06.060

Gulani, V., Webb, A. G., Duncan, I. D., & Lauterbur, P. C. (2001). Apparent diffusion tensor measurements in myelin-deficient rat spinal cords. *Magn Reson Med, 45*(2), 191-195. doi:10.1002/1522-2594(200102)45:2<191::aid-mrm1025>3.0.co;2-9

Haacke, E. M., Liu, S., Buch, S., Zheng, W., Wu, D., & Ye, Y. (2015). Quantitative susceptibility mapping: current status and future directions. *Magn Reson Imaging, 33*(1), 1-25. doi:10.1016/j.mri.2014.09.004

Hallgren, B., & Sourander, P. (1958). The effect of age on the non-haemin iron in the human brain. *J Neurochem, 3*(1), 41-51.

Hametner, S., Wimmer, I., Haider, L., Pfeifenbring, S., Bruck, W., & Lassmann, H. (2013). Iron and neurodegeneration in the multiple sclerosis brain. *Ann Neurol, 74*(6), 848-861. doi:10.1002/ana.23974

Han, H., Glenn, A. L., & Dawson, K. J. (2019). Evaluating Alternative Correction Methods for Multiple Comparison in Functional Neuroimaging Research. *Brain Sci, 9*(8). doi:10.3390/brainsci9080198

Haorah, J., Heilman, D., Knipe, B., Chrastil, J., Leibhart, J., Ghorpade, A., . . . Persidsky, Y. (2005). Ethanol-induced activation of myosin light chain kinase leads to dysfunction of tight junctions and blood-brain barrier compromise. *Alcohol Clin Exp Res, 29*(6), 999-1009.

Haorah, J., Knipe, B., Gorantla, S., Zheng, J., & Persidsky, Y. (2007). Alcohol-induced blood-brain barrier dysfunction is mediated via inositol 1,4,5-triphosphate receptor (IP3R)-gated intracellular calcium release. *J Neurochem, 100*(2), 324-336. doi:10.1111/j.1471-4159.2006.04245.x

Harding, A. J., Halliday, G. M., Ng, J. L., Harper, C. G., & Kril, J. J. (1996). Loss of vasopressin-immunoreactive neurons in alcoholics is dose-related and time-dependent. *Neuroscience, 72*(3), 699-708. doi:10.1016/0306-4522(95)00577-3

Hare, D. J., & Double, K. L. (2016). Iron and dopamine: a toxic couple. *Brain*. doi:10.1093/brain/aww022

Harper, C. (1998). The neuropathology of alcohol-specific brain damage, or does alcohol damage the brain? *J Neuropathol Exp Neurol, 57*(2), 101-110. doi:10.1097/00005072-199802000-00001

Harper, C. (2007). The neurotoxicity of alcohol. *Hum Exp Toxicol, 26*(3), 251-257. doi:10.1177/0960327107070499

Harper, C., Dixon, G., Sheedy, D., & Garrick, T. (2003). Neuropathological alterations in alcoholic brains. Studies arising from the New South Wales Tissue Resource Centre. *Prog Neuropsychopharmacol Biol Psychiatry, 27*(6), 951-961. doi:10.1016/s0278-5846(03)00155-6

Harper, C., & Kril, J. (1989). Patterns of neuronal loss in the cerebral cortex in chronic alcoholic patients. *J Neurol Sci, 92*(1), 81-89. doi:10.1016/0022-510x(89)90177-9

Harper, C., & Kril, J. (1991). If you drink your brain will shrink. Neuropathological considerations. *Alcohol Alcohol Suppl, 1*, 375-380.

Harper, C., Kril, J., & Daly, J. (1987). Are we drinking our neurones away? *Br Med J (Clin Res Ed), 294*(6571), 534-536. doi:10.1136/bmj.294.6571.534

Harris, G. J., Jaffin, S. K., Hodge, S. M., Kennedy, D., Caviness, V. S., Marinkovic, K., . . . Oscar-Berman, M. (2008). Frontal white matter and cingulum diffusion tensor imaging deficits in alcoholism. *Alcohol Clin Exp Res, 32*(6), 1001-1013. doi:10.1111/j.1530-0277.2008.00661.x

Harris, R. A., Trudell, J. R., & Mihic, S. J. (2008). Ethanol's Molecular Targets. *Science Signaling, 1*(28), re7. doi:10.1126/scisignal.128re7

Harsan, L. A., Poulet, P., Guignard, B., Steibel, J., Parizel, N., de Sousa, P. L., . . . Ghandour, M. S. (2006). Brain dysmyelination and recovery assessment by noninvasive in vivo diffusion tensor magnetic resonance imaging. *J Neurosci Res, 83*(3), 392-402. doi:10.1002/jnr.20742

Heatherton, T. F., Kozlowski, L. T., Frecker, R. C., & Fagerström, K. O. (1991). The Fagerström Test for Nicotine Dependence: a revision of the Fagerström Tolerance Questionnaire. *Br J Addict, 86*(9), 1119-1127.

Heinz, A., Dufeu, P., Kuhn, S., Dettling, M., Graf, K., Kurten, I., . . . Schmidt, L. G. (1996). Psychopathological and behavioral correlates of dopaminergic sensitivity in alcohol-dependent patients. *Arch Gen Psychiatry, 53*(12), 1123-1128.

Hermann, D., Weber-Fahr, W., Sartorius, A., Hoerst, M., Frischknecht, U., Tunc-Skarka, N., . . . Sommer, W. H. (2012). Translational magnetic resonance spectroscopy reveals excessive central glutamate levels during alcohol withdrawal in humans and rats. *Biol Psychiatry, 71*(11), 1015-1021. doi:10.1016/j.biopsych.2011.07.034

Herting, M. M., Schwartz, D., Mitchell, S. H., & Nagel, B. J. (2010). Delay discounting behavior and white matter microstructure abnormalities in youth with a family history of alcoholism. *Alcohol Clin Exp Res, 34*(9), 1590-1602. doi:10.1111/j.1530-0277.2010.01244.x

Hirth, N., Meinhardt, M. W., Noori, H. R., Salgado, H., Torres-Ramirez, O., Uhrig, S., . . . Hansson, A. C. (2016). Convergent evidence from alcohol-dependent humans and rats for a hyperdopaminergic state in protracted abstinence. *Proceedings of the National Academy of Sciences, 113*(11), 3024-3029. doi:10.1073/pnas.1506012113

Hobkirk, A. L., Bell, R. P., Utevsky, A. V., Huettel, S., & Meade, C. S. (2019). Reward and executive control network resting-state functional connectivity is associated with impulsivity during reward-based decision making for cocaine users. *Drug Alcohol Depend, 194*, 32-39. doi:10.1016/j.drugalcdep.2018.09.013

Hoefer, M. E., Pennington, D. L., Durazzo, T. C., Mon, A., Abe, C., Truran, D., . . . Meyerhoff, D. J. (2014). Genetic and behavioral determinants of hippocampal volume recovery during abstinence from alcohol. *Alcohol, 48*(7), 631-638. doi:10.1016/j.alcohol.2014.08.007

Hua, Y., Nakamura, T., Keep, R. F., Wu, J., Schallert, T., Hoff, J. T., & Xi, G. (2006). Long-term effects of experimental intracerebral hemorrhage: the role of iron. *J Neurosurg, 104*(2), 305-312. doi:10.3171/jns.2006.104.2.305

Hunt, J. R., Zito, C. A., & Johnson, L. K. (2009). Body iron excretion by healthy men and women. *Am J Clin Nutr, 89*(6), 1792-1798. doi:10.3945/ajcn.2009.27439

Hutton, C., Draganski, B., Ashburner, J., & Weiskopf, N. (2009). A comparison between voxel-based cortical thickness and voxel-based morphometry in normal aging. *Neuroimage, 48*(2), 371-380. doi:10.1016/j.neuroimage.2009.06.043

IBM Corp. (2011). IBM SPSS Statistics for Windows (Version 20.0). Armonk, NY: IBM Corp.

Im, S., Lee, S. G., Lee, J., Kim, S., Shin, C. J., Son, J. W., . . . Lee, S. I. (2016). Surface-Based Parameters of Brain Imaging in Male Patients with Alcohol Use Disorder. *Psychiatry Investig, 13*(5), 511-517. doi:10.4306/pi.2016.13.5.511

Ioannidis, J. P. (2011). Excess significance bias in the literature on brain volume abnormalities. *Arch Gen Psychiatry, 68*(8), 773-780. doi:10.1001/archgenpsychiatry.2011.28

Ito, R., Mori, S., & Melhem, E. R. (2002). Diffusion tensor brain imaging and tractography. *Neuroimaging Clin N Am, 12*(1), 1-19. doi:10.1016/s1052-5149(03)00067-4

Jenkinson, M. (2003). Fast, automated, N-dimensional phase-unwrapping algorithm. *Magn Reson Med, 49*(1), 193-197. doi:10.1002/mrm.10354

Jenkinson, M., Bannister, P., Brady, M., & Smith, S. (2002). Improved optimization for the robust and accurate linear registration and motion correction of brain images. *Neuroimage, 17*(2), 825-841.

Jenkinson, M., Beckmann, C. F., Behrens, T. E., Woolrich, M. W., & Smith, S. M. (2012). FSL. *Neuroimage, 62*(2), 782-790. doi:10.1016/j.neuroimage.2011.09.015

Jenkinson, M., & Smith, S. (2001). A global optimisation method for robust affine registration of brain images. *Med Image Anal, 5*(2), 143-156.

Jensen, G. B., & Pakkenberg, B. (1993). Do alcoholics drink their neurons away? *Lancet, 342*(8881), 1201-1204. doi:10.1016/0140-6736(93)92185-v

Jones, D. K., Knösche, T. R., & Turner, R. (2013). White matter integrity, fiber count, and other fallacies: the do's and don'ts of diffusion MRI. *Neuroimage, 73*, 239-254. doi:10.1016/j.neuroimage.2012.06.081

Juhás, M., Sun, H., Brown, M. R. G., MacKay, M. B., Mann, K. F., Sommer, W. H., . . . Greenshaw, A. J. (2017). Deep grey matter iron accumulation in alcohol use disorder. *Neuroimage, 148*, 115-122. doi:10.1016/j.neuroimage.2017.01.007

Jurczuk, M., Brzoska, M. M., Rogalska, J., & Moniuszko-Jakoniuk, J. (2003). Iron body status of rats chronically exposed to cadmium and ethanol. *Alcohol Alcohol, 38*(3), 202-207.

Kareken, D. A., Bragulat, V., Dzemidzic, M., Cox, C., Talavage, T., Davidson, D., & O'Connor, S. J. (2010). Family history of alcoholism mediates the frontal response to alcoholic drink odors and alcohol in at-risk drinkers. *Neuroimage, 50*(1), 267-276. doi:10.1016/j.neuroimage.2009.11.076

Kashem, M. A., Harper, C., & Matsumoto, I. (2008). Differential protein expression in the corpus callosum (genu) of human alcoholics. *Neurochem Int, 53*(1-2), 1-11. doi:10.1016/j.neuint.2008.04.003

Kelley, K. W., & Dantzer, R. (2011). Alcoholism and inflammation: neuroimmunology of behavioral and mood disorders. *Brain Behav Immun, 25 Suppl 1*, S13-20. doi:10.1016/j.bbi.2010.12.013

Kim, H., Kim, Y. K., Gwak, A. R., Lim, J. A., Lee, J. Y., Jung, H. Y., . . . Choi, J. S. (2015). Resting-state regional homogeneity as a biological marker for patients with Internet gaming disorder: A comparison with patients with alcohol use disorder and healthy controls. *Prog Neuropsychopharmacol Biol Psychiatry, 60*, 104-111. doi:10.1016/j.pnpbp.2015.02.004

Kim, S., Im, S., Lee, J., & Lee, S. G. (2017). Disrupted Control Network Connectivity in Abstinent Patients with Alcohol Dependence. *Psychiatry Investig, 14*(3), 325-332. doi:10.4306/pi.2017.14.3.325

Koeppen, A. H. (2003). A brief history of brain iron research. *J Neurol Sci, 207*(1-2), 95-97.

Kohgo, Y., Ikuta, K., Ohtake, T., Torimoto, Y., & Kato, J. (2008). Body iron metabolism and pathophysiology of iron overload. *International Journal of Hematology, 88*(1), 7-15. doi:10.1007/s12185-008-0120-5

Kohgo, Y., Ohtake, T., Ikuta, K., Suzuki, Y., Hosoki, Y., Saito, H., & Kato, J. (2005). Iron accumulation in alcoholic liver diseases. *Alcohol Clin Exp Res, 29*(11 Suppl), 189S-193S.

Kohgo, Y., Ohtake, T., Ikuta, K., Suzuki, Y., Torimoto, Y., & Kato, J. (2008). Dysregulation of systemic iron metabolism in alcoholic liver diseases. *J Gastroenterol Hepatol, 23 Suppl 1*, S78-81. doi:10.1111/j.1440-1746.2007.05290.x

Kohno, M., Dennis, L. E., McCready, H., & Hoffman, W. F. (2017). Executive Control and Striatal Resting-State Network Interact with Risk Factors to Influence Treatment Outcomes in Alcohol-Use Disorder. *Front Psychiatry, 8*, 182. doi:10.3389/fpsyt.2017.00182

Konrad, A., Vucurevic, G., Lorscheider, M., Bernow, N., Thummel, M., Chai, C., . . . Fehr, C. (2012). Broad disruption of brain white matter microstructure and relationship with neuropsychological performance in male patients with severe alcohol dependence. *Alcohol Alcohol, 47*(2), 118-126. doi:10.1093/alcalc/agr157

Koob, G. F., & Volkow, N. D. (2010). Neurocircuitry of addiction. *Neuropsychopharmacology, 35*(1), 217-238. doi:10.1038/npp.2009.110

Koob, G. F., & Volkow, N. D. (2016). Neurobiology of addiction: a neurocircuitry analysis. *Lancet Psychiatry, 3*(8), 760-773. doi:10.1016/S2215-0366(16)00104-8

Korbo, L. (1999). Glial cell loss in the hippocampus of alcoholics. *Alcohol Clin Exp Res, 23*(1), 164-168.

Kril, J. J., Halliday, G. M., Svoboda, M. D., & Cartwright, H. (1997). The cerebral cortex is damaged in chronic alcoholics. *Neuroscience, 79*(4), 983-998. doi:https://doi.org/10.1016/S0306-4522(97)00083-3

Kulaga-Yoskovitz, J., Bernhardt, B. C., Hong, S. J., Mansi, T., Liang, K. E., van der Kouwe, A. J., . . . Bernasconi, N. (2015). Multi-contrast submillimetric 3 Tesla hippocampal subfield segmentation protocol and dataset. *Sci Data, 2*, 150059. doi:10.1038/sdata.2015.59

Kurth, F., & Gaser, C. (2019). Computational Anatomy Toolbox - CAT12 Manual. In: University of Jena.

Kühn, S., Charlet, K., Schubert, F., Kiefer, F., Zimmermann, P., Heinz, A., & Gallinat, J. (2014). Plasticity of hippocampal subfield volume cornu ammonis 2+3 over the course of withdrawal in patients with alcohol dependence. *JAMA Psychiatry, 71*(7), 806-811. doi:10.1001/jamapsychiatry.2014.352

Kühn, S., Witt, C., Banaschewski, T., Barbot, A., Barker, G. J., Büchel, C., . . . Consortium, I. (2016). From mother to child: orbitofrontal cortex gyrification and changes of drinking behaviour during adolescence. *Addict Biol, 21*(3), 700-708. doi:10.1111/adb.12240

Laird, A. R., Fox, P. M., Eickhoff, S. B., Turner, J. A., Ray, K. L., McKay, D. R., . . . Fox, P. T. (2011). Behavioral interpretations of intrinsic connectivity networks. *J Cogn Neurosci, 23*(12), 4022-4037. doi:10.1162/jocn_a_00077

Langkammer, C., Schweser, F., Krebs, N., Deistung, A., Goessler, W., Scheurer, E., . . . Reichenbach, J. R. (2012). Quantitative susceptibility mapping (QSM) as a means to measure brain iron? A post mortem validation study. *Neuroimage, 62*(3), 1593-1599. doi:10.1016/j.neuroimage.2012.05.049

Lazar, M., Weinstein, D. M., Tsuruda, J. S., Hasan, K. M., Arfanakis, K., Meyerand, M. E., . . . Alexander, A. L. (2003). White matter tractography using diffusion tensor deflection. *Hum Brain Mapp, 18*(4), 306-321. doi:10.1002/hbm.10102

Le Berre, A. P., Fama, R., & Sullivan, E. V. (2017). Executive Functions, Memory, and Social Cognitive Deficits and Recovery in Chronic Alcoholism: A Critical Review to Inform Future Research. *Alcohol Clin Exp Res, 41*(8), 1432-1443. doi:10.1111/acer.13431

Le Bihan, D., Mangin, J. F., Poupon, C., Clark, C. A., Pappata, S., Molko, N., & Chabriat, H. (2001). Diffusion tensor imaging: concepts and applications. *J Magn Reson Imaging, 13*(4), 534-546. doi:10.1002/jmri.1076

Leclercq, S., De Saeger, C., Delzenne, N., de Timary, P., & Stärkel, P. (2014). Role of inflammatory pathways, blood mononuclear cells, and gut-derived bacterial products in alcohol dependence. *Biol Psychiatry, 76*(9), 725-733. doi:10.1016/j.biopsych.2014.02.003

Lee, J., Im, S. J., Lee, S. G., Stadlin, A., Son, J. W., Shin, C. J., . . . Kim, S. (2016). Volume of hippocampal subfields in patients with alcohol dependence. *Psychiatry Res Neuroimaging, 258*, 16-22. doi:10.1016/j.pscychresns.2016.10.009

LeVine, S. M., & Macklin, W. B. (1990). Iron-enriched oligodendrocytes: a reexamination of their spatial distribution. *J Neurosci Res, 26*(4), 508-512. doi:10.1002/jnr.490260415

Lewohl, J. M., Wang, L., Miles, M. F., Zhang, L., Dodd, P. R., & Harris, R. A. (2000). Gene expression in human alcoholism: microarray analysis of frontal cortex. *Alcohol Clin Exp Res, 24*(12), 1873-1882.

Li, W., Wu, B., Batrachenko, A., Bancroft-Wu, V., Morey, R. A., Shashi, V., . . . Liu, C. (2014). Differential developmental trajectories of magnetic susceptibility in human brain gray and white matter over the lifespan. *Hum Brain Mapp, 35*(6), 2698-2713. doi:10.1002/hbm.22360

Liu, C., Li, W., Tong, K. A., Yeom, K. W., & Kuzminski, S. (2015). Susceptibility-weighted imaging and quantitative susceptibility mapping in the brain. *J Magn Reson Imaging, 42*(1), 23-41. doi:10.1002/jmri.24768

Liu, I. C., Chiu, C. H., Chen, C. J., Kuo, L. W., Lo, Y. C., & Tseng, W. Y. (2010). The microstructural integrity of the corpus callosum and associated impulsivity in alcohol dependence: a tractography-based segmentation study using diffusion spectrum imaging. *Psychiatry Res, 184*(2), 128-134. doi:10.1016/j.pscychresns.2010.07.002

Liu, R., Liu, B. X., Ma, M., Kong, D., Li, G., Yang, J., . . . Dong, Y. (2018). Aberrant prefrontal-parietal-cerebellar circuits in alcohol dependence. *Neuropsychiatr Dis Treat, 14*, 3143-3150. doi:10.2147/NDT.S178257

Liu, R. S., Lemieux, L., Shorvon, S. D., Sisodiya, S. M., & Duncan, J. S. (2000). Association between brain size and abstinence from alcohol. *Lancet, 355*(9219), 1969-1970. doi:10.1016/s0140-6736(00)02332-1

Logothetis, N. K. (2003). The underpinnings of the BOLD functional magnetic resonance imaging signal. *J Neurosci, 23*(10), 3963-3971.

Logothetis, N. K. (2008). What we can do and what we cannot do with fMRI. *Nature, 453*(7197), 869-878. doi:10.1038/nature06976

Logothetis, N. K., Pauls, J., Augath, M., Trinath, T., & Oeltermann, A. (2001). Neurophysiological investigation of the basis of the fMRI signal. *Nature, 412*(6843), 150-157. doi:10.1038/35084005

Luigjes, J., Segrave, R., de Joode, N., Figee, M., & Denys, D. (2019). Efficacy of Invasive and Non-Invasive Brain Modulation Interventions for Addiction. *Neuropsychol Rev, 29*(1), 116-138. doi:10.1007/s11065-018-9393-5

Luo, J. (2015). Effects of Ethanol on the Cerebellum: Advances and Prospects. *Cerebellum, 14*(4), 383-385. doi:10.1007/s12311-015-0674-8

Luo, X., Guo, L., Dai, X. J., Wang, Q., Zhu, W., Miao, X., & Gong, H. (2017). Abnormal intrinsic functional hubs in alcohol dependence: evidence from a voxelwise degree centrality analysis. *Neuropsychiatr Dis Treat, 13*, 2011-2020. doi:10.2147/NDT.S142742

Mackey, S., Allgaier, N., Chaarani, B., Spechler, P., Orr, C., Bunn, J., . . . Group, E. A. W. (2019). Mega-Analysis of Gray Matter Volume in Substance Dependence: General and Substance-Specific Regional Effects. *Am J Psychiatry, 176*(2), 119-128. doi:10.1176/appi.ajp.2018.17040415

Mackiewicz Seghete, K. L., Cservenka, A., Herting, M. M., & Nagel, B. J. (2013). Atypical spatial working memory and task-general brain activity in adolescents with a family history of alcoholism. *Alcohol Clin Exp Res, 37*(3), 390-398. doi:10.1111/j.1530-0277.2012.01948.x

Manjón, J. V., & Coupé, P. (2016). volBrain: An Online MRI Brain Volumetry System. *Front Neuroinform, 10*, 30. doi:10.3389/fninf.2016.00030

Mann, K., Ackermann, K., Croissant, B., Mundle, G., Nakovics, H., & Diehl, A. (2005). Neuroimaging of gender differences in alcohol dependence: are women more vulnerable? *Alcohol Clin Exp Res, 29*(5), 896-901. doi:10.1097/01.alc.0000164376.69978.6b

Mann, K., Günther, A., Stetter, F., & Ackermann, K. (1999). Rapid recovery from cognitive deficits in abstinent alcoholics: a controlled test-retest study. *Alcohol Alcohol, 34*(4), 567-574. doi:10.1093/alcalc/34.4.567

Marchiafava, E. (1933). The Degeneration of the Brain in Chronic Alcoholism. *Proc R Soc Med, 26*(9), 1151-1158.

Marinkovic, K., Oscar-Berman, M., Urban, T., O'Reilly, C. E., Howard, J. A., Sawyer, K., & Harris, G. J. (2009). Alcoholism and dampened temporal limbic activation to emotional faces. *Alcohol Clin Exp Res, 33*(11), 1880-1892. doi:10.1111/j.1530-0277.2009.01026.x

Mayfield, R. D., Lewohl, J. M., Dodd, P. R., Herlihy, A., Liu, J., & Harris, R. A. (2002). Patterns of gene expression are altered in the frontal and motor cortices of human alcoholics. *J Neurochem, 81*(4), 802-813. doi:10.1046/j.1471-4159.2002.00860.x

McClure, S. M., Laibson, D. I., Loewenstein, G., & Cohen, J. D. (2004). Separate neural systems value immediate and delayed monetary rewards. *Science, 306*(5695), 503-507. doi:10.1126/science.1100907

McEvoy, L. K., Fennema-Notestine, C., Elman, J. A., Eyler, L. T., Franz, C. E., Hagler, D. J., Jr., . . . Kremen, W. S. (2018). Alcohol intake and brain white matter in middle aged men: Microscopic and macroscopic differences. *NeuroImage. Clinical, 18*, 390-398. doi:10.1016/j.nicl.2018.02.006

Melega, W. P., Lacan, G., Harvey, D. C., & Way, B. M. (2007). Methamphetamine increases basal ganglia iron to levels observed in aging. *Neuroreport, 18*(16), 1741-1745. doi:10.1097/WNR.0b013e3282f0d4f4

Meyerhoff, D. J., Blumenfeld, R., Truran, D., Lindgren, J., Flenniken, D., Cardenas, V., . . . Weiner, M. W. (2004). Effects of heavy drinking, binge drinking, and family history of alcoholism on regional brain metabolites. *Alcohol Clin Exp Res, 28*(4), 650-661. doi:10.1097/01.alc.0000121805.12350.ca

Miguel-Hidalgo, J. J., Wei, J., Andrew, M., Overholser, J. C., Jurjus, G., Stockmeier, C. A., & Rajkowska, G. (2002). Glia pathology in the prefrontal cortex in alcohol dependence with and without depressive symptoms. *Biol Psychiatry, 52*(12), 1121-1133. doi:10.1016/s0006-3223(02)01439-7

Milman, N., & Kirchhoff, M. (1996). Relationship between serum ferritin, alcohol intake, and social status in 2235 Danish men and women. *Ann Hematol, 72*(3), 145-151.

Momenan, R., Steckler, L. E., Saad, Z. S., van Rafelghem, S., Kerich, M. J., & Hommer, D. W. (2012). Effects of alcohol dependence on cortical thickness as determined by magnetic resonance imaging. *Psychiatry Res, 204*(2-3), 101-111. doi:10.1016/j.pscychresns.2012.05.003

Mon, A., Delucchi, K., Durazzo, T. C., Gazdzinski, S., & Meyerhoff, D. J. (2011). A mathematical formula for prediction of gray and white matter volume recovery in abstinent alcohol dependent individuals. *Psychiatry Res, 194*(2), 198-204. doi:10.1016/j.pscychresns.2011.05.003

Mon, A., Durazzo, T. C., Gazdzinski, S., Hutchison, K. E., Pennington, D., & Meyerhoff, D. J. (2013). Brain-derived neurotrophic factor genotype is associated with brain gray and white matter tissue volumes recovery in abstinent alcohol-dependent individuals. *Genes Brain Behav, 12*(1), 98-107. doi:10.1111/j.1601-183X.2012.00854.x

Monnig, M. A., Caprihan, A., Yeo, R. A., Gasparovic, C., Ruhl, D. A., Lysne, P., . . . Thoma, R. J. (2013). Diffusion tensor imaging of white matter networks in individuals with current and remitted alcohol use disorders and comorbid conditions. *Psychol Addict Behav, 27*(2), 455-465. doi:10.1037/a0027168

Monnig, M. A., Thayer, R. E., Caprihan, A., Claus, E. D., Yeo, R. A., Calhoun, V. D., & Hutchison, K. E. (2014). White matter integrity is associated with alcohol cue reactivity in heavy drinkers. *Brain Behav, 4*(2), 158-170. doi:10.1002/brb3.204

Monnig, M. A., Tonigan, J. S., Yeo, R. A., Thoma, R. J., & McCrady, B. S. (2013). White matter volume in alcohol use disorders: a meta-analysis. *Addict Biol, 18*(3), 581-592. doi:10.1111/j.1369-1600.2012.00441.x

Monnig, M. A., Yeo, R. A., Tonigan, J. S., McCrady, B. S., Thoma, R. J., Sabbineni, A., & Hutchison, K. E. (2015). Associations of White Matter Microstructure with Clinical and Demographic Characteristics in Heavy Drinkers. *PLoS One, 10*(11), e0142042. doi:10.1371/journal.pone.0142042

Moos, R. H., & Moos, B. S. (2006). Rates and predictors of relapse after natural and treated remission from alcohol use disorders. *Addiction, 101*(2), 212-222. doi:10.1111/j.1360-0443.2006.01310.x

Moos, T. (2002). Brain iron homeostasis. *Dan Med Bull, 49*(4), 279-301.

Moos, T., & Morgan, E. H. (1998). Kinetics and distribution of [59Fe-125I]transferrin injected into the ventricular system of the rat. *Brain Res, 790*(1-2), 115-128.

Moos, T., Rosengren Nielsen, T., Skjorringe, T., & Morgan, E. H. (2007). Iron trafficking inside the brain. *J Neurochem, 103*(5), 1730-1740. doi:10.1111/j.1471-4159.2007.04976.x

Mori, S., Wakana, S., Van Zijl, P. C., & Nagae-Poetscher, L. (2005). *MRI atlas of human white matter*: Elsevier.

Morris, L. S., Baek, K., Tait, R., Elliott, R., Ersche, K. D., Flechais, R., . . . Consortium, I. (2018). Naltrexone ameliorates functional network abnormalities in alcohol-dependent individuals. *Addict Biol, 23*(1), 425-436. doi:10.1111/adb.12503

Moulton, E. A., Elman, I., Becerra, L. R., Goldstein, R. Z., & Borsook, D. (2014). The cerebellum and addiction: insights gained from neuroimaging research. *Addict Biol, 19*(3), 317-331. doi:10.1111/adb.12101

Muller-Oehring, E. M., Schulte, T., Fama, R., Pfefferbaum, A., & Sullivan, E. V. (2009). Global-local interference is related to callosal compromise in alcoholism: a behavior-DTI association study. *Alcohol Clin Exp Res, 33*(3), 477-489. doi:10.1111/j.1530-0277.2008.00858.x

Munro, C. A., Saxton, J., & Butters, M. A. (2000). The neuropsychological consequences of abstinence among older alcoholics: a cross-sectional study. *Alcohol Clin Exp Res, 24*(10), 1510-1516.

Muuronen, A., Bergman, H., Hindmarsh, T., & Telakivi, T. (1989). Influence of improved drinking habits on brain atrophy and cognitive performance in alcoholic patients: a 5-year follow-up study. *Alcohol Clin Exp Res, 13*(1), 137-141. doi:10.1111/j.1530-0277.1989.tb00298.x

Müller-Oehring, E. M., Jung, Y. C., Pfefferbaum, A., Sullivan, E. V., & Schulte, T. (2015). The Resting Brain of Alcoholics. *Cereb Cortex, 25*(11), 4155-4168. doi:10.1093/cercor/bhu134

Neil, J. J., Shiran, S. I., McKinstry, R. C., Schefft, G. L., Snyder, A. Z., Almli, C. R., . . . Conturo, T. E. (1998). Normal brain in human newborns: apparent diffusion coefficient and diffusion anisotropy

measured by using diffusion tensor MR imaging. *Radiology, 209*(1), 57-66. doi:10.1148/radiology.209.1.9769812

Nickerson, L. D., Smith, S. M., Öngür, D., & Beckmann, C. F. (2017). Using Dual Regression to Investigate Network Shape and Amplitude in Functional Connectivity Analyses. *Front Neurosci, 11*, 115. doi:10.3389/fnins.2017.00115

Noble, S., Scheinost, D., & Constable, R. T. (2019). A decade of test-retest reliability of functional connectivity: A systematic review and meta-analysis. *Neuroimage, 203*, 116157. doi:10.1016/j.neuroimage.2019.116157

Noonberg, A., Goldstein, G., & Page, H. A. (1985). Premature aging in male alcoholics: "accelerated aging" or "increased vulnerability"? *Alcohol Clin Exp Res, 9*(4), 334-338.

Nordmann, R., Ribiere, C., & Rouach, H. (1987). Involvement of iron and iron-catalyzed free radical production in ethanol metabolism and toxicity. *Enzyme, 37*(1-2), 57-69.

Nordmann, R., Ribiere, C., & Rouach, H. (1990). Ethanol-induced lipid peroxidation and oxidative stress in extrahepatic tissues. *Alcohol Alcohol, 25*(2-3), 231-237.

Nutt, D. J., King, L. A., & Phillips, L. D. (2010). Drug harms in the UK: a multicriteria decision analysis. *Lancet, 376*(9752), 1558-1565. doi:10.1016/s0140-6736(10)61462-6

O'Neill, J., Cardenas, V. A., & Meyerhoff, D. J. (2001). Effects of abstinence on the brain: quantitative magnetic resonance imaging and magnetic resonance spectroscopic imaging in chronic alcohol abuse. *Alcohol Clin Exp Res, 25*(11), 1673-1682.

Oldfield, R. C. (1971). The assessment and analysis of handedness: the Edinburgh inventory. *Neuropsychologia, 9*(1), 97-113.

Oscar-Berman, M., & Marinkovic, K. (2003). Alcoholism and the brain: an overview. *Alcohol Res Health, 27*(2), 125-133.

Oscar-Berman, M., & Marinković, K. (2007). Alcohol: effects on neurobehavioral functions and the brain. *Neuropsychol Rev, 17*(3), 239-257. doi:10.1007/s11065-007-9038-6

Pan, P., Zhan, H., Xia, M., Zhang, Y., Guan, D., & Xu, Y. (2017). Aberrant regional homogeneity in Parkinson's disease: A voxel-wise meta-analysis of resting-state functional magnetic resonance imaging studies. *Neurosci Biobehav Rev, 72*, 223-231. doi:10.1016/j.neubiorev.2016.11.018

Pandey, A. K., Ardekani, B. A., Kamarajan, C., Zhang, J., Chorlian, D. B., Byrne, K. N., . . . Porjesz, B. (2018). Lower Prefrontal and Hippocampal Volume and Diffusion Tensor Imaging Differences Reflect Structural and Functional Abnormalities in Abstinent Individuals with Alcohol Use Disorder. *Alcohol Clin Exp Res, 42*(10), 1883-1896. doi:10.1111/acer.13854

Parks, M. H., Dawant, B. M., Riddle, W. R., Hartmann, S. L., Dietrich, M. S., Nickel, M. K., . . . Martin, P. R. (2002). Longitudinal brain metabolic characterization of chronic alcoholics with proton magnetic resonance spectroscopy. *Alcohol Clin Exp Res, 26*(9), 1368-1380. doi:10.1097/01.ALC.0000029598.07833.2D

Parks, M. H., Greenberg, D. S., Nickel, M. K., Dietrich, M. S., Rogers, B. P., & Martin, P. R. (2010). Recruitment of additional brain regions to accomplish simple motor tasks in chronic alcohol-dependent patients. *Alcohol Clin Exp Res, 34*(6), 1098-1109. doi:10.1111/j.1530-0277.2010.01186.x

Paula-Barbosa, M. M., & Tavares, M. A. (1985). Long term alcohol consumption induces microtubular changes in the adult rat cerebellar cortex. *Brain Res, 339*(1), 195-199. doi:10.1016/0006-8993(85)90645-6

Pernet, C. R., Latinus, M., Nichols, T. E., & Rousselet, G. A. (2015). Cluster-based computational methods for mass univariate analyses of event-related brain potentials/fields: A simulation study. *J Neurosci Methods, 250*, 85-93. doi:10.1016/j.jneumeth.2014.08.003

Petit, G., Luminet, O., Cordovil de Sousa Uva, M., Zorbas, A., Maurage, P., & de Timary, P. (2017). Differential spontaneous recovery across cognitive abilities during detoxification period in alcohol-dependence. *PLoS One, 12*(8), e0176638. doi:10.1371/journal.pone.0176638

Pfefferbaum, A., Adalsteinsson, E., & Sullivan, E. V. (2003). Replicability of diffusion tensor imaging measurements of fractional anisotropy and trace in brain. *J Magn Reson Imaging, 18*(4), 427-433. doi:10.1002/jmri.10377

Pfefferbaum, A., Adalsteinsson, E., & Sullivan, E. V. (2006a). Dysmorphology and microstructural degradation of the corpus callosum: Interaction of age and alcoholism. *Neurobiol Aging, 27*(7), 994-1009. doi:10.1016/j.neurobiolaging.2005.05.007

Pfefferbaum, A., Adalsteinsson, E., & Sullivan, E. V. (2006b). Supratentorial profile of white matter microstructural integrity in recovering alcoholic men and women. *Biol Psychiatry, 59*(4), 364-372. doi:10.1016/j.biopsych.2005.06.025

Pfefferbaum, A., Lim, K. O., Zipursky, R. B., Mathalon, D. H., Rosenbloom, M. J., Lane, B., . . . Sullivan, E. V. (1992). Brain gray and white matter volume loss accelerates with aging in chronic alcoholics: a quantitative MRI study. *Alcohol Clin Exp Res, 16*(6), 1078-1089.

Pfefferbaum, A., Rosenbloom, M., Rohlfing, T., & Sullivan, E. V. (2009). Degradation of association and projection white matter systems in alcoholism detected with quantitative fiber tracking. *Biol Psychiatry, 65*(8), 680-690. doi:10.1016/j.biopsych.2008.10.039

Pfefferbaum, A., Rosenbloom, M. J., Adalsteinsson, E., & Sullivan, E. V. (2007). Diffusion tensor imaging with quantitative fibre tracking in HIV infection and alcoholism comorbidity: synergistic white matter damage. *Brain, 130*(Pt 1), 48-64. doi:10.1093/brain/awl242

Pfefferbaum, A., Rosenbloom, M. J., Chu, W., Sassoon, S. A., Rohlfing, T., Pohl, K. M., . . . Sullivan, E. V. (2014). White matter microstructural recovery with abstinence and decline with relapse in alcohol dependence interacts with normal ageing: a controlled longitudinal DTI study. *Lancet Psychiatry, 1*(3), 202-212. doi:10.1016/S2215-0366(14)70301-3

Pfefferbaum, A., Rosenbloom, M. J., Fama, R., Sassoon, S. A., & Sullivan, E. V. (2010). Transcallosal white matter degradation detected with quantitative fiber tracking in alcoholic men and women: selective relations to dissociable functions. *Alcohol Clin Exp Res, 34*(7), 1201-1211. doi:10.1111/j.1530-0277.2010.01197.x

Pfefferbaum, A., & Sullivan, E. V. (2002). Microstructural but not macrostructural disruption of white matter in women with chronic alcoholism. *Neuroimage, 15*(3), 708-718. doi:10.1006/nimg.2001.1018

Pfefferbaum, A., & Sullivan, E. V. (2005). Disruption of brain white matter microstructure by excessive intracellular and extracellular fluid in alcoholism: evidence from diffusion tensor imaging. *Neuropsychopharmacology, 30*(2), 423-432. doi:10.1038/sj.npp.1300623

Pfefferbaum, A., Sullivan, E. V., Hedehus, M., Adalsteinsson, E., Lim, K. O., & Moseley, M. (2000). In vivo detection and functional correlates of white matter microstructural disruption in chronic alcoholism. *Alcohol Clin Exp Res, 24*(8), 1214-1221.

Pfefferbaum, A., Sullivan, E. V., Mathalon, D. H., Shear, P. K., Rosenbloom, M. J., & Lim, K. O. (1995). Longitudinal changes in magnetic resonance imaging brain volumes in abstinent and relapsed alcoholics. *Alcohol Clin Exp Res, 19*(5), 1177-1191. doi:10.1111/j.1530-0277.1995.tb01598.x

Pfefferbaum, A., Zahr, N. M., Mayer, D., Rohlfing, T., & Sullivan, E. V. (2015). Dynamic responses of selective brain white matter fiber tracts to binge alcohol and recovery in the rat. *PLoS One, 10*(4), e0124885. doi:10.1371/journal.pone.0124885

Picchietti, D. (2007). Is iron deficiency an underlying cause of pediatric restless legs syndrome and of attention-deficit/hyperactivity disorder? *Sleep Med, 8*(7-8), 693-694. doi:10.1016/j.sleep.2007.06.007

Pierpaoli, C., Barnett, A., Pajevic, S., Chen, R., Penix, L. R., Virta, A., & Basser, P. (2001). Water diffusion changes in Wallerian degeneration and their dependence on white matter architecture. *Neuroimage, 13*(6 Pt 1), 1174-1185. doi:10.1006/nimg.2001.0765

Pierpaoli, C., & Basser, P. J. (1996). Toward a quantitative assessment of diffusion anisotropy. *Magn Reson Med, 36*(6), 893-906. doi:10.1002/mrm.1910360612

Pitel, A. L., Chanraud, S., Sullivan, E. V., & Pfefferbaum, A. (2010). Callosal microstructural abnormalities in Alzheimer's disease and alcoholism: same phenotype, different mechanisms. *Psychiatry Res, 184*(1), 49-56. doi:10.1016/j.pscychresns.2010.07.006

Putzke, J., De Beun, R., Schreiber, R., De Vry, J., Tölle, T. R., Zieglgänsberger, W., & Spanagel, R. (1998). Long-term alcohol self-administration and alcohol withdrawal differentially modulate microtubule-associated protein 2 (MAP2) gene expression in the rat brain. *Brain Res Mol Brain Res, 62*(2), 196-205. doi:10.1016/s0169-328x(98)00253-8

Radlowski, E. C., & Johnson, R. W. (2013). Perinatal iron deficiency and neurocognitive development. *Front Hum Neurosci, 7*, 585. doi:10.3389/fnhum.2013.00585

Rando, K., Hong, K. I., Bhagwagar, Z., Li, C. S., Bergquist, K., Guarnaccia, J., & Sinha, R. (2011). Association of frontal and posterior cortical gray matter volume with time to alcohol relapse: a prospective study. *Am J Psychiatry, 168*(2), 183-192. doi:10.1176/appi.ajp.2010.10020233

Rao, H., Korczykowski, M., Pluta, J., Hoang, A., & Detre, J. A. (2008). Neural correlates of voluntary and involuntary risk taking in the human brain: an fMRI Study of the Balloon Analog Risk Task (BART). *Neuroimage, 42*(2), 902-910. doi:10.1016/j.neuroimage.2008.05.046

Robinson, S., Godfrey, K., Denne, J., & Cox, V. (1998). The determinants of iron status in early pregnancy. *Br J Nutr, 79*(3), 249-255.

Romero, J. E., Coupé, P., Giraud, R., Ta, V. T., Fonov, V., Park, M. T. M., . . . Manjón, J. V. (2017). CERES: A new cerebellum lobule segmentation method. *Neuroimage, 147*, 916-924. doi:10.1016/j.neuroimage.2016.11.003

Romero, J. E., Coupé, P., & Manjón, J. V. (2017). HIPS: A new hippocampus subfield segmentation method. *Neuroimage, 163*, 286-295. doi:10.1016/j.neuroimage.2017.09.049

Ron, M. A., Acker, W., Shaw, G. K., & Lishman, W. A. (1982). Computerized tomography of the brain in chronic alcoholism: a Survey and follow-up study. *Brain, 105 (Pt 3)*, 497-514. doi:10.1093/brain/105.3.497

Rosenbloom, M., Sullivan, E. V., & Pfefferbaum, A. (2003). Using magnetic resonance imaging and diffusion tensor imaging to assess brain damage in alcoholics. *Alcohol Res Health, 27*(2), 146-152.

Rosenbloom, M. J., Rohlfing, T., O'Reilly, A. W., Sassoon, S. A., Pfefferbaum, A., & Sullivan, E. V. (2007). Improvement in memory and static balance with abstinence in alcoholic men and women: selective relations with change in brain structure. *Psychiatry Res, 155*(2), 91-102. doi:10.1016/j.pscychresns.2006.12.019

Rossetti, Z. L., Melis, F., Carboni, S., & Gessa, G. L. (1992). Dramatic depletion of mesolimbic extracellular dopamine after withdrawal from morphine, alcohol or cocaine: a common neurochemical substrate for drug dependence. *Ann N Y Acad Sci, 654*, 513-516.

Rouach, H., Fataccioli, V., Gentil, M., French, S. W., Morimoto, M., & Nordmann, R. (1997). Effect of chronic ethanol feeding on lipid peroxidation and protein oxidation in relation to liver pathology. *Hepatology, 25*(2), 351-355. doi:10.1002/hep.510250216

Rouach, H., Houze, P., Gentil, M., Orfanelli, M. T., & Nordmann, R. (1994). Effects of acute ethanol administration on the uptake of 59Fe-labeled transferrin by rat liver and cerebellum. *Biochem Pharmacol, 47*(10), 1835-1841.

Rouach, H., Houze, P., Gentil, M., Orfanelli, M. T., & Nordmann, R. (1997). Changes in some pro- and antioxidants in rat cerebellum after chronic alcohol intake. *Biochem Pharmacol, 53*(4), 539-545.

Rouach, H., Houze, P., Orfanelli, M. T., Gentil, M., Bourdon, R., & Nordmann, R. (1990). Effect of acute ethanol administration on the subcellular distribution of iron in rat liver and cerebellum. *Biochem Pharmacol, 39*(6), 1095-1100.

Rouault, T. A. (2013). Iron metabolism in the CNS: implications for neurodegenerative diseases. *Nat Rev Neurosci, 14*(8), 551-564. doi:10.1038/nrn3453

Ryan, C., & Butters, N. (1984). Alcohol consumption and premature aging. A critical review. *Recent Dev Alcohol, 2*, 223-250.

Sanhueza, C., Garcia-Moreno, L. M., & Exposito, J. (2011). Weekend alcoholism in youth and neurocognitive aging. *Psicothema, 23*(2), 209-214.

Saunders, J. B., Aasland, O. G., Babor, T. F., de la Fuente, J. R., & Grant, M. (1993). Development of the Alcohol Use Disorders Identification Test (AUDIT): WHO Collaborative Project on Early Detection of Persons with Harmful Alcohol Consumption--II. *Addiction, 88*(6), 791-804.

Sawyer, K. S., Oscar-Berman, M., Mosher Ruiz, S., Gálvez, D. A., Makris, N., Harris, G. J., & Valera, E. M. (2016). Associations Between Cerebellar Subregional Morphometry and Alcoholism History in Men and Women. *Alcohol Clin Exp Res, 40*(6), 1262-1272. doi:10.1111/acer.13074

Schroth, G., Naegele, T., Klose, U., Mann, K., & Petersen, D. (1988). Reversible brain shrinkage in abstinent alcoholics, measured by MRI. *Neuroradiology, 30*(5), 385-389. doi:10.1007/bf00404102

Schulte, T., Muller-Oehring, E. M., Sullivan, E. V., & Pfefferbaum, A. (2012). White matter fiber compromise contributes differentially to attention and emotion processing impairment in alcoholism, HIV-infection, and their comorbidity. *Neuropsychologia, 50*(12), 2812-2822. doi:10.1016/j.neuropsychologia.2012.07.042

Schulte, T., Sullivan, E. V., Muller-Oehring, E. M., Adalsteinsson, E., & Pfefferbaum, A. (2005). Corpus callosal microstructural integrity influences interhemispheric processing: a diffusion tensor imaging study. *Cereb Cortex, 15*(9), 1384-1392. doi:10.1093/cercor/bhi020

Schweinsburg, A. D., Paulus, M. P., Barlett, V. C., Killeen, L. A., Caldwell, L. C., Pulido, C., . . . Tapert, S. F. (2004). An FMRI study of response inhibition in youths with a family history of alcoholism. *Ann N Y Acad Sci, 1021*, 391-394. doi:10.1196/annals.1308.050

Schweinsburg, B. C., Taylor, M. J., Videen, J. S., Alhassoon, O. M., Patterson, T. L., & Grant, I. (2000). Elevated myo-inositol in gray matter of recently detoxified but not long-term abstinent alcoholics: a preliminary MR spectroscopy study. *Alcohol Clin Exp Res, 24*(5), 699-705.

Segobin, S. H., Chetelat, G., Le Berre, A. P., Lannuzel, C., Boudehent, C., Vabret, F., . . . Pitel, A. L. (2014). Relationship between brain volumetric changes and interim drinking at six months in alcohol-dependent patients. *Alcohol Clin Exp Res, 38*(3), 739-748. doi:10.1111/acer.12300

Seo, D., & Sinha, R. (2015). Neuroplasticity and Predictors of Alcohol Recovery. *Alcohol Res, 37*(1), 143-152.

Shear, P. K., Jernigan, T. L., & Butters, N. (1994). Volumetric magnetic resonance imaging quantification of longitudinal brain changes in abstinent alcoholics. *Alcohol Clin Exp Res, 18*(1), 172-176. doi:10.1111/j.1530-0277.1994.tb00899.x

Shim, J. H., Kim, Y. T., Kim, S., & Baek, H. M. (2019). Volumetric Reductions of Subcortical Structures and Their Localizations in Alcohol-Dependent Patients. *Front Neurol, 10*, 247. doi:10.3389/fneur.2019.00247

Shirer, W. R., Ryali, S., Rykhlevskaia, E., Menon, V., & Greicius, M. D. (2012). Decoding subject-driven cognitive states with whole-brain connectivity patterns. *Cereb Cortex, 22*(1), 158-165. doi:10.1093/cercor/bhr099

Singh, A. K., Jiang, Y., Gupta, S., & Benlhabib, E. (2007). Effects of chronic ethanol drinking on the blood brain barrier and ensuing neuronal toxicity in alcohol-preferring rats subjected to intraperitoneal LPS injection. *Alcohol Alcohol, 42*(5), 385-399. doi:10.1093/alcalc/agl120

Singh, N., Haldar, S., Tripathi, A. K., Horback, K., Wong, J., Sharma, D., . . . Singh, A. (2014). Brain Iron Homeostasis: From Molecular Mechanisms To Clinical Significance and Therapeutic Opportunities. *Antioxidants & Redox Signaling, 20*(8), 1324-1363. doi:10.1089/ars.2012.4931

Sjoerds, Z., Stufflebeam, S. M., Veltman, D. J., Van den Brink, W., Penninx, B. W., & Douw, L. (2017). Loss of brain graph network efficiency in alcohol dependence. *Addict Biol, 22*(2), 523-534. doi:10.1111/adb.12346

Skikne, B. S., Flowers, C. H., & Cook, J. D. (1990). Serum transferrin receptor: a quantitative measure of tissue iron deficiency. *Blood, 75*(9), 1870-1876.

Skinner, H. A., & Allen, B. A. (1982). Alcohol dependence syndrome: measurement and validation. *J Abnorm Psychol, 91*(3), 199-209.

Smith, S. M. (2002). Fast robust automated brain extraction. *Hum Brain Mapp, 17*(3), 143-155. doi:10.1002/hbm.10062

Smith, S. M., Fox, P. T., Miller, K. L., Glahn, D. C., Fox, P. M., Mackay, C. E., . . . Beckmann, C. F. (2009). Correspondence of the brain's functional architecture during activation and rest. *Proc Natl Acad Sci U S A, 106*(31), 13040-13045. doi:10.1073/pnas.0905267106

Smith, S. M., Jenkinson, M., Johansen-Berg, H., Rueckert, D., Nichols, T. E., Mackay, C. E., . . . Behrens, T. E. (2006). Tract-based spatial statistics: voxelwise analysis of multi-subject diffusion data. *Neuroimage, 31*(4), 1487-1505. doi:10.1016/j.neuroimage.2006.02.024

Smith, S. M., & Nichols, T. E. (2009). Threshold-free cluster enhancement: addressing problems of smoothing, threshold dependence and localisation in cluster inference. *Neuroimage, 44*(1), 83-98. doi:10.1016/j.neuroimage.2008.03.061

Soares, J. M., Marques, P., Alves, V., & Sousa, N. (2013). A hitchhiker's guide to diffusion tensor imaging. *Front Neurosci, 7*, 31. doi:10.3389/fnins.2013.00031

Song, S. K., Sun, S. W., Ju, W. K., Lin, S. J., Cross, A. H., & Neufeld, A. H. (2003). Diffusion tensor imaging detects and differentiates axon and myelin degeneration in mouse optic nerve after retinal ischemia. *Neuroimage, 20*(3), 1714-1722. doi:10.1016/j.neuroimage.2003.07.005

Song, S. K., Sun, S. W., Ramsbottom, M. J., Chang, C., Russell, J., & Cross, A. H. (2002). Dysmyelination revealed through MRI as increased radial (but unchanged axial) diffusion of water. *Neuroimage, 17*(3), 1429-1436. doi:10.1006/nimg.2002.1267

Song, Z., Chen, J., Wen, Z., & Zhang, L. (2020). Abnormal functional connectivity and effective connectivity between the default mode network and attention networks in patients with alcohol-use disorder. *Acta Radiol*, 284185120923270. doi:10.1177/0284185120923270

Sorg, S. F., Squeglia, L. M., Taylor, M. J., Alhassoon, O. M., Delano-Wood, L. M., & Grant, I. (2015). Effects of aging on frontal white matter microstructure in alcohol use disorder and associations with processing speed. *Journal of studies on alcohol and drugs, 76*(2), 296-306. doi:10.15288/jsad.2015.76.296

Sorg, S. F., Taylor, M. J., Alhassoon, O. M., Gongvatana, A., Theilmann, R. J., Frank, L. R., & Grant, I. (2012). Frontal white matter integrity predictors of adult alcohol treatment outcome. *Biol Psychiatry, 71*(3), 262-268. doi:10.1016/j.biopsych.2011.09.022

Sotak, C. H. (2004). Nuclear magnetic resonance (NMR) measurement of the apparent diffusion coefficient (ADC) of tissue water and its relationship to cell volume changes in pathological states. *Neurochem Int, 45*(4), 569-582. doi:10.1016/j.neuint.2003.11.010

Soto-Insuga, V., Calleja, M. L., Prados, M., Castano, C., Losada, R., & Ruiz-Falco, M. L. (2013). [Role of iron in the treatment of attention deficit-hyperactivity disorder]. *An Pediatr (Barc), 79*(4), 230-235. doi:10.1016/j.anpedi.2013.02.008

Spadoni, A. D., Norman, A. L., Schweinsburg, A. D., & Tapert, S. F. (2008). Effects of family history of alcohol use disorders on spatial working memory BOLD response in adolescents. *Alcohol Clin Exp Res, 32*(7), 1135-1145. doi:10.1111/j.1530-0277.2008.00694.x

Spagnolli, F., Cerini, R., Cardobi, N., Barillari, M., Manganotti, P., Storti, S., & Mucelli, R. P. (2013). Brain modifications after acute alcohol consumption analyzed by resting state fMRI. *Magn Reson Imaging, 31*(8), 1325-1330. doi:10.1016/j.mri.2013.04.007

Spagnolo, P. A., & Goldman, D. (2017). Neuromodulation interventions for addictive disorders: challenges, promise, and roadmap for future research. *Brain, 140*(5), 1183-1203. doi:10.1093/brain/aww284

Spencer, R. L., & Hutchison, K. E. (1999). Alcohol, aging, and the stress response. *Alcohol Res Health, 23*(4), 272-283.

Stavro, K., Pelletier, J., & Potvin, S. (2013). Widespread and sustained cognitive deficits in alcoholism: a meta-analysis. *Addict Biol, 18*(2), 203-213. doi:10.1111/j.1369-1600.2011.00418.x

Stephens, M. A., & Wand, G. (2012). Stress and the HPA axis: role of glucocorticoids in alcohol dependence. *Alcohol Res, 34*(4), 468-483.

Stephenson, E., Nathoo, N., Mahjoub, Y., Dunn, J. F., & Yong, V. W. (2014). Iron in multiple sclerosis: roles in neurodegeneration and repair. *Nat Rev Neurol, 10*(8), 459-468. doi:10.1038/nrneurol.2014.118

Stuber, C., Pitt, D., & Wang, Y. (2016). Iron in Multiple Sclerosis and Its Noninvasive Imaging with Quantitative Susceptibility Mapping. *Int J Mol Sci, 17*(1). doi:10.3390/ijms17010100

Sullivan, E. V., Deshmukh, A., Desmond, J. E., Lim, K. O., & Pfefferbaum, A. (2000). Cerebellar volume decline in normal aging, alcoholism, and Korsakoff's syndrome: relation to ataxia. *Neuropsychology, 14*(3), 341-352. doi:10.1037//0894-4105.14.3.341

Sullivan, E. V., Harris, R. A., & Pfefferbaum, A. (2010). Alcohol's effects on brain and behavior. *Alcohol Res Health, 33*(1-2), 127-143.

Sullivan, E. V., & Pfefferbaum, A. (2005). Neurocircuitry in alcoholism: a substrate of disruption and repair. *Psychopharmacology (Berl), 180*(4), 583-594. doi:10.1007/s00213-005-2267-6

Sullivan, E. V., Rosenbloom, M. J., Lim, K. O., & Pfefferbaum, A. (2000). Longitudinal changes in cognition, gait, and balance in abstinent and relapsed alcoholic men: relationships to changes in brain structure. *Neuropsychology, 14*(2), 178-188.

Sullivan, E. V., Rosenbloom, M. J., & Pfefferbaum, A. (2000). Pattern of motor and cognitive deficits in detoxified alcoholic men. *Alcohol Clin Exp Res, 24*(5), 611-621.

Sullivan, E. V., Zahr, N. M., Saranathan, M., Pohl, K. M., & Pfefferbaum, A. (2019). Convergence of three parcellation approaches demonstrating cerebellar lobule volume deficits in Alcohol Use Disorder. *Neuroimage Clin, 24*, 101974. doi:10.1016/j.nicl.2019.101974

Sun, H., Seres, P., & Wilman, A. H. (2016). Structural and functional quantitative susceptibility mapping from standard fMRI studies. *NMR Biomed*. doi:10.1002/nbm.3619

Sun, H., Walsh, A. J., Lebel, R. M., Blevins, G., Catz, I., Lu, J. Q., . . . Wilman, A. H. (2015). Validation of quantitative susceptibility mapping with Perls' iron staining for subcortical gray matter. *Neuroimage, 105*, 486-492. doi:10.1016/j.neuroimage.2014.11.010

Sun, H., & Wilman, A. H. (2014). Background field removal using spherical mean value filtering and Tikhonov regularization. *Magn Reson Med, 71*(3), 1151-1157. doi:10.1002/mrm.24765

Sun, H., & Wilman, A. H. (2015). Quantitative susceptibility mapping using single-shot echo-planar imaging. *Magn Reson Med, 73*(5), 1932-1938. doi:10.1002/mrm.25316

Sutherland, G. T., Sheedy, D., & Kril, J. J. (2014a). Neuropathology of alcoholism. *Handb Clin Neurol, 125*, 603-615. doi:10.1016/b978-0-444-62619-6.00035-5

Sutherland, G. T., Sheedy, D., & Kril, J. J. (2014b). Using autopsy brain tissue to study alcohol-related brain damage in the genomic age. *Alcohol Clin Exp Res, 38*(1), 1-8. doi:10.1111/acer.12243

Tabakoff, B., & Hoffman, P. L. (2013). The neurobiology of alcohol consumption and alcoholism: an integrative history. *Pharmacol Biochem Behav, 113*, 20-37. doi:10.1016/j.pbb.2013.10.009

Takahashi, M., Hackney, D. B., Zhang, G., Wehrli, S. L., Wright, A. C., O'Brien, W. T., . . . Selzer, M. E. (2002). Magnetic resonance microimaging of intraaxonal water diffusion in live excised lamprey spinal cord. *Proc Natl Acad Sci U S A, 99*(25), 16192-16196. doi:10.1073/pnas.252249999

Tarnowska-Dziduszko, E., Bertrand, E., & Szpak, G. M. (1995). Morphological changes in the corpus callosum in chronic alcoholism. *Folia Neuropathol, 33*(1), 25-29.

The MathWorks Inc. (2018). MATLAB (Version R2018b). Natick, MA.: The MathWorks Inc,.

Todorich, B., Pasquini, J. M., Garcia, C. I., Paez, P. M., & Connor, J. R. (2009). Oligodendrocytes and myelination: the role of iron. *Glia, 57*(5), 467-478. doi:10.1002/glia.20784

Tomasi, D. G., Wiers, C. E., Shokri-Kojori, E., Zehra, A., Ramirez, V., Freeman, C., . . . Volkow, N. D. (2019). Association Between Reduced Brain Glucose Metabolism and Cortical Thickness in Alcoholics: Evidence of Neurotoxicity. *Int J Neuropsychopharmacol, 22*(9), 548-559. doi:10.1093/ijnp/pyz036

Trivedi, R., Bagga, D., Bhattacharya, D., Kaur, P., Kumar, P., Khushu, S., . . . Singh, N. (2013). White matter damage is associated with memory decline in chronic alcoholics: a quantitative diffusion tensor tractography study. *Behav Brain Res, 250*, 192-198. doi:10.1016/j.bbr.2013.05.001

Tu, X., Wang, J., Liu, X., & Zheng, J. (2018). Aberrant regional brain activities in alcohol dependence: a functional magnetic resonance imaging study. *Neuropsychiatr Dis Treat, 14*, 847-853. doi:10.2147/NDT.S158221

van den Heuvel, M. P., & Hulshoff Pol, H. E. (2010). Exploring the brain network: a review on resting-state fMRI functional connectivity. *Eur Neuropsychopharmacol, 20*(8), 519-534. doi:10.1016/j.euroneuro.2010.03.008

van Eijk, J., Demirakca, T., Frischknecht, U., Hermann, D., Mann, K., & Ende, G. (2013). Rapid partial regeneration of brain volume during the first 14 days of abstinence from alcohol. *Alcohol Clin Exp Res, 37*(1), 67-74. doi:10.1111/j.1530-0277.2012.01853.x

Vergara, V. M., Liu, J., Claus, E. D., Hutchison, K., & Calhoun, V. (2017). Alterations of resting state functional network connectivity in the brain of nicotine and alcohol users. *Neuroimage, 151*, 45-54. doi:10.1016/j.neuroimage.2016.11.012

Volkow, N. D., Wang, G.-J., Fowler, J. S., Tomasi, D., & Telang, F. (2011). Addiction: Beyond dopamine reward circuitry. *Proceedings of the National Academy of Sciences of the United States of America, 108*(37), 15037-15042. doi:10.1073/pnas.1010654108

Volkow, N. D., Wang, G. J., Hitzemann, R., Fowler, J. S., Overall, J. E., Burr, G., & Wolf, A. P. (1994). Recovery of brain glucose metabolism in detoxified alcoholics. *Am J Psychiatry, 151*(2), 178-183. doi:10.1176/ajp.151.2.178

Volkow, N. D., Wiers, C. E., Shokri-Kojori, E., Tomasi, D., Wang, G. J., & Baler, R. (2017). Neurochemical and metabolic effects of acute and chronic alcohol in the human brain: Studies with positron emission tomography. *Neuropharmacology, 122*, 175-188. doi:10.1016/j.neuropharm.2017.01.012

Walitzer, K. S., & Dearing, R. L. (2006). Gender differences in alcohol and substance use relapse. *Clin Psychol Rev, 26*(2), 128-148. doi:10.1016/j.cpr.2005.11.003

Walsh, D. O., Gmitro, A. F., & Marcellin, M. W. (2000). Adaptive reconstruction of phased array MR imagery. *Magn Reson Med, 43*(5), 682-690.

Wang, G. Y., Demirakca, T., van Eijk, J., Frischknecht, U., Ruf, M., Ucar, S., . . . Ende, G. (2016). Longitudinal Mapping of Gyral and Sulcal Patterns of Cortical Thickness and Brain Volume Regain during Early Alcohol Abstinence. *Eur Addict Res, 22*(2), 80-89. doi:10.1159/000438456

Wang, H. J., Zakhari, S., & Jung, M. K. (2010). Alcohol, inflammation, and gut-liver-brain interactions in tissue damage and disease development. *World J Gastroenterol, 16*(11), 1304-1313.

Wang, J. J., Durazzo, T. C., Gazdzinski, S., Yeh, P. H., Mon, A., & Meyerhoff, D. J. (2009). MRSI and DTI: a multimodal approach for improved detection of white matter abnormalities in alcohol and nicotine dependence. *NMR Biomed, 22*(5), 516-522. doi:10.1002/nbm.1363

Wang, Y., & Liu, T. (2015). Quantitative susceptibility mapping (QSM): Decoding MRI data for a tissue magnetic biomarker. *Magn Reson Med, 73*(1), 82-101. doi:10.1002/mrm.25358

Weiland, B. J., Sabbineni, A., Calhoun, V. D., Welsh, R. C., Bryan, A. D., Jung, R. E., . . . Hutchison, K. E. (2014). Reduced left executive control network functional connectivity is associated with alcohol use disorders. *Alcohol Clin Exp Res, 38*(9), 2445-2453. doi:10.1111/acer.12505

Weng, J. C., Chou, Y. S., Huang, G. J., Tyan, Y. S., & Ho, M. C. (2018). Mapping brain functional alterations in betel-quid chewers using resting-state fMRI and network analysis. *Psychopharmacology (Berl), 235*(4), 1257-1271. doi:10.1007/s00213-018-4841-8

Werring, D. J., Toosy, A. T., Clark, C. A., Parker, G. J., Barker, G. J., Miller, D. H., & Thompson, A. J. (2000). Diffusion tensor imaging can detect and quantify corticospinal tract degeneration after stroke. *J Neurol Neurosurg Psychiatry, 69*(2), 269-272. doi:10.1136/jnnp.69.2.269

Wessling-Resnick, M. (2010). Iron Homeostasis and the Inflammatory Response. *Annual review of nutrition, 30*, 105-122. doi:10.1146/annurev.nutr.012809.104804

Wheeler-Kingshott, C. A., & Cercignani, M. (2009). About "axial" and "radial" diffusivities. *Magn Reson Med, 61*(5), 1255-1260. doi:10.1002/mrm.21965

Whitfield, J. B., Zhu, G., Heath, A. C., Powell, L. W., & Martin, N. G. (2001). Effects of alcohol consumption on indices of iron stores and of iron stores on alcohol intake markers. *Alcohol Clin Exp Res, 25*(7), 1037-1045.

Wiggins, R. C., Gorman, A., Rolsten, C., Samorajski, T., Ballinger, W. E., & Freund, G. (1988). Effects of aging and alcohol on the biochemical composition of histologically normal human brain. *Metab Brain Dis, 3*(1), 67-80. doi:10.1007/BF01001354

Wilcox, C. E., Dekonenko, C. J., Mayer, A. R., Bogenschutz, M. P., & Turner, J. A. (2014). Cognitive control in alcohol use disorder: deficits and clinical relevance. *Rev Neurosci, 25*(1), 1-24. doi:10.1515/revneuro-2013-0054

Wilson, S., Bair, J. L., Thomas, K. M., & Iacono, W. G. (2017). Problematic alcohol use and reduced hippocampal volume: a meta-analytic review. *Psychol Med, 47*(13), 2288-2301. doi:10.1017/s0033291717000721

Winkler, A. M., Ridgway, G. R., Webster, M. A., Smith, S. M., & Nichols, T. E. (2014). Permutation inference for the general linear model. *Neuroimage, 92*, 381-397. doi:10.1016/j.neuroimage.2014.01.060

Winterburn, J. L., Pruessner, J. C., Chavez, S., Schira, M. M., Lobaugh, N. J., Voineskos, A. N., & Chakravarty, M. M. (2013). A novel in vivo atlas of human hippocampal subfields using high-resolution 3 T magnetic resonance imaging. *Neuroimage, 74*, 254-265. doi:10.1016/j.neuroimage.2013.02.003

Witkiewitz, K. (2011). Predictors of heavy drinking during and following treatment. *Psychol Addict Behav, 25*(3), 426-438. doi:10.1037/a0022889

Wobrock, T., Falkai, P., Schneider-Axmann, T., Frommann, N., Wolwer, W., & Gaebel, W. (2009). Effects of abstinence on brain morphology in alcoholism: a MRI study. *Eur Arch Psychiatry Clin Neurosci, 259*(3), 143-150. doi:10.1007/s00406-008-0846-3

Wong-Riley, M. T. (1989). Cytochrome oxidase: an endogenous metabolic marker for neuronal activity. *Trends Neurosci, 12*(3), 94-101.

Woo, C. W., Krishnan, A., & Wager, T. D. (2014). Cluster-extent based thresholding in fMRI analyses: pitfalls and recommendations. *Neuroimage, 91*, 412-419. doi:10.1016/j.neuroimage.2013.12.058

World Health Organization. (2014). Global status report on alcohol and health, 2014. Retrieved from http://apps.who.int/iris/bitstream/10665/112736/1/9789240692763_eng.pdf?ua=1

World Health Organization. (2018). *Global status report on alcohol and health 2018*. Geneva, Switzerland: World Health Organization.

Wu, B., Li, W., Guidon, A., & Liu, C. (2012). Whole brain susceptibility mapping using compressed sensing. *Magnetic Resonance in Medicine, 67*(1), 137-147. doi:10.1002/mrm.23000

Xia, J., Simonyi, A., & Sun, G. Y. (1999). Chronic ethanol and iron administration on iron content, neuronal nitric oxide synthase, and superoxide dismutase in rat cerebellum. *Alcohol Clin Exp Res, 23*(4), 702-707.

Xia, S., Zheng, G., Shen, W., Liu, S., Zhang, L. J., Haacke, E. M., & Lu, G. M. (2015). Quantitative measurements of brain iron deposition in cirrhotic patients using susceptibility mapping. *Acta Radiol, 56*(3), 339-346. doi:10.1177/0284185114525374

Xiao, P., Dai, Z., Zhong, J., Zhu, Y., Shi, H., & Pan, P. (2015). Regional gray matter deficits in alcohol dependence: A meta-analysis of voxel-based morphometry studies. *Drug Alcohol Depend, 153*, 22-28. doi:10.1016/j.drugalcdep.2015.05.030

Xu, X., Yuan, H., & Lei, X. (2016). Activation and Connectivity within the Default Mode Network Contribute Independently to Future-Oriented Thought. *Sci Rep, 6*, 21001. doi:10.1038/srep21001

Yang, X., Tian, F., Zhang, H., Zeng, J., Chen, T., Wang, S., . . . Gong, Q. (2016). Cortical and subcortical gray matter shrinkage in alcohol-use disorders: a voxel-based meta-analysis. *Neurosci Biobehav Rev, 66*, 92-103. doi:10.1016/j.neubiorev.2016.03.034

Yeh, P. H., Gazdzinski, S., Durazzo, T. C., Sjöstrand, K., & Meyerhoff, D. J. (2007). Hierarchical linear modeling (HLM) of longitudinal brain structural and cognitive changes in alcohol-dependent

individuals during sobriety. *Drug Alcohol Depend, 91*(2-3), 195-204. doi:10.1016/j.drugalcdep.2007.05.027

Yeh, P. H., Simpson, K., Durazzo, T. C., Gazdzinski, S., & Meyerhoff, D. J. (2009). Tract-Based Spatial Statistics (TBSS) of diffusion tensor imaging data in alcohol dependence: abnormalities of the motivational neurocircuitry. *Psychiatry Res, 173*(1), 22-30. doi:10.1016/j.pscychresns.2008.07.012

Yeo, B. T., Krienen, F. M., Sepulcre, J., Sabuncu, M. R., Lashkari, D., Hollinshead, M., . . . Buckner, R. L. (2011). The organization of the human cerebral cortex estimated by intrinsic functional connectivity. *J Neurophysiol, 106*(3), 1125-1165. doi:10.1152/jn.00338.2011

Yotter, R. A., Ziegler, G., Thompson, P. M., & Gaser, C. (2011). *Diffeometric Anatomical Registration on the Surface*. Paper presented at the *HBM 2011*.

Yu, R., Liu, B., Wang, L., Chen, J., & Liu, X. (2013). Enhanced functional connectivity between putamen and supplementary motor area in Parkinson's disease patients. *PLoS One, 8*(3), e59717. doi:10.1371/journal.pone.0059717

Zahr, N. M. (2014). Structural and microstructral imaging of the brain in alcohol use disorders. *Handb Clin Neurol, 125*, 275-290. doi:10.1016/b978-0-444-62619-6.00017-3

Zahr, N. M., & Pfefferbaum, A. (2017). Alcohol's Effects on the Brain: Neuroimaging Results in Humans and Animal Models. *Alcohol Res, 38*(2), 183-206.

Zahr, N. M., Pohl, K. M., Saranathan, M., Sullivan, E. V., & Pfefferbaum, A. (2019). Hippocampal subfield CA2+3 exhibits accelerated aging in Alcohol Use Disorder: A preliminary study. *Neuroimage Clin, 22*, 101764. doi:10.1016/j.nicl.2019.101764

Zahr, N. M., & Sullivan, E. V. (2008). Translational studies of alcoholism: bridging the gap. *Alcohol Res Health, 31*(3), 215-230.

Zang, Y., Jiang, T., Lu, Y., He, Y., & Tian, L. (2004). Regional homogeneity approach to fMRI data analysis. *Neuroimage, 22*(1), 394-400. doi:10.1016/j.neuroimage.2003.12.030

Zang, Y. F., He, Y., Zhu, C. Z., Cao, Q. J., Sui, M. Q., Liang, M., . . . Wang, Y. F. (2007). Altered baseline brain activity in children with ADHD revealed by resting-state functional MRI. *Brain Dev, 29*(2), 83-91. doi:10.1016/j.braindev.2006.07.002

Zecca, L., Youdim, M. B. H., Riederer, P., Connor, J. R., & Crichton, R. R. (2004). Iron, brain ageing and neurodegenerative disorders. *Nat Rev Neurosci, 5*(11), 863-873.

Zhao, Q., Pfefferbaum, A., Podhajsky, S., Pohl, K. M., & Sullivan, E. V. (2019). Accelerated aging and motor control deficits are related to regional deformation of central cerebellar white matter in alcohol use disorder. *Addict Biol*. doi:10.1111/adb.12746

Zheng, H., Kong, L., Chen, L., Zhang, H., & Zheng, W. (2015). Acute effects of alcohol on the human brain: a resting-state FMRI study. *Biomed Res Int, 2015*, 947529. doi:10.1155/2015/947529

Zhu, X., Cortes, C. R., Mathur, K., Tomasi, D., & Momenan, R. (2017). Model-free functional connectivity and impulsivity correlates of alcohol dependence: a resting-state study. *Addict Biol, 22*(1), 206-217. doi:10.1111/adb.12272

Zhu, X., Du, X., Kerich, M., Lohoff, F. W., & Momenan, R. (2018). Random forest based classification of alcohol dependence patients and healthy controls using resting state MRI. *Neurosci Lett, 676*, 27-33. doi:10.1016/j.neulet.2018.04.007

Zipursky, R. B., Lim, K. C., & Pfefferbaum, A. (1989). MRI study of brain changes with short-term abstinence from alcohol. *Alcohol Clin Exp Res, 13*(5), 664-666. doi:10.1111/j.1530-0277.1989.tb00401.x

Zois, E., Vollstadt-Klein, S., Hoffmann, S., Reinhard, I., Charlet, K., Beck, A., . . . Kiefer, F. (2017). Orbitofrontal structural markers of negative affect in alcohol dependence and their associations with heavy relapse-risk at 6 months post-treatment. *Eur Psychiatry, 46*, 16-22. doi:10.1016/j.eurpsy.2017.07.013

Zorlu, N., Gelal, F., Kuserli, A., Cenik, E., Durmaz, E., Saricicek, A., & Gulseren, S. (2013). Abnormal white matter integrity and decision-making deficits in alcohol dependence. *Psychiatry Res, 214*(3), 382-388. doi:10.1016/j.pscychresns.2013.06.014

Zorlu, N., Karavul Ucman, T., Gelal, F., Colak Kalayci, C., Polat, S., Saricicek, A., . . . Gulseren, S. (2014). Abnormal white matter integrity in long-term abstinent alcohol dependent patients. *Psychiatry Res, 224*(1), 42-48. doi:10.1016/j.pscychresns.2014.07.006

Zou, X., Durazzo, T. C., & Meyerhoff, D. J. (2018). Regional Brain Volume Changes in Alcohol-Dependent Individuals During Short-Term and Long-Term Abstinence. *Alcohol Clin Exp Res, 42*(6), 1062-1072. doi:10.1111/acer.13757

Zou, Y., Murray, D. E., Durazzo, T. C., Schmidt, T. P., Murray, T. A., & Meyerhoff, D. J. (2017). Effects of abstinence and chronic cigarette smoking on white matter microstructure in alcohol dependence: Diffusion tensor imaging at 4T. *Drug Alcohol Depend, 175*, 42-50. doi:10.1016/j.drugalcdep.2017.01.032

Zou, Y., Murray, D. E., Durazzo, T. C., Schmidt, T. P., Murray, T. A., & Meyerhoff, D. J. (2018). White matter microstructural correlates of relapse in alcohol dependence. *Psychiatry Res Neuroimaging, 281*, 92-100. doi:10.1016/j.pscychresns.2018.09.004

Zuo, X. N., Ehmke, R., Mennes, M., Imperati, D., Castellanos, F. X., Sporns, O., & Milham, M. P. (2012). Network centrality in the human functional connectome. *Cereb Cortex, 22*(8), 1862-1875. doi:10.1093/cercor/bhr269